UNIVERSITY OF SOUTHAMPTON

Linking the Thermal, Morphological and Electrical Properties of Thermoplastic Polymer Composites containing an Organoclay

by

Allison V. Shaw

A thesis submitted for the
degree of Doctor of Philosophy

in the
Faculty of Engineering and Physical Sciences
Department of Electronics and Computer Science

February 2020

UNIVERSITY OF SOUTHAMPTON

ABSTRACT

Faculty of Engineering and Physical Sciences
Department of Electronics and Computer Science

Doctor of Philosophy

by Allison V. Shaw

New material discovery to meet a list of property specifications is both slow and costly, whereas combining known materials to achieve a composite displaying a variety of properties from the constituent parts is widely regarded to be more effective. Blending polymers together with the incorporation of a nano-clay to form a nanocomposite alters the thermal, mechanical and electrical properties in particular.

This thesis investigates the ability to form composites and their resulting thermal, morphological and electrical properties. Within each material system, results of varying the relative ratio of their constituents will be investigated and a comment made on the compatibility of the constituents. The hypothesis being that, in each case, a link between these properties can be established such that understanding the interdependency can better inform future material development. The polymeric materials investigated include polyethylene, polypropylene, polystyrene and copolymers of ethylene and vinyl acetate.

Contents

List of Figures vii

List of Tables xi

Symbols and Abberivations xiii

Author's Declaration xvii

Acknowledgements xix

1 Introduction 1
- 1.1 Polymers . . . 1
- 1.2 Polymer Blends . . . 6
- 1.3 Organoclay . . . 6
- 1.4 Achieving Compatibilisation and Dispersion . . . 9
  - 1.4.1 Thermodynamic Considerations . . . 10
- 1.5 The Production of Polymer-Organoclay Composites . . . 11
- 1.6 Aim of this Thesis . . . 12
  - 1.6.1 Statement of Novelty . . . 14
- 1.7 Introducing the Composites in this Thesis . . . 16
  - 1.7.1 PE-EVA-Organoclay . . . 17
  - 1.7.2 PP-EVA-Organoclay . . . 19
  - 1.7.3 PP-PS-Organoclay . . . 20
- 1.8 Applications of Dielectrics in Capacitors . . . 23

2 Methods and Analysis Techniques 25
- 2.1 Processing . . . 25
  - 2.1.1 PE-EVA-Organoclay Samples . . . 25
  - 2.1.2 PP-EVA-Organoclay Samples . . . 26
  - 2.1.3 PP-PS-Organoclay Samples . . . 28
  - 2.1.4 Preparation of the Samples for the Xylene Immersion Tests . . . 29
  - 2.1.5 Preparation of the Samples for the Water Immersion Tests . . . 30
- 2.2 Thermal Analysis . . . 30
  - 2.2.1 Thermal Gravimetric Analysis . . . 30
- 2.3 Morphological Analysis . . . 31
  - 2.3.1 Differential Scanning Calorimetry . . . 31
  - 2.3.2 X-Ray Diffraction . . . 31
  - 2.3.3 Fourier-Transform Infrared Spectroscopy . . . 32

2.3.4 Scanning Electron Microscopy . . . 33
2.4 Electrical Analysis . . . 33
2.4.1 Dielectric Breakdown Strength . . . 33
2.4.2 DC Conductivity . . . 34
2.4.3 Dielectric Spectroscopy . . . 36

3 Thermal Analysis of the Composites 39
3.1 Introduction . . . 39
3.2 Experimental . . . 40
3.3 TGA for the PE-EVA-Organoclay System . . . 41
3.3.1 Evidence of Compatibilisation in PE-EVA-Organoclay Composites 43
3.4 TGA for the PP-EVA-Organoclay System . . . 45
3.4.1 TGA for the PP-EVA-Organoclay System Immersed in Xylene . . 47
3.5 TGA for the PP-PS-Organoclay System . . . 47
3.6 DSC for the PE-EVA-Organoclay samples . . . 50
3.7 DSC for the PP-EVA-Organoclay samples . . . 51
3.8 DSC for the PP-PS-Organoclay samples . . . 54
3.9 Conclusion . . . 56

4 Observing the Organoclay in the Composites 59
4.1 Experimental Techniques . . . 60
4.2 FT-IR: Confirming the Incorporation of Organoclay . . . 60
4.3 XRD for the Single Polymer-Organoclay Composites . . . 63
4.4 XRD for the PE-EVA-Organoclay Composites . . . 65
4.5 XRD for the Xylene Immersion tests . . . 67
4.6 XRD for the PP-EVA-Organoclay Composites . . . 68
4.7 XRD for the PP-PS-Organoclay Composites . . . 72
4.8 Conclusion . . . 77

5 Imaging the Composites 79
5.1 Experimental Techniques . . . 79
5.2 SEM of a single polymer with 5 wt.% organoclay . . . 80
5.3 SEM of PE-EVA-Organoclay Composites . . . 83
5.4 SEM of PP-EVA-Organoclay Composites . . . 86
5.5 SEM of PP-PS-Organoclay Composites . . . 89
5.6 Conclusion . . . 94

6 The Electrical Properties of the Composites 95
6.1 Experimental Techniques . . . 95
6.2 DC Conductivity . . . 95
6.2.1 DC Conductivity: PE-EVA-Organoclay . . . 95
6.2.2 DC Conductivity: PP-EVA-Organoclay Composites . . . 99
6.2.3 DC Conductivity: PP-PS-Organoclay Composites . . . 100
6.3 Dielectric Breakdown Strength Measurements . . . 103
6.3.1 Dielectric Breakdown Strength: Single Polymer-Organoclay Composites . . . 103
6.3.2 Dielectric Breakdown Strength: PE-EVA-Organoclay Composites 103
6.3.2.1 DC dielectric breakdown strength . . . 103

6.3.2.2 AC dielectric breakdown strength . . . 109
6.3.3 Dielectric Breakdown Strength: PP-EVA-Organoclay Composites 110
6.3.3.1 AC dielectric breakdown strength . . . 110
6.3.3.2 DC dielectric breakdown strength . . . 112
6.3.4 DC Dielectric Breakdown Strength: PP-PS-Organoclay Composites 114
6.4 Dielectric Spectroscopy . . . 116
6.5 Conclusion . . . 123

7 Effect of Xylene and Water Immersion on the Composites 125
7.1 Experimental . . . 126
7.2 Results and Discussion of Xylene Immersion . . . 127
7.2.1 Investigating Xylene Uptake and Removal . . . 127
7.2.2 The Dielectric Response . . . 134
7.2.2.1 Dielectric Spectroscopy . . . 134
7.2.2.2 Dielectric Breakdown . . . 139
7.3 Effect of Water Immersion on the Composites: a counterpart to the Xylene Immersion Work . . . 142
7.4 Conclusion . . . 146

8 Conclusions 147
8.1 Conclusions on the Compatibility of the PE-EVA-Organoclay Composites . . . 149
8.2 Conclusions on the Compatibility of the PP-EVA-Organoclay and PP-PS-Organoclay Composites . . . 150
8.3 A summary of the general principles discovered that allow predictability in material development . . . 151

9 Future Work 153

A Appendix: Introducing the Characterisation Methods 155
A.1 Introducing Dielectric Spectroscopy: The Frequency-Dependent Dielectric Response . . . 155
A.1.1 Plotting and Interpreting the Results . . . 156
A.1.2 Predicting the Real Permittivity . . . 157
A.2 Introducing the Dielectric Breakdown Strength . . . 157
A.3 Introducing Conductivity . . . 159
A.4 The Interplay between the Dielectric Properties . . . 161
A.5 Introducing Thermal Gravimetric Analysis . . . 161
A.6 Introducing Differential Scanning Calorimetry . . . 162
A.7 Introducing X-ray Diffraction . . . 163
A.8 Introducing Fourir-Transform Infrared Spectroscopy . . . 163
A.8.1 Normalising the Data . . . 164
A.9 Introducing Scanning Electron Microscopy . . . 164

B Appendix: Supplementary Material 167

Bibliography 169

List of Figures

1.1 *Schematic Diagram of a Spherulite* 2
1.2 *Diagram of the Crystalline and Amorphous Regions of a Spherulite* 2
1.3 *Schematic Diagram of Polyethylene* 3
1.4 *Schematic Diagram of Polypropylene* 4
1.5 *Schematic Diagram of Ethylene Vinyl Acetate* 4
1.6 *Schematic Diagram of Polystyrene* 5
1.7 *Schematic Diagram of Organoclay* 7

3.1 *TGA data: evidence of nanocomposite formation in the PE-EVA-Organoclay composites* 42
3.2 *TGA data: decomposition temperature versus organoclay content for the PE-EVA-Organoclay composites* 43
3.3 *TGA data: comparing the decomposition temperature of the PE-EVA-Organoclay composites under air and nitrogen* 44
3.4 *TGA data: decomposition temperature against organoclay content for the PP-EVA-Organoclay composites* 46
3.5 *TGA data: comparing the decomposition of a PP-EVA-organoclay composite* . . 46
3.6 *TGA data: decomposition temperature versus organoclay content for the PP-PS-organoclay composites* 48
3.7 *TGA data: decomposition traces for the PPa/PSb/X/Y samples* 49
3.8 *DSC data: crystallisation temperature with organoclay loading for the PE-EVA-Organoclay composites* 51
3.9 *DSC data: crystallisation time changes with temperature for the PP-EVA-Organoclay composites* 52
3.10 *DSC data: crystallisation temperature with organoclay loading for the PP-EVA-Organoclay composites* 53
3.11 *DSC data: crystallisation time changes with temperature for the PP-PS-organoclay composites samples* 55
3.12 *DSC data: crystallisation temperature with organoclay loading for the PP-PS-Organoclay samples* 56

4.1 *FT-IR data examining organoclay incorporation and oxidation of the PE-EVA-Organoclay samples* 61
4.2 *FT-IR data examining organoclay incorporation and oxidation of the PP-EVA-Organoclay samples* 61
4.3 *FT-IR data examining organoclay incorporation and oxidation of the PP-PS-Organoclay samples* 62
4.4 *Normalised XRD data of the single polymer-clay composites.* 64

4.5 *XRD data: examining the interlayer distance changes for the PE-EVA-Organoclay composites* . . . 66
4.6 *XRD data: examining the effect of xylene on a PE-EVA-Organoclay composite* 68
4.7 *XRD data for the PP-EVA-Organoclay composites* . . . 70
4.8 *XRD data of the clay region of the PP-EVA-Organoclay composites* . . . 71
4.9 *XRD data for comparing the quenched PP-PS-Organoclay composites* . . . 73
4.10 *XRD data for comparing the other thermal treatments of the PP-PS-Organoclay composites* . . . 74
4.11 *Normalised XRD data comparing the organoclay and the PP-PS-Organoclay composites* . . . 76

5.1 *SEM micrographs of the pure polymers PE, PP and PS* . . . 80
5.2 *SEM of the PE-organoclay Composite* . . . 81
5.3 *SEM of the PP-organoclay Composite* . . . 81
5.4 *SEM of the EVA-organoclay Composite* . . . 82
5.5 *SEM of the PS-organoclay Composite* . . . 82
5.6 *SEM micrographs of the PE-EVA-organoclay composites* . . . 85
5.7 *SEM micrographs of the PP-EVA-organoclay composites* . . . 88
5.8 *SEM of PP/EVA9/0.5/Q* . . . 88
5.9 *SEM micrographs of the PP7/PS3/0/Y Blends* . . . 90
5.10 *SEM micrographs of the PP9/PS1/0/Y Blends* . . . 90
5.11 *SEM micrographs of the PP7/PS3/X/Y composites* . . . 92
5.12 *SEM micrographs of the PP9/PS1/X/Y composites* . . . 93

6.1 *The current decay of PE/EVA20/X/Q samples taken under dry or ambient conditions* . . . 96
6.2 *DC conductivity data of the PE/EVA9/X/Q composites* . . . 97
6.3 *DC conductivity data of the PE/EVA9/X/Y composites at 70* °C . . . 98
6.4 *DC conductivity summary of data from the PP-EVA-Organoclay composites* . 99
6.5 *DC conductivity plotted to compare current decay over time for the PP-EVA-Organoclay composites* . . . 101
6.6 *DC conductivity data summary of the PP-PS-Organoclay composites* . . . 102
6.7 *DC dielectric breakdown Weibulls for the PE/EVA9/0/Y samples* . . . 105
6.8 *DC dielectric breakdown Weibulls for the PE/EVA9/X/Q samples* . . . 106
6.9 *DC dielectric breakdown Weibulls for the PE/EVA9/X/SC samples* . . . 107
6.10 *DC dielectric breakdown Weibulls for the PE/EVA9/X/ISO samples* . . . 108
6.11 *AC dielectric breakdown Weibulls for the PE/EVA9/X/Q samples* . . . 109
6.12 *AC dielectric breakdown summary of the PP-EVA-organoclay composites* . . . 111
6.13 *AC dielectric breakdown summary of pure PP* . . . 112
6.14 *DC dielectric breakdown summary of the PP-EVA-Organoclay composites* . . . 114
6.15 *DC dielectric breakdown summary of the PP-PS-organoclay composites* . . . 115
6.16 *Permittivity against frequency graphs for all the samples* . . . 117
6.17 *Cole-Cole plots of the Dielectric Spectroscopy results obtained under several different temperatures for the PE-EVA-organoclay samples* . . . 120
6.18 *Cole-Cole plots of the Dielectric Spectroscopy results obtained under several different temperatures for the PP-EVA-organoclay samples* . . . 121
6.19 *Cole-Cole plots of the Dielectric Spectroscopy results obtained under several different temperatures for the PP-PS-organoclay samples* . . . 122

7.1 *Mass changes upon immersion of the PP/EVA9/X/Y composites in xylene* . . . 127
7.2 *TGA data: decomposition of the dried and immersed PP/EVA9/X/Y composites* 128
7.3 *Mass changes upon immersion and subsequent removal of xylene from PP/EVA9/0/Y composites* 129
7.4 *Mass changes upon immersion and subsequent removal of xylene from PE/EVA9/X/Y composites* 130
7.5 *FT-IR data examining organoclay incorporation and oxidation of the PP/EVA9/X/Y composites* 131
7.6 *FT-IR transmission mode data of dried, immersed and re-dried PP/EVA9/X/Y composites* 132
7.7 *FT-IR data of the PE/EVA9/X/Y composites* 133
7.8 *Dielectric spectroscopy data from the xylene immersion tests of the PE/EVA9/X/Y composites* 134
7.9 *Dielectric spectroscopy data from the xylene immersion tests of the PP/EVA9/X/Y composites* 135
7.10 *AC dielectric breakdown strength data for the dried and immersed samples of PP/EVA9/2.5* 140
7.11 *Normalised FT-IR of Composites Immersed in Water* 143
7.12 *Dielectric Spectroscopy results from Water Immersion Tests* 145

List of Tables

3.1 *DSC data: from the PE-EVA-organoclay composites* 50
3.2 *DSC data: the percent crystallinity for the PP-EVA-organoclay composites* . . 53

4.1 *Results from the Scherrer equation applied to PP-EVA-organoclay composites* . 69

6.1 *DC dielectric breakdown data from the single polymer-organoclay composites and the pristine polymers* 104
6.2 *AC dielectric breakdown strength data from the PE-EVA-organoclay composites* 110
6.3 *AC dielectric breakdown data from the PP-EVA-organoclay composites* 112

7.1 *Weibull statistics from the AC dielectric breakdown data studying the effect of the xylene on the PP/EVA9/X/Y composites* 139
7.2 *Weibull data from the DC dielectric breakdown data studying the effect of the xylene on the PE/EVA9/X/Y composites* 141

B.1 *DC conductivity data for the PE/EVA9/X/Q water immersion tests* 167

Symbols and Abberivations

σ	Conductivity
ϵ'	Real Relative Permittivity
ϵ''	Imaginary Relative Permittivity
α	Weibull Distribution Scale Parameter
β	Weibull Distribution Shape Parameter

AC alternating current

ATR attenuated total reflection

DSC differential scanning calorimetry

EVA Ethylene-vinyl acetate

FT-IR Fourier-transform infrared spectroscopy

HDPE high density PE

LDPE Low density PE

MMT montmorillonite

PE polyethylene

phr parts per hundred rubber

PP polypropylene

PS polystyrene

SEM scanning electron microscopy

TEM transmission electron microscopy

TGA thermal gravimetric analysis

VA vinyl acetate

XRD X-ray diffraction

Author's Declaration

I, Allison Shaw, declare that this thesis entitled 'LINKING THE THERMAL, MORPHOLOGICAL AND ELECTRICAL PROPERTIES OF THERMOPLASTIC POLYMER COMPOSITES CONTAINING AN ORGANOCLAY' and the work presented in it are my own and has been generated by me as the result of my own original research.

I confirm that:

1. This work was done wholly or mainly while in candidature for a research degree at this University;
2. Where any part of this thesis has previously been submitted for a degree or any other qualification at this University or any other institution, this has been clearly stated;
3. Where I have consulted the published work of others, this is always clearly attributed;
4. Where I have quoted from the work of others, the source is always given. With the exception of such quotations, this thesis is entirely my own work;
5. I have acknowledged all main sources of help;
6. Where the thesis is based on work done by myself jointly with others, I have made clear exactly what was done by others and what I have contributed myself;
7. Parts of this work have been published as:

   (a) Conference paper, entitled 'THE DIELECTRIC EFFECT OF XYLENE ON AN ORGANOCLAY-CONTAINING COMPOSITE', at the *2018 IEEE 2nd International Conference on Dielectrics*; Budapest, Hungary

   Paper DOI: 10.1109/ICD.2018.8470055; Data DOI: 10.5258/SOTON/D0518

   (b) Journal paper published in *IEEE Transactions on Dielectrics and Electrical Insulation* entitled 'THE DIELECTRIC EFFECT OF XYLENE ON AN ORGANOCLAY-CONTAINING COMPOSITE'

   Paper DOI: 10.1109/TDEI.2019.8726038; Data DOI: 10.5258/SOTON/D0537

(c) Journal paper published in the *Journal of Materials Science* entitled 'THE EFFECT OF ORGANOCLAY LOADING AND MATRIX MORPHOLOGY ON CHARGE TRANSPORT AND DIELECTRIC BREAKDOWN IN AN ETHYLENE-BASED POLYMER BLEND'

Paper DOI: 10.1007/s10853-019-03765-5; Data DOI:10.5258/SOTON/D0746

(d) Conference paper, entitled 'THE DIELECTRIC PROPERTIES OF PP-EVA-ORGANOCLAY COMPOSITES', at the *2019 Conference on Electrical Insulation and Dielectric Phenomena*; Richland WA, USA

Paper DOI: *pending*; Data DOI: 10.5258/SOTON/D0876

(e) Conference paper, entitled 'COMPARING THE INFLUENCE OF ORGANOCLAY ON THE MORPHOLOGY AND DIELECTRIC PROPERTIES OF THREE THERMOPLASTIC POLYMERS', at the *2019 Conference on Electrical Insulation and Dielectric Phenomena*; Richland WA, USA

Paper DOI: *pending*; Data DOI: 10.5258/SOTON/D0877

(f) Journal paper accepted, awaiting publication in *IET Special Issue: Interface Charging Phenomena for Dielectric Materials* entitled 'THE EFFECT OF ORGANOCLAY LOADING ON THE DIELECTRIC PROPERTIES AND CHARGE DYNAMICS OF A PP-RUBBER NANOCOMPOSITE'

Paper DOI: *pending*; Data DOI: 10.5258/SOTON/D1160

(g) Journal paper submitted to *IET Nanodielectrics* entitled 'ON THE INFLUENCE OF XYLENE ON THE DIELECTRIC RESPONSE OF AN ORGANOCLAY-CONTAINING NANOCOMPOSITE'

Paper DOI: *pending*; Data DOI:10.5258/SOTON/D0787

Signed:

Date:

Acknowledgements

I have many, many people to acknowledge for their help, support, and prayer during my time working towards the completion of this thesis. I could list them all, but that would serve little purpose because they already know who they are.

To all of you - Thank you.

Chapter 1

Introduction

1.1 Polymers

Polymers are long-chained molecules comprised of repeating units called monomers that are linked together to form chains of thousands of monomer units in length. Polymers can be found everywhere - some are synthetic, like many plastics and some are naturally occurring like viruses. Polymers have a range of properties and hence a number of applications.

Due to the size of polymer chains being thousands of monomers long, the crystal structure is markedly different to small molecules as the whole chain does not necessarily form one crystal. The result is that polymer chains solidify out from a nucleation point spherically, the resulting spherical structures are called spherulites. These consist of crystalline regions of neatly stacked chains called lamellae (50-500 Å thick with a folded width of 1 - 25 μm) and amorphous regions between the lamellae,[1] this has been represented by the schematic in Figure 1.1. Since the regular folding increases the ability of the bulk to scatter light, as the amount of crystallinity increases, the transmissive properties are decreased. Figure 1.2 highlights the crystalline and amorphous regions in a spherulite reproduced from a journal paper published by Upadhyay *et al.*.[2]

The most common, and arguably the simplest synthetic polymer, is polyethylene (PE). Near the end of the nineteenth century PE was discovered by accident by a German chemist named Pechmann. However, a commercial synthesis was not found until 1933 by Gibson and Fawcett in England. During the second world war efforts research into polyethylene increased due to the desirably low-loss properties at high frequencies, making applications in radar possible. The commercial production increased significantly when catalysts were developed in the 1950s. These catalysts facilitated the polymer synthesis under milder temperatures and pressures (making the processing cheaper and more facile) and made the product density tunable.[3]

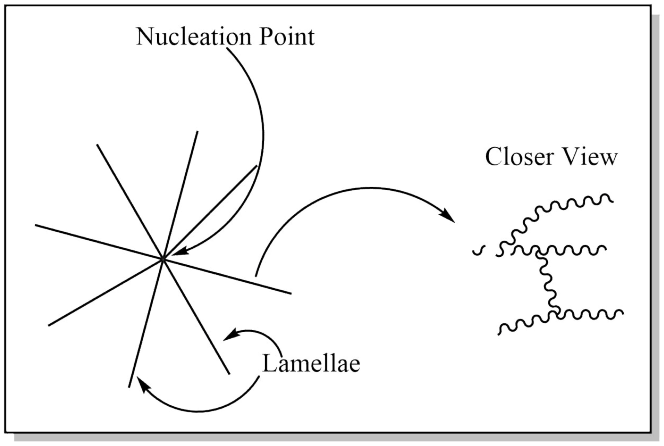

Figure 1.1: *A schematic diagram of a spherulite. The closer view of the crystalline lamella shows the polymer chain folding together and branching, forming an ordered structure.*

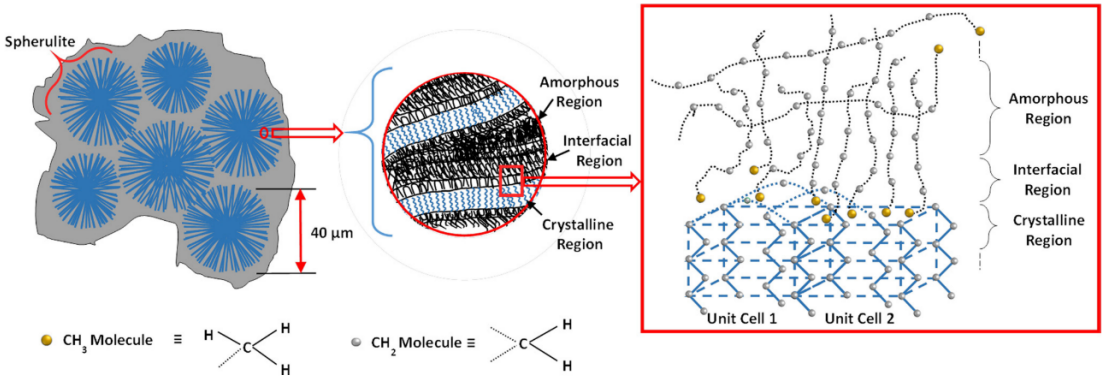

Figure 1.2: *A schematic diagram of a spherulite highlighting the amorphous and cyrstalline regions reproduced from a journal paper published by Upadhyay et al..*[2]

As a semi-crystalline, thermoplastic polymer, PE has applications in packaging, textiles, insulation and structural furnishings.[4,5,6] Compared to other polymers, it has good chemical resistance, low cost, low processing energy requirements and low permeability. However, compared to other polymers it has poor stress crack resistance, creep resistance and a low compatibility with other materials, all of which prevent PE from being used in many other applications.[7,8]

PE is comprised of ethylene monomers, which have a carbon-carbon double bond that breaks during the polymerisation process with the electrons from the broken bond forming bonds to neighbouring monomer units. PE gains the low density or high density classification depending on the branching of the polymer chains, which dictates how the polymer chains arrange together. Figure 1.3 shows the detailed chemical structure and the overview of the polymer chain. Low density PE (LDPE) has random branching and depicted in the figure is an example of such branching however this does not precisely represent the structure of the polymers used. The most stable crystal structure of PE is orthorhombic but the monoclinic phase can form when the sample

has been subjected to mechanical stress.[9]

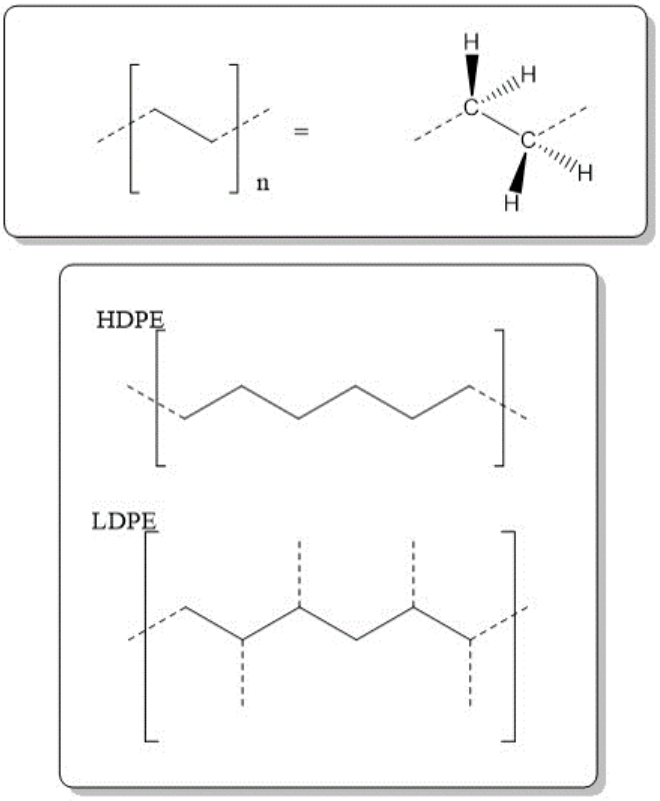

Figure 1.3: *The chemical structure of high density and low density polyethylene. The brackets show a unit that can be repeated n times to form the polymer chain.*

The structure of PE consists of crystalline lamellae growing out from nucleating sites to form spherulites. Between these crystalline lamellae are areas of amorphous polymer. Due to the lack of branches in high density PE (HDPE), the chains can pack together closely and so crystallise in an ordered structure giving HDPE a crystallinity of around 80 % while LDPE has a crystallinity around 32 %.[10] Residual water, solvents and other small molecules exist in amorphous regions surrounding spherulites since the growth of the spherulite excludes them.[4,11]

Polypropylene is a thermoplastic polymer and is one of the most widely used non-polar polymers, alongside PE.[12,13] Figure 1.4 shows the chemical structure of the monomer unit, which is larger than the PE monomer by one methyl group. Due to this methyl group, polypropylene can have a variety of structures depending on the orientation of the group relative to the carbon backbone and the surrounding monomer units. Isotactic polypropylene (PP) has been employed in this study. This polymer has all the methyl groups on the carbon backbone in the same orientation. Compared to having a mixture of orientations of the methyl group, this allows the regular arrangement of the polymer chains into crystalline structures.

Commercial production of polypropylene began in 1957 and has become popular due

to the versatility (mostly through structural alterations) and the many beneficial properties such as low density, facile processability, and corrosion resistance as well as being a cheap material. Due to this, polypropylene has many applications in common with PE. One of the main differences between the two is that PE has a lower melting point than PP. Additionally, polypropylene has poor toughness (impact resistance) and stiffness.[14,15]

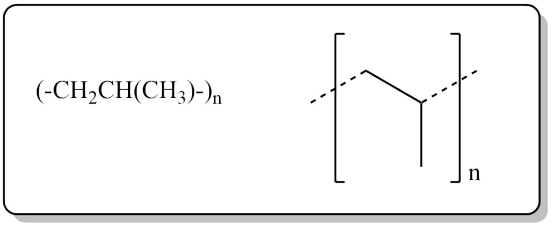

Figure 1.4: *The chemical formula and structure of polypropylene. The brackets show a monomer unit that can be repeated n times to form the polymer chain.*

Ethylene-vinyl acetate (EVA) is frequently employed in blends due to the low temperature flexibility, good impact strength and low permeability.[16] EVA was developed by several research groups but it was DuPont who claimed the patent in 1955 using a catalysed synthesis and subsequently produced a range of commercial products.[17] EVA is also a semi-crystalline polymer and is comprised of two types of monomer units (ethylene groups and vinyl acetate groups), therefore it is defined as a copolymer. The content ratio of the two types of monomers alters the properties of the copolymer, for example the crystallinity decreases with increasing vinyl acetate (VA) content.[16] The VA content of the EVA has influence on the glass transition temperature and causes a decrease in the crystalline spherulitic structure of ethylene.[18] The copolymer offers control of the properties via the variation of the VA content.

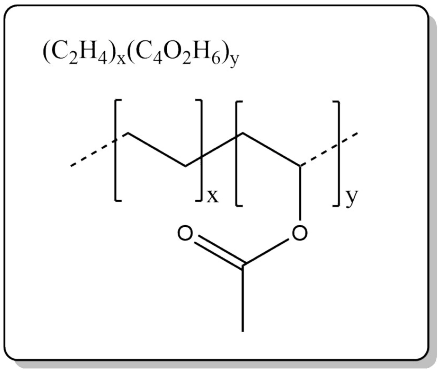

Figure 1.5: *The chemical formula and structure of EVA. The brackets show the ethylene (x) and vinyl acetate (y) units which are repeated to form the polymer chain.*

The two EVA copolymers used in this study were EVA9 and EVA20 (produced by Elvax), differing by variations of VA content. Referring to Figure 1.5, EVA9 contained enough y monomers that VA comprised 9 wt.% of the EVA while and EVA20 contained

20 wt.% VA. The presence of carbonyl groups (carbon double bonded to oxygen) in EVA makes the polymer polar, the extent depends on the relative VA content, which in turn affects the melting points: EVA with 9 wt.% of VA melts at 100 °C whereas EVA with 20 wt.% of VA melts at 78 °C.

Formed from styrene monomers, polystyrene (PS) is another thermoplastic polymer. PS has a number of possible chain structures, much like for PP, due to the orientation of the styrene monomer on the carbon backbone. PS was first developed in 1839, however it took until the 1930s for PS to become manufactured and utilised.[19] PS is inert, cost effective and long-lasting and is frequently employed in solid or foam forms in car parts, protective packaging and for sound dampening. The crystalline melting point is around 240 °C. However, due to the amorphous nature of the polymer, it undergoes the glass transition and begins to flow at around 100 °C. Figure 1.6 shows the chemical structure of the monomer unit comprising of PS.

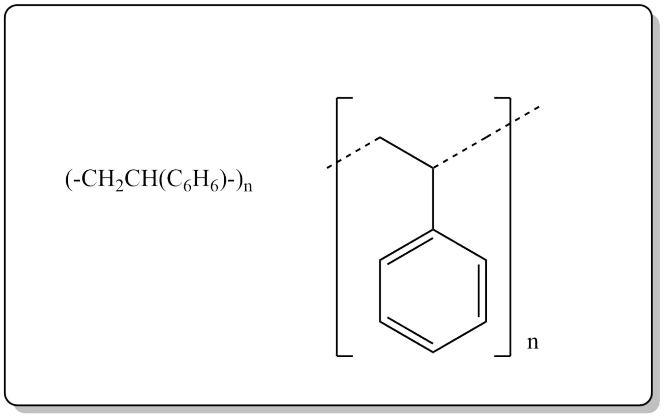

Figure 1.6: *The chemical formula and structure of PS.*

1.2 Polymer Blends

A mixture of polymers can be used to amalgamate their properties for a specific application. EVA is frequently employed in blends due to its flexibility at low temperatures, good impact strength and low permeability.[16] Both EVA and PE offer low electrical conductivity ($< 1x10^{-16}$ S/cm) and the PE-EVA blend is known for its high Youngs modulus (around 400 MPa), transparency, and good stress crack resistance (coping with 60% strain).[20,8] The blend is possible because of the compatibility of the non-polar ethylene monomers of EVA with PE.

PP-EVA blends are incompatible.[21] This is due to the methyl group in PP inhibiting polymer chain interactions with the linear EVA and hence the formation of sufficient intermolecular interactions. A search of the literature revealed that the PP-EVA blend has mostly been investigated in the context of being a base matrix for the formation of a nanocomposite. As such, little information about the properties of the blend exist and it might be deduced that this blend is not feasible in terms of the resulting properties without a nanofiller. The literature on PP-EVA based nanocomposites refers to the addition of the nanofiller being necessary to compatibilise the binary combination of the polymers.[22,23,15,24] Without the nanofiller, phase separation was reported and the resulting inhomogeneity is often undesirable, since it produces non-uniform material properties that tend to be weaker in terms of breakdown strength than the individual parts. For example, Hosier *et al.*[25] found that as VA content increased in a PE-EVA blend, the alternating current (AC) dielectric breakdown strength of the blend decreased.

Similarly to the PP-EVA blend, blending PP with PS, although also incompatible, has received a good deal of interest in the literature. Combining two of the most widely used plastics has led to researchers incorporating copolymers, nanofillers and modifiers to achieve a material that contains the advantages of both polymers.[26]

1.3 Organoclay

The filler chosen for nanocomposite studies varies depending on the desired outcome, for example boron nitride can increase the thermal conductivity of the material[27] while graphene oxide can increase resistance to gas permeability and mechanical strength.[28] However, a significant problem faced when incorporating a filler is the compatibility with the polymer matrix. This can be overcome by using an anisotropic filler like an organically-modified clay (or organoclay): the organic parts can increase the compatibility of the filler with the polymers, while the clay provides the inorganic filler that can alter the properties of the polymer blend.[29,30,31] Industrial applications of organoclays

include reinforcements to polymers, photo-physical devices, rheological agents and as an adsorbent of pollutants in soil and aquatic environments.[32]

The organoclay employed in this study was a montmorillonite (MMT) clay, a soft phyllosilicate with two tetrahedral sheets of silicates fused to an edge-shared octahedral sheet of silica. The stacking of the sheets gives a regular van der Waals gap between the layers (referred to as the interlayer or gallery spacing) where the counter ions to the silicates sit. The cationic counter ions (mostly sodium ions but occasionally aluminium ions) to the silicates had been exchanged by the commercial vendor for ammonium ions with coordinated organic chains of tallow and methylene groups (illustrated in Figure 1.7).

The organoclay is anisotropic since it has both the polar silicate parts of the clay and the non-polar parts of the co-ordinated organic chains. This is exploited with the PE-EVA-organoclay studied herein where the organoclay can interact with the VA and the ethylene in the blend respectively. This makes the EVA the compatibilising agent for the system since PE and the organoclay are not compatible without it.[33,34] However, in the PP-EVA-organoclay and PP-PS-organoclay systems it was seen that the organoclay is the compatibiliser since without it, the PP and EVA would phase separate, this finding has also been reported elsewhere for other PP-containing blends.[26]

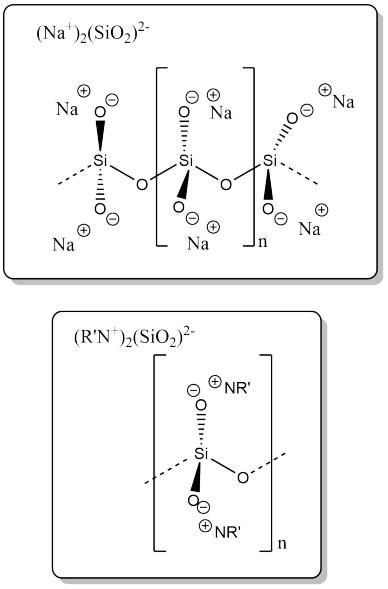

Figure 1.7: *The chemical formula and structure the organoclay. The brackets show a tetrahedral silicate unit that can be repeated n times to form the silicate structure. Sodium ions are shown to be the counter ions to the silicate structure. R' represents the four organic chains attached to the nitrogen atom making it a quaternary ammonium ion and hence capable of countering the negative charge from the oxygen atoms in the silicate structure.*

The organoclay has a nanoplatelet structure with the layers being about 1 nm thick and between 50 - 150 nm long. This high aspect ratio nature means that layers can be delaminated by intercalating polymer chains and hence become dispersed throughout

the polymer matrix.[35]

In some cases it has been found that the filler loading has a critical amount, after which the properties initially enhanced by the addition of organoclay decrease again. For example, Jaeverberg *et al.*[36] and Hui *et al.*[37] both found this to the be case for breakdown strength for alumina and silica-filled polyethylene-based nanocomposites, respectively.

Gherbaz *et al.*[38] compared two organoclays, one the same as used herein and another, chemically similar organoclay. They found that the chemical nature of the organoclay can change the properties of the nanocomposite: different AC dielectric breakdown strengths, shifting the EVA melting peak in differential scanning calorimetry (DSC) and changing the influence of solution blending time. Therefore comparisons of findings in the present work to published work on similar organoclays should be made with caution.

Zhong *et al.*[39] studied the X-ray diffraction (XRD) peaks of EVA-organoclay and PE-organoclay systems and found that there was no significant change in intercalation extent in the loading range 2-5 wt.%. A different report found that the introduction of between 1-5 wt.% of organoclay into the polymer matrix improved the mechanical strength as well as enhanced the barrier properties leading to flame retardancy and an increased thermal stability.[40] The same study reports that while there are several types of layered silicates (including mica, hectorite and saponite), MMT is of great commercial interest. This is due largely to the structure having loosely held ions, which allows for facile ion exchange for organic modification purposes and its natural abundance, keeping costs low.[32]

The thermal degradation resistance achieved in the nanocomposite has been directly related to the degree of exfoliation of the organoclay in the polymer matrix.[40] In turn, the degree of exfoliation was found to be dependant on the concentration of MMT because it is necessary to have a homogeneous exfoliation throughout the sample. The mechanism for the thermal stability improvement is reported to be via the accelerated formation of char acting as a barrier to oxygen permeation and the loss of the degradation products. The organoclay itself also forms a physical barrier which acts in the same way as the char to delay degradation. The published evidence presented to support these conclusions were isothermal thermal gravimetric analysis (TGA) tests.[40]

Kumar *et al.*[41] found that for their thermoplastic-based nanocomposites, the samples containing an MMT-based organoclay intercalated into the polymer matrix whereas the unmodified MMT clay showed no signs of intercalation. In view of their polymer matrix being more polar than PE, one would expect there would be even less intercalation of the unmodified MMT into PE. This illustrates the need for the organic modifications to the clay.

A general search of the literature shows that the addition of an organoclay to polymers

such as poly(methyl methacrylate) and PS and blends such as PP-PS, have shown an increase in thermal degradation temperature. In the latter, the miscibility of the blend was also increased by the presence of the organoclay.[42,43,26]

Functionalising the surface of the clay with organics reduces nanofiller agglomeration and therefore is more likely to achieve a homogeneous dispersion in a polymer matrix, which is favourable for achieving the properties unique to nanocomposites and not microcomposites. This can be explained by the thermodynamic interactions between the similar hydrophobic properties of the organic modifications to the clay and the hydrophobic polymer matrix. It has been reported that the nature of the organic modification impacts the mechanical strength, thermal properties, water uptake ability and dielectric response of the sample.[44,45,46] However, this report will not consider this effect as it will focus on only one type of organic modification.

1.4 Achieving Compatibilisation and Dispersion

Making polymers compatible with clay so that in a composite the clay is well dispersed is an essential part of the composite development. When the intercalation reaches a point whereby the sheets are completely separated and dispersed into the continuous polymer matrix, the clay is said to be exfoliated.[47] If the clay is dispersed well enough to have at least one dimension less than 100 nm, the composite is referred to as a nanocomposite. Depending on the extent of polymer chain intercalation, the filler transitions from the micro- to the nano-scale, which can fundamentally change the properties of the system due to the increased interfacial area and via minimising the phase separation of the polymers.[48,26]

The first nanocomposites employing clays were formed with polycaprolactam (Nylon-6), a polymer that contains a polar amide group that enables the intercalation of the polar clay.[43,49] While dispersion of the polar clay into polar polymers such as polyamides is relatively straightforward, the incorporation of these clays into non-polar host matrices is problematic even with an organoclay. One solution, which has seen much work, involves altering the chemical properties of the polymer matrix through grafting polar groups, such as maleic anhydride or glycidyl methacrylate, to non-polar polymers to form polar regions that act as a compatibiliser between the polymer and the clay.[50,51,47,49] The drawback of using the grafting technique is that it requires a radical reaction to incorporate the polar groups leading to a range of products, a decrease in the melting temperature of the polymer and can produce some cross-linking of polymer chains.[52] These are undesirable as the matrix composition and crystallising nature will change and maybe difficult to keep consistent between experiments.

An alternative strategy, employs a second polymer that is compatible with both the non-polar polymer and the organoclay as a means of creating a homogeneous blend.[24,53]

EVA was employed as a compatibilising polymer in the PE-EVA-organoclay composite. EVA does not require modification or a compatibiliser to intercalate into the organoclay[39] or into PE (though the compatibility with PE decreases at higher VA contents).[54] Using EVA as a compatibiliser between the non-polar polymers and the organoclay has a secondary benefit of increasing the insulation lifetime of the polymer matrix.[55]

In a similar way to EVA compatibilising the PE and organoclay interaction, it has been reported that organoclay can act as a compatibilising agents to polymer blends that would otherwise phase separate.[26,56] This was observed herein for the PP-EVA-Organoclay and the PP-PS-Organoclay composites.

Another route to achieving dispersion is using organoclay supplied in masterbatch form (where the organoclay is already dispersed into polymer pellets by the manufacturer). Compared with using the organoclay in a powdered form (as herein), a disadvantage of the masterbatch method is that other polymers are introduced into the blend with the organoclay so the polymer composition is altered. However, an advantage is that the organoclay is pre-dispersed into a polymer, which would make it easier to disperse into the polymer blend and less likely to aggregate.

The organoclay employed in this study was also used, in masterbatch form, by Gopakumar *et al*.[6] while a similar organoclay was used by Vaughan *et al*.[57] Since working with organoclay from a masterbatch is popular and the results should largely be transferable to samples prepared from organoclay powder, this literature review will include work produced from both powder and masterbatch organoclay.

1.4.1 Thermodynamic Considerations

In brief, thermodynamics is concerned with the energy of the system, with enthalpy referring to the total equivalent heat energy of the system, and entropy referring to the disorder in the system representing the unavailability of the thermal energy for conversion into some form of work.

Thermodynamically considering a thermoplastic-clay nanocomposite, the driving force of polymer-chain intercalation is the total entropy change while the enthalpy change is considered negligible. (For polymer blends and solutions, it is the other way around.) The entropy change is the difference between the entropy gained in the system due to expansion of the clay galleries and the entropy lost due to polymer chain confinement in the clay.[58] There are three types of polymer-layered silicate (modified or un-modified clay) that are thermodynamically feasible.[59] These are: intercalated, flocculated and exfoliated nanocomposites. The first occurring when the polymer matrix inserts between the clay layers in a regular pattern, the second is similar just with an additional hydroxylated edge-edge interaction between the clay layers while exfoliated nanocomposites

occurs when the clay layers are separated by a continuous polymer matrix most common at lower filler loadings. It is worth noting that thermodynamics only predicts the structure of the nanocomposite at equilibrium and it has been reported that kinetic products have been produced when composites are slowly dried from a colloidal suspension.[59]

A compatibiliser works, in terms of thermodynamics, in three ways by:

- interacting with both of the otherwise immiscible components,
- the adsorption resulting in free energy gains and
- altering tensions between the phases through existing in the interfaces.

Clay localisation, as a means of assessing the compatibilisation capabilities, has been calculated by many authors via a thermodynamical approach using the wetting coefficients determined by Young's equation.[60] This effect is greater with compatibilisers with greater surface areas. By way of example, MMT (a common base for organoclays) can act as an efficient compatibiliser with a specific surface area of around 750 m^2/g.[61] For context, hexagonal boron nitride, an alternative nanofiller, has a specific surface area of 20 m^2/g[62] and silver microflakes have a specific surface area of 1.16 m^2/g.[63]

Thermodynamically immiscible blends leads to poor mechanical, thermal properties and affects the dielectric properties. Examples of such blends include PP-PS, EVA-PS, and PP-EVA.[23,61,64,65] This thesis will address some of these blends with the employment of compatibilisers.

1.5 The Production of Polymer-Organoclay Composites

Published synthetic techniques for the synthesis of nanocomposites are mostly via the melt mixing route using a mechanical blender or via solution blending involving dissolution of polymers into a solvent.

Solution blending is not environmentally friendly in that it requires use of a solvent, often xylene. Additionally, solution blending has the disadvantage that sample preparation is significantly longer than melt mixing on account of having to remove the solvent from the material. Further, solution blending can be restrictive because it is required that all the polymers for the blend are soluble in the same solvent. Herein, for the case of the PE-EVA, PP-EVA and PP-PS blends, all the polymers are soluble in xylene so this does not place a limitation on the method.

A benefit of solution blending over melt mixing is that the former fragments the clay aggregates, which later facilitates the intercalation with the polymer upon the application of heat to achieve dispersion of the filler.[49] Further, solution blending allows the

pre-treatment of the organoclay by means of sonication in the solvent, which has been shown to exfoliate the clay by providing the energy to separate the clay layers.[66]

Another advantage of solution blending is that the solvent can mediate the mixing of the materials via lowering the viscosity of the mixture, such that the extent of dispersion is influenced by factors such as the filler loading level, temperature and length of solution reflux time.[67,30] Whereas, for the melt mixing method, the order of material addition and the number of times the material was passed through the extruder is an important consideration.[47,15] Furthermore, although heat is required for the proper mixing of clay and polymer, the organic ion in the organoclay decomposes at the high temperatures that the melt mixing process requires[30] making solution blending a safer option.

A further advantage of the solution blending technique is that the equipment set up is trivial to dismantle for cleaning and it can be conducted entirely in a fume cupboard, unlike the melt mixing method that involves equipment that would be harder to decontaminate and the clay powder could be more easily released into the laboratory risking respiratory problems and eye irritation.

A literature search revealed that Carastan *et al.*[68] used the same organoclay as used herein for a PS-organoclay composite and showed that solution or master batch routes were better than melt mixing, the latter resulting in poor dispersion of the organoclay.

In light of these advantages and disadvantages, solution blending was employed for the purposes of this thesis.

1.6 Aim of this Thesis

This thesis will consider three polymer composites: PE with EVA and an organoclay, PP with EVA and an organoclay, and PP with PS and an organoclay together with single polymer-organoclay composites made with each of the aforementioned polymers and organoclay as a baseline. The compatibility, thermal, morphological and electrical properties of the composites will be investigated. The hypothesis being that these properties are interdependent. The aim is that the work presented herein will identify principles that will allow the properties in other composites to be predictable and thus make future material development more efficient.

Chapter 3 will discuss the thermal properties of the composites by presenting the TGA and DSC results of the composites. The aim of this avenue of analytical research was to understand firstly the effect of the organoclay on the thermal degradation temperature of the composite as well as establish the influence of the organoclay on the melting and crystallisation temperatures and enthalpies of the polymers. These are important to

the overarching aim of this thesis since these data will give an insight into both the dispersion and the morphological impact (nucleating ability and the extent of spherulite growth) of the organoclay respectively, which will aid the understanding of the composites and interpretation of the dielectric results.

Chapter 4 will present and discuss results from the techniques used to analyse the organoclay within the composite, namely FT-IR and XRD. The aim of using FT-IR analysis was to confirm that organoclay had been incorporated into the composite (lending support to the aforementioned TGA data). The XRD analysis was used primarily to assess the affinity of the organoclay to the polymer matrix (and therefore the dispersion of the organoclay). However, both techniques had additional benefits. Firstly, FT-IR was used to assess whether the sample had been chemically changed (for example, oxidised) during processing, which would have been undesirable since this would itself impact the dielectric properties.[69] Secondly, from XRD analysis, the influence the organoclay had on the crystal structure of the polymers was assessed. This was significant as different crystal structures confer different macro-scale properties to the material such as density, which would in turn impact the dielectric properties.[48,70]

Chapter 5 will present the scanning electron microscopy (SEM) micrographs of the composites. These results will be used to discuss the influence of the thermal treatment and organoclay on the sample morphology and to assess the dispersion of the organoclay. Although these aims are equivalent to those met by employing TGA, DSC, FT-IR and XRD, the more approaches one has to assess a certain aspect of a material, the conclusions drawn can be made more confidently and related more securely to the dielectric results.

Chapter 6 will present the results and discussions of the dielectric tests on the composites. The dielectric testing includes DC conductivity, both AC and DC dielectric breakdown and dielectric spectroscopy measurements. The results were interrelated between techniques and understood in terms of the morphology and dispersion established in the previous chapters. The conductivity and breakdown data are closely related to the filler dispersion whilst the dielectric spectroscopy data is key to understanding the frequency dependence of the sample conductivity.

Chapter 7 considers the effects of immersing the composites in xylene and in water. The aim of this chapter is to present an understanding of the probable outcomes from a potential inadequacy in the sample processing procedure. The effects were assessed using TGA and FT-IR (to measure the solvent uptake), XRD (to check for swelling of the organoclay layers), and, in order to assess changes to the dielectric properties: dielectric spectroscopy and dielectric breakdown strength.

Chapter 2 details the experimental methods and analysis techniques. Whilst the remaining chapters will have the conclusions, the future work proposed following this PhD, and appendices containing an introduction to the various analytical techniques

(Chapter A) and any data relevant that would otherwise disrupt the flow of the text (Chapter B).

1.6.1 Statement of Novelty

A key area of research in this thesis has surrounded compatibilising otherwise immiscible polymer blends. In the PE-EVA-organoclay composites, EVA acted as a compatibilising agent whilst organoclay compatibilised PP-EVA and PP-PS blends. Understanding the limits of compatibility, the resulting morphologies and linking this to the dielectric properties of the composites, has furthered scientific understanding. The novelty of this work has resulted in conference presentations, conference papers and a journal publication:

1. Conference poster, entitled 'THE THERMAL AND ELECTRICAL PROPERTIES OF PE-CLAY NANOCOMPOSITES COMPATIBILISED BY EVA', at the *Euromat 2017 International Conference*; Thessaloniki, Greece

   This work has been included in Chapters 3.3, 6.2.1 and 6.3.2.

2. Conference oral presentation, entitled 'MORPHOLOGICAL AND ELECTRICAL INVESTIGATIONS INTO POLYMER-CLAY COMPOSITES', at the *2018 UHVnet Colloquium*, Winchester, UK for which I was awarded 'Best Oral Presentation'.

   This work has been included in Chapters 4.6, 5.4, 6.2.2 and 6.3.3.

3. Journal paper published in the *Journal of Materials Science* entitled 'THE EFFECT OF ORGANOCLAY LOADING AND MATRIX MORPHOLOGY ON CHARGE TRANSPORT AND DIELECTRIC BREAKDOWN IN AN ETHYLENE-BASED POLYMER BLEND'

   Paper DOI: 10.1007/s10853-019-03765-5; Data DOI: 10.5258/SOTON/D0746

   This work has been included in Chapters 3.3, 4.4, 5.3, 6.2.1 and 6.3.2.

4. Conference paper, entitled 'THE DIELECTRIC PROPERTIES OF PP-EVA-ORGANOCLAY COMPOSITES', at the *2019 Conference on Electrical Insulation and Dielectric Phenomena*; Richland WA, USA

   Paper DOI: *pending*; Data DOI: 10.5258/SOTON/D0876

   This work was presented in a 1 minute poster preview and during a poster session at the conference.

   This work has been included in Chapters 5.4, 4.6, 6.2.2, 6.3.3 and 6.4.

5. Conference paper, entitled 'COMPARING THE INFLUENCE OF ORGANOCLAY ON THE MORPHOLOGY AND DIELECTRIC PROPERTIES OF THREE THERMOPLASTIC POLYMERS', at the *2019 Conference on Electrical Insulation and Dielectric Phenomena*; Richland WA, USA

Paper DOI: *pending*; Data DOI: 10.5258/SOTON/D0877

This work was presented as a poster presentation at the conference.

This work has been included in Chapters 5.2, 4.3, 6.3.1 and 6.4.

6. Journal paper accepted, awaiting publication in *IET Special Issue: Interface Charging Phenomena for Dielectric Materials* entitled 'THE EFFECT OF ORGANOCLAY LOADING ON THE DIELECTRIC PROPERTIES AND CHARGE DYNAMICS OF A PP-RUBBER NANOCOMPOSITE'

   Paper DOI: *pending*; Data DOI: 10.5258/SOTON/D1160

   This work has been included in Chapters 5.4, 4.6, 6.2.2, 6.3.3 and 6.4.

Understanding the dielectric effects of solvent remaining in the composites following the sample production procedure is of significance for several reasons including correctly attributing phenomena to the composite or solvent, refining procedures and appreciating sample operating condition limits. As such, PP-EVA-organoclay samples were tested, producing novel findings. Subsequently, PE-EVA-organoclay samples were tested to explore the generality of the results and create a firmer understanding of the phenomena occurring. This work has resulted in publications:

1. Conference paper, entitled 'THE DIELECTRIC EFFECT OF XYLENE ON AN ORGANOCLAY-CONTAINING COMPOSITE' at the *2018 IEEE 2nd International Conference on Dielectrics*; Budapest, Hungary

   Paper DOI: 10.1109/ICD.2018.8470055; Data DOI: 10.5258/SOTON/D0518

   The paper was presented as a keynote, oral presentation and awarded one of the three 'Best Presentation' prizes.

   This work has been included in Chapters 3.4.1 and 7.

2. Journal paper published in *IEEE Transactions on Dielectrics and Electrical Insulation* entitled 'THE DIELECTRIC EFFECT OF XYLENE ON AN ORGANOCLAY-CONTAINING COMPOSITE'

   Paper DOI: 10.1109/TDEI.2019.8726038; Data DOI: 10.5258/SOTON/D0537

   This work has been included in Chapters 3.4.1 and 7.

3. Journal paper submitted to *IET Nanodielectrics* entitled 'ON THE INFLUENCE OF XYLENE ON THE DIELECTRIC RESPONSE OF AN ORGANOCLAY-CONTAINING NANOCOMPOSITE'

   Paper DOI: *pending*; Data DOI: 10.5258/SOTON/D0787

   This work has been included in Chapters 4.5 and 7.

In order to best convey the findings of this thesis as a whole, the work from each of these publications has been presented in chapters that are specific to each analytical technique while Chapter 8 contains the discussion and conclusions that link the individual chapters.

1.7 Introducing the Composites in this Thesis

This chapter will contain a general overview of the literature before the following chapters will contain literature reviews specifically tailored to each of the composites investigated in this thesis. The aim is to give some background information and reasoning as to why these composites were selected before the results chapters present the experimental data and make comparisons and contrasts between the composites.

While the bulk of the literature concerning the nanocomposite materials has focused on particulate systems, such as silica, alumina, titanium dioxide, and gold, in other areas, plate-like nanofillers, such as clays, nickel oxide, boron nitride, and graphite, have received great attention. For example, graphene oxide, an exfoliated form of graphite, can increase the conductivity of nanocomposites[51] while post-curing reduces the graphene oxide causing a significant increase in permittivity.[71] Another material that has certain structural similarities with graphene is hexagonal boron nitride. This filler has been investigated in both thermoplastic and thermosetting polymers with the resulting properties being closely linked to the interaction of the surface of the filler with the polymer.[62,72] Finally, the current interest in nanocomposites is frequently attributed to pioneering work on systems based upon the reinforcement properties that organoclay confers to polymer blends (for example Toyota employing the material for car parts[73]). Such materials form the focus of this thesis.

Organoclay is anisotropic since it has both the polar silicate parts of the clay and the non-polar organic chains, which can interact with the polar and the non-polar parts of the polymer blend respectively, creating a composite. A holistic view of the morphology can be revealed under SEM since the compatibility of the blend and the dispersion of the filler can be seen. While XRD shows the extent of polymer intercalation increasing the distances between the clay layers, which can be used to assess the dispersion of the filler.[74,6,64] It is widely accepted that the organoclay loading has an optimum, around 5 wt.%, whereby the material properties (such as dielectric breakdown strength) are enhanced most significantly.[55,75,76]

The crystallography, or the physical arrangement of a polymer on the atomic scale, is changed by the addition of organoclay, which, on a microscale alters the overall structure of the material via influencing spherulite growth. This in turns alters properties of the material including thermal,[74,29] mechanical,[74,29] gas permeability[35,77] and electrical.[78,79] The organoclay brings about this change in two ways: through having a

nucleating effect and through preventing polymer chain movement whilst in the melt phase.[80] This can be assessed using an SEM and investigating materials from a range of thermal treatments from the melt phase.

To image samples under SEM, an etching technique capable of revealing the dispersed MMT and the polymer matrix is frequently used,[78,81,82,83,84] therefore a similar technique was employed on each of the composites in this report for the same reasons.

Many published papers on blends similar to those studied herein investigate the gas barrier effects of the composites using TGA. However, in this thesis, TGA will be used to assess the organoclay loading achieved during the synthesis and to assess the dispersion of the organoclay since the pyrolysis of composites under nitrogen or air atmospheres using TGA have the same degradation temperature if the dispersion is sufficient to form a nanocomposite.[85] Although this seems a somewhat arbitrary line to draw, it highlights the effects of well distributed organoclay: it prevents oxygen penetration so the sample decomposes as if in a nitrogen atmosphere.

The performance of composites under dielectric tests can be affected by the organoclay loading - through the dispersion, availability of charge carriers; the boundary conditions, the extent of interfacial sites acting as charge traps and the nucleation and restriction of polymer chain movement during crystallisation.[86,87,88,79,89] For example, the organoclay increases the DC conductivity of the material since it gives rise to charge carriers - with more carriers generated at higher temperatures due to thermal energy.[87,90] The organoclay has been reported to increase the AC breakdown strength when well-dispersed[55,78,80] and decrease it if less well dispersed.[91,92,93,94]

1.7.1 PE-EVA-Organoclay

When PE is required to have an improved mechanical, thermal or electrical performance, composites of PE can be employed. It is widely accepted that the enhanced properties in composites are due to the increased interfacial area per unit volume between polymer and a well-dispersed filler, herein an organoclay.[95,96,6] However, as has been found by many other studies, due to the incompatibility of the non-polar PE and the relatively polar organoclay, a compatibiliser is required to form a homogeneous mixture and prevent phase separation.[6,35] Reviewing previous publications, EVA does not require modification or the use of a compatibiliser to mix with PE or intercalate into, and promote dispersion of, the organoclay used herein.[54,39,97,55]

Vaughan *et al.* have previously worked on the PE-EVA blend finding that the breakdown strength was largely independent of composition,[98] whilst in another paper the same group looked at the PE-organoclay blend finding that the organoclay had no impact on the breakdown strength.[57] Work presented in this thesis on the PE-EVA-organoclay composites seeks to bridge the gap between these two papers by address-

ing the dispersion difficulties by using EVA as a compatibiliser between the PE and the organoclay and in doing so forming a matrix that has properties that are a combination of the two polymers.

Zhong *et al.*[39] investigated the speed of intercalation of an organoclay into both EVA and PE polymers. Firstly, they report that the PE had to be maleated in order to be compatible with the organoclay whereas the EVA did not require treatment to induce intercalation with the organoclay due to the flexibility and polarity of the co-polymer chain. They found that the intercalation of EVA into the organoclay was rapid due to the polarity and flexibility of the chain, but that this was also the result of the temperature the blend was mixed at being considerably higher than the melting point of EVA.

Green *et al.*[78] investigated PE blends with a masterbatch containing the same organoclay as employed in this study. It is worth noting that the masterbatch contains organoclay loadings of around 40 wt.% within linear LDPE and the addition of this polymer could be influencing the overall properties of the blend along with the organoclay. Green found that the morphology of the blends showed little evidence of the organoclay affecting the nucleation or crystal growth implying that the two components are not interacting. They note that this is in contrast to their previous findings[57] on a similar system with a different masterbatch organoclay where the platelets were shown to reduce the mobility of the polymer chains and therefore lead to less ordered structures forming.

Good dispersion of MMT has been shown to provide nucleating points to PE but subsequently decrease crystallisation due to the organoclay physically impeding crystal growth,[57] which itself will influence the conductivity of the material[2] and, furthermore, large aggregates have been shown to have adverse effects on breakdown strength performances.[57] This trend was also seen when Roy *et al.*[79] compared micron-sized and nano-sized silica nanoparticles. Additionally, Vaughan *et al.*[57] found that the thermal history (the speed at which it was cooled from the melt phase) of a PE-blend has no influence on breakdown behaviour if the organoclay is present. However, when the organoclay was absent, slow cooling yielded higher breakdown strengths than quenched samples, clearly illustrating that the morphology of the blend is important in the electrical properties of the samples.

Although no effect on morphology was seen, the PE-organoclay composites investigated by Green *et al.*[78] showed an increased AC dielectric breakdown strength with organoclay content. However, the improvement of electrical breakdown strength was not seen in their previous study on a different organoclay.[57] They attribute the differences to either the nature of the organic chains on the clay or the processing conditions used in the production of the masterbatch, both of which may lead to an orientated crystal growth.

PE is a semicrystalline polymer so charge trapping sites exist at the amorphous-crystalline interface. The addition of clay to this structure introduces polymer-clay interfaces and therefore new charge trapping sites. Overall these interfaces affect the current flow through the system depending on their distribution.[86] When dispersion is poor, the sample is more conductive.[99]

In this thesis, copolymer EVA was employed as a compatibiliser to a system involving PE and an organoclay. Keeping the PE:EVA ratio constant and adding varying amounts of organoclay and changing the thermal treatments, the interplay between the morphology and the dielectric properties of the blends was explored.

1.7.2 PP-EVA-Organoclay

The thermoplastic polymer PP has been studied extensively with various nano-fillers to adapt its properties.[100,101,27] In order to effectively disperse the filler the compatibility issue of the filler being hydrophilic and the PP being hydrophobic needs to be addressed. A solution has often been found in grafting maleic anhydride to the polymer or modifying the nano-filler.[100,101,102,103]

Zilg *et al.*[104] reported on PP-organoclay and EVA-organoclay nanocomposites. Firstly, they noted that it was necessary to graft maleic anhydride to the PP to promote dispersion of the organoclay. Although using a different organoclay to that employed in this thesis, the loadings used herein are approximately the same so their findings were considered relevant. They found that, for both their nanocomposites, the thermal stability was improved by the matrix stabilisation caused by the organoclay. Both Goodarzi *et al.*[23] and Martins *et al.*[15] also used maleic anhydride to disperse the organoclay in the PP-based blend containing EVA.

Another method to achieve dispersion in a PP-EVA blend was described by Ma *et al.*[105] who employed 'intercalative polymerisation' (where the polymerisation is initiated from the filler), to form a nanocomposite - shown using XRD. Another published report showed that the PP-organoclay nanocomposite was achievable if the organoclay was first dispersed in EVA to form a masterbatch.[24]

An alternative compatibilising method for immiscible polymers is where the filler acts as a compatibiliser between the two polymers via two emulsifying mechanisms. Firstly, the filler increases the interfacial tensions, preventing coalescence of the polymer.[61] While secondly, the organoclay decreases the crystallite size.[106] Goodarzi *et al.*[23] showed that in a PP-EVA blend, although the organoclay reduced the domain size of the polymer, it can be reduced further when the PP is maleated (i.e. when the emulsifier effect is further enhanced). Goodarzi *et al.*[23] also showed that the organoclay had a higher affinity to the EVA than the PP which, drawing parallels with the PE-EVA system, is in line with expectations.

Shafiee *et al.*[24] studied a nanocomposite of PP-EVA and an organoclay and reported that the crystallinity and melting point, determined by DSC, was decreased by the organoclay until a loading of 5 wt.% before the extent of the changes decreased. Furthermore, as has been seen for other polymer-organoclay composites, organoclay increased the thermal degradation temperature, measured by TGA, of the PP-composite.[105]

Compared to PE-organoclay nanocomposites, the PP-based systems have relatively little work investigating their electrical properties. However, linking the morphology and the electrical properties could be significant since PP-blends are highly sensitive to the cooling procedure from the melt phase and PP is known to form large spherulites that reduce electrical strength and increase rigidity.[84] To mention the highlights on the electrical properties of the PP-based systems: Bulinski *et al.*[107] reported on a PP-organoclay composite and found that the addition of a mica-based organoclay increased both the AC dielectric breakdown strength, conductivity and the dielectric loss factor. Zilg *et al.*[104] reported that the organoclay changes the charge trap distribution and acts as a mobile ion scavenger in a PP-based system. Further, they report that the DC dielectric breakdown tests showed that the filler increased the breakdown strength for the PP-based nanocomposites whilst having the opposite affect on the EVA-based nanocomposites. Montanari *et al.*[50] investigated the same material systems and agreed with these findings - attributing the results to the organoclay altering the space charge accumulation properties and the mechanical strength of the material.

Herein it is shown that an organoclay can be used to compatibilise the blending of PP with the copolymer EVA. The investigation will take the current published knowledge on this sample system forward by investigating the influence that the morphology has on the electrical properties.

1.7.3 PP-PS-Organoclay

Several different routes to creating a PS-organoclay nanocomposite have been published including in-situ polymerisation of the styrene monomers, using copolymers containing styrene as a compatibiliser, solution blending with sonication and melt blending.[108,66] Although in-situ methods have most successfully yielded exfoliated nanocomposites, the use of compatibilisers has increased the successes of using melt and solution blending methods.[30] However, another consideration needs to be that organoclay exfoliation is particularly sensitive to the tacticity (the stereochemistry of the monomers in the polymer chain) of PS and the type of organic modifier used.[109]

PS and PP polymers are immiscible without a compatibiliser. In order to compatibilise the blend, several papers have employed fillers in the form of an organoclay,[110,111,112,26] or silica nanoparticles[56] whilst others have used copolymers and grafting techniques[113,114,115] or, indeed, a mixture of these.[61,116]

Organoclay was first employed as a compatibiliser for the PP-PS blend by Wang *et al.*[26] in 2003. They used an MMT organoclay for a PP-PS blend in a 70:30 by weight blend with a range of organoclay loadings up to 30 wt.%. Wang *et al.*[26] presented XRD, peel strength and SEM micrographs. At time of writing, this seminal paper has been cited by 342 papers, many of which explore the use of an organoclay as a compatibiliser for this polymer blend.

Salehiyan *et al.*[60] concluded that, for the same organoclay as used herein, an organoclay loading of 3 wt.% was required to stabilise a 80:20 PP-PS blend. Morgan *et al.*[66] described the optimum loading for maximum exfoliation succinctly: a high dilution of the organoclay is necessary to prevent re-aggregation; concluding that the optimal loading for MMT-organoclay in PS is around 2-3 wt.%. Krishna *et al.*[67] used a xylene-based solution blending method to create PS-organoclay nanocomposites with several filler loadings between 3 and 20 wt.%. They concluded that exfoliation was achieved in the composites of lower filler contents and, the longest reflux times during the composite synthesis.

Morgan *et al.*[66] also used solution blending and found that the sonication energy used on the clay in the solvent at the start of the synthesis had an effect on the dispersion achieved. Employing chlorobenzene as the solvent, they found that the effectiveness of solvent blending in exfoliating the clay depends on the clay type - MMT performing better than fluorinated synthetic mica despite both being modified with the same organic ammonium ions as employed in the organoclay in this thesis. They attribute this difference to the layers in the two silicates having different chemistry, aspect ratios and cation exchange capacity, which highlights the need for caution when comparing different composites in the literature.

Whether the organoclay in the composite exists in the PS or PP polymer phases, the interphase or indeed a mixture of these is frequently discussed in the literature. In the original paper on this composite system, Wang *et al.*[26] suggest that the organoclay exists in both the PP and PS, using XRD data. They suggest that due to confinement, the polymers are forced to mix and as such, a more homogeneous sample is achieved, seen through a decrease in the phase size of PS. Salehiyan *et al.*[60] reported that when hydrophilic, the organoclay existed in the PS phase but when hydrophobic, the organoclay encapsulated the PS phase thereby occupying the interphase region. Istrate *et al.*,[64] Wu *et al.*[116] and Sinha Ray *et al.*[61] all used the same, largely hydrophobic, organoclay as employed herein but disagreed on the location of the organoclay. The latter two using transmission electron microscopy (TEM) micrographs to conclude the organoclay existed in the PP-PS interface whilst the former concluded the organoclay existed in the PS phase using XRD and TEM. However Sinha Ray *et al.* conceded that when the PP had been grafted with maleic anhydride, the organoclay existed in both phases and the interface, which corroborates with Tiwari *et al.*[117] Perhaps an explanation to this apparent discrepancy lies in whether the thermodynamic or kinetic product was

achieved: with evidence that after 1 minute of mixing the organoclay existed in the PS phase, however after longer mixing times, the clay had migrated to the interfaces. In conclusion, the chemical affinity between a polymer phase and the organoclay causes the filler to migrate to achieve the most stable configuration.[118]

As seen elsewhere in other polymer matrices, the interlayer distance of the organoclay was increased by PS.[67] Depending on the nature of the organic modification on the clay and the filler loading, the interlayer spacing was increased above 4 nm by PS.[67,108,43] Abbasi *et al.*[119] and Istrate *et al.*[64] present XRD data wherein the interlayer distance of the clay, compared to the pristine clay, was increased by PS more than PP. Further, when the two polymers coexisted an interlayer distance was achieved between that of the PS-clay and PP-clay composites. However, Sinha Ray *et al.*,[61] who used the same organoclay as employed herein, did show that when both the polymers were present the interlayer distance was larger than when either one of the polymers was present alone. Regardless, this leads to the conclusion that the organoclay exists and interacts with both the polymers.

SEM micrographs presented by Wu *et al.*,[116] Cho *et al.*[120] and Salehiyan *et al.*[60] showed that the PS domain size decreased with the addition of organoclay. Specifically, Salehiyan *et al.*,[60] using the same organoclay as used herein, showed that the decrease in the PS domain size occurred by a loading of 3 wt.% and no further change was observed across the rest of the loadings (up to 11 wt.%). This was attributed to the clay encapsulating the PS domains and preventing them merging to create larger domains, via increased viscosity and the repulsion caused by steric hindrance. TEM was also used frequently to assess the organoclay dispersion.[67,108,43,66,64]

Istrate *et al.*[64] considered the crystallinity of PP-PS-organoclay composites using DSC and found that the presence of organoclay did not alter the melting or glass transition temperatures of the materials. Further they reported that the clay has a nucleating ability for the PP-PS blend whilst decreasing the domain size (observed under SEM). They also reported that when the polymer chains were functionalised to increase their affinity to the clay, due to the increase in stiffness of the material, the crystallinity was decreased.

As reported elsewhere for other polymer matrices, the presence of the organoclay increases the thermal decomposition temperature, however this increase is determined by the nature of the organoclay dispersion: the greater the exfoliation the higher the thermal decomposition temperature.[67] Istrate *et al.*[64] also considered TGA results and, as seen elsewhere upon the addition of organoclay, the data show an increase in thermal degradation temperature.

Following a thorough search of the literature, the only paper found with dielectric breakdown strength measurements on a composite containing PS and an organoclay was published in 2018 by Helal *et al.*[121] They report a positive correlation between

mechanical strength and AC dielectric breakdown strength results. The report details materials with three different clay morphologies: orientated, partially-orientated or isotropic and it was found that the lowest mechanical properties and breakdown strength occurred in the samples where the clay was aligned perpendicular to the electric field.

Like many others who have studied PP-PS-organoclay,[26,60,117,120] herein samples will be of 70:30 by weight ratio of PP:PS. Although many papers exist discussing the morphology of this blend, there is a lack of publications on their electrical properties. As such, in this thesis the electrical properties of these composites will be investigated and linked to the morphological properties.

1.8 Applications of Dielectrics in Capacitors

Polymer-clay composites, first developed by Toyota for use in car engines,[122] have many possible applications, including food packaging, electrical insulation and various structures for household products. Of particular interest in this thesis, however, is their use as a dielectric for a capacitor, even though producing the capacitor is beyond the scope of this project. Nonetheless, the electrical properties of the materials will be investigated by means of dielectric spectroscopy, both DC and AC dielectric breakdown strength and DC conductivity. This chapter will introduce briefly the electrical principles involved in dielectrics and capacitors while the principles behind the measurement techniques and the relevant equations can be found in Chapter 2.4.

A dielectric is a material that can be polarised by an applied electric field but does not permit a current (it is an electrical insulator). The relative permittivity of the dielectric, often referred to as the dielectric constant, is the ability of the dielectric to store electrical energy in an electric field due to the field polarising the material. A dielectric forms a capacitor when a dielectric separates two parallel electrodes and stores potential energy in an electric field. As shown in Equation 1.1, the capacitance (C, measured in Farads) of a capacitor is inversely proportional to the distance between the electrodes, (d), and is proportional to the dielectric constant of the material, ($\epsilon_r(\omega)$), between the electrodes multiplied by the dielectric constant of a vacuum, (ϵ_o), and the overlap area, (A), of the electrodes. In order achieve a high capacitance, A needs to be maximised and d needs to be minimised. A common way to achieve this yet still create a space efficient capacitor, is to vacuum deposit electrodes onto both sides of a polymer thin film before rolling up the material similar to a Swiss-roll cake.

$$C = \epsilon_r(\omega)\epsilon_o A/d \tag{1.1}$$

Chapter 2

Methods and Analysis Techniques

2.1 Processing

The processing procedure for creating the samples studied herein was adapted from published studies to include the materials desired for this report and the use of a rotary evaporator (instead of a hot stage).[92,123,67] The rotary evaporator allows rapid solvent removal leaving a solid product, which makes precipitating the dissolved material redundant and reduces the solvent waste. In general, the materials were produced via solution blending in xylene using a rotary evaporator. The organoclay was dispersed in xylene using a probe sonicator, to disperse the clay,[66] before being added to the rotary evaporator along with the polymer pellets. The mixture was heated and agitated until the polymer had dissolved. The samples were dried in a vacuum oven for one week (at ca. 2 mbar) before being pressed into films using a hydraulic press. The method of cooling from the melt phase depended on the investigation and will be detailed in the relevant sections below.

The same organoclay was used throughout this thesis: an MMT-based organoclay with 35-45 wt.% organic, used as received from Sigma Aldrich (682624).

2.1.1 PE-EVA-Organoclay Samples

This chapter will detail the sample preparation for the PE-EVA-Organoclay samples.

The following materials were used as supplied: LDPE (LD100BW, Exxon Mobil Chemicals); HDPE (Rigidex HD5813EA, BP Chemicals); and EVA (Elvax 750 and Elvax 450, DuPont - 9 and 20 wt.% VA respectively).

The organoclay was sonicated in xylene for 30 minutes before being added with the EVA into the rotary evaporator at 140 °C. When the polymer had completely dissolved,

the LDPE and HDPE were added and mixed until dissolved. The mixture was put under vacuum (at ca. 2 mbar) to remove the xylene once the polymers were completely dissolved and had been left stirring for 10 minutes. The product was dried under vacuum (at ca. 2 mbar) at 70 °C for 48 hours. A hot press (set to 140 °C) was used to produce films of around 100 μm in thickness with one of three different thermal treatments.

Three different thermal profiles were used to vary the morphology/phase structure of the final specimens. First, samples were quenched directly after melt pressing, to produce materials where liquid/liquid phase separation in the melt would be minimised and where rapid crystallisation would lead to a simple morphology (designated Q). For this, the samples were removed from the press and cooled to room temperature rapidly in the air. Second, the press was allowed to cool slowly to 70 °C, with the pressure applied to the sample; this process occurred over a period of 3 h, such that, in principle, the final morphology would result from a combination of liquid/liquid phase separation in the melt and subsequent liquid/solid phase separation during slow crystallisation of the polymer (designated SC). Finally, samples were held isothermally at 140 °C in the melt for 3 hours before being quenched (as above for Q), in order to combine liquid/liquid phase separation in the melt with rapid subsequent crystallisation (designated ISO). These thermal treatments were used to probe the impact of the organoclay on the response of the material to the thermal treatments because many published studies on nanocomposites also investigate these effects and one can use it to be an indicator of the dispersion.[6,57,99]

The relative ratio of LDPE:HDPE was always 80:20, and is referred to as PE. The ratio of PE:EVA was always 80:20. The nomenclature of EVA9 or EVA20 will be used for a VA content of 9 wt.% and 20 wt.% respectively. Six organoclay loadings were made and tested - 0, 1, 3, 5, 9 and 13 wt.%. When referred to in this thesis, either *Q*, *ISO* or *SC* will be appended to the sample name to signify the thermal treatment: for example, the sample PE/EVA9/5/SC has an 80:20 ratio for PE:EVA9 with a 5 wt.% loading of organoclay and was slowly cooled from the press.

In order to achieve a baseline, PE/5/Q was also produced containing 95:5 by weight of PE:organoclay (where PE = 80:20 LDPE:HDPE) and was quenched from the melt phase.

2.1.2 PP-EVA-Organoclay Samples

This chapter will detail the sample preparation for the PP-EVA-Organoclay samples.

The following materials were used as supplied: PP (product number: 427888, from Sigma Alrich) and EVA (Elvax 750, 9 wt.% VA from DuPont).

The processing protocol followed the general procedure described in Chapter 2.1. The

organoclay was sonicated in xylene for 30 minutes before being added with the EVA into the rotary evaporator at 140 °C. When the polymer had completely dissolved the PP was added and the temperature was increased to 155 °C to aid dissolution. The mixture was left stirring for 30 minutes before it was put under vacuum (ca. 2 mbar) to remove the xylene. The product was dried under vacuum (ca. 2 mbar) at 70 °C for one week whilst monitoring the mass change.

The samples were pressed into films (around 100 μm in thickness) using a hydraulic press to ensure a constant thickness film was obtained. Samples were held in the press at 180 °C for 5 mins before being treated with one of the three thermal treatments: held isothermally at 120 °C for 10 minutes (iso120) or 135 °C for 120 minutes (iso135) before being quenched by a room temperature water bath or directly quenched (Q) from the press. The required temperature and time were determined using DSC analysis.

These thermal treatments from the melt phase were employed in order to achieve a range of morphologies. Firstly, the quenched samples will have the simplest morphology given they pass through the crystallisation temperature rapidly, which limits crystal structure growth. The temperatures at which the samples were held isothermally facilitate nucleation and crystallistion on the order of minutes. This extended time in the melt phase allows opportunity for phase separation and for more ordered crystal growth upon nucleation. The two temperatures chosen for the isothermal treatments will create two different lengths of time that a sample will crystallise over and hence achieve different morphologies. In this way, investigating the same material over different thermal treatments will allow insight to the compatibility and interplay of the components of the composites.

The sample nomenclature has the form PP/EVA9/X/Y where X= 0, 0.5, 2.5 or 5 depending on the clay loading in wt.%, Y is the thermal treatment from the melt phase in the press. The ratio of PP to EVA was always 80:20. For example, the sample PP/EVA9/2.5/iso135 has 80:20 PP:EVA9 and 2.5 wt.% loading of organoclay and was isothermally cooled at 135 °C from the press.

For this material system, rather than making many composites with a wide range of organoclay loadings, a more focussed approach was adopted. Drawing from the literature and from experience gained through the PE-EVA-organoclay system, initially only composites with X = 0 and X = 2.5 were made. These were tested and, in particular, studied under SEM. Since the results showed a relatively saturated composite at only 2.5 wt.% loading (compared to the PE-based system), it was decided to make composites with X = 0.5 and 5.

In order to achieve a baseline, PP/5/Q was also produced containing 95:5 by weight of PP:organoclay and was quenched from the melt phase.

2.1.3 PP-PS-Organoclay Samples

This chapter will detail the sample preparation for the PP-PS-Organoclay samples.

The following materials were used as supplied: PS (product number: 430102, from Sigma Aldrich) and PP (product number: 427888, from Sigma Alrich).

The processing protocol followed the general procedure described in Chapter 2.1. The organoclay was sonicated in xylene for 30 minutes before being added with the polymer pellets into the rotary evaporator at 155 °C. The mixture was left stirring for 30 minutes before it was put under vacuum (ca. 2 mbar) to remove the xylene. The product was dried under vacuum (ca. 2 mbar) at 70 °C for one week whilst monitoring the mass change.

The samples were pressed into films (around 100 μm in thickness) using a hydraulic press to ensure a constant thickness film was obtained. Samples were held in the press at 180 °C for 5 mins before being treated with one of the three thermal treatments: held isothermally at 125 °C for 40 minutes (iso125) or 180 °C in the press for 40 mins (iso40min) before being quenched or directly quenched (Q) from the press in the air. The required temperature and time were determined using DSC analysis.

These thermal treatments from the melt phase were employed in order to achieve a range of morphologies. Firstly, the quenched samples will have the simplest morphology given they have the shortest time in the melt phase, therefore limiting phase separation, and pass through the crystallisation temperature rapidly therefore limiting crystal structure growth. The samples held isothermally at 125 °C will nucleate and crystallise much more slowly than samples following the other two thermal treatments. This extended time in the melt phase allows opportunity for phase separation and for more ordered crystal growth upon nucleation. To contrast this and the quenched samples, the iso40min samples were made by being held in the melt phase for 40 minutes before being quenched in the air. These samples have the longest length of time in the melt phase, meaning they have the longest time to phase separate into thermodynamically favoured configurations before being crystallised rapidly to effectively trap the morphology achieved. This gives rise to a different morphology than the iso125 samples as the iso40min samples do not have a slow nucleation and crystallisation period. The length of time chosen (40 minutes) was simply to match the samples being isothermally held at 125 °C. In this way, investigating the same material over different thermal treatments will allow insight to the compatibility and interplay of the components of the composites.

The sample nomenclature has the form PPa/PSb/X/Y where X= 0, 0.5, 1, 2, 3 or 5 depending on the clay loading in wt.%, Y is the thermal treatment from the melt phase in the press (either Q, iso125 or iso40min). The ratio of PP to PS was either 7:3 or 9:1. For example, the sample PP7/PS3/1/iso40min has 7:3 PP:PS, 1 wt.% loading of organ-

oclay and was held isothermally at 180 °C for 40 minutes before being quenched in the air from the melt phase in the press. The choice of organoclay loadings in this sample system were based largely on the findings from the PP-EVA-organoclay system (it was established from the literature that the two polymer blends were likely to interact similarly with the organoclay), and the desire to have a more composites representing the organoclay loading range so that results and conclusions could be thorough.

In order to achieve a baseline, PS/5/Q was also produced containing 95:5 by weight of PS:organoclay and was quenched from the melt phase.

2.1.4 Preparation of the Samples for the Xylene Immersion Tests

In order to investigate and develop an understanding of the probable outcomes from a potential inadequacy in the sample processing procedure, samples were immersed in xylene. This section describes the process of these experiments.

The PP-EVA-organoclay composites used for the xylene immersion investigations were produced as described in Chapter 2.1.2. The PE-EVA-organoclay composites used in this investigation were produced as described in Chapter 2.1.1.

From the press, all of the films were further dried for one week under dynamic vacuum (ca. 2 mbar) at 70 °C, whilst monitoring the mass change, to remove any absorbed water or residual solvent. These samples will hereafter be referred to as dried. Subsequent immersion in a xylene bath achieved samples termed immersed. Some immersed samples were dried under dynamic vacuum (ca. 2 mbar) at 70 °C and are termed re-dried.

The PP-EVA-organoclay composites were immersed in the xylene bath for one week and subsequently dried for two weeks while the PE-EVA-Organoclay composites were immersed for 4 days and subsequently dried for four days. The PE-EVA-Organoclay composites had shorter time scales because it was found that the time allowed for the PP-EVA-organoclay system was unnecessarily long.

Prior to performing the dielectric measurements on immersed samples, they were removed from the solvent bath and left open in the fume cupboard for 30 minutes before the experiment. This was to remove solvent from the surface to ensure that measurements reflected the influence of any solvent in the bulk of the sample.

Sample nomenclature will be appended with either D, I or R depending on the sample status of dried, immersed and re-dried respectively. For example, PP/EVA9/5/R is a sample that has been immersed in solvent and subsequently re-dried.

2.1.5 Preparation of the Samples for the Water Immersion Tests

In order to investigate and develop an understanding of the probable outcomes from any potential exposure of the nanocomposites to water, samples were immersed in water. This section describes the process of these experiments.

The samples used in the water immersion tests were fully dried PE/EVA9/X/Q films. The samples were immersed in a room temperature, deionised water bath. After 1 day, and again after 4 days, the mass, conductivity and dielectric spectroscopy measurements were performed according to the protocols set out in Chapter 2.4. The samples were removed from the water bath, patted dry and left exposed to the ambient laboratory conditions for 20 minutes to remove the water from the sample surface so that measurements would be the result of only the water taken up into the samples.

2.2 Thermal Analysis

2.2.1 Thermal Gravimetric Analysis

This analysis technique has been introduced in A.5.

TGA was used to determine the organoclay loading of the samples achieved when making the samples. This was realised by taking the ratio of the mass remaining from the sample and the mass remaining from the pristine organoclay and taking into account the mass of the organic moieties that would have been removed by the pyrolysis. This was possible because the only material resistant to pyrolysis in the samples was the silicate from the organoclay.[34]

Another use of the TGA data was through comparing the degradation data of the sample measured on the TGA under air and nitrogen atmospheres has been used in literature as a method of assessing the dispersion of the organoclay and therefore whether or not a nanocomposite has been formed.[85,124] The comparison was made by simply plotting the data on the same graph and observing the overlap of the graphs.

A further use of the TGA data was to assess the temperature of thermal degradation of the nanocomposite samples. As done elsewhere,[44] a comparison point was chosen - either the temperature at the maximum rate of material loss or the temperature at which 50 % of the material had been lost.

The analysis was conducted on the pressed films under both air and nitrogen atmospheres to 900 °C at 10 °C per minute using a Perkin Elmer Pyris 1 instrument. Data are plotted using percentage weight change (in order to normalise data across samples) versus temperature.

2.3 Morphological Analysis

2.3.1 Differential Scanning Calorimetry

This analysis technique has been introduced in A.6.

The purpose of employing DSC measurements was to understand the changes to the melting and crystallisation temperatures upon addition of organoclay, and to calculate the percent crystallinity of the samples.

The DSC data were collected under nitrogen at 10 °C per minute on a Perkin Elmer DSC-7 instrument, calibrated using the published procedure.[125] Data are plotted using Watts per gram of sample (in order to normalise data between samples) on a y-axis versus temperature on the x-axis.

The enthalpy of melting and crystallisation were obtained from the peaks for PE or PP using integration on the instrument software. The percent crystallinity ($\%_{crys}$) of the sample was determined by following Equation 2.1 as given by an application note supplied by the manufactures of the DSC instrument.[126] Where ΔH_f is the enthalpy of melting, ΔH_c is the enthalpy of crystallisation and ΔH_f° is the enthalpy of the totally crystalline polymer measured at the equilibrium melting point - a value that was obtained from a data table.[127] In brief, the equation says that the percent crystallinity of the sample is given by the difference between the enthalpy of melting and crystallisation divided by the enthalpy of the totally crystalline polymer multiplied by 100.

$$\%_{\mathrm{crys}} = 100 \times (\Delta H_{\mathrm{f}} - \Delta H_{\mathrm{c}}) / \Delta H_{\mathrm{f}}^{\circ} \tag{2.1}$$

2.3.2 X-Ray Diffraction

This analysis technique has been introduced in A.7.

XRD analysis was performed to determine the crystal structure of the organoclay and the polymers and to determine how these change with relative compositional changes as well as the polymer crystallite size.

Low angle XRD measurements were performed on a Rigaku Smartlab between 0.014-7.1 q using increments of 0.02°, a 0.2 mm slit and a source with λ = 1.54 Å.

The 2θ values obtained from the instruments have been converted into q values (units: nm^{-1}) for the x-axis in order that data are independent of the wavelength, (λ), of the radiation source and therefore comparable; Equation 2.2 shows the conversion.

$$q = (4\pi/\lambda).sin\theta \tag{2.2}$$

Data are plotted on graphs of intensity against the diffraction angle with the traces often being off-set for clarity.

The Scherrer equation, shown in Equation 2.3, was applied using the PDXL2 version 2.4.2.0, Rigaku Corporation (2007-2015) software to determine the volume-averaged crystallite size, τ, using the breadth of the peak, β; a shape factor, K=0.97; the Bragg angle, θ; and wavelength of the X-ray source, λ.

Errors in the results from the Scherrer equation primarily arise due to peak broadening effects caused by factors other than the crystal, these include crystal dislocations, micro-stresses, grain boundaries and crystal imperfections due to contaminants.[128]

$$\tau = K\lambda/\beta cos(\theta) \tag{2.3}$$

Comparing the interlayer distance (or d-spacing) of the organoclay is a method of comparing intercalation and therefore assessing the compatibility of the system. Equation 2.4 gives Bragg's law, which was used for calculating the d-spacing. The terms in the equation are defined as: $n = 1$ (due to the position of the organoclay peaks investigated); λ, the wavelength of the X-ray source; and θ is the angle at which the peak that one is investigating the d-spacing of appears (taking care to divide the number read off the 2θ axis by 2).

$$d = n\lambda/2sin(\theta) \tag{2.4}$$

2.3.3 Fourier-Transform Infrared Spectroscopy

This analysis technique has been introduced in A.8.

Fourier-transform infrared spectroscopy (FT-IR) was performed using a Thermo Scientific Nicolet iS5 operating in transmission mode or attenuated total reflection (ATR) mode depending on the application. This technique indicates the types of bonds present and so was used for two purposes. Firstly, the presence of organoclay in the polymer blends was confirmed by the appearance of a peak around 1050 cm^{-1} corresponding to an asymmetric stretch of Si-O-Si of the organoclay. Secondly the technique was used to check that the thermal exposure during the drying procedures had not caused oxidation of the polymers by checking that peak patterns had not changed before and after cooling and in particular, no peaks had appeared to correspond to the formation of a carbonyl group or other oxide group.

Data are plotted on a graph of intensity against wavelength and the spectra are sometimes off-set for clarity. To be able to compare the samples, data were normalised using Z-scores (also known as the Standard Normal Variate Correction) using the *Origin* software. Refer to Chapter A.8.1 for specific details on this normalisation method.

2.3.4 Scanning Electron Microscopy

This analysis technique has been introduced in A.9.

The SEM was used to study the internal morphology of the samples, to observe changes caused by the thermal treatment and to check for aggregation of the organoclay. To reveal the sample morphology, the samples were cut to reveal an internal morphology that was unaffected by the pressing process. The samples were chemically etched following an established etching technique.[81] The etchant comprised of 1 wt.% potassium permanganate in a solution of sulfuric acid, phosphoric acid and deionised water in a 5:2:1 ratio and the quenching solution was sulfuric acid, deionised water and hydrogen peroxide in a 2:7:2 ratio. The etching procedure was performed under constant agitation before the samples were decanted into the quenching solution and then washed once in deionised water and then ethanol. The samples were sputter coated with gold before being imaged. So that artefacts from the pressing process did not interfere with the observed morphology, the cut-edge surfaces of the films were imaged using SEM (EVO LS25, produced by Zeiss).

2.4 Electrical Analysis

2.4.1 Dielectric Breakdown Strength

This analysis technique has been introduced in A.2.

AC breakdown strength was measured following ASTM D149-97a, with the sample immersed in silicone oil between vertically opposed spherical electrodes (6.3 mm diameter). Each film was divided into a grid containing 20 boxes, the thickness of each was recorded before being tested, until breakdown, at a rate of 500 V/s. The results were analysed by dividing the breakdown strength of each boxed position by the respective sample thickness so each film had 20 results in the form kV/mm. These were applied to the two-parameter Weibull distribution with 90 % confidence limits using *Origin*.

In a similar way, the DC dielectric breakdown strength was measured in a test cell immersed in silicon oil with the sample held between two vertically opposed spherical electrodes (6.3 mm diameter) with a ramp rate of 350 V/s. Each film was tested 16-20

times and the results were analysed using the two-parameter Weibull statistics with 90 % confidence limits using the *Origin* software package. (It is noted that this is not truly a DC system as the voltage is not constant however for the purposes of this thesis and due to equipment limitations in the laboratory these results will be treated as DC.)

Variation in the measured breakdown strength is a result of the statistical nature of the dielectric breakdown and was analysed using the Weibull Distribution. The two-parameter distribution was employed as it is a commonly used method for characterising electrical breakdown in solid insulators.[129,130] The two parameters are defined by Equation 2.5 where P_F represents the proportion of specimens tested which will fail by the electric field limit, x.

$$P_F = 1 - exp[(-x/\alpha)^{\beta}] \tag{2.5}$$

Where α is the scale parameter and β is the shape parameter; each must be > 0. The scale parameter, which has units of the electric field (kV/mm), represents the field by which $\approx$ 63.2 % (1 - e^{-1})% of the specimens have failed.[131]

The shape parameter is dimensionless and represents the dispersion of the breakdown fields. The larger the shape parameter, the narrower the spread in the breakdown fields.

The two parameters are properties of the dielectric material, and the scale parameter is also a function of the applied electric field.[131,132] Equation 2.5 can be linearised to aid plotting and visualisation of the parameters, shown in Equation 2.6.

$$log[-ln(1 - P_F)] = \beta log(x) - \beta log(\alpha) \tag{2.6}$$

A three parameter distribution exists but in the two parameter distribution employed here, the simplification has been made that the location parameter, γ, is equal to zero. This approximation is also commonly used in the literature in comparable studies to that conducted herein.[91,133,130]

2.4.2 DC Conductivity

This analysis technique has been introduced in A.3.

It is noted that true DC conductivity is the point where all the polarisation has occurred. This may require hours and consequently be influenced by environmental changes during this time. Therefore an approximation of the DC conductivity has been measured herein and referred to as simply DC conductivity.

For these measurements, samples were pressed into films of thickness 100 μm. This was a compromise between being thin enough to maximise the field and not being so thin that thickness variation across the sample would be significant compared to the thickness of the material and that the conductivity of the bulk (and not just the surface interphase) could be measured.

DC conductivity tests were used to determine the polarising nature and resistivity of the samples, to explore the influence of the organoclay loading and temperature on sample conductivity. The tests were performed using Keithley Instruments: test fixture 8009 and picoameter 6517B with a guarded electrode of diameter 54 mm. The electrodes were conductive rubber pads so no further sample preparation (such as gold coating) was required. Tests were under constant voltage conditions creating a 3 kV/mm field for the PE-EVA-organoclay composites, 9 kV/mm for the PP-EVA-organoclay composites and 8 kV/mm for the PP-PS-organoclay composites.

Different fields were used for each system, somewhat un-intentionally, due to the progression and development of the project over the course of time. To start with a field of 3 kV/mm was used as it was well within equipment capabilities. The disadvantage of using a field this low was that the results were sometimes, particularly in samples with the lowest organoclay loadings, too low to be meaningfully interpreted against background noise. As such, for the latter material systems, the maximum possible field achievable was chosen, taking into account the sample thickness and the maximum voltage the test set-up could supply (1000 V). Another disadvantage is that possible applications of these materials have significantly higher fields and conductivity does not necessarily change linearly with electric field. Specifically, in cables the field could be 20-30 kV/mm while in capacitors the field could be greater.

The time of electrification was defined as 1000 seconds following an investigation into appropriate time scales for these sample systems, using recommendations in ASTM D257. It was decided that by 1000 seconds under a constant voltage, steady state would have been achieved or was not going to be achieved within a practical time scale. Although 1000 seconds is somewhat arbitrary, especially given the potential applications of these materials, it served as a standard point at which all the materials were measured. Furthermore, this length of time allowed for the presence of bubbles in the samples to breakdown (and therefore cause the experiment to fail) so that another, more representative sample could be tested. Moreover after 1000 seconds, the variations in current readings were approximately 9% of the final value so it could be said that the current had stabilised and these variations were mitigated by measuring three samples per sample composition in order to present the mean and standard deviation results herein.

The four temperatures investigated (28, 40, 55 and 70 °C) were chosen as a representative spread over the temperature range that the equipment could achieve. Similarly,

the choice of field used was capped by the capability of the equipment to supply a maximum of 1 kV.

$$Resistivity = Resistance \times \frac{Area\ of\ electrode}{Thickness\ of\ sample} = \Omega \times \frac{cm^2}{cm} = \Omega cm \tag{2.7}$$

$$Conductivity = \frac{1}{Resistivity} = \frac{1}{\Omega cm} = S/cm \tag{2.8}$$

The equipment software published the current and resistance measured throughout the 1000s experiment. Using Equations 2.7 and 2.8, and by taking the resistance to be the average of the final ten measurements of each experiment, the conductivity was calculated.

2.4.3 Dielectric Spectroscopy

This analysis technique has been introduced in A.1.

For this analysis, samples of thickness 200 μm were used in order to produce a signal that was representative of the bulk properties. Gold coating the sample was shown to have no effect on the signal therefore, so that the samples could be re-used for other analysis, the measurements were made without gold coating.

Dielectric spectroscopy measures, as a function of frequency, the dielectric response of a material. The equipment measures the magnitude and phase angle of the current relative to the applied AC field. From this, the capacitance is deduced and the relative permittivity is calculated by taking the ratio of the capacitance of a dielectric to that of a vacuum.

Dielectric spectra were acquired using a Solartron 1296 dielectric interface together with a Schlumberger SI1260 impedance/phase gain analyser system. For this, an AC voltage of amplitude 1 V RMS was applied across electrodes 30 mm in diameter with a guard electrode and the frequency range of 10^{-1} to 10^5 Hz was considered.

Data are plotted with frequency on the x-axis in logarithmic form against real permittivity in linear form or imaginary permittivity in logarithmic form on the y-axis. The shapes and gradients of the traces on the graphs allow for interpretation of the frequency dependent dielectric response of the material.

It is possible to estimate the value of the real part of the relative permittivity, using any one of a number of effective medium mixing theories.[134] Herein, the widely used Lichtenecker logarithmic mixing rule[135] (Equation 2.9) will be employed using permittivity values from data tables such as *'The CRC Handbook of Chemistry and Physics'*.[136]

$$(V_1 + V_2).log(\epsilon_{\text{composite}}) = V_1.log(\epsilon_1) + V_2.log(\epsilon_2) \tag{2.9}$$

Where V_x is the volume fraction of a component, x.

In order to probe the processes occurring in response to frequency, dielectric spectroscopy data was gathered at a range of temperatures above room temperature.

Chapter 3

Thermal Analysis of the Composites

3.1 Introduction

This chapter will use TGA and DSC to investigate the thermal properties of the composites made before the following chapters will detail the compatibility and the electrical properties.

TGA measures the mass change with temperature under a controlled atmosphere and can be used to give insight to the material properties. Firstly, the thermal degradation temperature can be determined from the position of the mass loss curve. The temperature at which the pyrolysis occurs can be affected by the chemical nature of the polymer and the dispersion of the organoclay. Since, for each material system the polymer is constant, it is the organoclay loading that causes the variation in the temperature at which pyrolysis occurs. This is because organoclay can act as a physical barrier to the permeation of oxygen and therefore char forms from the polymer burning in insufficient oxygen levels. Charring further prevents the permeation of oxygen or the loss of material so mass loss is postponed until higher temperatures when the char is removed.[29,34,76]

A second use for TGA is confirming the formation of a nanocomposite. Several published studies use the criteria that if the mass loss traces obtained from burning the sample in air and nitrogen are the same in terms of shape and temperature then a nanocomposite has been formed.[85,29,34] (It is noted that determining the equivalence is somewhat subjective but nevertheless provides a guide for interpreting the results.) This phenomena is an unusual occurrence as, usually, pyrolysis in air occurs at a lower temperature than in nitrogen due to the absence of oxygen in the latter that would otherwise react and break the covalent bonds in the polymer. If the organoclay is sufficiently dispersed to form a barrier to the permeation of oxygen, then the sample burning in air would effectively be exposed to no oxygen as in a nitrogen atmosphere. This

means that the mass loss occurs as if there was no oxygen present until the temperature is high enough to remove the char and burn the previously protected material, hence the traces appear the same.

However, the products of the organoclay degradation - formed from the ammonium groups via Hofmann Elimination and hence independent of the type of organoclay used - degrade the polymer matrix.[29] This means that the organoclay can also decrease the degradation temperature of the material. Therefore the net effect of the presence of organoclay on the pyrolysis depends on the amount of organoclay present due to how the two processes can counteract.

In terms of aiding the material investigations by confirming the legitimacy of the samples produced, TGA has two further uses. TGA can be used to determine the precise organoclay loading achieved by the material synthesis. This means that rather than working with nominal values for the organoclay loading, a more accurate value can be used which may reveal trends in the data. TGA can also reveal if the sample contained any residue solvent from the solution blending protocol through potential mass loss at temperatures below 300 °C.

DSC measures the heat flow to a sample compared to an indium calibrant. This can yield results to inform of the optimum temperature for the crystallisation of the sample, the percent crystallinity of the sample (via the enthalpies of crystallisation and melting and Equation 2.1) and the melting point of the sample.

The crystallinity of the sample can be important information as amorphous regions are susceptible to water permeation and allow the initiation and development of electrical treeing.[137] Together with the crystallinity, the melting point data can be used as a way of comparing the samples as it can be affected by the purity of the polymer phase - in turn affected by the compatibility of the phase with the rest of the sample phases and the nucleating ability of the organoclay.[101]

3.2 Experimental

The processing procedure of the PE-EVA-organoclay, PP-EVA-organoclay and the PP-PS-organoclay composites are detailed in Chapters 2.1.1, 2.1.2 and 2.1.3 respectively. The thermal analysis was conducted using TGA and DSC, detailed in Chapters 2.2.1 and 2.3.1 respectively.

3.3 TGA for the PE-EVA-Organoclay System

Figure 3.1 compares TGA traces obtained in air and in nitrogen for samples from the PE-EVA material system. Of the five organoclay loadings investigated, a comparison of the TGA data from samples pyrolysed in air and nitrogen confirmed the formation of nanocomposites for all organoclay loadings apart for 13 wt.% since all but this loading had equivalent traces (see Chapter 3.1 for details) obtained from air and nitrogen atmospheres.

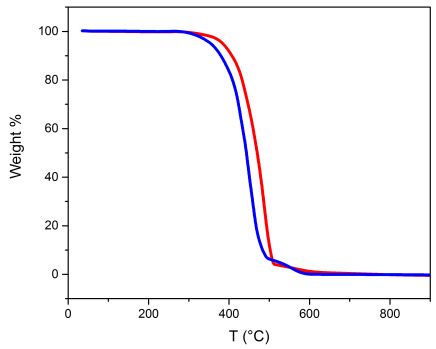

(a) PE/EVA9/0 (contains no organoclay)

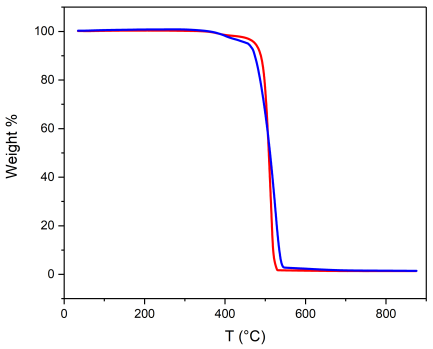

(b) PE/EVA9/1 (contains 1 wt.% organoclay)

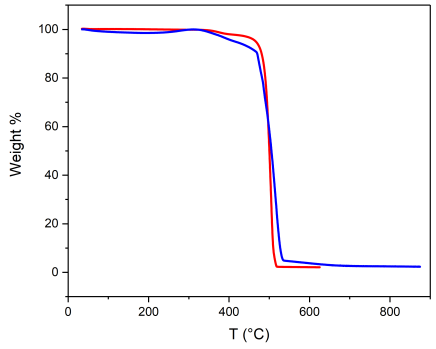

(c) PE/EVA9/3 (contains 3 wt.% organoclay)

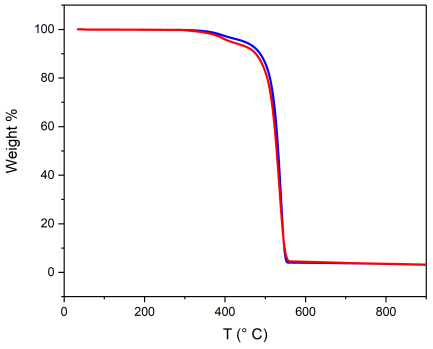

(d) PE/EVA9/5 (contains 5 wt.% organoclay)

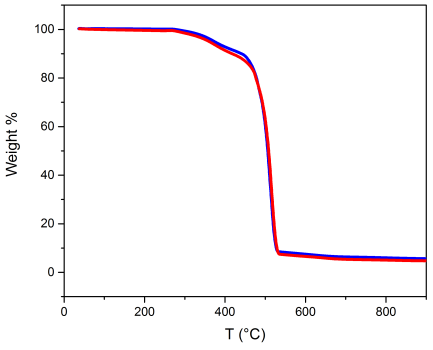

(e) PE/EVA9/9 (contains 9 wt.% organoclay)

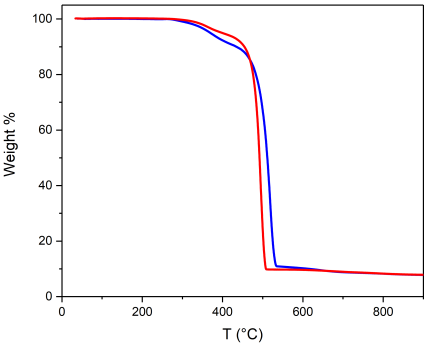

(f) PE/EVA9/13 (contains 13 wt.% organoclay)

Figure 3.1: *TGA data showing the effect of organoclay on the thermal decomposition of the samples and the presence of nanocomposites. Blue represents TGA in air while red represents TGA in nitrogen.*

Figure 3.2 shows a plot of the organoclay loading calculated for each material sample run in the TGA with the temperature at the maximum rate of material loss (chosen as a comparative temperature point between the samples). It can be seen that there is some variation in the obtained organoclay loading to that nominally assigned from the processing, nevertheless, the samples shall still be referred to by their nominal loading

herein. Overall, it can be seen that the maximum rate of material loss occurred at higher temperatures when the blends contained organoclay. This was seen elsewhere and was attributed to the barrier effect of the organoclay.[76]

In more detail, the degradation temperature increases with organoclay loading until around 5 wt.%. This correlates with more organoclay causing more of a barrier effect and delaying pyrolysis to higher temperatures. However, increasing organoclay content above 5 wt.% causes a decrease in degradation temperature, though it remained higher than samples without organoclay. This is because the organoclay degradation products are off-setting the barrier effect of the organoclay. It is proposed that another contributing factor to the lower degradation temperature is that aggregation is more likely at higher loadings, causing non-uniform char formation that would therefore limit the barrier effect.

Figure 3.2 also shows data from a set of samples made identical to PE/EVA9/X/Y apart for the VA content of the EVA was 20 wt.%. It can be seen that the relative VA content between the samples containing EVA9 and EVA20 apparently causes no difference in the degradation temperature. This implies that the more polar blend makes no difference to the dispersion of the organoclay to form a nanocomposite.

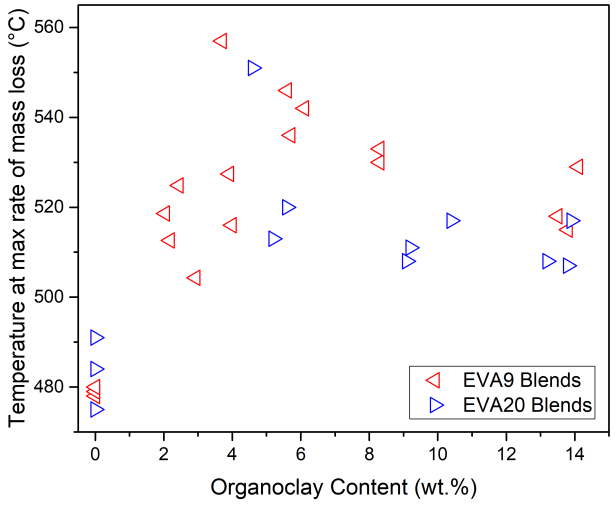

Figure 3.2: *Graph showing the actual organoclay loading of each sample compared to the temperature of the maximum rate of thermal decomposition for both the PE-EVA systems containing EVA9 and EVA20.*

3.3.1 Evidence of Compatibilisation in PE-EVA-Organoclay Composites

To compare the dispersion of the organoclay as a means of assessing the compatibility of the composite, Figure 3.3 shows the actual organoclay content against the temperature at 50 % material loss for the PE-EVA-organoclay composites.

It is worth noting that, though not directly related to the dispersion, all of the composites showed a higher thermal degradation temperature than the unfilled polymer, which is as expected from the literature.[76] This has been discussed in more detail in Chapter 3.1.

TGA traces from the experimental runs in air and from nitrogen were indistinguishable in all the composites apart for the highest organoclay loading (13 wt.%). This is shown by the proximity of the data points for each respective loading in Figure 3.3. This suggests that, in line with other published work,[85] a nanocomposite has been formed in the composites when the loading was less than or equal to 9 wt.%. This highlights the successful use of EVA as a compatibiliser to the system until the organoclay reached 13 wt.% where the ratio of EVA to organoclay was too low to enable compatibility and dispersion with the PE.

Comparable TGA results from the PP-EVA-organoclay and PP-PS-organoclay composites did not show the same equivalence between results obtained in air and nitrogen (see Chapter 3.1 for details), which was taken to mean that the dispersion was not as effective as in the PE-EVA-organoclay samples.

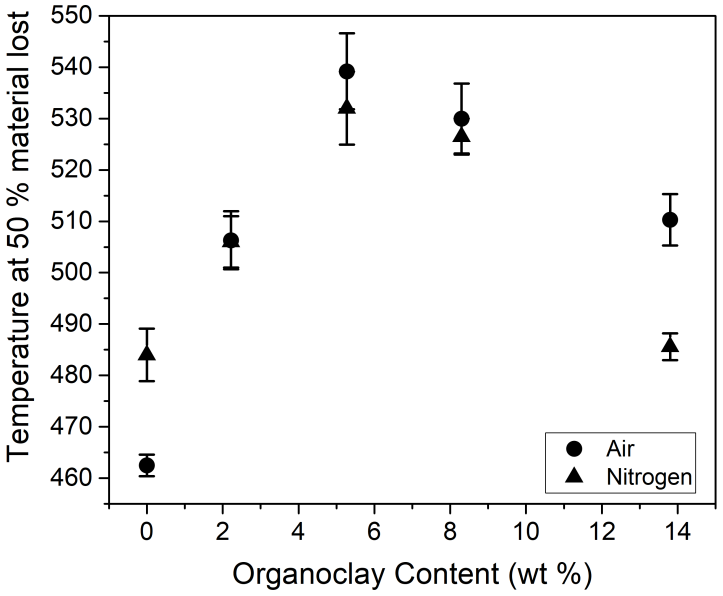

Figure 3.3: *TGA results of composites conducted in air and nitrogen atmospheres showing their respective temperature at which 50 % of the material had been lost.*

3.4 TGA for the PP-EVA-Organoclay System

TGA was performed on the samples to confirm the organoclay loading achieved during the sample processing (taken to be the average of several runs). As seen in Figure 3.4, the results varied from the desired 0.5, 2.5 and 5 wt.% - the actual organoclay loadings were found, after averaging three experimental runs, to be 0.4, 1.5 and 4.7 wt.% respectively. Nevertheless, the samples shall be referred to herein by their nominal loadings.

As with the PE-EVA-organoclay system, the TGA data from the PP-EVA-organoclay system (shown in Figure 3.4) reveal that the presence of organoclay increases the thermal degradation temperature of the blend by around 40 °C. This is entirely in line with expectations as discussed previously for the PE-EVA-organoclay system. Furthermore, it can be seen that degradation occurs at a higher temperature in an oxygen-free atmosphere, this is a well understood phenomenon of pyrolysis. This also indicates that the organoclay did not prevent the permeation of oxygen to the extent seen with the PE-EVA-organoclay composites.

Notable exceptions to these two observations occur at around 0.5 wt.% organoclay loading where two of the results have a lower degradation temperature than the unfilled polymer blend and the degradation temperature of the material in nitrogen is only around 20 °C higher than their counterparts. The cause of these is unclear but may involve a combination of factors including organoclay loading and dispersion being too low to significantly influence the degradation temperature, and the dispersion favouring the Hofmann elimination mechanism that in turn accelerates the degradation of the polymer matrix.

The comparison of the representative selection of samples in Figure 3.5, run in nitrogen and in air, showed that this sample, as with the other PP-EVA-organoclay composites, has insufficient organoclay dispersion to be termed a nanocomposite according to the accepted published criterion (see Chapter 3.1 for details).[85]

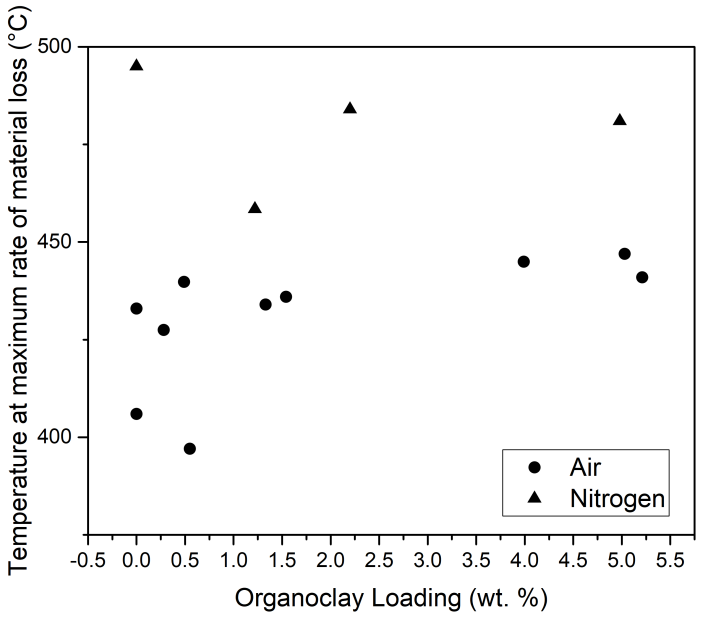

Figure 3.4: *Graph showing the actual organoclay loading of each sample compared to the temperature of the maximum rate of thermal decomposition for the PP-EVA-organoclay system.*

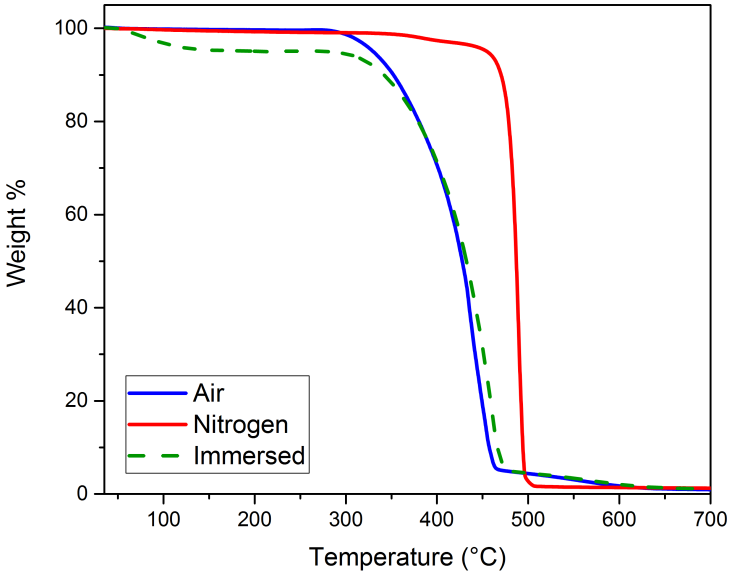

Figure 3.5: *Graph showing traces from the TGA of dried PP/EVA9/2.5/Q samples in conducted in air and in nitrogen and a trace from a sample of PP/EVA9/2.5/Q that had been immersed in xylene conducted in air.*

3.4.1 TGA for the PP-EVA-Organoclay System Immersed in Xylene

Additional TGA tests to those described by Chapter 3.4 were run on the samples involved in the xylene immersion tests. These were run to determine if there was solvent residue present and to determine how the presence of xylene in the sample affected the thermal degradation temperature. This has been discussed in detail in Chapter 7 but Figure 3.5 shows a brief overview of the findings.

Most pertinent to the tests in Chapter 7, the data from the immersed sample show a mass loss around 150 °C (before the polymer degradation), which was ascribed to the removal of the solvent from the sample.

Furthermore, there is no significant difference between the traces of the immersed sample and the dried sample so it can be said that the introduction and subsequent removal of xylene does not change the thermal degradation temperature.

3.5 TGA for the PP-PS-Organoclay System

Figure 3.6 shows the temperature at the maximum rate of thermal degradation plotted against the calculated organoclay loading for each of the TGA experiments on the PP-PS-organoclay samples conducted in both air and nitrogen. It is clear from the graph that there was a considerable spread in the calculated organoclay loading results of between multiple tests on each sample composition, which highlights that the organoclay was not evenly distributed throughout the sample. On average, the organoclay loading achieved for PP7/PS3/1/Q, PP7/PS3/3/Q and PP7/PS3/5/Q was 1.2 wt.%, 3.3 wt.% and 4.6 wt.% respectively whilst for PP9/PS1/0.5/Q and PP9/PS1/2/Q the organoclay loading achieved was actually 0.3 and 1.7 wt.% respectively. Nevertheless, the samples shall be referred to herein by their nominal loadings.

Other observations from Figure 3.6 include that the degradation temperature of the samples containing organoclay are higher than the degradation temperature of the sample without organoclay and the degradation temperature continues to increase with loading across the loadings investigated. This is because the organoclay (and the char that forms from it) acts as a barrier to oxygen penetrating the sample. This delays the oxidation degradation until a higher temperature since at a higher temperature the char is itself burned off and there has been more time for the oxygen to penetrate. Similar findings were reported upon by Arora *et al.*[138] who studied PS-organoclay composites.

Further, there is no significant difference between the results obtained between the experiments conducted in nitrogen. This highlights that in the absence of oxygen the degradation is effectively the same between samples. And, reflecting this onto the data

collected from the experiments conducted in air: with increasing organoclay content the degradation in air approaches the degradation temperatures for nitrogen. This implies that at higher organoclay loadings the samples are effectively degrading as if in a nitrogen atmosphere since the char is excluding the oxygen. This was as expected and similar results were found for the PP-EVA-organoclay composites.

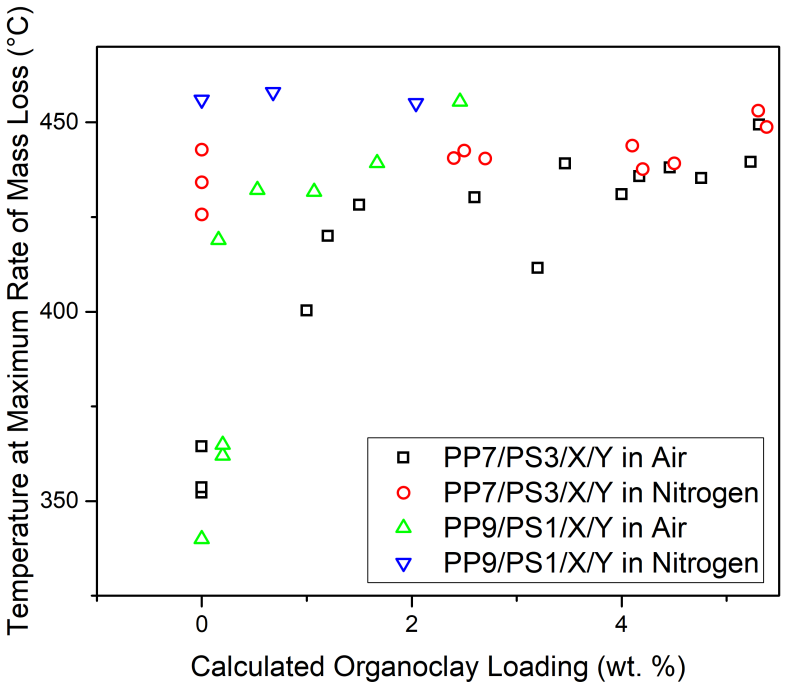

Figure 3.6: *Graph showing the actual organoclay loading of each sample compared to the temperature of the maximum rate of thermal decomposition for the PP-PS-organoclay composites.*

Figure 3.7 shows the degradation traces for both PP-PS-organoclay systems. These show that degradation is not equivalent between air- and nitrogen-based experiments and hence that loading and/or dispersion was not sufficient to prevent oxygen penetration. This means that the samples degrade non-equivalently under both environments and hence do not achieve the benchmark rule for nanocomposite formation (see Chapter 3.1 for details).[85]

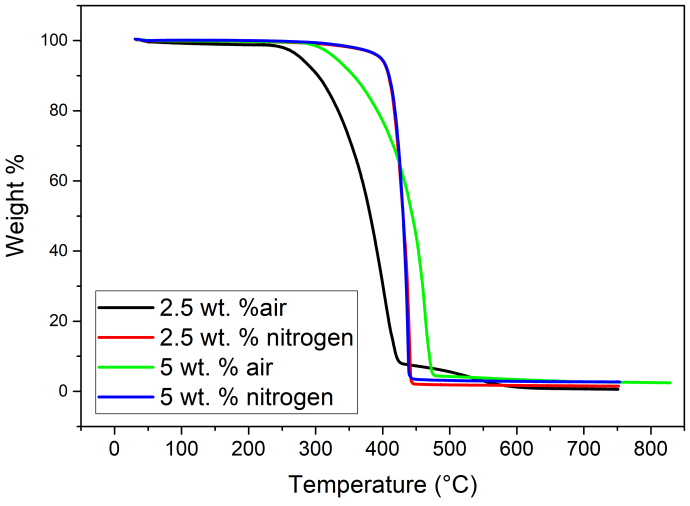

(a) PP7/PS3/X/Y

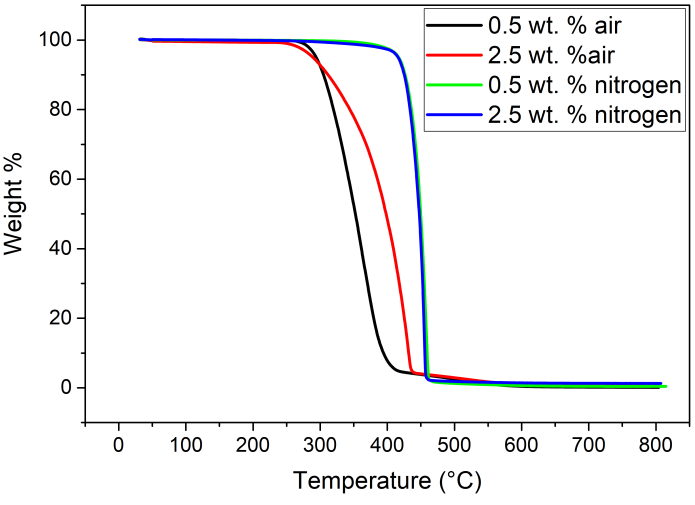

(b) PP9/PS1/X/Y

Figure 3.7: *TGA data showing the effect of organoclay on the thermal decomposition of the samples under air and nitrogen.*

Sample	Temperature of Crystallisation (°C)	% Crystallinity	Error (Standard Deviation)
PE/EVA9/0/Q	106.0	20.8	0.53
PE/EVA9/1/Q	112.0	20.0	0.02
PE/EVA9/5/Q	105.0	18.7	0.34
PE/EVA9/9/Q	105.5	19.3	0.06
PE/EVA9/13/Q	107.0	19.9	0.04

Table 3.1: *The temperature of crystallisation and percent crystallinity results from the DSC data of the PE-EVA-organoclay composites. See also Figure 3.8*

3.6 DSC for the PE-EVA-Organoclay samples

Table 3.1 shows the DSC results for the PE-EVA-organoclay samples. It can be seen that, with the addition of organoclay, the crystallinity of the samples decreased to a minimum at 5 wt.% organoclay loading before the crystallinity increased again with further additions of organoclay. However, when taking into account the standard deviation, this trend is less clear.

A filler like organoclay can prevent the movement of the polymer chains (through bonding interactions, confinement or facilitating nucleation) and so hinder the formation of crystalline areas of polymer.[87,6] It is suggested that this is the cause of the decreased crystallinity compared to pure LDPE (around 32 %) published by Hosier *et al.*[10]

Another study showed that well-dispersed MMT decreased crystallinity due to the organoclay physically inhibiting crystal growth.[57] It is suggested that the changes in the crystallinity seen in the DSC data in Table 3.1 can be related to the dispersion of the organoclay: the well-dispersed organoclay at 5 wt.% showed the minimum crystallinity (the maximum crystal growth disruption) while further increases in the loading, agglomeration decreased the effectiveness of the organoclay at inhibiting the polymer chain movement. Since herein the samples showed a decrease in crystallinity upon the addition of organoclay, it can be reasoned that they have well-dispersed organoclay.

Figure 3.8 shows the crystallisation curves for the PE/EVA9/X/Q samples. The crystallisation of PE in samples containing organoclay occurs at different temperatures to the PE/EVA9/0/Q sample. However there is not a clear trend in the results: the sample with the highest crystallisation temperature contains 1 wt.% organoclay whilst the sample with the lowest crystallisation temperature contains 5 wt.% organoclay, thereafter, further increases in organoclay loading increase the temperature of crystallisation again. It should be noted that the data for all but the PE/EVA9/1/Q sample was collected on the same day and it is possible that a temperature calibration problem has resulted in PE/EVA9/1/Q not fitting well with the trend.

Zazoum *et al.*[139] found that the organoclay does not have a nucleating effect on a PE-organoclay composite whereas Vaughan *et al.*[57] found the organoclay to have some nucleating effects. Discounting the PE/EVA9/1/Q sample, it can be seen that the crystallisation temperature increases with organoclay loading and with an increase in percent crystallinity. This is consistent with the organoclay acting as a nucleating agent.[31]

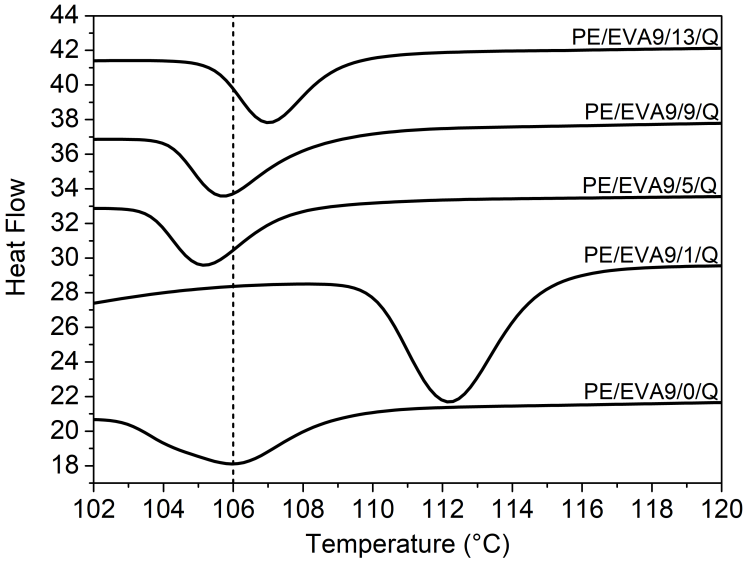

Figure 3.8: *Graph showing how the temperature of crystallisation changes with organoclay loading using the crystallisation curves from the PE/EVA9/X/Q samples.*

3.7 DSC for the PP-EVA-Organoclay samples

The most appropriate conditions for the isothermal crystallisation of the samples were decided using the DSC to determine the crystallisation time of the PP. The samples were melted and then held isothermally at certain temperatures in the range 105-135 °C. Figure 3.9 shows that the results from two samples and pure PP. As has be found elsewhere, at the higher temperatures the samples required exponentially longer lengths of time to crystallise.[84,140] This is related to the higher temperatures being closer to the melting point so the material has higher mobility and kinetic energy meaning that there are fewer successful nucleation points for crystallisation to occur. Another consideration is that the longer time in the melt phase, more phase separation is likely to occur, which will create interfaces that in turn influence the electrical properties.[38,141] Therefore the temperatures chosen for this study were a compromise to maximise the length of time in the melt phase to allow larger crystallites to form whilst working within a feasible length of time.

As can be seen in Figure 3.9, isothermally crystallising the samples with and without the organoclay makes little difference to the length of crystallisation time below 130

°C. Comparing the results of the composites with the pure PP, the former took longer to crystallise at all of the temperatures investigated. This could be attributed to the organoclay and EVA inhibiting the PP moving into a favourable crystal structure and so increasing the amount of time required for the PP to crystallise. This is supported by the blend containing organoclay and EVA taking longer to crystallise since the PP was inhibited.

From Figure 3.9 it can be noted that the crystallisation time at 120 °C and 135 °C of the PP component was about 2.5 minutes and 55 minutes respectively. It was decided that the length of time that the samples would be held at their respective temperatures would be at least twice what was determined from the DSC data to ensure that the sample had crystallised fully. For this investigation it was decided that samples would be treated with one of the three thermal treatments from the melt phase: held isothermally at 120 °C for 10 minutes or 135 °C for 120 minutes before being quenched in a room temperature water bath or directly quenched.

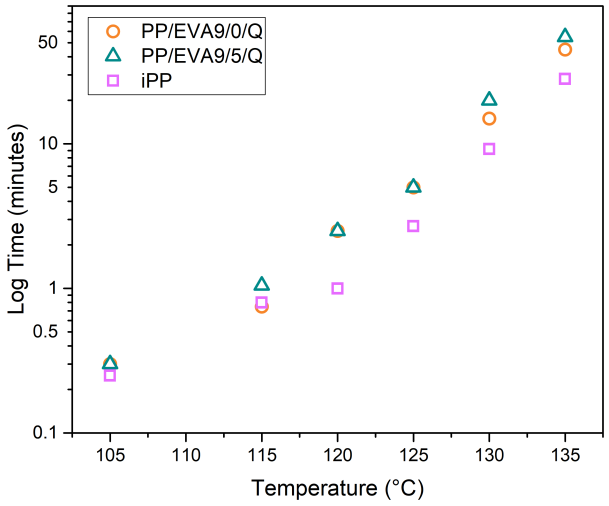

Figure 3.9: *Graph showing DSC data used to decide the temperatures at which the thermal treatments should be conducted for the PP-EVA-Organoclay composites.*

DSC was also used to compare the percentage crystallinity of the samples to investigate the influence of the organoclay on the cooling procedure. The averaged results are shown in Table 3.2. Although a general decrease in the crystallinity of PP was seen upon the addition of organoclay, variations between samples gave standard deviation error bars that overlapped. Further, there was no significant difference on the crystallinity caused by the different heat treatments of samples of equivalent composition. This indicates that the length of time in the melt phase does not impact the percentage of the sample in a crystalline phase. Elsewhere, the percentage crystallinity was not found to be a dominant factor in the electrical strength of a material.[79] Therefore, and especially because the differences in crystallinity observed were small, an attempt will

Sample Name	Enthalpy of Melting (J/g)	Enthalpy of Crys-tallisation (J/g)	Percent Crys-tallinity of PP	Error (Standard Deviation)
PP/EVA9/0/Q	49.4	71.3	62	6
PP/EVA9/0/iso120	48.5	73.1	63	7
PP/EVA9/0.5/Q	44.0	73.5	61	2
PP/EVA9/2.5/Q	44.0	70.9	60	4
PP/EVA9/2.5/iso120	51.0	70.1	63	5
PP/EVA9/5/Q	48.9	65.3	59	6
PP/EVA9/5/iso120	42.8	68.0	57	3

Table 3.2: *Table listing the averaged results from the three experimental runs on the DSC for each sample.*

not be made to ascribe the electrical breakdown strength to the crystallinity.

It is worth noting the much larger standard deviation values in the PP-EVA-organoclay system compared to the PE-EVA-organoclay system presented in Tables 3.2 and 3.1 respectively. This difference was ascribed to the incompatibility and therefore inhomogeneity of the PP-EVA blend compared to the PE-EVA blend causing more variation between experimental runs.

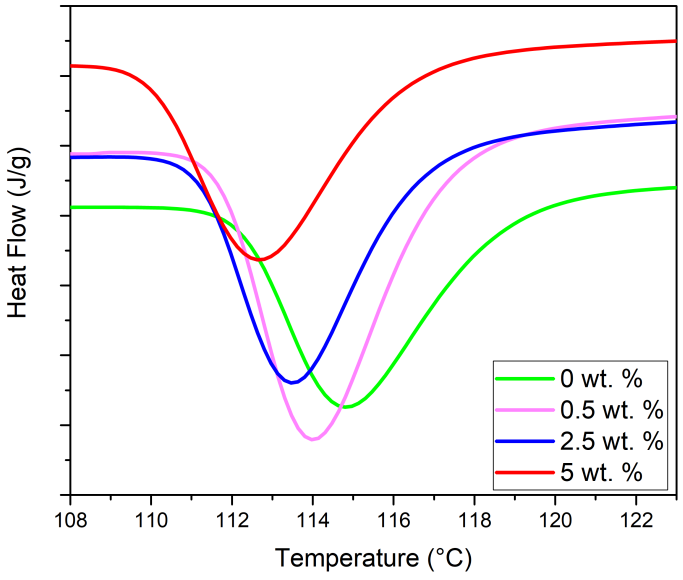

Figure 3.10: *Graph showing how the temperature of crystallisation changes with organoclay loading using the crystallisation curves from the PP/EVA9/X/Q samples.*

Figure 3.10 shows DSC results investigating the temperature at which the PP crystallised. A correlation can be seen where there is a higher organoclay loading, the

crystallisation temperature is lower. However, it is suggested that this is not a causal relationship because when comparing these to results from Dong *et al.*,[101] who investigated the crystallisation temperature variation of PP with organoclay and another polymer, it is believed that herein the effect of the organoclay acting as a compatibiliser is observed. Dong *et al.* reported that an organoclay had a nucleating effect that increased the crystallisation temperature but that the influence of the organoclay was off-set by the presence of another polymer in the matrix that had a lower crystallisation temperature.[101] It is suggested that the crystallisation temperature for PP in the blend studied herein without organoclay was highest because it was not influenced by the presence of EVA. However, when the organoclay compatibilised PP with EVA, the EVA did not phase separate from the PP matrix which caused a decrease in the PP crystallisation temperature. Therefore it is suggested that in this case the enhanced nucleation effect of the organoclay has been off-set by the EVA and is observed by the overall decrease in crystallisation temperature. The aforementioned paper found that the organoclay had the dominating effect but the influence of the additional polymer at higher loadings decreased the organoclay dominance, lending support to the theory proposed herein.

3.8 DSC for the PP-PS-Organoclay samples

Due to the small compositional differences between PP9/PS1/X/Y and PP7/PS3/X/Y and for the sake of brevity, only the PP7/PS3/X/Y composites shall be considered in this chapter. Figure 3.11 shows the data acquired that informed the decisions about the thermal treatments for the PP-PS-organoclay composites. The graph shows temperature plotted against the log of the time taken to crystallise and the data show a positive linear correlation. The PP7/PS3/0/Y samples took the longest to crystallise at any given temperature whilst the PP7/PS3/1/Y and PP7/PS3/3/Y samples crystallised in approximately the same time for each temperature.

Figure 3.11 was used in deciding a temperature to isothermally hold the samples at from the melt phase so that the crystallisation would create a variety of morphologies compared to the quenched samples. In practise, the length of time the sample is held in the melt was doubled so as to ensure crystallisation had occurred a technique used elsewhere.[10,84] At 125 °C, PP7/PS3/0/Q, PP7/PS3/1/Q and PP7/PS3/3/Q took 21.0, 5.5 and 7.0 minutes to crystallise, respectively. At 130 °C the time had increased to be impractical whilst at 120 °C the crystallisation was deemed to be too quick that the morphology would not be significantly different from the quenched samples. Therefore, it was decided that the samples would be held at 125 °C for 40 minutes.

Figure 3.12 shows the crystallisation curves for the PPa/PSb/X/Q samples (though the nature of the thermal treatment from the melt phase was erased during the DSC experimental run). It can be seen that the crystallisation temperature is significantly

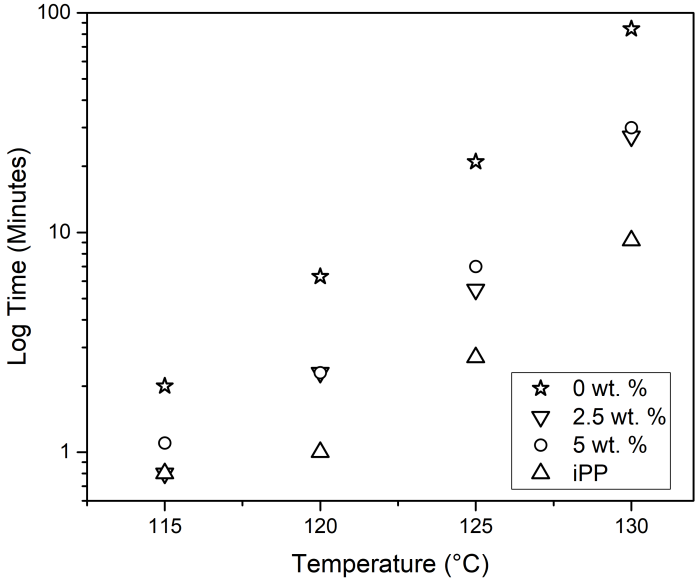

Figure 3.11: *Graph showing DSC data for PP7/PS3/X/Y samples used to decide the temperatures at which the thermal treatments should be conducted for the PP-PS-organoclay composites.*

lower for the sample without organoclay while the samples with organoclay crystallise at approximately the same temperature. This suggests that the organoclay had a nucleating effect causing the polymers to crystallise from the melt sooner than without the organoclay present.

The percent crystallinity of the PP7/PS3/0/Q, PP7/PS3/1/Q and PP7/PS3/3/Q samples was 51.7, 62.0 and 49.3 % respectively. These do not follow a trend nor are significantly different from each other.

Although publications exist on PP-PS-organoclay composites stating that the organoclay acts as a nucleating agent, they use the decrease in percent crystallinity as evidence since the temperature of crystallisation changed very little.[116,64] Herein, the opposite seems true but, nevertheless, it can be concluded that the organoclay had a nucleating effect on the polymer blend, albeit not a particularly strong one.

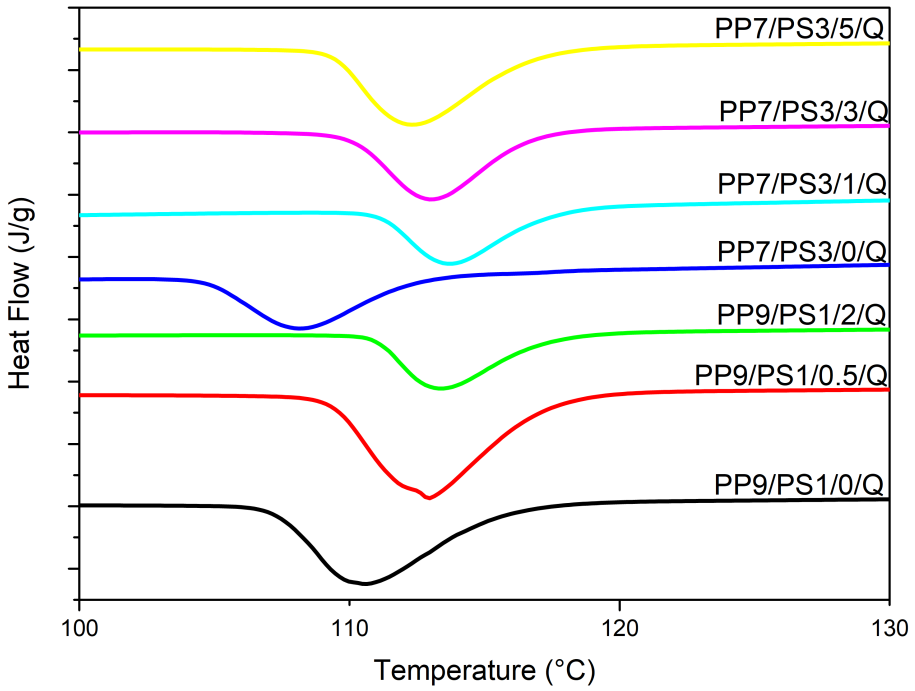

Figure 3.12: *Graph showing how the temperature of crystallisation changes with organoclay loading using the crystallisation curves from the PPa/PSb/X/Q samples.*

3.9 Conclusion

From this brief overview of the TGA results, a few general conclusions can be drawn.

Firstly, the organoclay increased the thermal degradation temperature in all three of the material systems studied. Furthermore, it was the PE-EVA-organoclay composites that achieved a sufficient dispersion for the samples to be deemed nanocomposites based on their performance under TGA.

The samples that were immersed in xylene showed evidence of solvent absorption on the TGA trace but it appeared that the overall degradation temperature of the sample was not affected.

More generally, it can be said that the solution blending protocol was reasonably successful in achieving the organoclay loadings desired.

From the DSC results, decisions about the crystallisation conditions were made for the PP-EVA-organoclay and the PP-PS-organoclay systems.

Although the percent crystallinity was calculated for each of the material systems, no significant difference or trends were seen in any of the systems.

The crystallisation temperature for PE in the PE-EVA-organoclay system increases

slightly with organoclay loading indicating some weak nucleating effect. By contrast, in the PP-PS-organoclay system the crystallisation temperature was clearly affected by the nucleating ability of the organoclay. However, the crystallisation temperature for PP in the PP-EVA-organoclay system is apparently unaffected by the nucleation effect of the organoclay and instead influenced by the EVA (made possible by the compatibilising effect of the organoclay).

This insight into the filler dispersion and nucleating effect will be built upon by the forth coming results from XRD and SEM before being used to interpret the dielectric results.

Chapter 4

Observing the Organoclay in the Composites

This chapter will detail the results of the investigations specifically performed to observe and analyse the organoclay in the composites: FT-IR spectroscopy and XRD.

FT-IR data on the dried samples was used for two purposes. Firstly, it was used to determine whether the isothermal cooling or the drying process had oxidised the surface of the films by looking for a change in the wavenumber regions where one would expect an oxidised group to appear. While secondly, the incorporation of the organoclay can be assessed by the appearance of a peak at 1075 cm^{-1} corresponding to the Si-O group.[31]

XRD at low angles was used to look at the polymer intercalation of the clay layers. Even though this chapter is dedicated to considering the organoclay, some XRD results are also presented for the 2θ range 10 - 25 $^{\circ}$ since this region gives an insight to the crystal structure of the polymer matrix and this can be affected by the organoclay loading and thermal treatment.[142,127]

PP exhibits polymorphism, meaning it can crystallise into more than one crystal form. These crystals can co-exist within a sample. The type and size of crystal growth will be influenced by the organoclay acting as a nucleating agent and also the thermal treatment of the material from the melt phase (including the length of time in the melt phase and the time taken to pass through the crystallisation temperature).[96,123] The interface between these phases significantly influence the physical properties of the composite.[143] β-PP exhibits a higher impact resistance and ductility but lower density, yield and elastic modulus than α-PP.[48,70] Since the properties determined by the crystal structure (including density and ductility) can also influence the electrical performance of the material, it is important to understand the nature of the crystalline form of PP present in the samples - this can be determined using XRD analysis.

4.1 Experimental Techniques

The processing of the PE-EVA-organoclay, PP-EVA-organoclay and the PP-PS-organoclay composites are detailed in Chapters 2.1.1, 2.1.2 and 2.1.3 respectively. Chapters 2.3.3 and 2.3.2 detail the FT-IR and XRD techniques used herein, respectively.

Comparing the interlayer distance (or d-spacing) of the organoclay is a method of comparing intercalation and therefore assessing the compatibility of the system. The equation for calculating the d-spacing (Bragg's law) is given in Equation 2.4; see Chapter 2.3.2 for details.

Comparing the average crystallite size can be a useful method for comparing the influence of organoclay on the polymers. The equation for calculating the average crystallite size (the Scherrer Equation) is given in Equation 2.3; see Chapter 2.3.2 for details.

4.2 FT-IR: Confirming the Incorporation of Organoclay

FT-IR data acquired in ATR mode from dried films of PE/EVA20/X/Q, PP/EVA9/X/Q and PP7/PS3/X/Q are shown in Figures 4.1 and 4.2 and 4.3, respectively. The data confirm both that no oxidation has occurred during sample processing and that the organoclay has been incorporated (highlighted by the respective insets) across all the material systems. This means that the sample processing conditions were appropriate - they did not introduce another variable that would influence the dielectric properties.[69]

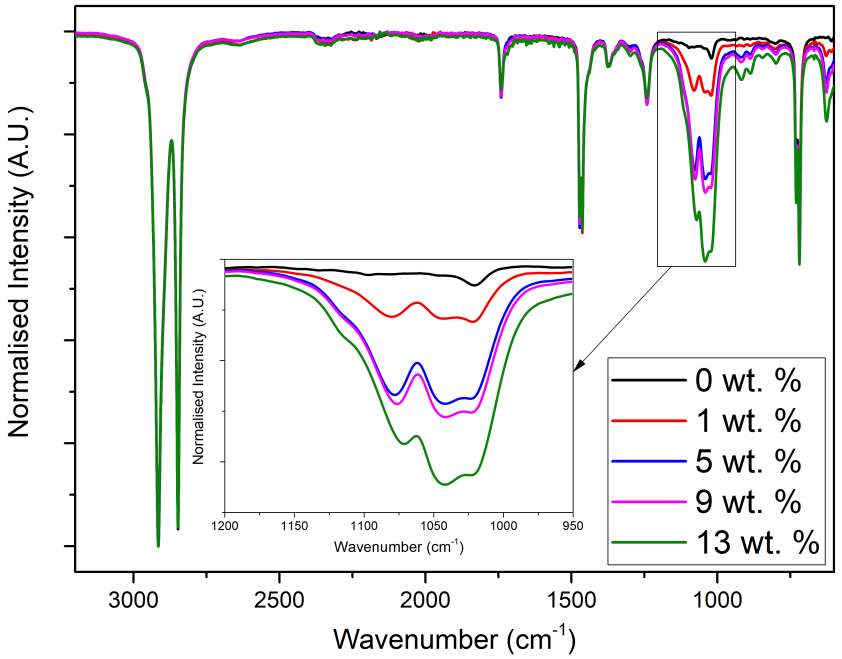

Figure 4.1: *Graph showing FT-IR data of PE/EVA20/X/Q samples with no evidence of oxidation while the inset highlights the evidence of the successful addition of the organoclay.*

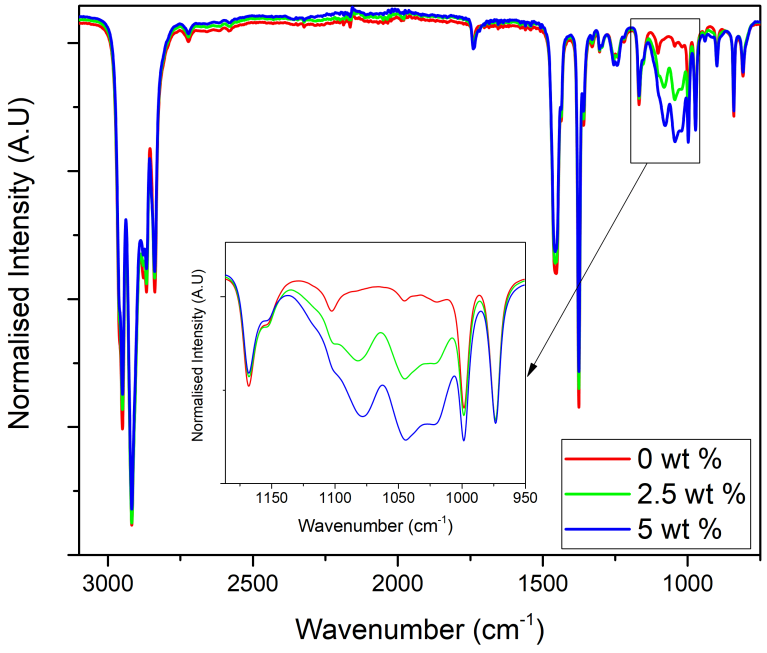

Figure 4.2: *Graph showing FT-IR data of PP/EVA9/X/Q samples with no evidence of oxidation while the inset highlights the evidence of the successful addition of the organoclay.*

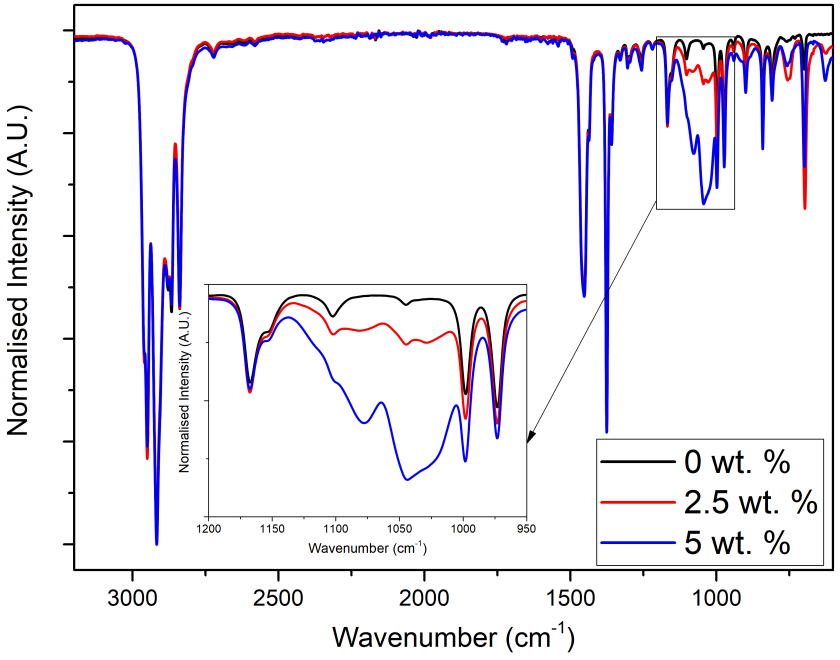

Figure 4.3: *Graph showing FT-IR data of PP7/PS3/X/Q samples with no evidence of oxidation while the inset highlights the evidence of the successful addition of the organoclay. The PP9/PS1/X/Y samples have been omitted for brevity.*

4.3 XRD for the Single Polymer-Organoclay Composites

The data presented in this chapter should be viewed as preliminary to the results of two polymers mixed with the organoclay, which will be presented later in this chapter. As such, discussion about the organoclay trace will be detailed later.

As frequently reported upon,[138,31,120] if the organoclay is incorporated into a polymer and the chains are compatible, intercalation will lead to a shift in the d_{001} peak to lower angles corresponding to an increase in interlayer distance. However, Figure 4.4(a) shows only a marginal increase of the interlayer distance of the organoclay in the composites, which suggests limited intercalation and implies relative incompatibility between the organoclay and polymers. This, in turn, will seriously hinder the ability of the polymer to disperse the organoclay throughout the matrix.[31,120] The differences seen between PS/5 and PP/5 are not surprising given that, when studying composites made with the same organoclay as used herein, Cho *et al.*[120] found, using XRD analysis, that organoclay had a higher compatibility to PS than PP. Amongst the single-polymer clay composites, the most significant increase in interlayer distance from the pristine organoclay was seen for the PS/5 composite.

Figure 4.4(b) shows the region where peaks relating to the polymer can be seen. The traces obtained were as expected for the unfilled polymers of PE,[49] PP[101] and PS.[144]

The composites show shifts in the polymer peaks towards lower angles compared to their respective unfilled counterparts. It is suggested that this is a result of the polymer-organoclay interaction creating a pseudo solid-solution, wherein only the unit cell size of the polymer is increased - the crystal structure of the polymer does not change. Although a shift to lower angles implies an increase in unit cell size,[145] there is nothing in the literature to suggest that a change in the unit cell size alone constitutes to significant changes to the physical, macroscale properties of the material. Furthermore, the additional peaks seen in the composites, highlighted by the arrows, are a result of the organoclay.[144]

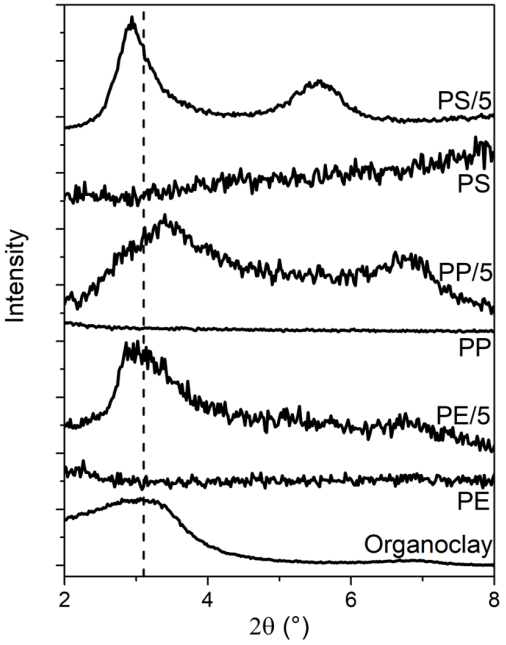

(a)

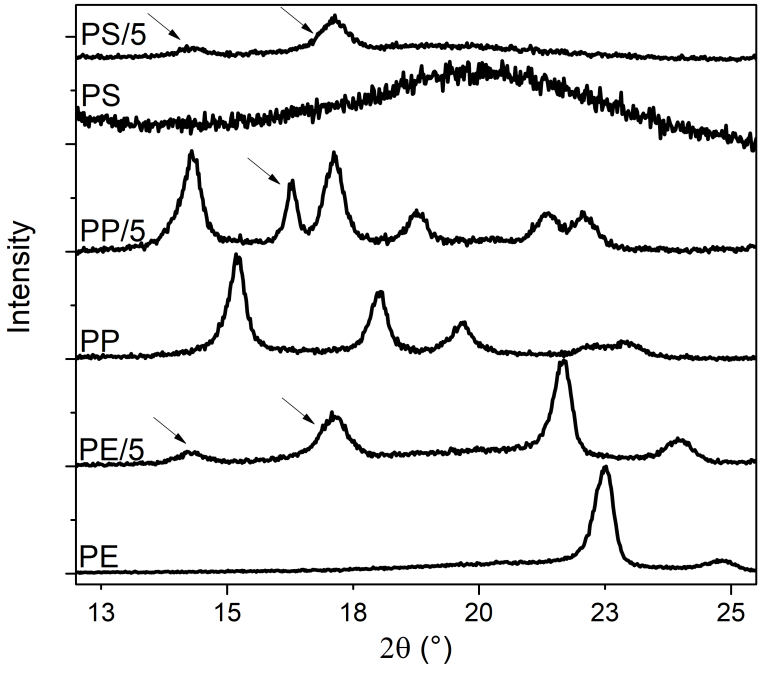

(b)

Figure 4.4: *Normalised XRD data of the (a) clay and (b) polymer regions for the single polymer-organoclay composites.*

4.4 XRD for the PE-EVA-Organoclay Composites

Figure 4.5 compares XRD data obtained from the PE/EVA9/X/Q sample set and pristine organoclay; the vertical line in this figure has been positioned to provide a marker to aid comparison of the data. First, the pristine organoclay can be seen to be characterised by a broad peak with a maximum at $2\theta = 3.1^\circ$; crystallographically, this corresponds to the interlayer periodicity within the organoclay and is, conventionally, represented d_{001}.[58,146] Here, this peak corresponds to a basal spacing of 2.8 nm, a result that is in line with expectations.[147,49] Second, as anticipated, the unfilled PE/EVA9/0/Q exhibits no diffraction peaks in the angular range shown, since it contains no organoclay. As such, any diffraction features seen in the following nanocomposites must be related to the state of the included organoclay which, from the data presented, is characterised by two diffraction peaks, one which falls between $2\theta = 2.5^\circ$ and $2\theta = 3.0^\circ$ and a smaller feature between $2\theta = 5.0^\circ$ and $2\theta = 6.0^\circ$.

The former peak occurs at the lowest diffraction angle for PE/EVA9/1/Q, which indicates an increase in the interlayer spacing from 2.8 nm seen in the pristine clay to 3.4 nm. Increasing the organoclay loading leads to a general reduction in the measured value of 2θ for this diffraction peak, indicating a general reduction in the interlayer spacing and hence intercalation. For example, the peak maximum at $2\theta = 2.8^\circ$ in the data obtained from PE/EVA9/9/Q corresponds to an interlayer distance of 3.1 nm. For organoclays, the interlayer distance is determined by both the organic components of the clay and the degree of intercalation of polymer chains between the clay layers[31,49,148] and, therefore, the data suggest that the degree of intercalation in the systems is higher for the lower organoclay loadings. Behradfar *et al.*,[149] Mahmoudi *et al.*[55] and Zanetti *et al.*[53] all showed that intercalation in systems based upon PE and an organoclay is mediated by the presence of EVA. Elsewhere, Liang *et al.*[150] showed that intercalation could be enhanced by grafting polar moieties into the PE structure - maleic anhydride in this case; the key finding being that the presence and concentration of the compatibilising agent is influential in the intercalation process. Wu *et al.*[116] found similar results upon varying the organoclay concentration however they used entirely different polymers and offered no substantial explanation for their results. We suggest that our results can be readily interpreted in the context of the aforementioned published work. That is, at higher organoclay loadings, the ratio of polar compatibilising moieties to organoclay is lower (the equivalent of decreasing the compatibilising agent concentration), such that the capacity for enhanced intercalation is reduced.

The data obtained from the organoclay show an additional small and broad peak around $2\theta = 6.8^\circ$, within an angular range that is twice that of the principal d_{001} peak. This is consistent with data from four MMT-based organoclays published by Araujo *et al.*[31] In view of this, the origin of the feature located between $2\theta = 5.0^\circ$ and $2\theta = 6.0^\circ$ in each of the composites is, similarly, most reasonably associated with second order scattering

(d_{002}) from the layered structure of the clay, albeit that its intensity appears to increase somewhat at higher loading levels. Although such second order scattering features have not universally been reported for MMT-based nanocomposites,[55,149] this interpretation is consistent with published work relating to the same organoclay as used here in a HDPE-organoclay nanocomposite compatibilised by grafted maleic anhydride.[49]

The variations in scattering behaviour described above are reflective of varying degrees of ordering within the systems. The presence of the d_{002} peak in all the data sets shown in Figure 4.5 is indicative of the presence of extensive organoclay tactoids, while the variations seen in both the d_{001} and d_{002} diffraction peaks imply variations in basal spacing and degrees of intercalation. Also, it is conceivable that some extraction of the bulky quaternary ammonium salts from the organoclay galleries may occur during solution processing; although this phenomenon has previously been reported to result from mechanical forces experienced during mixing in the melt phase,[55,149] a search of the literature found no reports of any comparable effects resulting from processing in solution.

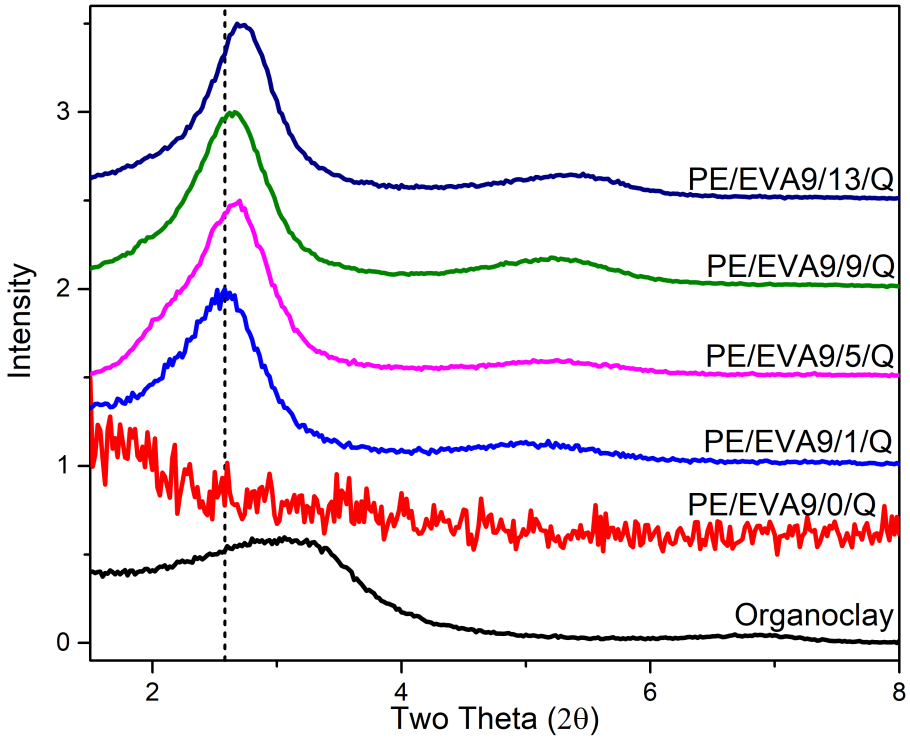

Figure 4.5: *Graph showing the changes in the interlayer distance seen in the PE/EVA9/X/Q composites compared to pristine organoclay.*

4.5 XRD for the Xylene Immersion tests

The changes to the organoclay in the composite following xylene immersion and subsequent removal were studied using XRD. Figure 4.6 shows XRD results from the dried, immersed and re-dried composites compared to pristine organoclay. The results are discussed in the context of the other xylene immersion tests in Chapter 7.

In the case of PE/EVA9/5/D, the d_{001} peak from the pristine organoclay is displaced to lower angles of around $2\theta = 2.5^\circ$, indicating a basal spacing, d_{001}, of 3.5 nm, which is expanded compared to the organoclay, and as expected from published literature.[49,148] The peak of PE/EVA9/5/I, around $2\theta = 2.1^\circ$, indicates a further increase in the basal spacing to 4.2 nm, which can be attributed to diffusion of the xylene into the system as a consequence of favourable thermodynamic interactions,[151,1] and causing swelling of the organoclay.[152]

Comparison of PE/EVA9/5/D data with those obtained from PE/EVA9/5/R reveals that the position of the d_{001} scattering is displaced to a higher angle in PE/EVA9/5/R. This indicates a reduction in interlayer periodicity to about 2.6 nm, and implies that the xylene immersion has caused some permanent physical change to the structure. In light of published literature showing that an organoclay was preferentially intercalated by EVA in a PE-EVA blend[149] and that EVA can be extracted from a PP/EVA blend by a solvent similar in nature to xylene,[21] the above changes can, *in toto*, be interpreted as follows. During immersion, swelling of the organoclay by xylene occurs in parallel with extraction of a fraction of the organic intercalants (EVA and/or a fraction of the amphiphilic compatibiliser), such that the interlayer periodicity increases. However upon removal of the solvent during the subsequent drying process, the interlayer distance decreases and becomes smaller than before the xylene treatment.

In the XRD data obtained from PE/EVA9/5/D and PE/EVA9/5/R, a weak and broad second peak ($2\theta = 5.0^\circ$ and $2\theta = 5.9^\circ$ respectively) can be seen located at close to twice the scattering angle of their respective d_{001} peak. Such features have been reported in previous studies and associated with second order scattering from the smectic structure of the clay. Therefore these peaks were similarly considered to be the d_{002} peak.[31] Similarly, and since the graph for the PE/EVA9/5/I sample has effectively been shifted to the left, within the 2θ range investigated both the d_{002} and d_{003} peaks can be seen at $2\theta = 4.3^\circ$ and 6.7° respectively; suggesting long range order of the intercalated clay structure.[153,65] Significantly though, d_{002} scattering in PE/EVA9/5/I appears to be weak and therefore present only in small amounts, indicating a greater degree of disorder when the clay is swollen with xylene.

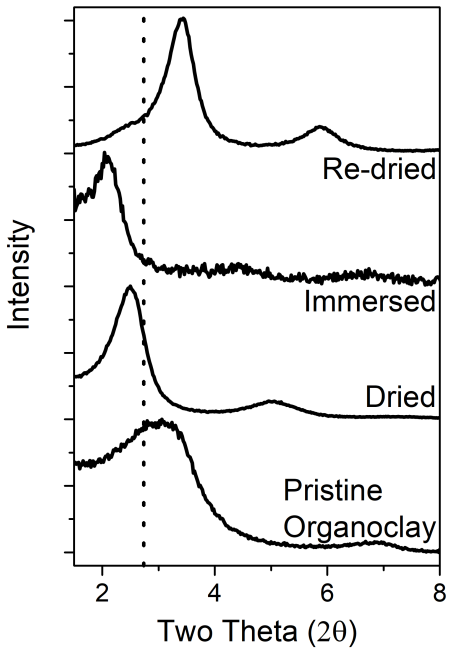

Figure 4.6: *Graph showing the changes in the interlayer distance seen in the PE/EVA9/5/Y composites compared to pristine organoclay and off-set for clarity, at the various stages of the xylene immersion tests.*

4.6 XRD for the PP-EVA-Organoclay Composites

XRD data from the PP/EVA9/X/Y samples of the three different thermal treatments are presented in Figure 4.7. These data were used in the Scherrer equation (Equation 2.3) to determine the average crystallite size of the PP in each sample to investigate the link with the thermal treatment. Although the Scherrer equation gives the dimension of the crystal in the direction perpendicular to the reflecting plane, herein it was assumed that there is enough random orientation in the matrix that the stated crystal length is essentially the average length. The results from the Scherrer equation applied to the peak at $2\theta = 17\,^{\circ}$, highlighted by the box, are shown in Table 4.1. This peak was chosen since it is the only peak representing a single phase. PP is polymorphic, although the alpha (monoclinic) phase is the most common. Thermal treatments and nucleating agents give rise to several crystalline phases at different relative concentrations, including α (monoclinic), β (hexagonal), γ (triclinic) and δ (smectic).[48,127,154]

The results reveal that samples had a larger average crystallite size when isothermally cooled compared to being quenched. This can be understood as the quenched samples have the shortest time to crystallise (and hence the shortest time in which to phase separate) and so form the smallest regions of pure polymer, meaning these samples had the smallest crystallite size.

The PP/EVA9/X/iso135 samples show a smaller average crystallite than the

Sample	Average Crystallite Size (Å)
PP/EVA9/0/Q	124
PP/EVA9/0/iso120	221
PP/EVA9/0/iso135	190
PP/EVA9/2.5/Q	139
PP/EVA9/2.5/iso120	200
PP/EVA9/2.5/iso135	194
PP/EVA9/5/Q	134
PP/EVA9/5/iso120	218
PP/EVA9/5/iso135	180
PP, quenched	203

Table 4.1: *Results from the Scherrer equation applied to the peak from the α-phase at 2θ = 17 ° for PP and PP/EVA9/X/Y composites and quenched PP. The results have an accuracy of approximately ± 10 Å*

PP/EVA9/X/iso120 samples. This is surprising given the former had longer in the melt phase allowing more phase separation to occur. Therefore, the origin of these results must lie in the interplay between length of time in the melt phase and the length of time of crystallisation. Establishing which has a stronger influence on the results presented herein requires further work, involving varying the crystallisation times and temperatures.

The average crystallite size of quenched PP is larger than the PP/EVA9/X/Q samples. This comparison clearly reveals that both EVA and organoclay disrupt crystallite growth, limiting crystallite size. This is unsurprising given literature published elsewhere on a PE-EVA blend[16] and a PE-organoclay composite.[78]

Figure 4.7 shows a representative selection of the XRD results obtained for the PP-EVA-organoclay composites compared with pure PP that was quenched from the melt phase. The box in Figure 4.7 highlights evidence for the formation of the β (hexagonal) phase, present only in the materials quenched from the press.

Since the results show no difference between the PP and the unfilled PP-EVA blend, it can be concluded that the EVA does not nucleate or promote an alternative crystalline structure. This is likely due to the relatively small proportion that the EVA comprises and the fact that the crystallisation temperature of EVA is around 30 °C lower than that of PP.

The presence of the β-phase only in the quenched samples is likely because there is a temperature gradient during nucleation - the sample crystallises whilst cooling whereas the other samples were held isothermally during crystallisation.[155]

Crystalline phases infer different properties to the material such as mechanical strength, conductivity and permittivity, which in turn can affect the electrical breakdown strength

due to the mismatch at interface boundaries.[101,154] Therefore these findings should be considered when seeking to understand the dielectric properties.

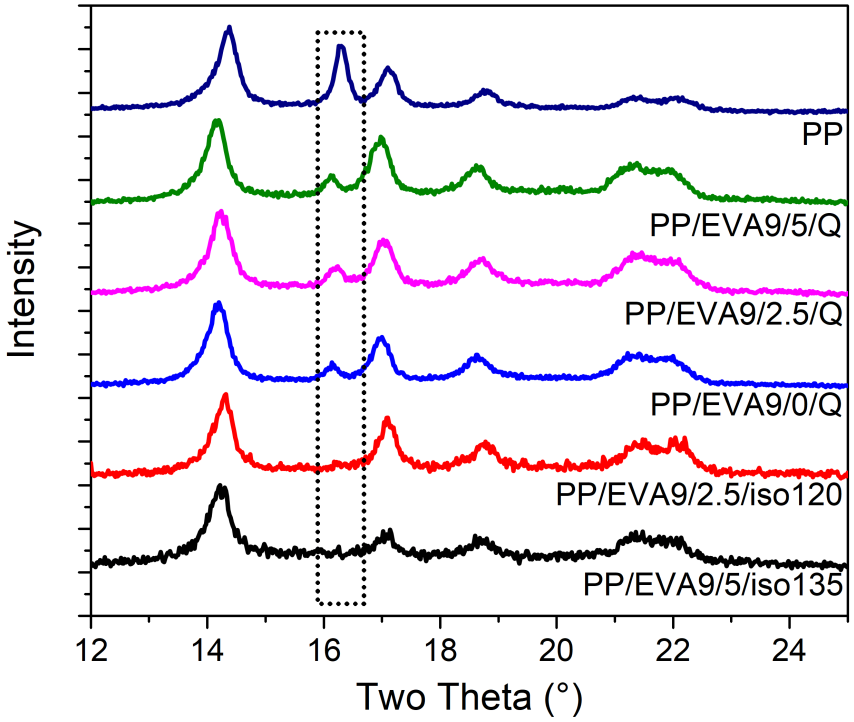

Figure 4.7: *XRD traces for the quenched (Q), isothermally cooled at 120 °C (iso120) and isothermally cooled at 135 °C (iso135) samples of PP/EVA9/X/Y and PP quenched from the press, off-set for clarity. The peaks highlighted in the box are the (300) reflection of the beta (hexagonal) phase. The peaks at 2θ = 14.2, 17.0, 18.7, 21.2 and 21.9 ° correspond to α-crystal planes (110), (040), (130), (131) and (041) respectively.*[48,156]

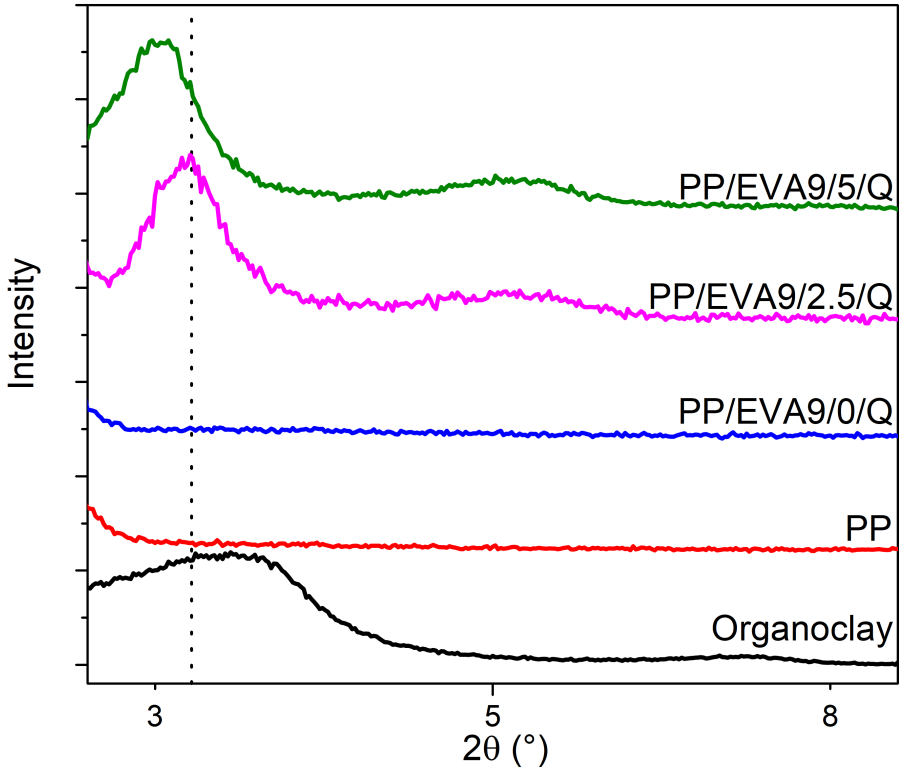

Figure 4.8: *XRD data of the clay region of the PP-EVA-Organoclay composites compared to pure PP and pristine organoclay*

Figure 4.8 shows data for three of the composites compared to pristine organoclay and pure PP from the XRD region where the organoclay can be observed. It can be seen that both the PP and the unfilled composite (PP/EVA9/0/Q) have no peaks in this region suggesting the peaks in the composites are solely due to the organoclay. Similarly to the PE-EVA-organoclay composites, the PP/EVA9/2.5/Q and PP/EVA/5/Q show both the d_{001} and d_{002} diffractions peaks seen in the pristine organoclay. Furthermore, as previously, the organoclay in the composites has an increased interlayer spacing compared to the pristine organoclay. Specifically, the interlayer spacing of the organoclay increased from 2.8 nm in the pristine specimen to 3.2 nm and 3.5 nm in the PP/EVA9/2.5/Q and PP/EVA/5/Q composites respectively. To highlight this, a dotted vertical line has been added to Figure 4.8. The increase in the interlayer distance with organoclay loading may be a result of the compatibilising effect of the organoclay being greater at the higher loading and therefore more polymer chains are able to intercalate with the clay.

4.7 XRD for the PP-PS-Organoclay Composites

Figure 4.9 shows the XRD traces of the PP7/PS3/X/Q composites while Figure 4.10 shows XRD traces for PP7/PS3/X/iso125 and PP7/PS3/X/iso40min composites. Figure 4.11 focusses only on the region specifically relevant to the organoclay.

The published literature on PP-PS-organoclay composites has presented XRD data focussed only on the low angles relevant to the organoclay. Therefore discussion on Figures 4.9 and 4.10 will rely on literature from other composites.

Since PS is an amorphous polymer, published XRD data reveals broad peaks around 2θ = 10 ° and 20 °.[157,67] However, neither of these peaks were seen in Figure 4.9, likely due to the low intensity of the peaks meaning they are lost in the background noise compared to the crystalline, high intensity peaks caused by the PP. The peaks observed for PP7/PS3/0/Q in the 2θ = 13 - 25 ° region are all due to the α-crystal of PP.[156,48,127]

Figure 4.9 also shows the presence of the β phase, highlighted by the arrows, in the quenched PP, PP7/PS3/3/Q and PP7/PS3/5/Q. However, Figure 4.10 shows the PP7/PS3/X/iso125 and PP7/PS3/iso40min samples do not have the β phase.

Since the β phase forms in quenched PP, the absence of this phase from certain samples implies that the presence of PS and organoclay affects the crystallisation of PP under certain conditions. Namely, when the samples were isothermally crystallised from the press, and when the quenched samples contained little or no organoclay. These results are similar to the PP-EVA-organoclay composites, which also show the formation of the β-phase exclusively in the quenched samples. The reason behind this occurrence can be similarly ascribed to the temperature gradient during crystallisation.[155]

The literature concludes that MMT has an α-nucleating ability for PP. Indeed, many studies have tried to enhance β nucleation by altering the surface of the MMT or by including β-nucleators such as aryl amide-containing compounds.[158,159]
Medellin-Rodriguez *et al.*[160] found an MMT-based organoclay (different to that used herein) had a β-nucleating effect at 2 and 4 wt.% loadings but not at 6 wt.%. This discrepancy was ascribed to the extent of the exfoliated layers common only at the lower filler loadings. Although, the results presented herein cannot be used as evidence that organoclay has a β-nucleating ability, it can be said that the presence of organoclay does not preclude the formation of the crystal structure. Furthermore, since PP/EVA9/0/Q shows evidence of the β phase, the absence of this phase from PP7/PS3/0/Q implies that PS, at least to some extent, inhibits the β phase formation.

Another observation that can be drawn from Figure 4.10 is that the intensity of the peaks decrease as the organoclay loading increases within each of the thermal treatment sets. Since these data have been normalised, it is valid to compare the peak intensities. The intensity of the peaks can be related to the occurrence rate of a par-

ticular crystal plane. Therefore it can be said that as the organoclay loading increases, the occurrence of the crystal plane decreases, implying that the organoclay disrupts the crystal growth of PP. This phenomenon not occurring in the PP7/PS3/X/Q system can be rationalised since these samples, unlike the other thermal treatments, rapidly pass through the crystallisation temperature meaning effects of the organoclay on crystallisation are not felt.

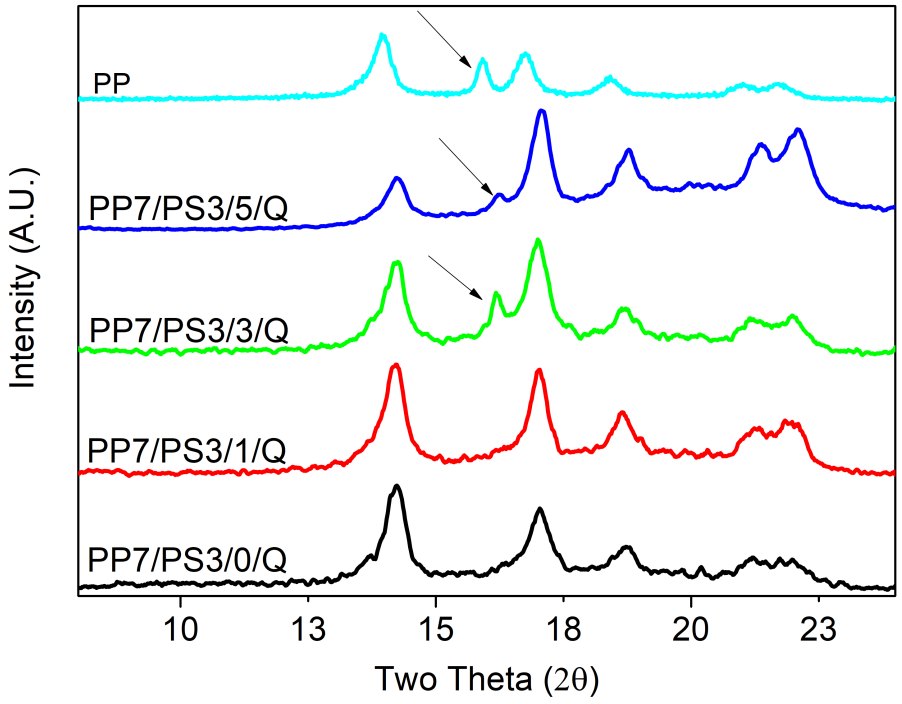

Figure 4.9: *Normalised XRD traces for quenched, pristine PP and PP7/PS3/X/Q, off-set for clarity. The peaks at 2θ = 14.2, 17.0, 18.7, 21.2 and 21.9 ° correspond to α-crystal planes (110), (040), (130), (131) and (041) respectively.*[48,156]

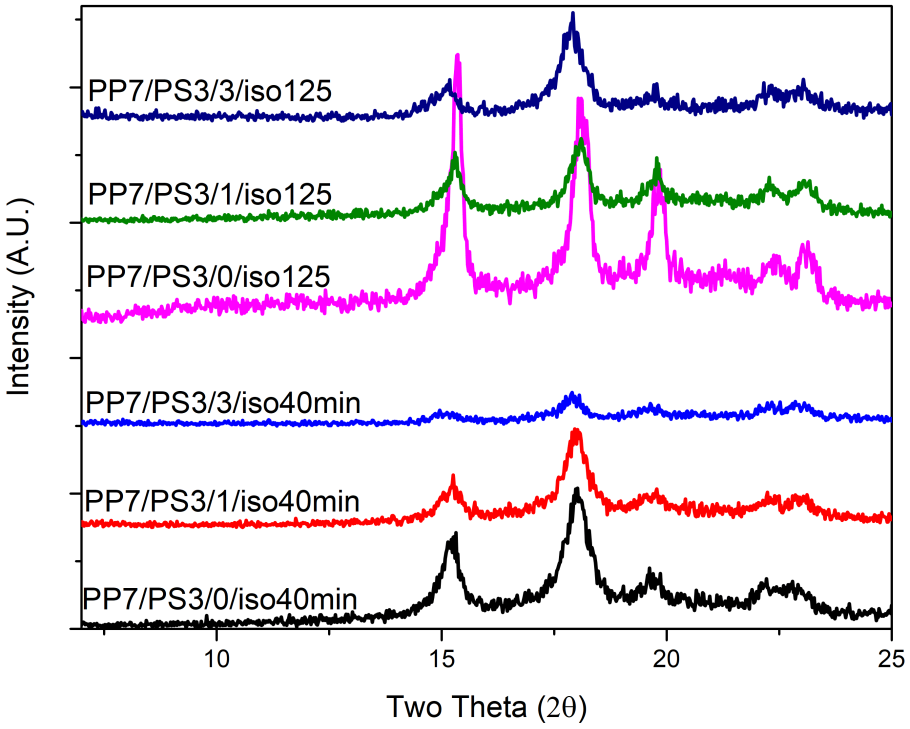

Figure 4.10: *Normalised XRD traces for PP7/PS3/X/iso125 and PP7/PS3/X/iso40min, off-set for clarity. The peaks at 2θ = 14.2, 17.0, 18.7, 21.2 and 21.9 ° correspond to α-crystal planes (110), (040), (130), (131) and (041) respectively.*[48,156]

Figure 4.11 shows the XRD traces of the PPa/PSb/X/Q composites compared to pristine organoclay. PP7/PS3/0/Q and PP9/PS1/0/Q show no peaks in this region since these do not contain organoclay.

The organoclay peaks in the composites appear shifted to lower angles compared to that of the pristine organoclay suggesting that the basal spacing was increased by the polymer matrix and implying that intercalation has occurred. Behradfar *et al.*[149] found that the intensity of the d_{001} peak became larger and shifted to lower angles when they added EVA (a polymer known to have good affinities to organoclays both in literature and reported herein) to LDPE-organoclay composites. They concluded that the introduction of this polymer means intercalation of the organoclay galleries occurs. It is suggested that an equivalent occurred with the PPa/PSb/X/Q composites.

The pristine organoclay contains a small, broad peak at approximately twice the angle of the broad d_{001} peak, which is consistent with published work on four other organoclays and can be labelled as the second reflection: the d_{002} peak.[31] The PP7/PS3/X/Q composites, unlike the PP9/PS1/X/Q composites, did not show a d_{002} peak. Additionally, peaks equivalent to those in the pristine organoclay appear in all of the composites except for PP7/PS3/1/Q. This, together with the peaks being less noisey and having a greater intensity count in the PP9/PS1/X/Q system, suggests that the organoclay in the PP7/PS3/X/Q samples had less long-range order than in the PP9/PS1/X/Q samples. It is suggested that this is a result of the latter having less amorphous PS, which would disrupt the long-range order of the organoclay crystalline structure.

Both PP7/PS3/X/Q and PP9/PS1/X/Q composites show an increase in interlayer distance from 2.8 nm to around 3.4 nm and around 3.2 nm, respectively. The similarity in the interlayer distance between the PPa/PSb/X/Q composites despite the PS loading changing, implies that PS has little affect on the interlayer distance - and therefore it is likely that PP is the primary intercalant of the organoclay layers. This is further supported by the PP9/PS1/X/Q samples - the samples with the lower PS loading - having a greater interlayer distance. This is surprising given the single polymer-organoclay work and suggests that the organoclay maybe influenced by the PP-PS interaction.

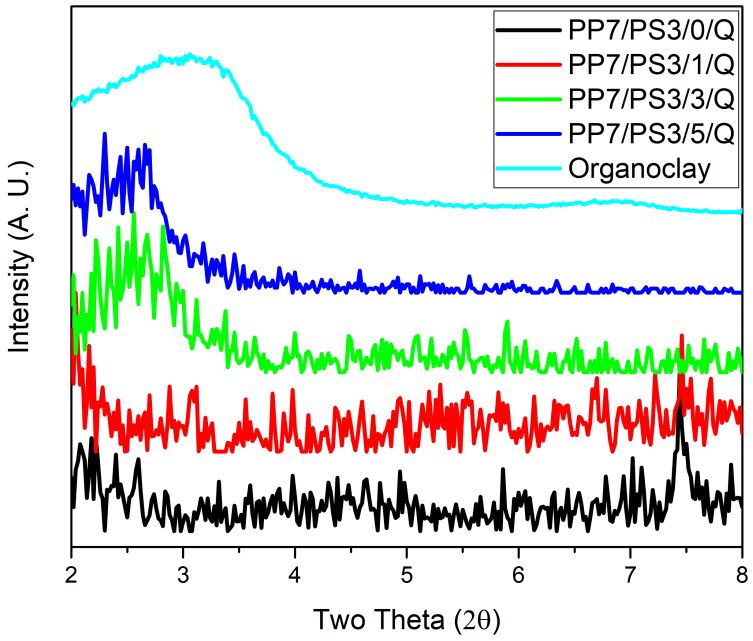

(a)

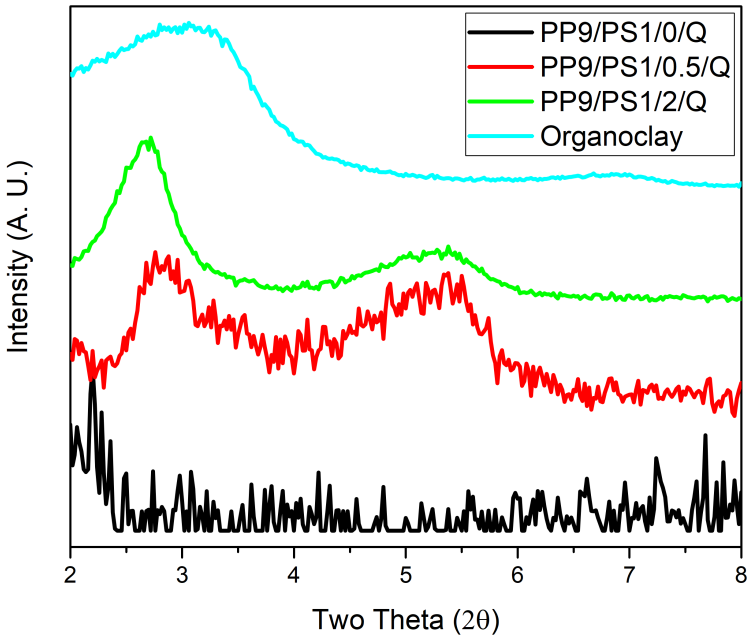

(b)

Figure 4.11: *Normalised XRD traces, off-set for clarity, zoomed to specifically study the region relevant to the organoclay for the PPa/PSb/X/Q composites.*

4.8 Conclusion

The presence of organoclay in the composites was observed successfully using FT-IR. Furthermore, FT-IR confirmed that the sample processing conditions did not cause oxidation of the samples, ruling out any possible influence on the dielectric properties.

By comparison the XRD data revealed much more: the crystal structures of the samples and the intercalation of the polymer matrix between the clay layers. Respectively, this gave an insight into the nucleation effects of the species in the composites and the compatibility of the matrix with the organoclay in terms of the dispersion achieved. A general summary of the conclusions follows:

Intercalation, and therefore interlayer expansion, was observed in the PE-EVA-organoclay, PP-EVA-organoclay composites and in the PP-PS-organoclay composites. Comparatively, the results suggest the organoclay was least compatible with the PP-PS matrix and was expanded most by the PP-EVA-organoclay composites.

The crystallite structure of PP was altered in both the PP-EVA-organoclay and PP-PS-organoclay composites by the thermal treatments from the melt phase. Specifically, only quenched samples showed evidence of the β-phase formation together with the α-phase whilst the isothermally treated samples showed exclusively the α-phase. However, in the PP-PS-organoclay system, samples containing 0 and 1 wt.% organoclay showed no evidence of β-phase formation, suggesting that PS and organoclay can influence the polymer crystallisation at certain compositional conditions. This, again, could be due to the compatibility between the polymer and organoclay resulting in differing nucleation and crystal growth disruption effects.

Together with the aforementioned TGA results, the organoclay addition was confirmed by FT-IR and XRD analysis. Furthermore, the TGA results viewed together with the XRD results continues to build an understanding of the organoclay dispersion, which will be further contributed to by the SEM micrographs in the next chapter.

Chapter 5

Imaging the Composites

This chapter will present and discuss the micrographs obtained from the SEM for samples investigated in this thesis.

5.1 Experimental Techniques

The processing of the PE-EVA-organoclay, PP-EVA-organoclay and the PP-PS-organoclay composites are detailed in Chapters 2.1.1, 2.1.2 and 2.1.3 respectively. The details of sample preparation for SEM and the SEM details are given in Chapter 2.3.4. In each case, an internal cross section of the sample was imaged so that artefacts from the pressing of the films would not interfere with the morphology being assessed.

The organoclay, being comprised of nano-platelets, appears in the micrographs as white flakes of around 10 μm. However, raised areas of the polymer morphology may also appear flake-like. Discerning between the two can sometimes be challenging however, a judgement can be made by looking at the micrograph as a whole and comparing whether:

- the area in question appears part of a larger pattern (and is therefore likely part of a polymer spherulite);
- similar structures occupy about the proportion of the micrograph would one expect for the filler loading of that particular sample;
- other areas of the micrographs appear to contain filler agglomerates (and therefore how likely it is that a comparatively well-dispersed flake is likely to be seen);
- other micrographs from the same sample and samples of different filler loadings, thermal treatments and even polymer ratios differ.

5.2 SEM of a single polymer with 5 wt.% organoclay

Before imaging the composites, it is necessary to gain an understanding of how, separately, each of the polymers interact with the organoclay. To this end, micrographs of PE, PP and PS are shown in Figures 5.1(a), 5.1(b), and 5.1(c) respectively. Furthermore, micrographs of PE-organoclay, PP-organoclay, EVA-organoclay and PS-organoclay are shown in Figures 5.2, 5.3, 5.4, and 5.5 respectively. In brief, these micrographs are consistent with the XRD results presented in Chapter 4.3. The organoclay can be seen throughout the SEM micrographs as white flakes. The dispersion can be assessed qualitatively by observing uniformity of the distribution and the size of the organoclay flakes.

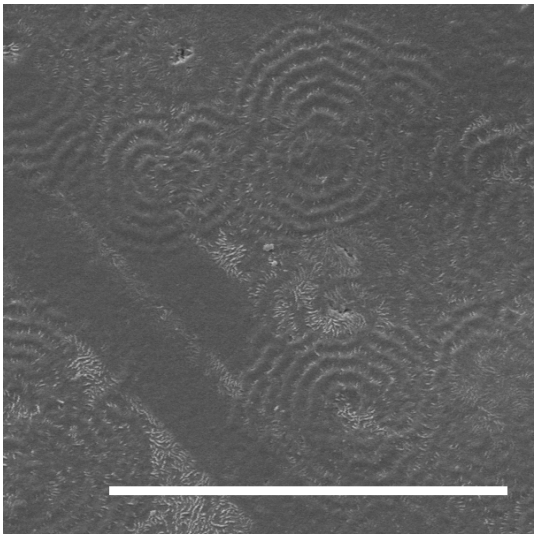

(a) PE Q

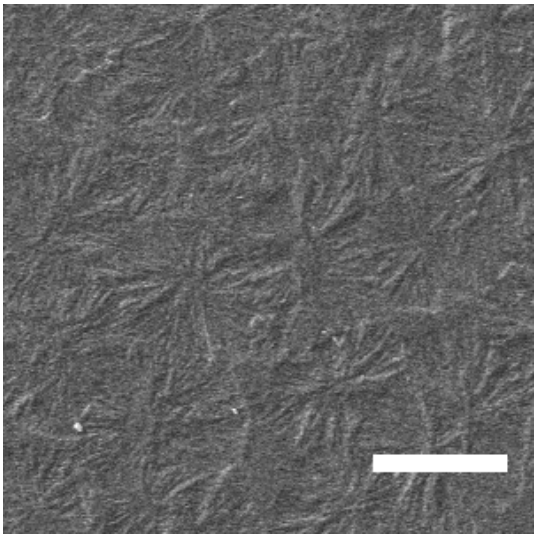

(b) PP Q

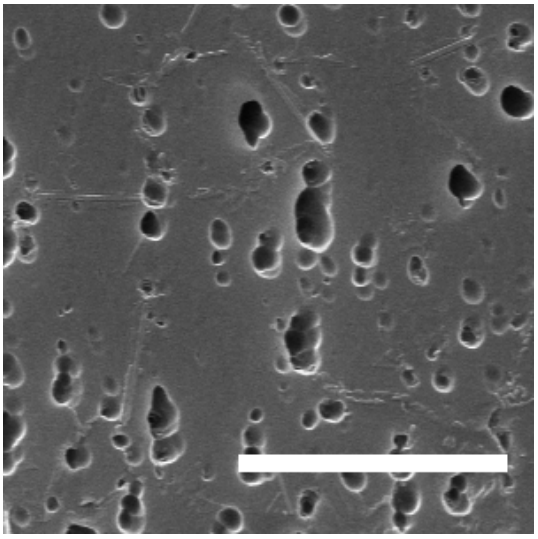

(c) PS Q

Figure 5.1: *SEM micrographs of the pure polymers PE, PP and PS. The scale bar represents 20 µm.*

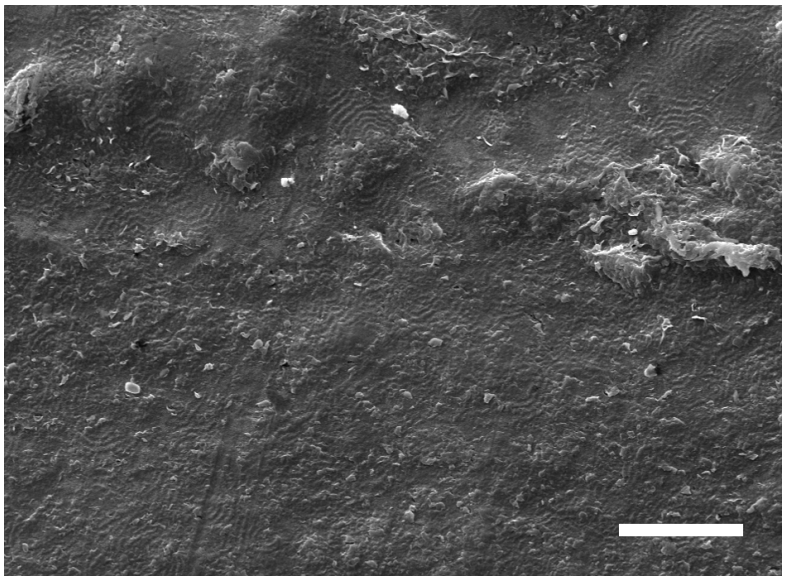

Figure 5.2: *SEM of PE/5/Q, scale bar: 20 µm.*

The SEM micrograph of pure PE shows extensive spherulite growth however the SEM micrograph of PE-organoclay (Figure 5.2) shows spherulites growing only in regions without organoclay, with the absence of spherulitic structures where the organoclay exists. This implies that the organoclay disrupts the spherulite growth, which is in line with the literature.[57] The micrograph also shows non-uniform dispersion throughout the polymer implying that there are some compatibility issues for this composite.

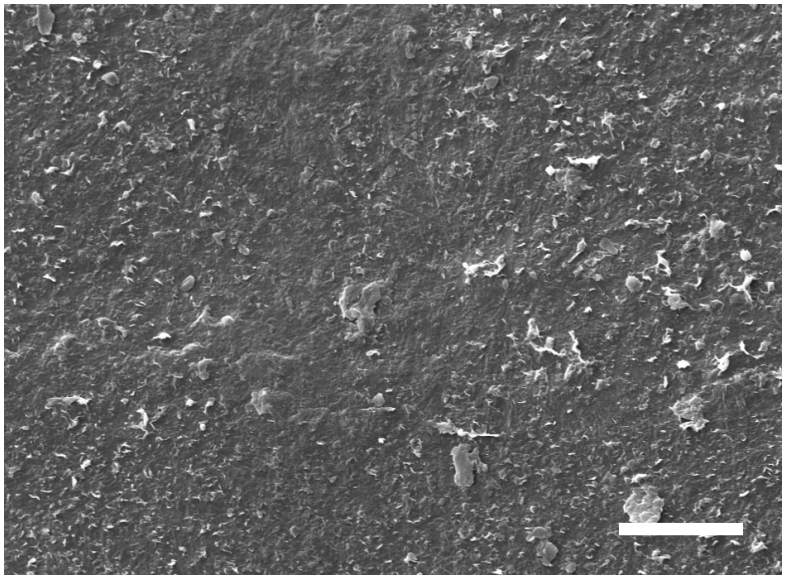

Figure 5.3: *SEM of PP/5/Q, scale bar: 20 µm.*

The PP-organoclay and EVA-organoclay (Figures 5.3 and 5.4 respectively) both show, despite aggregation, a uniform dispersion of organoclay and polymer matrices with no significant texture. They differ in the apparent depth of the etch, which is in line with the understanding that the etch is more potent to EVA than PP due to the polarity or

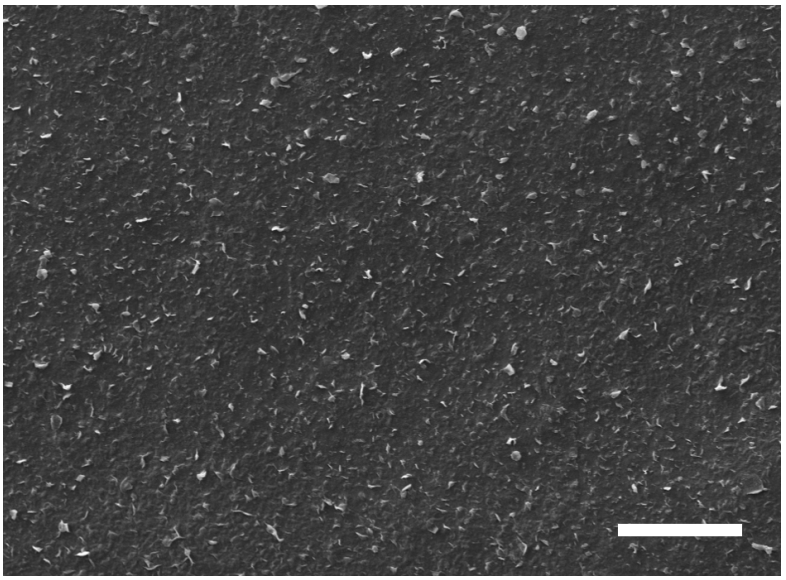

Figure 5.4: *SEM of EVA/5/Q, scale bar: 20 µm.*

crystallinity of the former.[54] The literature, and Figure 5.1(b) shows unfilled, quenched, isotactic PP has a spherulitic structure.[84] Therefore, similarly to the PE/5 composite, this implies that the organoclay disrupts polymer crystallisation by acting as a nucleating agent.[74] Due to the level of aggregation observed, it can be said that there are also some compatibility issues for this composite. On the other hand, the literature shows[161] that pure EVA does not have crystalline regions of spherulites so it is unclear how the organoclay is disrupting the crystal-structure of the EVA in Figure 5.4.

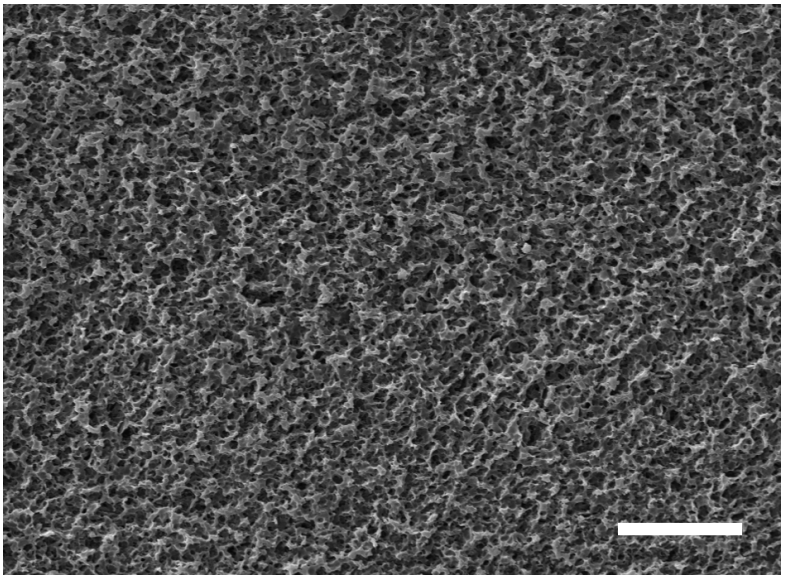

Figure 5.5: *SEM of PS/5/Q, scale bar: 20 µm.*

Figures 5.1(c) and 5.5, of pure PS and PS-organoclay respectively, show significant depth as if a large volume has been removed by the etching procedure. Although potentially difficult to compare due to there being very different preparation techniques before imaging, the porous structure of both is similar to that seen elsewhere.[162,163] The cause of the holes was not addressed in either of those papers though is possibly due to the processing conditions of the samples from the melt phase. This requires further investigations.

Both the filled and unfilled samples show an amorphous morphology expected for PS and both are homogeneous. The only difference is the extent of the holes being more significant in the PS/5/Q micrograph than the micrograph of the unfilled polymer. This suggests that the additional holes are either a result of the organoclay being removed from the polymer during the etching process or the organoclay changes the polymer chain movement and solidification. Determining which is the case would require producing samples using different cooling techniques and organoclay loadings to compare the morphology achieved.

5.3 SEM of PE-EVA-Organoclay Composites

The SEM micrographs shown in Figure 5.6 are a representative selection to describe the morphology observed in the PE-EVA-organoclay composites.

First, consider Figures 5.6(a), 5.6(b) and 5.6(c), which illustrate the effect of increasing the organoclay content in samples slowly crystallised (PE/EVA9/X/SC) and which, consequently, possess the most highly developed morphology. From Figure 5.6(a), it is evident that in the absence of any organoclay, crystallisation during slow cooling from the melt results in a well-developed spherulitic texture. Elsewhere,[123,164] equivalent structures have been shown to evolve in blends of HDPE and LDPE through the initial formation at relatively high temperatures of a framework of dominant lamellae composed, predominantly of the HDPE fraction of the system, followed by crystallisation of the LDPE (at a lower temperature) within the existing dominant lamellar framework. In the case of the PE/EVA blend shown here, there is no evidence of discrete EVA phases within the morphology, signifying miscibility between the EVA and the PE, such that crystallisation of the former occurs along with the LDPE within the HDPE-rich dominant lamellar framework. Adding the organoclay affects the observed morphology in two ways, as evinced in Figure 5.6(b) and 5.6(c) which, show PE/EVA9/5/SC to PE/EVA9/13/SC respectively. First, the spherulitic morphology becomes suppressed, which can be explained both through enhanced nucleation and inhibited crystal growth.[57] (This was also seen in Figure 5.2 where regions absent of organoclay had spherulites whereas areas with organoclay had a disrupted morphology.) Second, the clay, which is barely visible in PE/EVA9/5/SC becomes much more

apparent in PE/EVA9/13/SC. This is consistent with the TGA and XRD results presented previously.

Figures 5.6(d) and 5.6(e), show samples crystallised rapidly on quenching - this strategy being employed deliberately to limit morphological complexity with the polymer matrix. Comparison of the structure of PE/EVA9/1/Q and PE/EVA9/9/Q (Figures 5.6(d) and 5.6(e) respectively) reinforces the point made above concerning the tendency for increased organoclay agglomeration with increased loading level. Also, despite the system shown in Figure 5.6(d) only containing 1 wt.% of organoclay, no well-developed spherulitic texture is evident, an observation that is, presumably, a combination of both enhanced nucleation and rapid crystallisation, factors that inhibit the time and space available for spherulite growth respectively. Finally, Figure 5.6(f) shows the morphology of PE/EVA9/1/ISO which, despite being held in the melt for 3 h prior to quenching, exhibits a morphology that is equivalent to that of PE/EVA9/1/Q, which was quenched immediately after being formed. This supports the assertion made concerning miscibility of the EVA used here, since any significant degree of liquid/liquid phase separation would led to the formation of discrete EVA phase regions, which is not the case.

The absence of phase separation in the SEM micrographs highlights the effectiveness of the compatibilising nature of EVA in this composite. Since the ratio of PE to EVA was the same across all these samples, the changing morphology observed with organoclay loading cannot be ascribed to the presence of another polymer diluting the matrix causing disruption of polymer crystal growth. It can be seen that the introduction of the organoclay results in an apparently rather less well organised structure, consisting of fewer and smaller lamellar rings. Elsewhere, organoclay has been shown to inhibit the growth of extensive polymer crystals.[87] Together with the results from the DSC, it is proposed that the changes seen are a result of the changing crystallisation ability of the polymer in the presence of the organoclay, including the nucleating effect of organoclay on the polymer.

The presence of lamellae despite the organoclay is in agreement with a study on PE-organoclay nanocomposites which used organoclay loadings up to 4.5 wt.%.[57] Herein a decrease in the extent of the formation of spherulites with an increasing organoclay content was observed, particularly above 5 wt.%, possibly due to a change in the nucleating nature that the organoclay has at higher loadings - also seen in the DSC results. This further highlights the compatibilising nature of the EVA polymer in allowing such interactions between the organoclay and the PE.

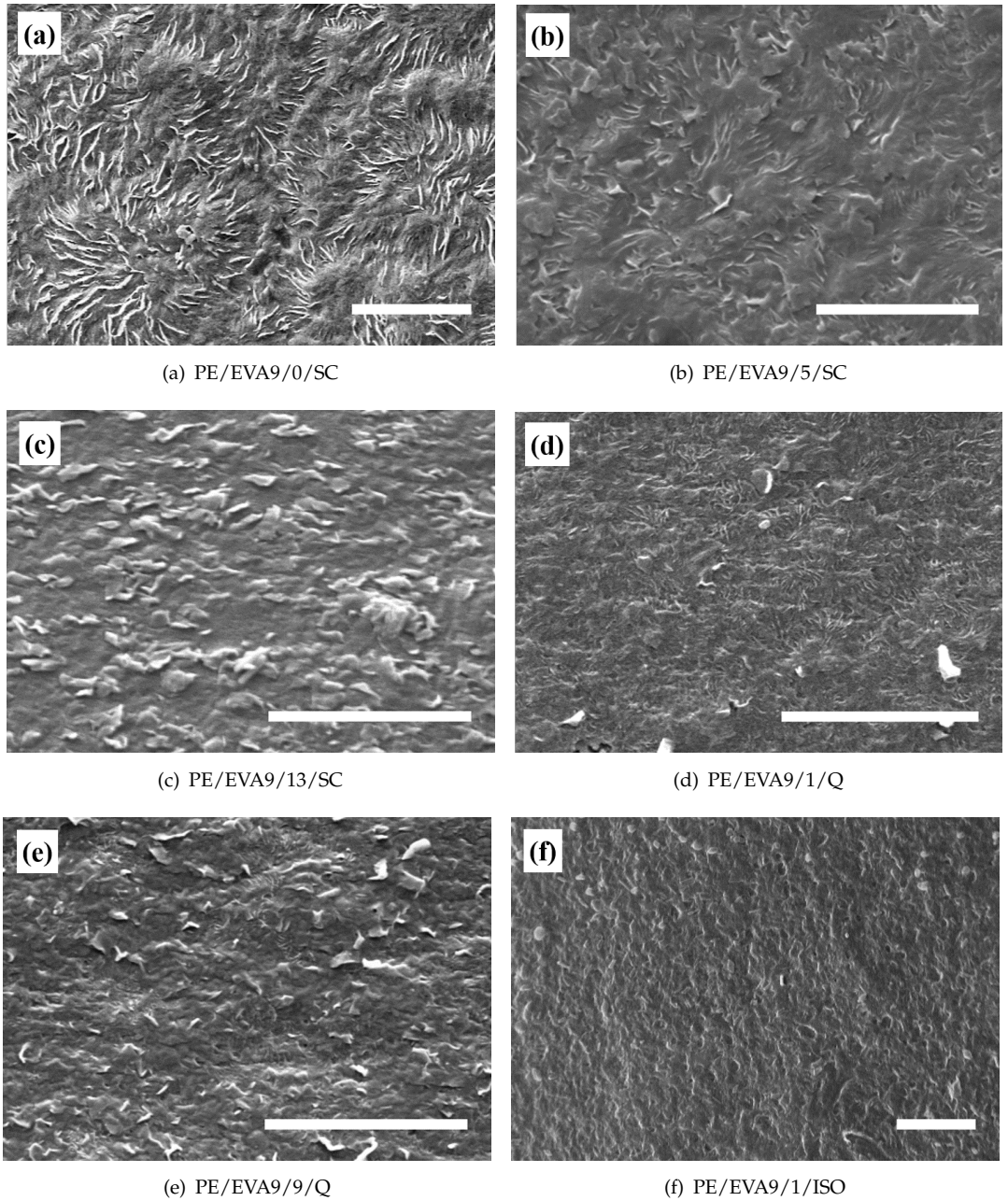

(a) PE/EVA9/0/SC

(b) PE/EVA9/5/SC

(c) PE/EVA9/13/SC

(d) PE/EVA9/1/Q

(e) PE/EVA9/9/Q

(f) PE/EVA9/1/ISO

Figure 5.6: *A representative selection of the SEM micrographs from the PE-EVA-organoclay composites, where the bar in each represents 10 µm.*

5.4 SEM of PP-EVA-Organoclay Composites

The SEM micrographs of the PP-EVA-organoclay composites are shown in Figure 5.7. The EVA copolymer is more susceptible to being removed by the etching process so the darker regions that appear to be sunken into the material represent areas where there was once EVA. The organoclay appears in the SEM micrographs as white specks protruding from the polymer surface. There is a clear difference in the morphology obtained from the different thermal treatments and organoclay loadings that will be discussed in more detail below:

Figures 5.7(a), 5.7(b) and 5.7(c) show PP/EVA9/0/Q, PP/EVA9/0/iso120 and PP/EVA9/0/iso135 samples respectively, that is, samples containing the polymer blend without organoclay under the three thermal treatments: quenched, isothermally crystallised at 120 °C and isothermally crystallised at 135 °C. The micrographs show that without organoclay, there is significant phase separation, which allows the PP to form spherulites and the EVA to coalesce to minimise interfacial area and therefore energy. The difference between the PP/EVA9/0/Q and PP/EVA9/0/iso120 samples is the size of the spherulites: in the former, the spherulites are smaller and have no obvious boundary line with the neighbouring spherulite. However, the PP/EVA9/0/iso135 sample shows no gap between the spherulites and deeper EVA regions. This suggests that the sample, having had longer in the melt phase, has formed larger spherulites and more EVA has coalesced meaning that larger gaps have been left following the etching procedure.

Considering the samples containing organoclay, the PP/EVA9/2.5/Q and PP/EVA9/2.5/iso120 samples (Figures 5.7(d) and 5.7(e) respectively) show no evidence of phase separation but some evidence of spherulites whereas the PP/EVA9/2.5/iso135 sample (Figure 5.7(f)) shows significant phase separation. In each of these samples, there are some small organoclay pieces. The PP/EVA9/2.5/iso135 sample appears to have the majority of the organoclay in the regions once containing the EVA, suggesting the organoclay has a chemical preference for this phase, which, from the literature, is as expected.[165,15] The PP/EVA9/2.5/iso135 sample shows phase separation, unlike the PP/EVA9/2.5/iso120 sample, this could be because at the higher temperature, the organoclay is less effective at preventing the polymer chain movement since the polymer would have more kinetic energy. In contrast to this, at a higher organoclay loading, in PP/EVA9/5/iso135 (shown in Figure 5.7(i)), there was no phase separation, suggesting that the increased organoclay could offset the increased polymer chain mobility at the higher temperature.

Figures 5.7(g), 5.7(h) and 5.7(i) show PP/EVA9/5/Q, PP/EVA9/5/iso120 and PP/EVA9/5/iso135 samples respectively, that is, the samples with the highest organoclay loading investigated. Unlike the other compositions, there is relatively little difference observed between the thermal histories. Neither phase separation nor spherulite

structures were seen. However, the organoclay is visible in bigger structures to that seen in the PP/EVA9/2.5/Y samples. Therefore it is believed that there is sufficient organoclay to prevent phase separation of the polymer blend, apparently regardless of the thermal treatments investigated.

Comparing Figures 5.7(a) and 5.7(g) highlights the compatibilising effects of the organoclay. Clearly, phase separation has occurred in the unfilled polymer blend, since the spherulitic morphology of the PP and the smooth, circular morphology of the EVA are distinct. This is in line with expectations, since incompatibility between PP and EVA has been reported elsewhere.[23] However, the micrograph of a cross section through PP/EVA9/5, suggests that, in the presence of the organoclay, phase separation of the polymeric constituents is prevented, or at least, markedly suppressed. Also, it appears that the organoclay has disrupted the crystalline morphology of the PP, inhibiting spherulite growth. Since the organoclay has been shown to be compatible, separately, with both PP and EVA matrices,[50] this suppression of morphological evolution could result from the retardation of chain movement by the organoclay[23] and/or by the clay acting to promote nucleation.[24] Elsewhere, Shafiee *et al.*[24] examined a PP-EVA-organoclay system and suggested that the EVA enhanced compatibility between the PP and the organoclay, leading to a morphology which, when imaged using SEM, appeared equivalent to Figure 5.7(g). In contrast, Goodarzi *et al.*[165] claimed that maleic anhydride grafting played a critical role in compatibilising their PP-EVA-organoclay system. This variation in interpretation may be related to the use of different PP and EVA ratios. Nevertheless, comparison of the micrographs in Figure 5.7 clearly demonstrates suppression of EVA phase separation in the presence of the organoclay.

At a later stage in this project work, when the significance of the organoclay loading effects was investigated further, PP/EVA9/0.5/Q was produced and imaged using SEM. The resulting micrograph, shown in Figure 5.8 fits in as expected to the trend displayed in Figure 5.7. Specifically, for the quenched samples, with the addition of organoclay, fewer and smaller spherulites are formed until, at 5 wt.% loading, no spherulites are observed. Along with this, phase separation is eliminated by a loading of 2.5 wt.% and greater. The suppression of both the phase separation and spherulite formation can be attributed to the organoclay suppressing chain movement, similarly to elsewhere.[101] Clearly, for the quenched thermal treatment, the lowest organoclay loading investigated (0.5 wt.%) is insufficient to achieve this, the 2.5 wt.% loading is able to suppress the phase separation but not the spherulite formation while the 5 wt.% loading achieves both.

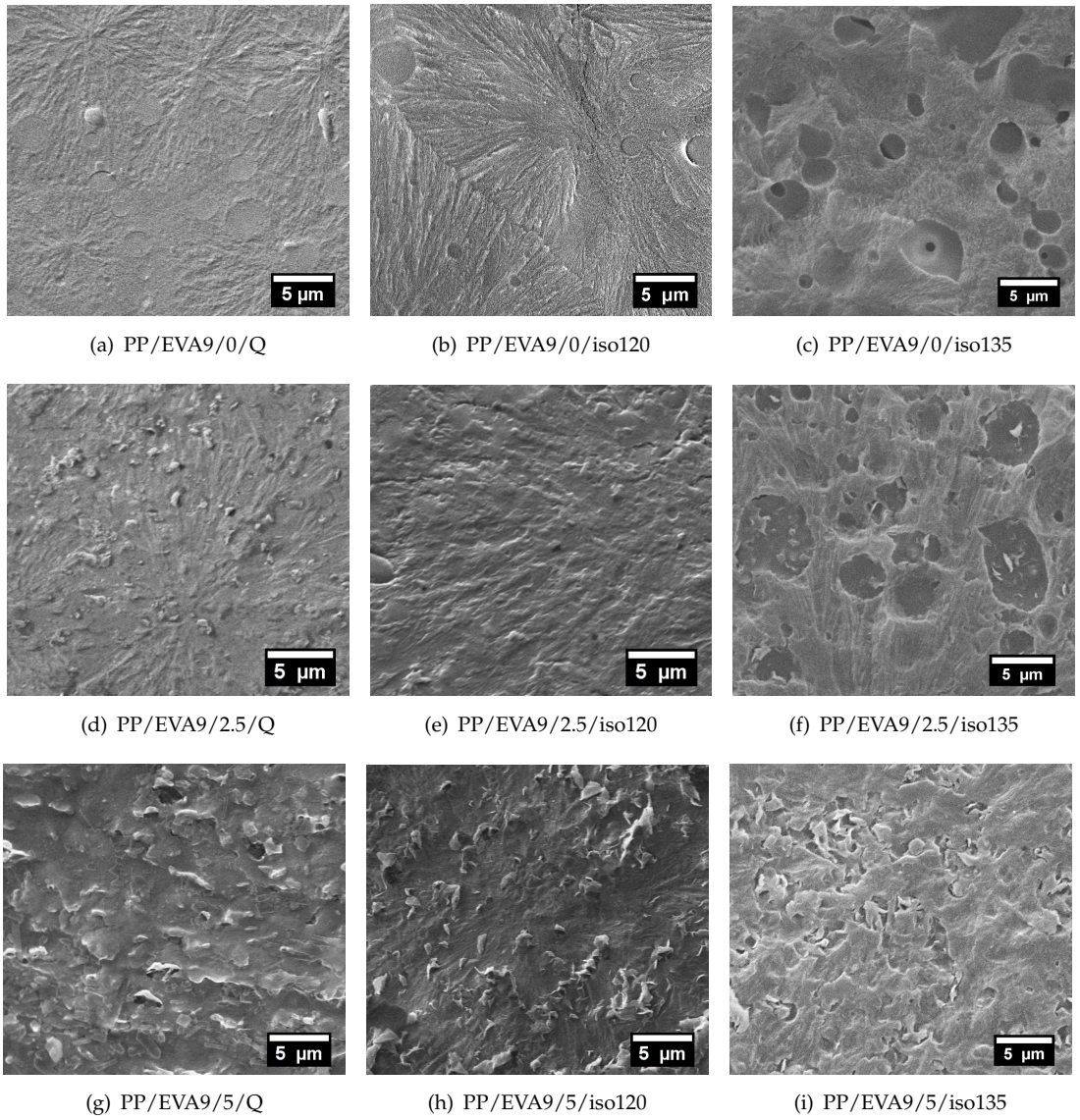

(a) PP/EVA9/0/Q (b) PP/EVA9/0/iso120 (c) PP/EVA9/0/iso135

(d) PP/EVA9/2.5/Q (e) PP/EVA9/2.5/iso120 (f) PP/EVA9/2.5/iso135

(g) PP/EVA9/5/Q (h) PP/EVA9/5/iso120 (i) PP/EVA9/5/iso135

Figure 5.7: *SEM micrographs of the PP-EVA-organoclay composites.*

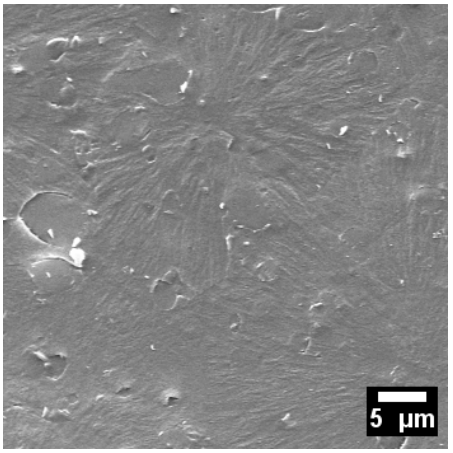

Figure 5.8: *SEM of PP/EVA9/0.5/Q.*

5.5 SEM of PP-PS-Organoclay Composites

Figures 5.9 and 5.11 show a representative selection of the SEM micrographs obtained from the PP7/PS3/X/Y composites while Figures 5.10 and 5.12 show a representative selection from the PP9/PS1/X/Y composites. Although in the literature solvents such as toluene,[26] dimethylbenzene[56] and tetra-hydro-furan[60] were used to chemically etch the PS out of the blend, herein the permanganate etching procedure was used, as for the other composites herein. Aided by the composition variations, (in comparing Figures 5.9 and 5.10), the single polymer-organoclay investigations, the micrographs of the PP-EVA-organoclay system, and the presence of the holes only in certain regions, it was determined that PP is more susceptible to the etchant than PS and that PS is the polymer that appears brighter in the micrographs.

Due to the immiscibility of the PP and PS polymers,[64,26] the phase separation of the PP-PS blend seen in Figures 5.9 and 5.10 was expected. Moving between the PP7/PS3/0/Q, PP7/PS3/0/iso125 and PPP7/PS3/0/iso40min micrographs the samples have had longer in the melt phase, resulting in the polymer domain size increasing (most clearly seen with the voids where the polymer has been etched away) since this allowed for more coalescence to occur.

It is clear that in PP7/PS3/0/Q, the time in the melt phase was insufficient for the polymers to flow into thermodynamically favourable spheres that would minimise the contact surface area with each other. The evolution of the spheres has begun in the PP7/PS3/0/iso125 sample, whilst in the sample with the longest amount of time in the melt, PP7/PS3/0/iso40min, the spheres are readily apparent.

The evolution of the spheres indicating the extent of phase separation is also apparent in the PP9/PS1/0/X samples. Also evident, is the more extensive spherulites, understood by there being less PS disrupting spherulite growth of PP than in PP7/PS3/0/Y. The apparent layering effect seen in Figure 5.10(a) is likely a result of a combination of: poor homogeneity of the crude material before the pressing procedure, the melt flow effects, and the quenching process not allowing enough time for mixing in the melt phase. These suggestions are supported by discussions following a conference presentation by Cavallini *et al.*[166] and in the literature,[167] though the precise cause in this case would require investigating further mixing ratios and thermal treatments.

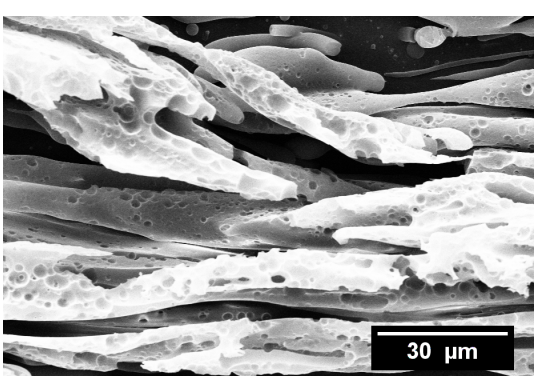

(a) PP7/PS3/0/Q

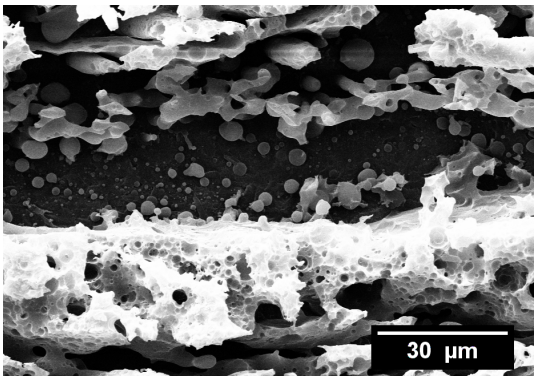

(b) PP7/PS3/0/iso125

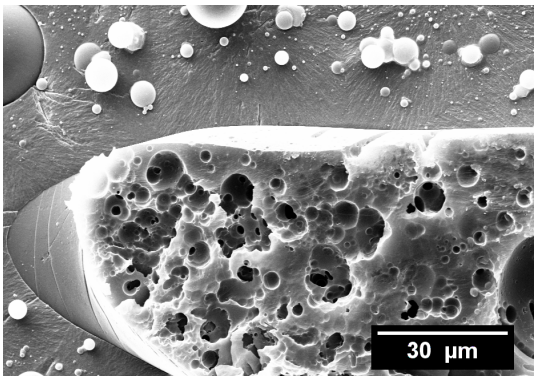

(c) PP7/PS3/0/iso40min

Figure 5.9: *SEM micrographs of the PP7/PS3/0/Y blends.*

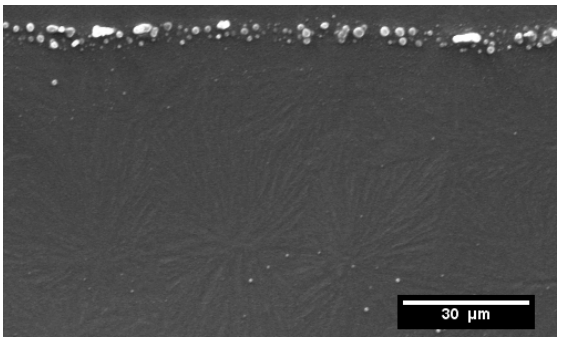

(a) PP9/PS1/0/Q

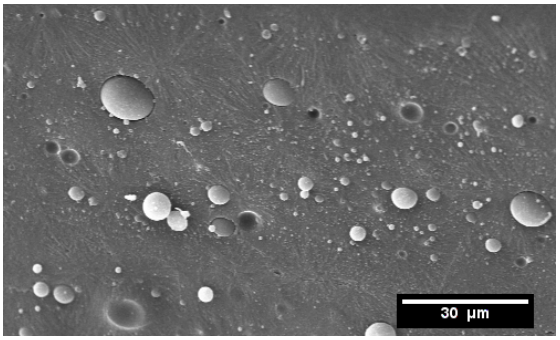

(b) PP9/PS1/0/iso40min

Figure 5.10: *SEM micrographs of the PP9/PS1/0/Y blends.*

It can be seen from Figures 5.11 and 5.12 that organoclay acts as a nucleating agent, that disrupts spherulite growth - evinced by the notable decline in the number of spherulites with increasing organoclay loading. From the micrographs it can be seen that the organoclay acts as a compatibiliser since both polymers migrate between the clay layers.[26,64] In the literature, it was shown that the organic modifications on the MMT were significant in facilitating the compatibilisation since unmodified MMT did not have the same influence.[26,40,75]

Unlike in the other composites discussed in this thesis, organoclay is not readily apparent in the micrographs in Figures 5.11(a), 5.11(b), 5.11(c), 5.11(d) and 5.11(e). According to the literature, in a PP-PS-organoclay composite, the organoclay exists in the PS phase, or, given time to migrate, at the interface between the polymer phases.[64,117,118] Furthermore, the literature is clear that in order for the organoclay to exist in the PP phase, polar modifications such as maleic anhydride must be present.[64,117] Given that the polarity of the PP used was not increased by modifiers, it is likely that the organoclay exists in the PS phase or at the interface between the two polymers. In either case, some of the organoclay would have been removed by the etching procedure. The remaining organoclay is likely to be difficult to discern in the micrographs due to the already bright colour of the PS phase.

Another finding frequently reported on in the literature is that the addition of organoclay decreases the domain size of polymers. The mechanism of this includes discussion of the organoclay increasing the viscosity of the polymers and creating a barrier effect preventing coalescence.[64,116,26] The prevention of coalescence is evinced by there being an optimum loading of organoclay, whereby a complete covering of the PS droplets is achieved leaving no particle-free surface capable of coalescing, before no further reduction in domain size is seen upon further additions of organoclay.[116,60] Although, as with the unfilled samples (PPa/PSb/0/Y) the domain size increases with time in the melt phase for the PP7/PS3/1/X and PP9/PS1/2/X samples, the size of these phases is significantly smaller. This indicates that the organoclay is somewhat suppressing phase separation but the ability to do this decreases with length of time in the melt phase - likely due to the extended amount of time the polymer chains are mobile.

Contrary to this, for the PP7/PS3/3/X samples, it appears that the domain size decreases with time in the melt phase. This could be attributed to the organoclay loading being sufficient for barrier formation preventing coalescence and/or for polymer intercalation between the clay layers during the melt phase. The former being supported by two articles in the literature reporting that at loadings of 3 parts per hundred rubber (phr) and above, an effective barrier is formed preventing coalescence for PP:PS ratio, by weight, of 70:30 and 80:20.[116,60] While the latter is supported by the effect of organoclay being most noticeable in the sample with the highest organoclay loading and the longest length of time in the melt phase (PP7/PS3/3/iso40min in Figure 5.11(f)).

Compared with the randomly changing nature of the other samples, appears relatively uniform and organoclay is observed suggesting that the organoclay is associated, at least in part, with the persisting PP phase.

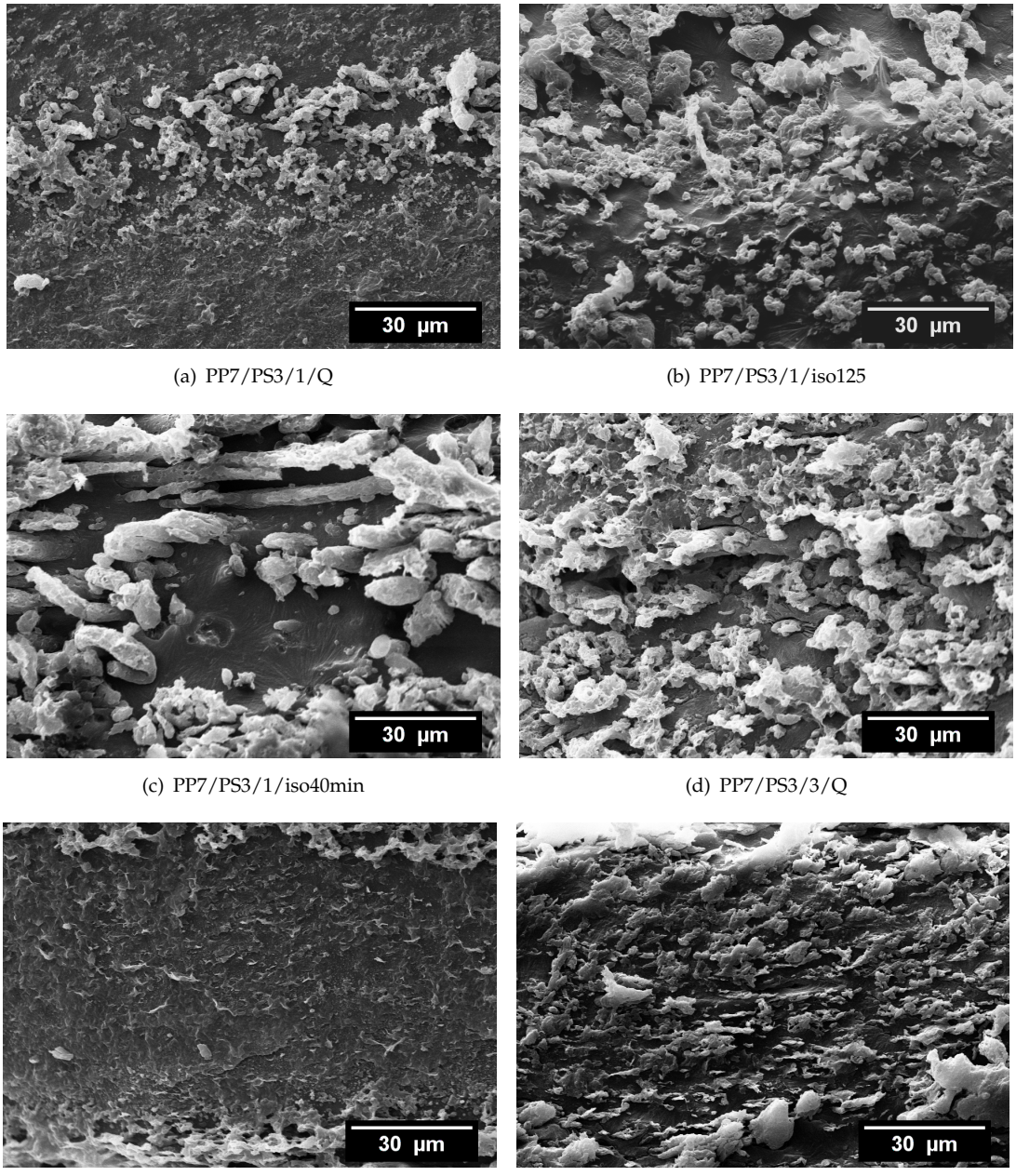

(a) PP7/PS3/1/Q (b) PP7/PS3/1/iso125

(c) PP7/PS3/1/iso40min (d) PP7/PS3/3/Q

(e) PP7/PS3/3/iso125 (f) PP7/PS3/3/iso40min

Figure 5.11: *SEM micrographs of the PP7/PS3/X/Y composites.*

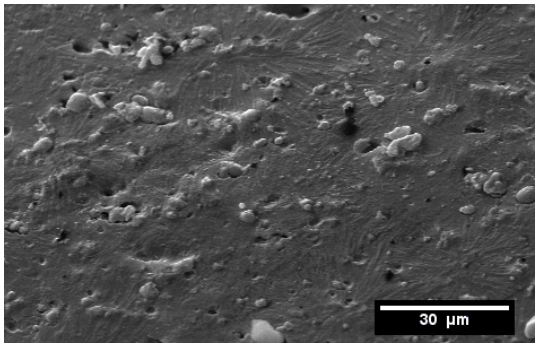

(a) PP9/PS1/0.5/Q

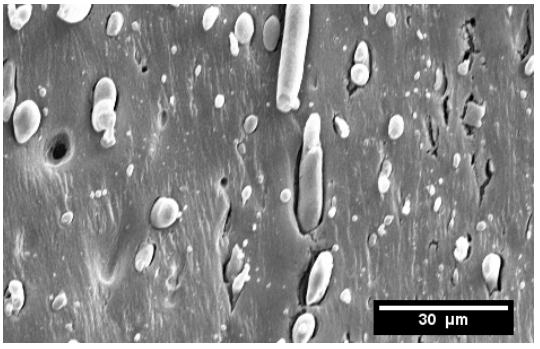

(b) PP9/PS1/0.5/iso40min

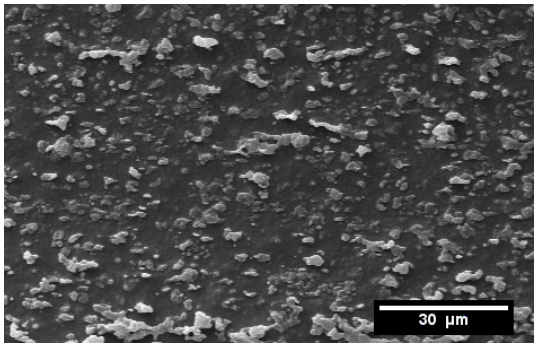

(c) PP9/PS1/2/Q

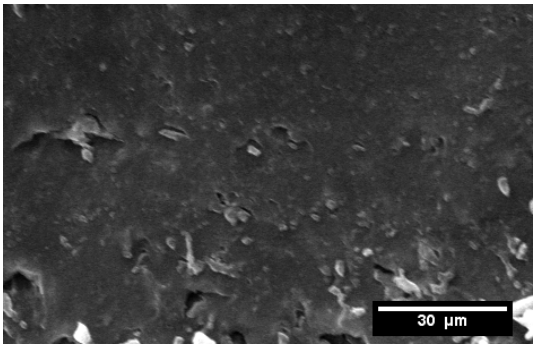

(d) PP9/PS1/2/iso40min

Figure 5.12: *SEM micrographs of the PP9/PS1/X/Y composites.*

In Figure 5.12, it can be seen that there is, little difference between the two thermal treatments of PP9/PS1/2/Y. This suggests that the organoclay is dominating the morphology of the sample rather than the length of time the polymer existed in the mobile, melt phase. Whereas, the PP9/PS1/0.5/Y samples show significant differences depending on thermal treatment - the phase separation is greater in the iso40min. This suggests that an organoclay loading of 0.5 wt.% is too low to prevent the polymer blend from being unaffected by the thermal treatment and prevent phase separation.

5.6 Conclusion

In general, it was seen that the organoclay can prevent phase separation in the PP-EVA-organoclay and PP-PS-organoclay composites. The limitation on the ability of organoclay to prevent phase separation was the balance between organoclay loading and time in the melt phase - a higher loading is required to prevent phase separation in samples held for longer lengths of time in the melt phase. For example, in the PP-EVA-organoclay system, an organoclay loading of 2.5 wt.% was enough to prevent phase separation in the samples held in the melt phase for around 5 minutes (isothermally crystallised at 120 °C) but was unable to prevent phase separation in samples held in the melt phase for around 60 minutes (isothermally crystallised at 135 °C).

Somewhat in contrast to this, the PE-EVA-organoclay composites were compatibilised by the EVA copolymer. EVA was effective in this role under all three thermal treatments investigated but did have an upper limit on its ratio with organoclay loading before agglomeration of the organoclay occurred.

Across all the composites, it was seen that the presence of the organoclay and/or additional polymers disrupted the spherulite structure of the PE or PP polymers. Also, in all cases, the organoclay showed evidence of acting as a nucleating agent and an inhibitor to crystal growth.

Overall, it can be seen that the SEM has provided an insight into the morphologies of the samples investigated, the interplay of the thermal treatments, filler dispersion, and the organoclay altering the extent of polymer phase separation. This is invaluable in building upon the results from the previous chapters to generate a clear understanding of samples allowing for confident interpretation of the dielectric results presented in Chapter 6.

Chapter 6

The Electrical Properties of the Composites

In this chapter the results from the dielectric tests will be presented and compared. Since the conductivity results can be used to understand the dielectric breakdown and dielectric spectroscopy data, they will be presented first. The interpretation of these results will rely upon the understanding of the filler dispersion and sample morphology built by the previous chapters.

6.1 Experimental Techniques

The processing of the PE-EVA-organoclay, PP-EVA-organoclay and the PP-PS-organoclay composites are detailed in Chapters 2.1.1, 2.1.2 and 2.1.3 respectively. The electrical investigations were conducted using DC conductivity, AC and DC dielectric breakdown measurements and dielectric spectroscopy, all of which are detailed in Chapter 2.4.

For simplicity and brevity, the PPa/PSb/X/iso125 samples have, on the most part, been omitted so the dielectric data will consider samples from the two extremes on the length of time in the melt phase.

6.2 DC Conductivity

6.2.1 DC Conductivity: PE-EVA-Organoclay

DC conductivity measurements were taken over 24 hours under both ambient and dry conditions to check the suitability of the 1000 second electrification time and the sus-

ceptibility of the sample to the environmental conditions in the testing chamber. The results are shown in Figure 6.1. The results show that the plateau was reached before 1000 seconds and the samples were not susceptible to changes in the environmental conditions when the chamber was open to the controlled laboratory atmosphere (around 20 °C and 50 % relative humidity, referred to as 'ambient'). The mass change of samples left under ambient conditions was studied over 5 days; the sample containing the most organoclay showed the largest change but this was still only a 0.5% increase and within experimental uncertainties. Therefore it can be said that testing the samples for 1000 seconds would be sufficient and the samples are not susceptible to water uptake from the atmosphere. See Chapter 7.3 for a more in-depth study of the effect of water on these composites.

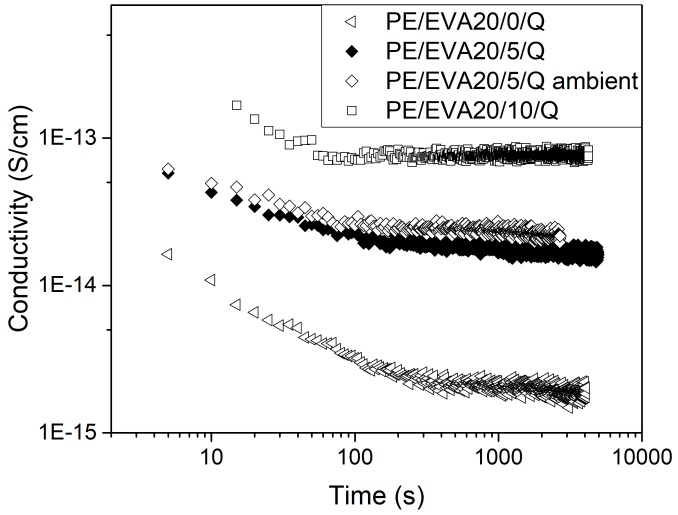

Figure 6.1: *The current decay of PE/EVA20/X/Q samples in a field of 3 kV/mm for one day to check the appropriability of the electrification time. All the tests were performed under dry vacuum unless marked 'ambient' for which the chamber was open to the atmosphere.*

Figure 6.2 compares measures of DC conductivity, as defined above, obtained at four different temperatures for the PE/EVA9/X/Q sample set. Values below the sensitivity limit of the equipment were deemed unreliable and were omitted, leaving the samples containing no organoclay and 1 wt.% with results at only 70 °C. From these data, it is evident that conductivity increases with temperature, as would be anticipated[90,129] and, with filler loading level from zero to 9 wt.% of organoclay. The effect of further addition of organoclay is unclear, since at 55 °C and 70 °C the systems containing 9 wt.% and 13 wt.% are statistically equivalent whilst at lower temperatures, the latter shows a decrease in conductivity compared to the former. The increased conductivity with organoclay loading may be related to a number of processes, such as the formation of localised shallow charge trapping states that can promote charge carrier mobility[168] and the introduction of additional ionic species that act as charge carriers.[169] Never-

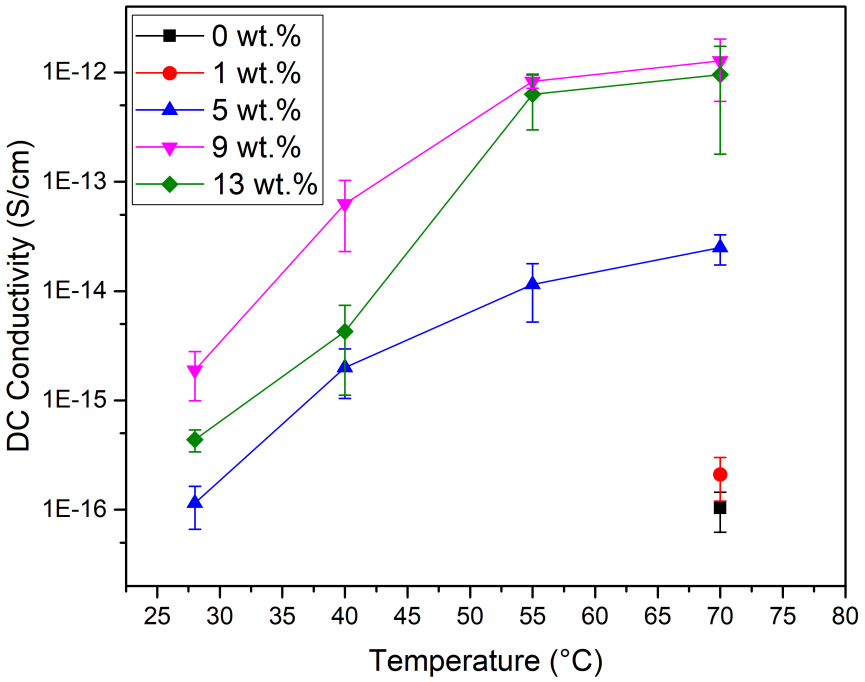

Figure 6.2: *DC Conductivity of PE/EVA9/X/Q blends in a field of 3 kV/mm (the maximum field possible for the samples due to an equipment supply limit of 1 kV) under different temperatures. The equipment limit was 1x10^{-17} S/cm and results that fell below this value have been omitted.*

theless, whatever the precise origin of the marked increase in conductivity with clay loading, the results presented in Figure 6.2 clearly show that the presence of the clay dominates the charge transport process.

Figure 6.3 shows DC conductivity data taken at 70 °C in order to compare the effect of each thermal treatment. In the absence of any organoclay, the measured conductivity values all fall around 10^{-16} S/cm and no clear influence of sample thermal history is evident. Similarly, the samples containing either 9 wt.% or 13 wt.% of the organoclay all exhibit conductivities in the range 10^{-12} - 10^{-11} S/cm and while their respective PE/EVA9/X/ISO and PE/EVA9/X/SC samples behave equivalently, the conductivity of both their respective PE/EVA9/X/Q samples is reduced. This is contrary to the unfilled samples, where sample thermal history does not appear to affect DC conduction processes. Differentiation between the thermal treatments are even more marked at lower organoclay loading levels with, for example, the conductivity of PE/EVA9/1/Q falling two orders of magnitude below that of both PE/EVA9/1/ISO and PE/EVA9/1/SC.

Taken together, Figures 6.2 and 6.3 suggest that charge transport through an assembly of organoclay tactoids dispersed within an insulating polymer is dominated by

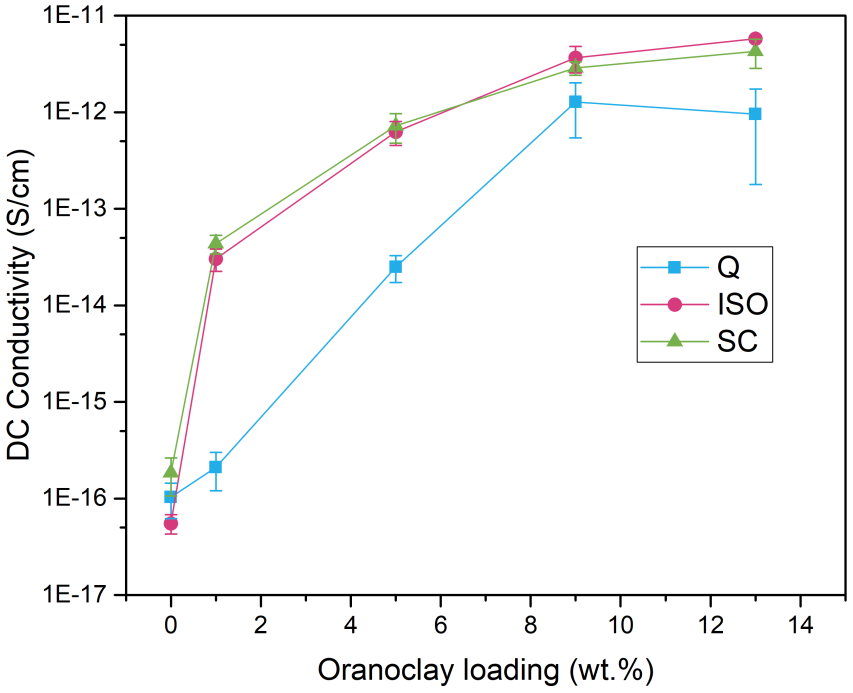

Figure 6.3: *DC Conductivity of PE/EVA9/X/Y blends in a field of 3 kV/mm (the maximum field possible for the samples due to an equipment supply limit of 1 kV) at 70* °C.

the organoclay and, as such, it is suggested that it depends upon (a) the chemical and physical characteristics of the organoclay, (b) the loading level and (c) the dispersion of the organoclay throughout the matrix. The influence of this final factor on the physical properties of composite materials has been studied in connection with numerous phenomena and material systems. For example, the formation of percolating networks within graphene-based materials has been considered extensively as a means of producing composites with increased electrical conductivity. In this context, Stankovich *et al.*[170] showed that, although graphene oxide is semiconducting, upon reduction with hydrazine the conductivity increases to the point where it is comparable to graphite. They ascribe this, despite the oxygen acting as potential acceptor sites, to the particle interfaces being conductive, a dense conductive network and possible ionic channels allowing electron transfer. Elsewhere, the effect of particle distribution on the thermal conductivity of polymers has attracted great interest in attempts to generate electrically insulating materials capable of effectively dissipating unwanted heat. In the case of hexagonal boron nitride (hBN), which exhibits a platelet structure, Zhou *et al.*[171] described a sample preparation technique that was specifically chosen to restrict dispersion throughout their HDPE matrix, thereby significantly enhancing thermal conductivity compared with equivalent systems generated by conventional melt mixing. In view of effects such as those described above, it is suggested that the variations

in electrical conductivity seen in Figure 6.3 can be explained in terms of variations in the organoclay dispersion within the matrix polymer. That is, the long residence time in the melt that characterises both the PE/EVA9/X/ISO and PE/EVA9/X/SC sample sets serves to facilitate a degree of self-assembly of the organoclay within the final system. In the absence of organoclay, the resulting variations in matrix morphology have no significant effect on charge transport. At high organoclay loadings, the initially formed organoclay distributions result in vastly increased electrical conductivities such that further modification in the structure is unimportant. Only at intermediate levels - 1 wt.% and 5 wt.% - does the arrangement of the clay tactoids evolve to a sufficient degree to affect the overall electrical conductivity of the system. From this, it is clear that there are two limits on EVA compatibilising the composite: the organoclay loading and the length of time in the melt.

6.2.2 DC Conductivity: PP-EVA-Organoclay Composites

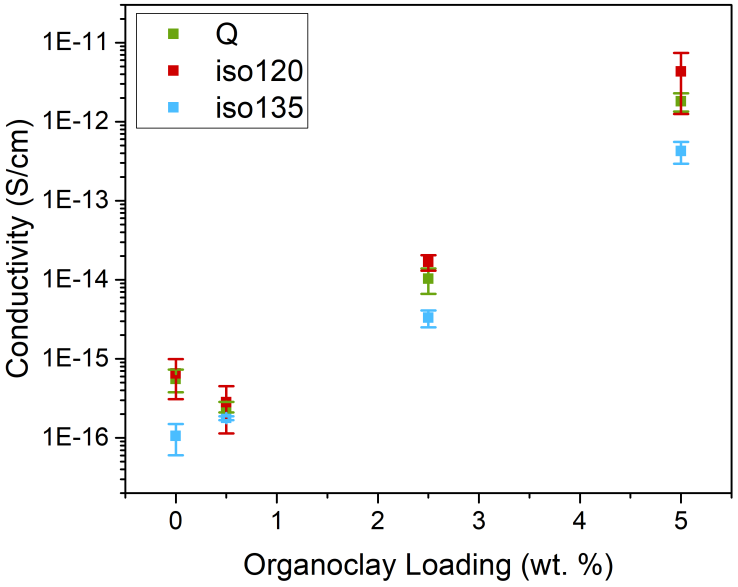

Figure 6.4: *Graph summarising the DC conductivity at 60 °C under a constant field of 9 kV/mm for the PP/EVA9/X/Y composites. The error bars represent the standard deviation of the results from the three repeats of each experiment.*

Figure 6.4 shows that the nominal conductivity of the nanocomposites increases with increasing temperature and with organoclay loading level, with good levels of reproducibility (evinced by the small error bars). The correlation with organoclay loading is a result of the polymer/filler interface controlling charge carrier transport,[172,173,107] and the nanofiller providing additional charge carriers.[173] Both of which can be increased by thermal activation.

Another contribution the organoclay brings is that, as previously noted, it decreases the ability of PP and EVA to phase separate.[174,101] This means that fewer phase boundaries are formed that would otherwise act as charge traps or scatter the charge and decrease the conductivity, as seen elsewhere.[107]

From the DC conductivity data summarised in Figure 6.4, it is clear that the conductivity is also influenced by the thermal treatment of the composite from the melt phase. Most notable is that between samples of equivalent composition, the iso135 samples have the lowest DC conductivity while the iso120 and Q samples have statistically equivalent conductivity. It is suggested that the effect is likely caused by how the thermal treatment affects the organoclay dispersion amongst the crystallites. The iso135 samples were able to crystallise over the longest length of time meaning that more of the impurities (in this case organoclay) are left at the crystallite/amorphous boundary (as opposed to in the amorphous phase).[4] (Unfortunately the SEM micrographs did not have sufficient resolution to provide evidence of this occurrence.) If this is the case, and since more organoclay at the interface results in a lower conductivity,[129,169] one can understand why the iso135 samples have the lowest conductivity. Meanwhile the similarity between the Q and iso120 samples may arise from the time in the melt phase varying only by around 5 minutes.

Considering all of this, and together with the fact that the conductivity of solid dielectrics also has a positive dependence on temperature,[130] the results in Figure 6.4 are in line with expectations.

Figure 6.5 shows the DC conductivity results presented as log current against log time at 50 °C and 60 °C. The current decay traces allow the time dependence to be assessed. For the organoclay-containing composites, it can clearly be seen that the samples reach time independence more quickly at higher temperatures and greater organoclay loadings. In particular, the PP/EVA9/0.5/Q sample shows the decay reaching time independence within 1000 s at 60 °C but not at 50 °C. Further, the PP/EVA9/0.5/Q sample shows a much slower decay than the other organoclay-containing composites, together this indicates that this sample composition is much less conductive. Meanwhile the sample without organoclay reached time independence within 1000 s only at the higher temperature, which again highlights the temperature-dependent conductivity of the polymer blend.

6.2.3 DC Conductivity: PP-PS-Organoclay Composites

Figure 6.6 summarises the conductivity of the PP-PS-organoclay composites. The results show that the samples without organoclay have the lowest conductivity, these samples show large error bars since the readings were around the limit of the equipment and are therefore more prone to random noise, producing unreliable results. De-

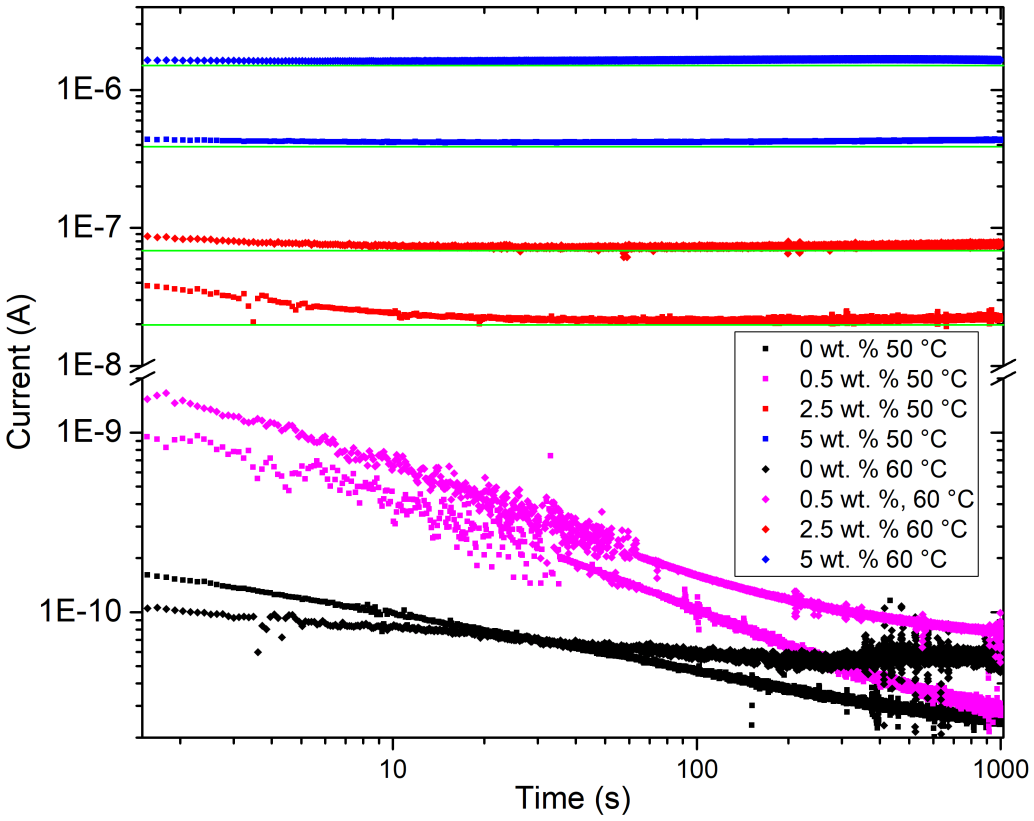

Figure 6.5: *DC conductivity results of PP/EVA9/X/Q (under a field of 5 kV/mm) plotted on a log-log graph of current against time with horizontal green lines added to aid comprehension.*

spite this, these results have been included in the graph in order to provide a baseline.

Given that the PP-PS-organoclay samples were measured at 70 °C and at a higher field than the other composites measured herein, the PPa/PSb/0/Y composites are the most insulating of the composites investigated in this thesis.

The results of the PP7/PS3/1/Y, PP7/PS3/3/Y and PP7/PS3/5/Y samples all have a conductivity four orders of magnitude larger than the unfilled systems. The PP7/PS3/1/Y samples have a lower conductivity than the other two loadings however the difference is small: all the results of the samples with organoclay fall within one order of magnitude. Organoclay increasing the conductivity of the samples has been seen with both the other systems investigated in this thesis and in published literature.[173] Therefore these results are entirely in line with expectations.

Figure 6.6 also shows that the thermal treatments result in small or insignificant differences in the conductivity between equivalent sample compositions. This was also observed in the PE/EVA9/X/Y composites and the PP/EVA9/X/Y composites when the organoclay loading was high enough to form a percolating network of organoclay. However, unlike those other samples, the samples in Figure 6.6 appear to have achieved

a percolating network at a lower organoclay loading. This difference has been attributed to the fact that organoclay is more compatible with PE and EVA than both PP and PS,[39,78,104,64] giving rise to a morphology with better dispersion and hence a lower conductivity.

Of particular note is the PP9/PS1/0.5/Y samples, highlighted by the green circle, as they are the only samples that have a conductivity significantly affected by the thermal treatment. This suggests that the organoclay has not reached a percolating loading level and instead the conductivity is dominated by the morphology of the sample. This gives an insight into the effect of the morphology changes observed in Chapter 5.5 with organoclay loading and thermal treatment. Further, given that PP7/PS3/1/Y and PP9/PS1/2/Y show no significant difference between the thermal treatments, it is suggested that the percolation loading level lies between 0.5 and 1 wt.%.

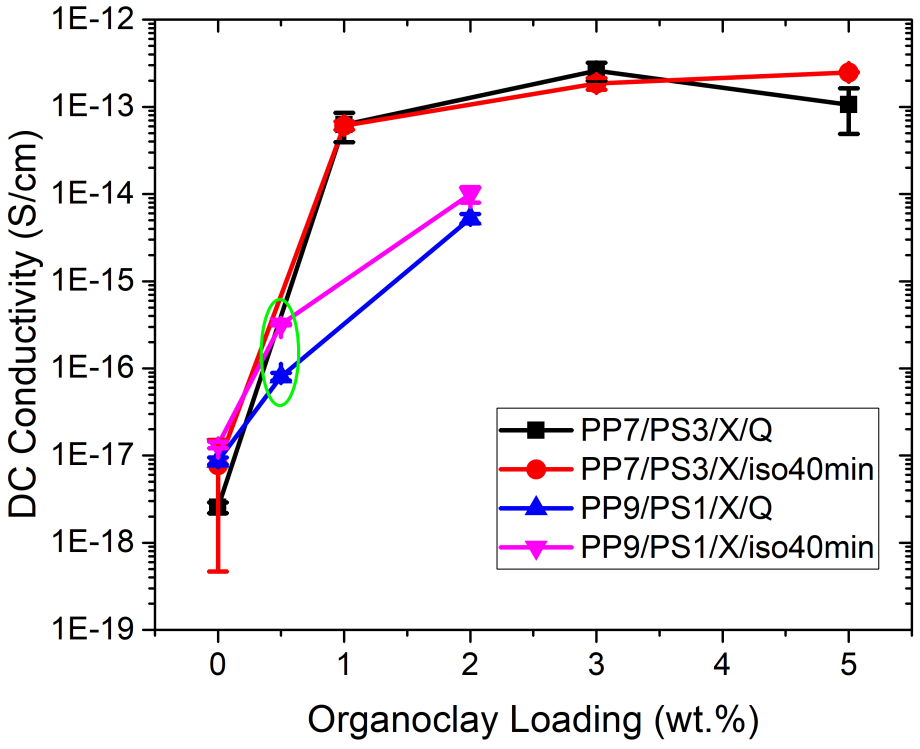

Figure 6.6: *Graph summarising the DC conductivity data of the PP-PS-Organoclay composites, measured at 70 °C, following different thermal treatments from the melt phase.*

6.3 Dielectric Breakdown Strength Measurements

This chapter will discuss the DC dielectric breakdown strength results for all the samples and the AC dielectric breakdown strength results for the PE-EVA-organoclay and PP-EVA-organoclay composites. AC dielectric measurements were not performed on all the composites since DC measurements are more pertinent to the capacitor applications that these materials are destined for and due to laboratory equipment limitations.

6.3.1 Dielectric Breakdown Strength: Single Polymer-Organoclay Composites

The DC dielectric breakdown strength measurements of the single polymer-organoclay composites compared to the three pristine polymers are displayed in Table 6.1.

In each case the breakdown strength decreased upon addition of organoclay. Specifically, the organoclay led to a percentage change of -16 %, -33 % and -44 % in PE, PP and PS matrices respectively. This is in line with the literature, where, taking just one example, LDPE was reported to have a breakdown strength of 470 kV/mm which dropped 22 % upon addition of 5 wt.% organoclay.[75] Although the exact breakdown mechanism is difficult to determine, it is reasonable, and indeed has been reported elsewhere,[50,62] that the increased conductivity of the material directly causes a decrease in breakdown strength. This could occur via changes in the thermal properties, charge trapping behaviour and/or filler agglomeration enhancing the local electric field.[75,50,62] However, in terms of applicability, the beta value, representing the spread of the breakdown results, is more important than the breakdown strength, *per se*. Notably, from these results, the spread of the breakdown strength results is decreased (and therefore is improved by) the addition of organoclay for the PP and PS systems and is almost unchanged for the PE system. This has been attributed to the morphological change resulting from the organoclay, in particular, the absence of phase boundaries.[57]

6.3.2 Dielectric Breakdown Strength: PE-EVA-Organoclay Composites

6.3.2.1 DC dielectric breakdown strength

Figure 6.7 contains Weibull plots of DC dielectric breakdown data, obtained from the PE/EVA9/0/Y sample set from which it is evident that the indicated confidence bounds of each data set largely overlap. As such, any dependence of DC dielectric breakdown strength on thermal history for the polymer blend considered here is small. However, it is clear that the spread of the results (shown by the β value) increases with an increase in time in the melt phase.

Sample	Thermal Treatment	α (kV/mm)	Change in α from unfilled sample	β	Average Thickness (mm)
PE	Q	449.8 ± 15.7	–	11.0	0.10
PE/5	Q	378.5 ± 13.5	-16%	10.7	0.10
PP	Q	481.4 ± 30.2	–	6.2	0.09
PP/5	Q	322.5 ± 10.3	-33%	12.0	0.10
PS	Q	429.7 ± 17.8	–	9.3	0.11
PS/5	Q	241.5 ± 8.2	-44%	11.2	0.11

Table 6.1: *Summary of the two parameter Weibull statistics analysis for the DC dielectric breakdown data from the single polymer-organoclay composites and the pristine polymers.*

Figures 6.7, 6.8, 6.9 and 6.10 contain Weibull plots of DC dielectric breakdown data. From these, it is evident that the DC dielectric breakdown strength is adversely affected by the presence of the organoclay and, in both systems containing 5 wt.% and 9 wt.% of organoclay, it is the sample that was quenched that exhibits the highest DC dielectric breakdown strength. As such, these breakdown data are consistent with the DC conductivity data described previously in that increases in conductivity are paralleled by reductions in DC dielectric breakdown strength, suggesting that DC dielectric breakdown in these systems are thermal in nature (since avalanche mechanisms occur only when thermal mechanisms are absent).[129,75]

Another observation from these data is the variation in β value with organoclay loading and time in the melt phase. This gives an indication of the organoclay dispersion and general variation created between the samples by varying these two factors alone. In brief, the results in Figures 6.7, 6.8, 6.9 and 6.10 show that the 13 wt.% loading causes a wide spread in the results (and therefore supports the conclusion that this loading is too high for good dispersion); and that quenching from the melt phase improves the breakdown strength results in terms of the spread of the data.

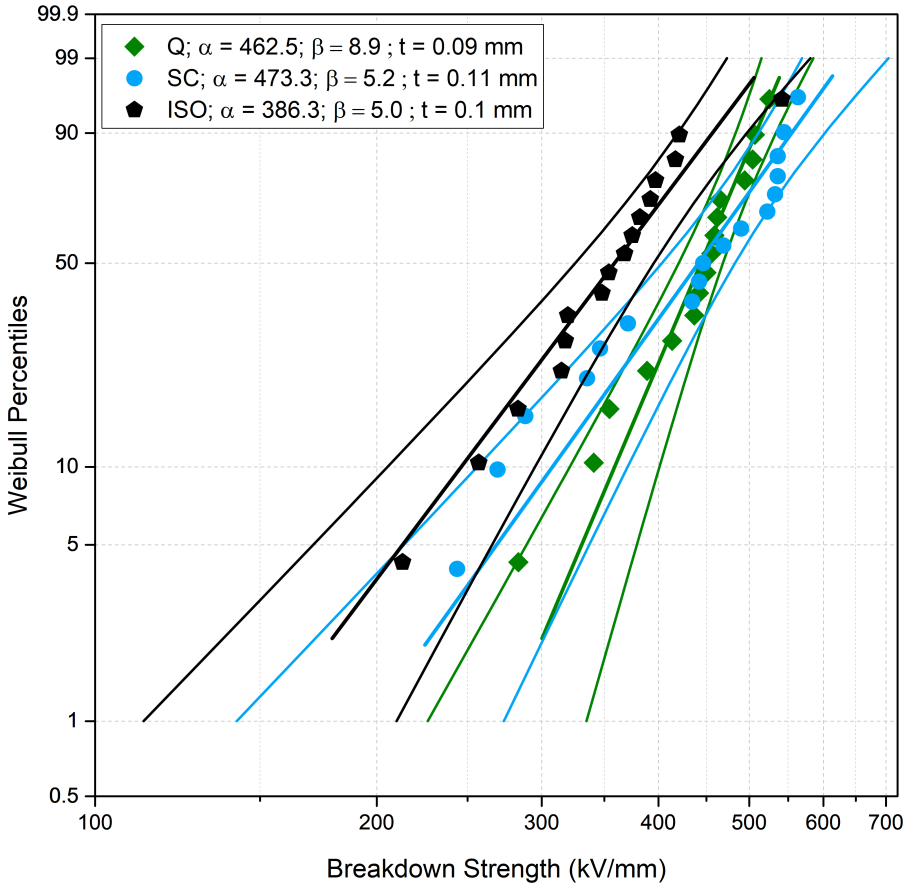

Figure 6.7: *DC dielectric breakdown Weibulls for the PE/EVA9/0/Y samples*

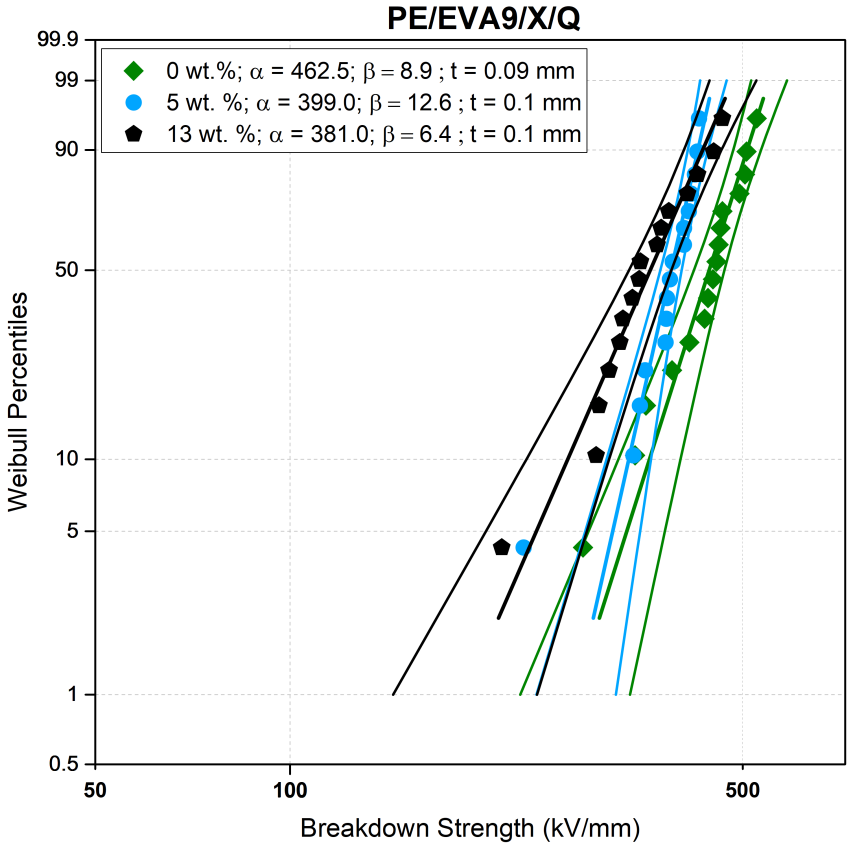

Figure 6.8: *DC dielectric breakdown Weibulls for the PE/EVA9/X/Q samples*

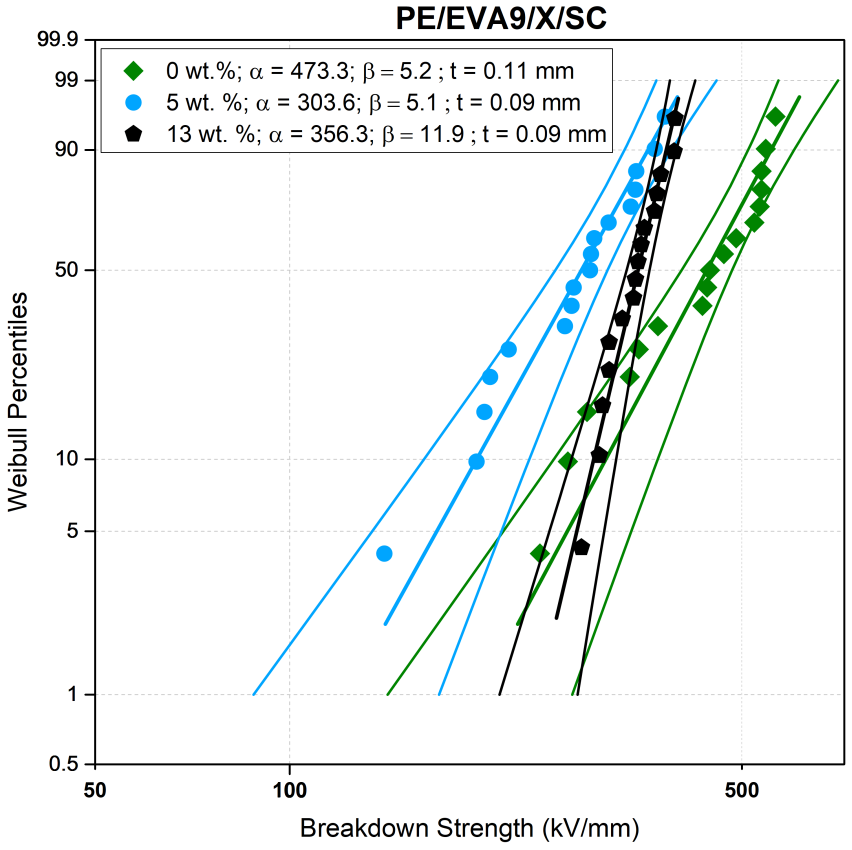

Figure 6.9: *DC dielectric breakdown Weibulls for the PE/EVA9/X/SC samples*

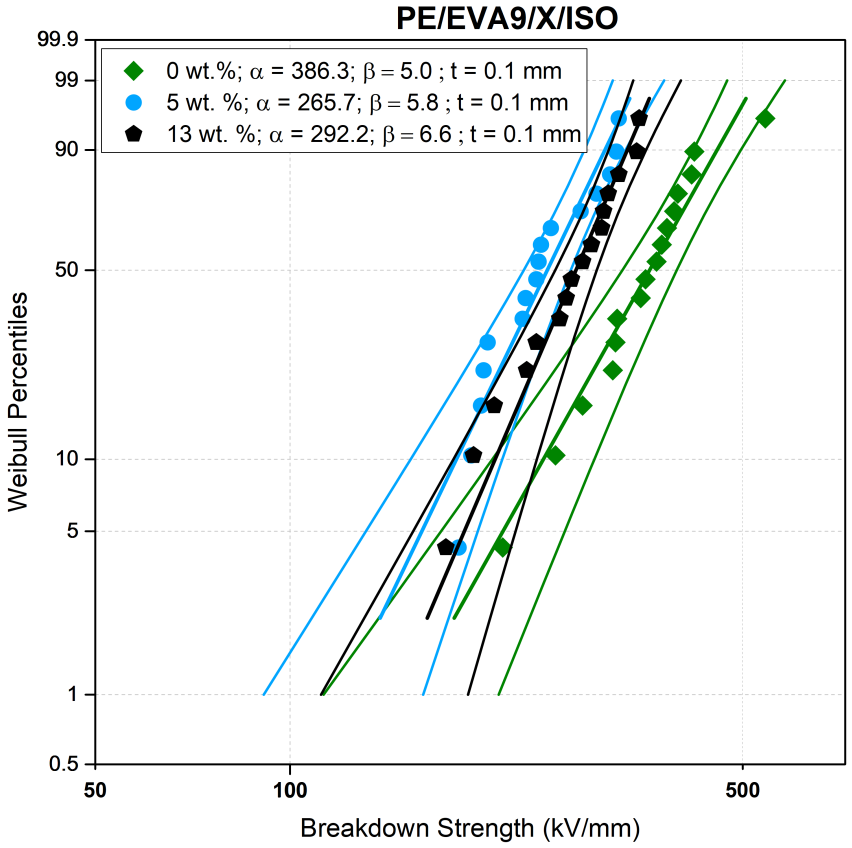

Figure 6.10: *DC dielectric breakdown Weibulls for the PE/EVA9/X/ISO samples*

6.3.2.2 AC dielectric breakdown strength

Table 6.2 shows the AC dielectric breakdown strength results for the samples for both thermal treatments together with the average sample thickness while Figure 6.11 shows the Weibull plots for the PE/EVA9/X/Q samples.

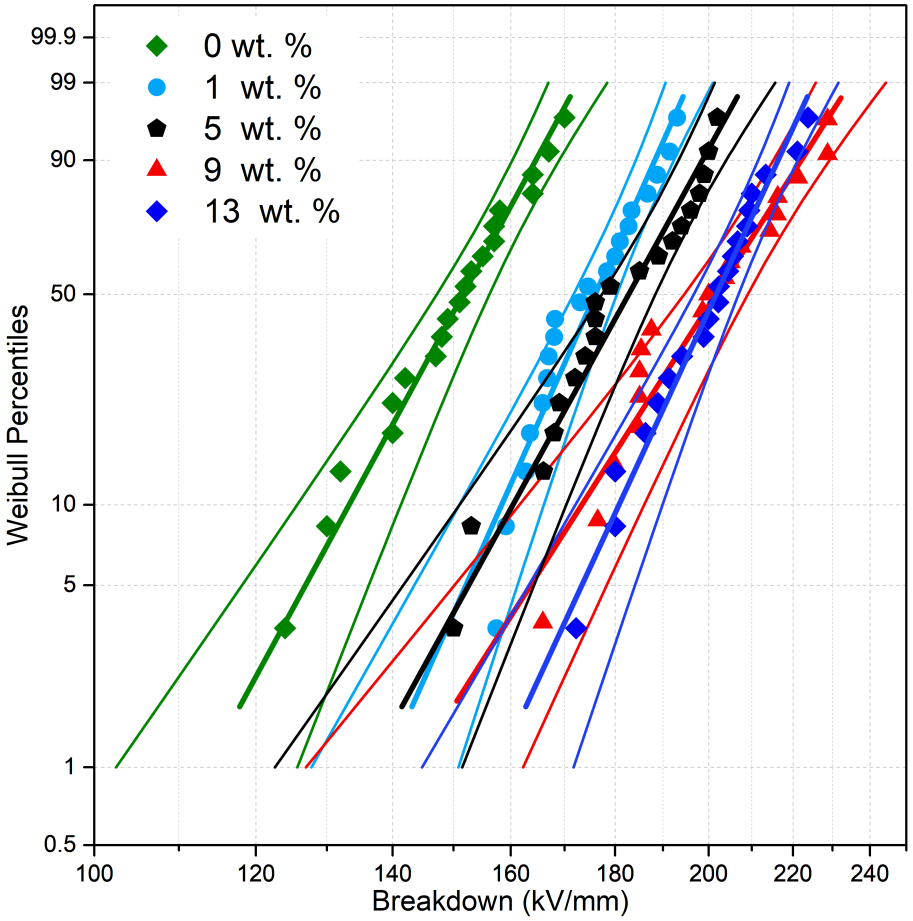

Figure 6.11: *AC dielectric breakdown Weibulls for the PE/EVA9/X/Q samples*

In marked contrast to the DC dielectric breakdown behaviour reported previously, under AC conditions, the inclusion of the organoclay results in a monotonic increase in breakdown strength with organoclay loading level. It has previously been shown in a PE-EVA-organoclay composite that the AC dielectric breakdown strength increased up to a content of 5 wt.%, but thereafter, further increases in organoclay reduced the breakdown strength, an affect ascribed to organoclay agglomeration.[55,75] Since the results presented herein reveal no comparable reduction in performance, it would seem that, in the material system considered here, such composition-related agglomeration effects are not sufficient to adversely impact the dielectric breakdown strength. This illustrates the capabilities of EVA as a compatibiliser because our maximum filler loading was significantly higher than in the aforementioned paper. Furthermore, all of the systems considered here are characterised by increased AC dielectric breakdown

X	Y	α (kV/mm)	Change in α from unfilled sample	β	Average Thickness (mm)
0	Q	150 ± 4	–	15	0.10
0	SC	151 ± 7	–	9	0.09
1	Q	180 ± 4	+20%	18	0.11
1	SC	176 ± 5	+17%	12	0.11
5	Q	182 ± 5	+21%	14	0.10
5	SC	173 ± 8	+15%	18	0.09
9	Q	200 ± 7	+30%	11	0.08
9	SC	200 ± 8	+32%	11	0.08
13	Q	201 ± 5	+34%	17	0.09
13	SC	182 ± 8	+21%	10	0.08

Table 6.2: *Table listing the AC dielectric breakdown strength Weibull statistics data from the PE/EVA9/X/Y composites.*

strength compared with the unfilled matrix, an occurrence that is generally linked to well-dispersed systems.[55,78,80] Therefore, these AC dielectric breakdown strength results further support the assertion that this material system achieved a good dispersion of the organoclay and the capability of the EVA to compatibilise the system, regardless of the thermal treatment.

6.3.3 Dielectric Breakdown Strength: PP-EVA-Organoclay Composites

6.3.3.1 AC dielectric breakdown strength

The AC dielectric breakdown data of the three different sample compositions and the three different thermal treatments are shown in Figure 6.12 and for pure PP samples in Figure 6.13. Data for PP/EVA9/0/Y, PP/EVA9/2.5/Y and PP/EVA9/5/Y were obtained but, due to equipment breakages, data for the PP/EVA9/0.5/Y samples were not obtained.

It can be seen that although there are overlapping error bars, some trends are clear. Firstly, the breakdown strength increases with the presence of organoclay, which was also reported by Bulinski *et al.*[107] for a composite of PP and a mica-based organoclay.

Another trend seen in the data is that the breakdown strength is higher for the quenched samples than the isothermally cooled samples. Furthermore the data show that for two of the three samples, the breakdown strength decreased with increased time in the melt phase, which was also true for the pure PP samples.

It is proposed that these observations could be due to the organoclay acting via three

mechanisms, or, indeed, a mixture of the three. Firstly, the enhanced mechanical strength of the sample caused by the organoclay means that the electromechanical strength of the sample is improved.[175] A further possible explanation is that the organoclay acts as an effective barrier to partial discharge and electrical tree formation, essentially delaying the breakdown mechanism until higher fields.[176] An alternative or contributing factor, is supported by the SEM micrographs in Figure 5.6. From these micrographs it was seen that for each organoclay loading, the longer the time in the melt phase, the more phase separation occurred. This would weaken the material as phase separation leads to phase boundaries where impurities gather, creating a defect that essentially provides a conductive pathway, ultimately leading to premature breakdown.[129,62] The compatibilising nature of the organoclay helps to prevent phase separation of the polymer blends and less phase separation means the sample has fewer phase boundaries where impurities gather and provide a breakdown pathway that weakens the material.

Furthermore, the decrease in breakdown strength is less significant with a longer time in the melt phase for the composites compared to pure PP. This shows that the composites are stronger mechanically (and so better at distributing the electrical stresses), which, again, can be attributed to the phase separation inhibition by the compatibilising nature of the organoclay.[75,76]

Overall, in comparing all the breakdown data (summarised in Table 6.3) the composites have a higher breakdown strength than pure PP. This is likely due to the EVA and organoclay causing charge scattering and thereby increasing the path length of the charge carriers and so decreasing the chances of breakdown.[177]

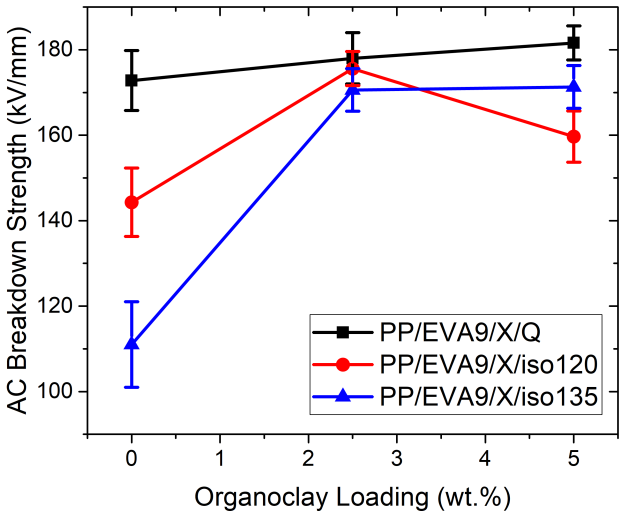

Figure 6.12: *Graph summarising the AC dielectric breakdown data for the PP-EVA-organoclay samples.*

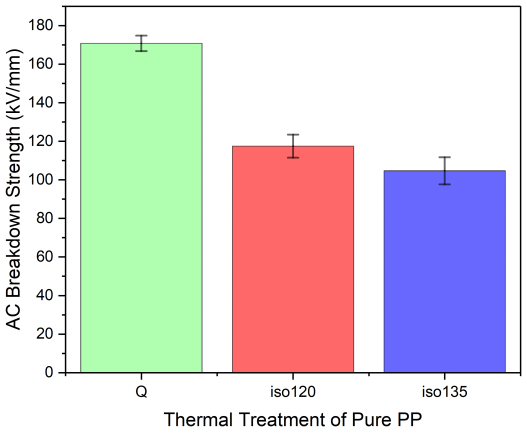

Figure 6.13: *Graph summarising the AC dielectric breakdown data of pure PP following different thermal treatments from the melt phase.*

Sample Name	Thermal Treatment	α (kV/mm)	Change in α from pure PP	β	Average Thickness (mm)
PP	Q	170.8 $\pm$4	–	16.0	0.11
PP	iso120	117.5 $\pm$6	–	7.6	0.12
PP	iso135	104.7 $\pm$7	–	5.6	0.11
PP/EVA9/0	Q	172.8 $\pm$7	1.1%	9.0	0.09
PP/EVA9/0	iso120	144.3 $\pm$8	22.8%	6.9	0.11
PP/EVA9/0	iso135	111.0 $\pm$10	6.0%	3.8	0.11
PP/EVA9/2.5	Q	178.0 $\pm$6	4.2%	11.5	0.11
PP/EVA9/2.5	iso120	175.6 $\pm$4	49.4%	16.6	0.10
PP/EVA9/2.5	iso135	170.6 $\pm$4	62.9%	13.7	0.12
PP/EVA9/5	Q	181.6 $\pm$8	6.3%	16.4	0.10
PP/EVA9/5	iso120	159.7 $\pm$6	35.9%	10.5	0.09
PP/EVA9/5	iso135	171.3 $\pm$5	64.2%	13.0	0.11

Table 6.3: *Summary of the two parameter Weibull statistics analysis on the AC dielectric breakdown data from the PP-EVA-organoclay composites.*

6.3.3.2 DC dielectric breakdown strength

The Weibull plots of the DC dielectric breakdown strength data, shown in Figure 6.14, reveal a marked decrease in DC breakdown strength with increased organoclay loading, which aligns well with the literature for organoclay, silica, oxide and nitride based nano-fillers.[75,91,94] Clearly, the presence of the organoclay increases the conductivity of the system, which suggests that DC breakdown occurs through a thermal runaway

mechanism. Montanari *et al.*[50] reported comparable findings for PP-EVA-organoclay composites, where increases in conductivity and reductions in breakdown strength were observed and attributed to the thermal instability of the matrix to the heat generated by the current flow.

There are alternative and/or contributing possible mechanisms explaining the causal link between breakdown strength and organoclay loading. One suggested mechanism relates to the charge trapping sites created by the organoclay: under DC fields, space charge accumulates at the trap sites, enhancing the field at this position leading to a breakdown.[75] The occurrence of this mechanism depends largely on the length of time to breakdown allowing enough time for space charge accumulation. Since the authors of this proposal[75] used a ramp rate of 5000 V/s compared to the 350 V/s used herein is certainly plausible that there was enough time (around 2 minutes) for space charge to accumulate and breakdown to have occurred via this mechanism. Furthermore, electric field enhancement due to agglomerations leading to premature breakdown, is more likely at higher filler loadings.[75] In light of this, it can be concluded that the results reported herein are in line with expectations and the insignificant difference observed between PP/EVA9/0/Q and PP/EVA9/0.5/Q may be attributed to the morphology being similar (see Chapter 5.4) and the organoclay loading being insufficient to affect the sample conductivity unlike the other composites (shown in Figure 6.4).

A notable feature of the Weibull plots is the better breakdown performance of the samples containing organoclay compared to the unfilled polymer matrix, shown by the narrower spread of results in the former. Indeed, it is suggested that the data obtained from PP/EVA9/0/Q may be indicative of two distinct breakdown mechanisms occurring. The breakdown at the highest fields can be ascribed to the inherent strength of the polymer blend and the breakdown at the lowest fields can be ascribed to failure through weak points generated by EVA phase separation. The latter is something that the addition of organoclay prevented (shown in the SEM micrographs in Chapter 5.4).

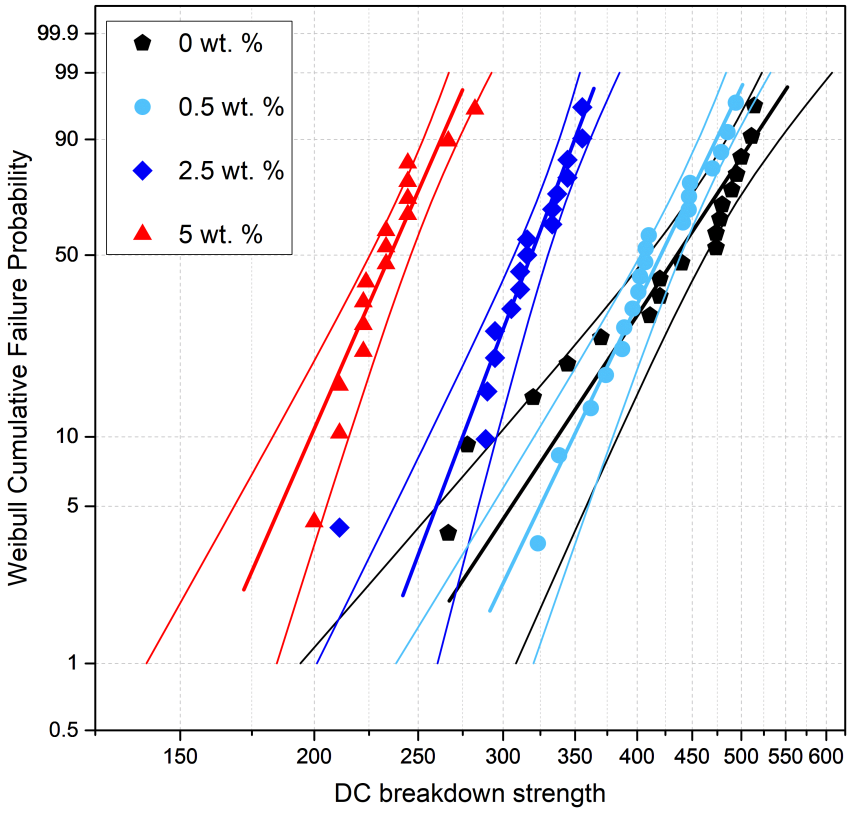

Figure 6.14: *Graph summarising the DC dielectric breakdown data of the PP/EVA/X/Q composites.*

6.3.4 DC Dielectric Breakdown Strength: PP-PS-Organoclay Composites

The DC dielectric breakdown results of the PP-PS-organoclay composites are shown in Figure 6.15. The PPa/PSb/0/Y samples clearly have the highest breakdown strength. Further, there is a decrease in breakdown strength in the samples with increases in organoclay loading. This correlates with an increased conductivity (shown in Figure 6.6), which is a well-accepted and reported phenomenon,[99,178] and is consistent with the two other composite systems studied herein.

The PP9/PS1/0.5/Y samples show a significant difference in breakdown strength following different thermal treatments, highlighted by the green circle. Since the conductivity and breakdown strength are closely linked, the significance of these results have been discussed previously for Figure 6.6.

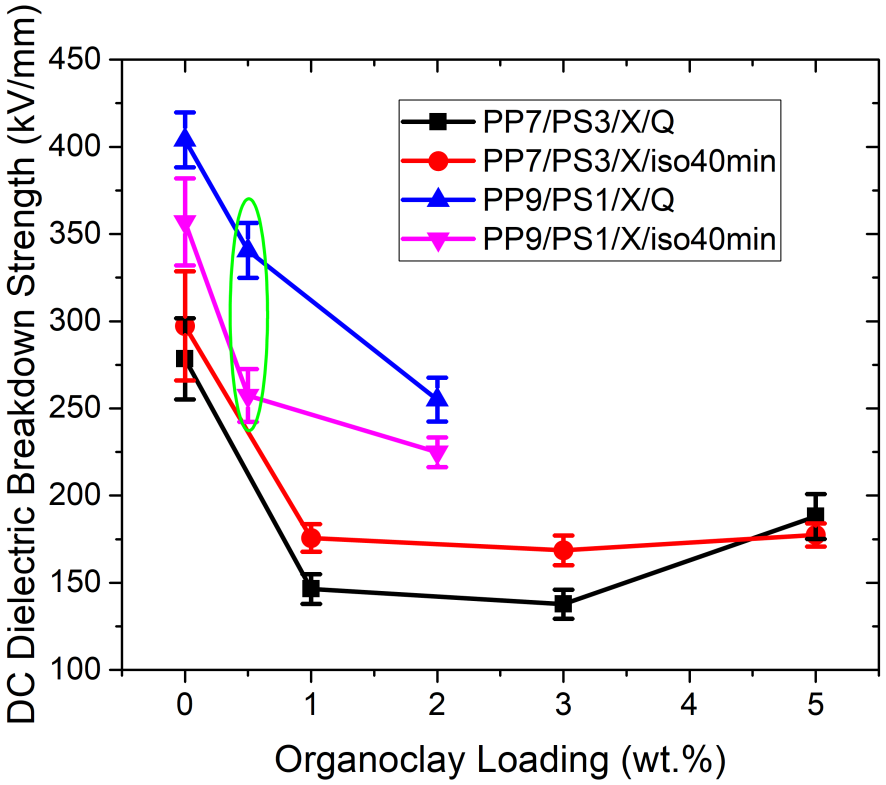

Figure 6.15: *Graph summarising the DC dielectric breakdown data of the PPa/PSb/X/Y composites.*

6.4 Dielectric Spectroscopy

Using the Lichtenecker mixing rule,[135] (see Chapter A.1.2) a prediction of the dielectric constant at 1 kHz can be made using a dielectric constant value of 2.3 for PE,[136] 2.7 for EVA,[179] 2.3 for PP,[136] and 2.6 for PS.[136] The result of the prediction calculations, rounded to two significant figures, was 2.4 for all the composites; as noted on Figures 6.16(a), 6.16(c) and 6.16(e). The Lichtenecker mixing rule consistently over-predicted the permittivity of these blends. This discrepancy could be due to several reasons including: the permittivity value for EVA being inaccurate as, due to limits in the published data tables, the value used for a polymer with a higher VA content than that used; the effect of the various polymer additives introduced by the manufacturer to combat oxidation or equipment uncertainties.

Real relative permittivity data for the PE-EVA-organoclay, PP-EVA-organoclay and PP-PS-organoclay systems are shown in 6.16(a), 6.16(c) and 6.16(e) respectively, whilst the corresponding data for the single polymer-organoclay composites are shown in Figure 6.16(g). The unfilled polymers and unfilled polymer blends all display no change in permittivity across the frequency range considered. This is in line with expectations as the literature on pure PE,[180,139] EVA,[178] PP,[181] and PS.[182]

In each case, the addition of organoclay had a clear effect on the real permittivity. Firstly, the addition of an upturn at low frequencies and secondly, as the amount of organoclay increases the real permittivity increases. This suggests the nature of the polarisation causing the loss peak is interfacial, namely Maxwell-Wagner-Sillars. This arises due to the differences in the real permittivity and conductivity of the types of materials at the interface or their nature (crystalline or amorphous).[183,169,184,185] Since there was no such loss upturn in the unfilled blend, it can be reasoned that this interfacial region is between the polymer and the organoclay. Meanwhile, the apparent increase in real permittivity with filler loading can be attributed to the increase in the number of polar moieties, in this case carbonyl groups, present.[186]

The corresponding imaginary relative permittivity data for the PE-EVA-organoclay, PP-EVA-organoclay and PP-PS-organoclay systems are shown in Figures 6.16(b), 6.16(d) and 6.16(f) respectively, whilst the single polymer-organoclay composites are shown in Figure 6.16(h). The unfilled systems show a slight increase in imaginary permittivity with frequency, however the equipment limit is around 10^{-3} so these data, being below this point, are likely inaccurate and invalid. However, there is a dominant feature in the samples containing organoclay: an increase in imaginary permittivity towards lower frequencies with a gradient between -1 and 0. This gradient indicates that there is a combination of mechanisms contributing to this phenomenon including a conductivity component and also an electrode polarisation component.[139,187]

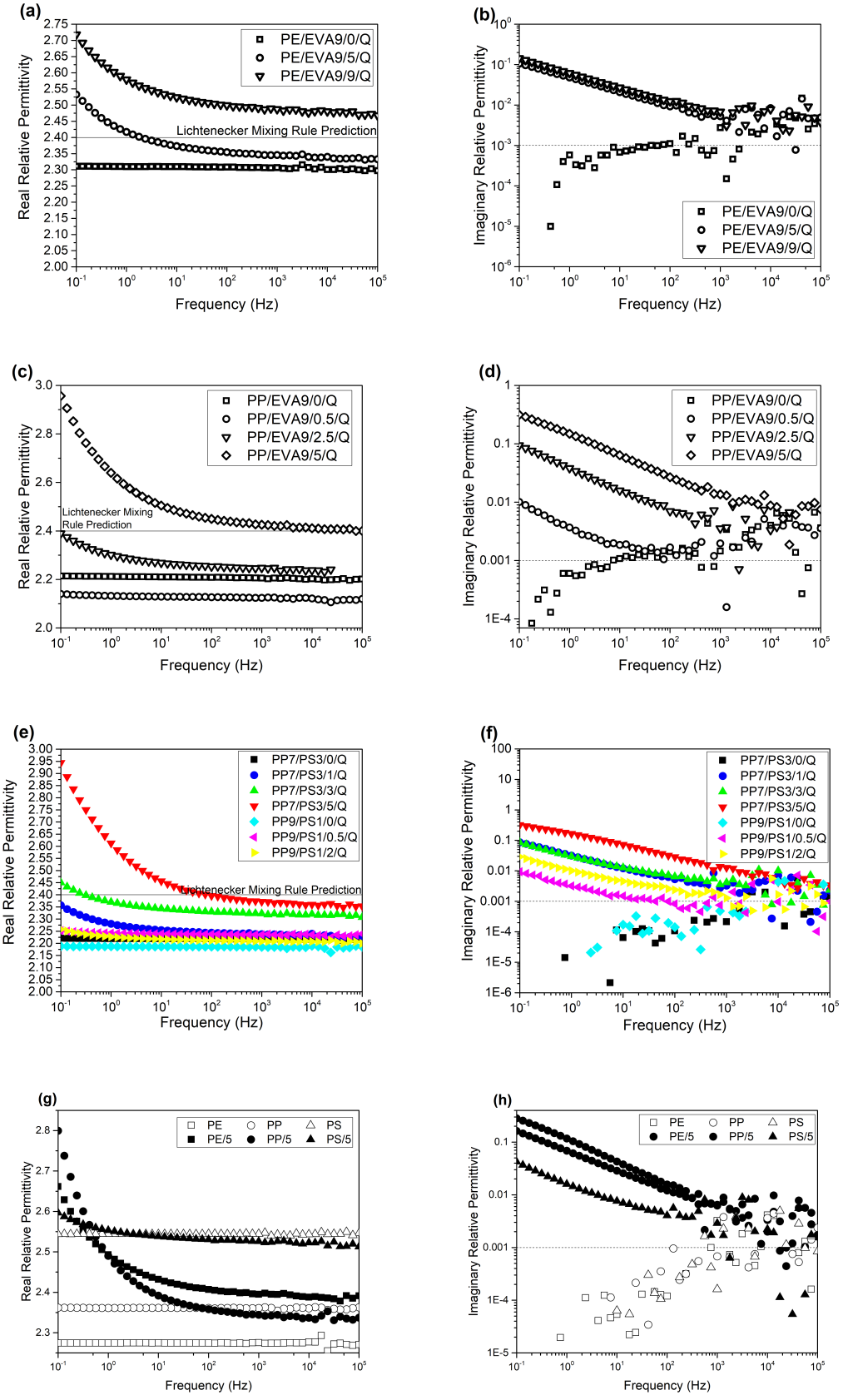

Figure 6.16: *The real and imaginary permittivities for (a) and (b) PE/EVA9/X/Q, (c) and (d) PP/EVA/X/Q, (e) and (f) for PPa/PSb/X/Q and (g) and (h) the single polymer-organoclay composites. The horizontal dashed line indicates the equipment limit.*

An alternative way to scrutinise the dielectric spectroscopy results involves plotting an Argand diagram in the form of the imaginary permittivity on the y-axis and the real permittivity on the x-axis. This has become known as a Cole-Cole plot, named after the authors of the seminal paper published in 1941.[188] Although not frequently used, a Cole-Cole plot can be useful in revealing the dielectric spectroscopy data. It should be noted that ideally, and in order for the arc to appear complete, results should have been gathered to a lower frequency. However, due to equipment sensitivity limitations at low frequencies this was not possible and instead, in order to shift the relaxation to higher frequencies, the temperature of the experiment was increased.

Figures 6.17, 6.18 and 6.19 show Cole-Cole plots for the PE-EVA-organoclay, PP-EVA-organoclay and PP-PS-organoclay systems, respectively. So that measurements could be made at a range of temperatures, the data plotted were collected using a different test cell to the data plotted in Figure 6.16 (hence the permittivity readings differing slightly). Within each material system, the plots have equivalent scales on the axes in order to make comparison facile, however, where necessary, zoomed-in plots have also been included so that details were not lost.

A semi-circular arc in a Cole-Cole plot is indicative of a single dielectric relaxation. Where the arc shape is looser or distorted, the material is either less polarisable or has multiple relaxation processes.[188,189,190,191] Given that Figure 6.16 shows only one relaxation, it is suggested that the distortions away from the arc shape in these Cole-Cole plots are due to the polarisability of the material. From Figures 6.17(a), 6.19(a) and 6.18(a) it is clear that unfilled samples are less polarisable, regardless of the polymer matrix or temperature, compared to the samples containing organoclay. This makes sense given that samples without organoclay contain less polarisable species. The fact that the samples containing organoclay are much more polarisable gives clear evidence of the origin of the dipole responding to the field. Since there is one polarisable species dominating in the samples, the distortion of the semicircular arc may be attributed to the different environments the organoclay is exposed to within the material. As such, a homogeneous composite where the organoclay is evenly dispersed amongst the co-existing polymer chains (i.e. not phase separated) will give rise to the most uniform arc shape. In this way, Cole-Cole plots reveal something about the nature of the dispersion of the organoclay in the materials. Applying this to Figures 6.17, 6.18 and 6.19, it can be concluded that dispersion is best at the lowest organoclay loadings for each material system and, between these, is best in the PE-EVA-organoclay system.

In samples of relatively low organoclay loading, (such as PE/EVA9/1/Q, PP/EVA9/0.5/Q and PP9/PS1/0.5/Q in Figures 6.17(a), 6.18(a) and 6.19(b), respectively) the semicircular arcs become more pronounced with temperature indicating an increase in the polarisability of the sample with temperature. This makes sense with the understanding that at higher temperatures, the sample has higher thermal energy and therefore dipoles are more likely to have sufficient energy to respond to the field.

Deviations from the semicircular arc are seen across all of the samples containing organoclay when measured above room temperature. In particular, the samples containing relatively high organoclay loadings have the arc relatively dwarfed by the conducting component increasing rapidly in real relative permittivity. This indicates the samples are frequency-dependently conductive.[192] All the samples containing organoclay, show an increase in conductivity towards the lowest frequencies investigated i.e. as DC is approached. Across all of the samples containing organoclay, regardless of polymer matrix, the tendency of AC conductivity to increase with temperature was observed. This was also seen elsewhere for a polar co-polymer.[192] These results align well with the model of there being more charge carriers in the conduction band at higher temperatures and more generally with the 'hopping charge carrier' model of conductivity. Therefore, overall, the interpretations of the Cole-Cole plots are in line with expectations.

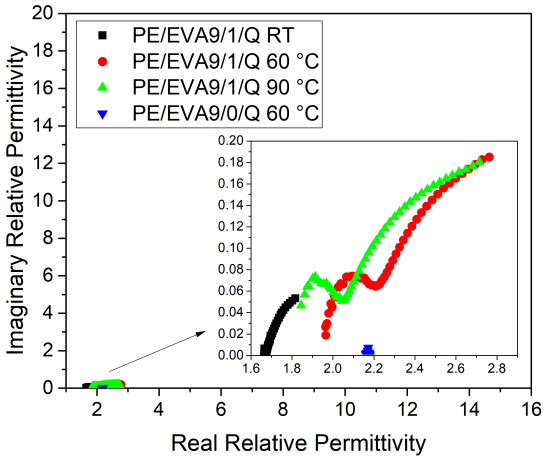

(a) nb if zoomed in further it would be revealed that the blue triangles appear in a small arc shape

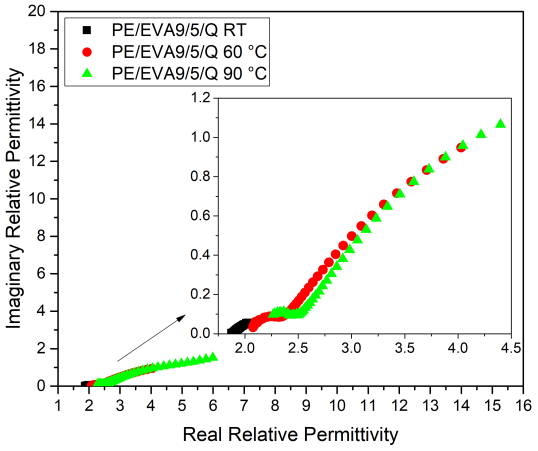

(b)

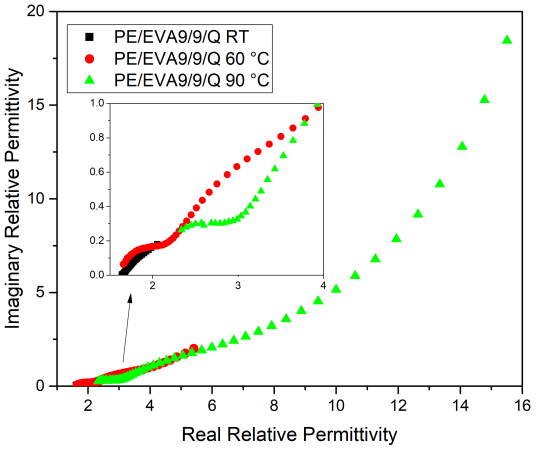

(c)

Figure 6.17: *Cole-Cole plots of the dielectric spectroscopy results obtained under several different temperatures for (a) PE/EVA9/0/Q and PE/EVA9/1/Q, (b) PE/EVA9/5/Q and (c) PE/EVA9/9/Q.*

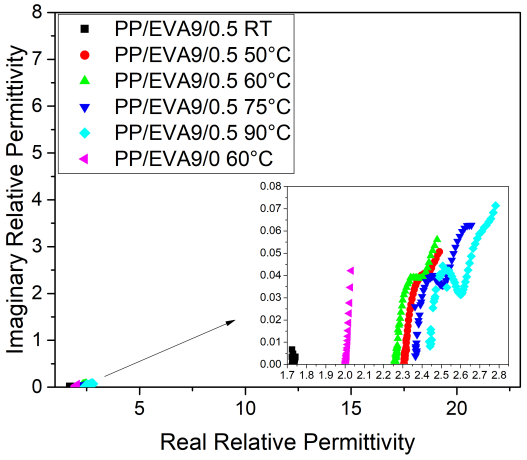

(a)

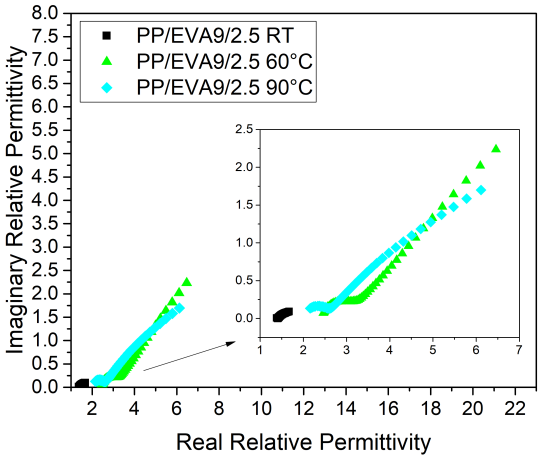

(b)

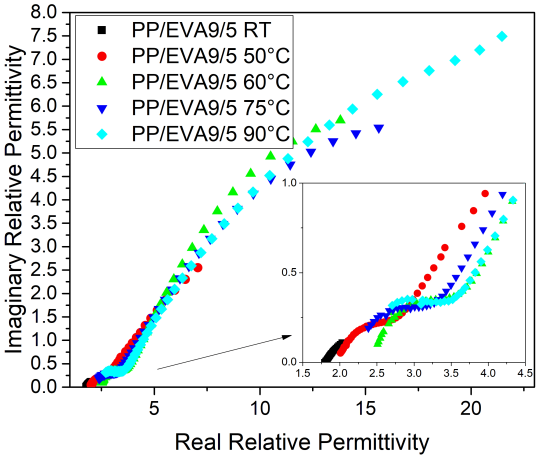

(c)

Figure 6.18: *Cole-Cole plots of the dielectric spectroscopy results obtained under several different temperatures for (a) PP/EVA/9/0/Q and PP/EVA9/0.5/Q, (b) PP/EVA9/2.5/Q and (c) PP/EVA9/5/Q.*

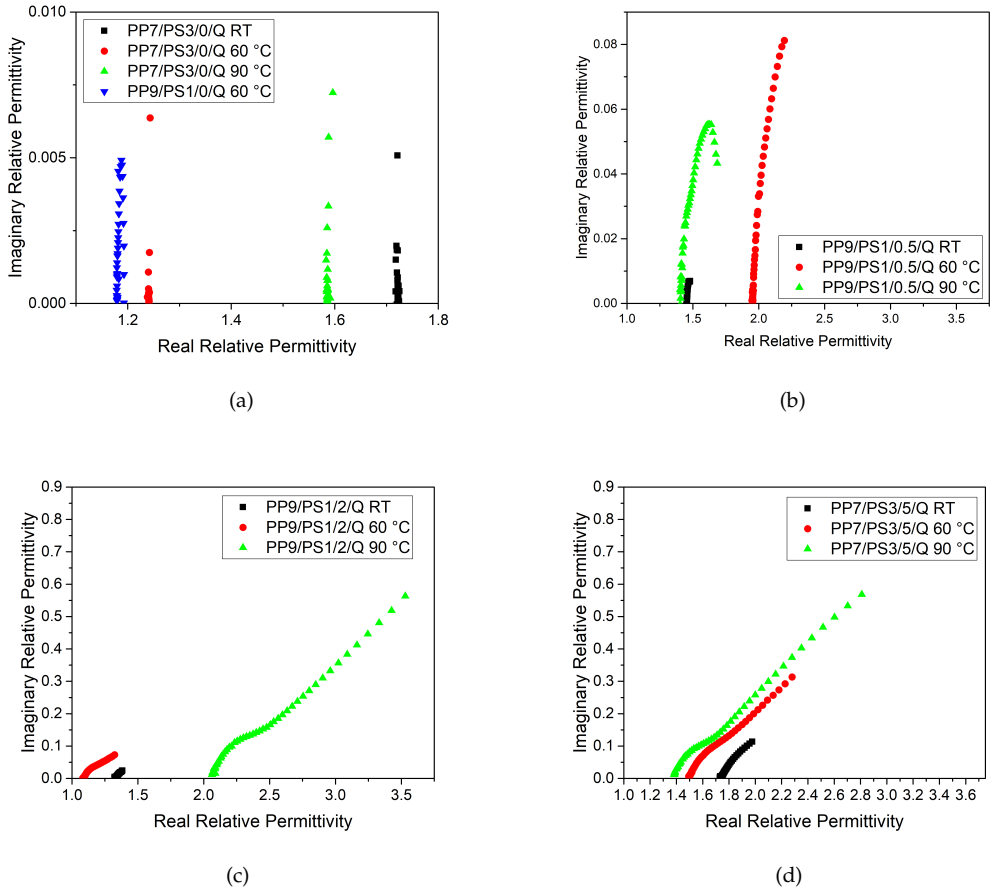

Figure 6.19: *Cole-Cole plots of the dielectric spectroscopy results obtained under several different temperatures for (a) PP7/PS3/0/Q and PP9/PS1/0/Q, (b) PP9/PS1/0.5/Q, (c) PP9/PS1/2/Q and (d) PP7/PS3/5/Q.*

6.5 Conclusion

In all the composites studied, the DC conductivity increase correlated with the increased organoclay loading and a decrease in the DC dielectric breakdown strength. This causal relationship makes sense and has been reported upon previously. This result, nonetheless, highlights the disadvantages of the addition of a nanofiller to the polymer matrix, which will need to be considered, alongside the benefits, by material developers with their specific application in mind.

The AC dielectric breakdown strength results of the PE-EVA-organoclay and PP-EVA-organoclay systems were consistent in that the breakdown strength increased with organoclay loading. In both composite systems the AC dielectric breakdown strength was used to infer some morphological properties of the systems depending on their thermal treatments from the melt phase. In the case of the PE-EVA-organoclay system, no significant change highlighted the effectiveness of the EVA compatibilising the system while in the PP-EVA-organoclay system, the different thermal cooling techniques from the melt phase changed the ability of the organoclay to compatibilise the system.

It is worth noting that most of these breakdown results overlap at the low percentiles (meaning that there is no significant difference at these points) and, so as to keep the material operating within its capabilities, these lower percentiles (and not the α value taken at approximately 63%) are of the most interest for real world applications. Nonetheless, the principles shown in the trends between the α values stand and can be useful for informing future material development.

When considering together the results from the DC conductivity and the DC dielectric breakdown strength measurements with the morphological results, it can be seen that at or above the organoclay percolation point the morphological differences do not affect the dielectric properties. This is an important result in informing material development for specific applications, in particular, in the material processing stages.

The dielectric spectroscopy data show the samples containing organoclay are polarisable and, at high enough loadings, are dominated by conduction losses. Further, the results gave an insight into the relative dispersion of the organoclay being greatest in the PE-EVA-organoclay system, which corroborates with results previously discussed in this thesis.

Chapter 7

Effect of Xylene and Water Immersion on the Composites

This chapter will detail the results from immersing the PP-EVA-organoclay and PE-EVA-organoclay composites in xylene and PE-EVA-organoclay composites in water. This is relevant to the research topic of this thesis since the samples are produced using solution blending in xylene and are exposed to water in the air. Therefore, it is possible that one could be measuring the solvent effects on the material and not those integral of the material itself such as filler loading and morphology. As such, an understanding of the possible side-effects of having remnants of the solvent remaining in the sample is important so that the properties discussed in the previous chapters can be correctly assigned and understood. In order to probe this with some reproducibility the samples were exposed post-synthetically to xylene and, separately, water.

The experiments exposing the samples to xylene were novel - the literature contains no evidence that this approach had been done before. The results from the first material system were established as being general principles, since the experiments were repeated for a second material system yielding similar results. The findings from this work, therefore, have made a valuable contribution and have been published (see Chapter 1.6.1 for details).

The experiments exposing samples to water were undertaken as a counterpoint to the xylene tests, that way, the effects of both polar and non-polar solvents on the samples (and, in particular the organoclay, which has both polar and non-polar elements) would be known. Though exposing samples to water is not an original idea, testing samples containing this type of organoclay, and viewing the results in light of the xylene tests, makes this work novel.

Due to the ubiquity of water, many studies have investigated the effects of the presence of water on the dielectric properties of nanocomposites. For example, Ayoob *et*

al.[193] found that the permittivity increased with nanofiller content when samples were immersed in water, while Lau *et al.*[194] found there to be a significant difference in the dielectric response after immersion in water, depending on the surface treatment of the nanofiller. These effects were interpreted in relation to the adsorption of dipolar water molecules at nanoparticle surfaces, whereupon, the precise dynamics were governed by local hydrogen bonding effects. Hosier *et al.*[99] noted that, although there are relatively few studies in the literature on the effect of water on breakdown, such work consistently shows that the presence of water adversely affects breakdown strength.

While absorption of water will be an inevitable consequence of environmental exposure, this is not the only labile molecular species that may be present, since a solvent processing step is often used in the production of nanocomposites. An investigation into the electrical properties of a PP-based composite containing an organoclay and EVA initially showed some atypical results. It was established that if the samples were not fully dried from the solution blending procedure, the remaining solvent, in this case xylene, could artificially decrease the AC dielectric breakdown strength when organoclay was present and increase the permittivity. The work set out to examine the influence of a labile, but non-polar, species (xylene) on the electrical characteristics of a polymeric nanocomposite and contrast this to the effects of water on the materials.

7.1 Experimental

The samples were prepared and tested using protocols outlined in Sections 2.1.4, 2.1.5, 2.2, 2.3 and 2.4.

For the xylene immersion investigations the samples were PP/EVA9/X/iso120, where X = 0, 2.5 or 5 wt.%, and PE/EVA9/X/Q, where X = 0 or 5 wt.%. For simplicity the samples will be referred to without their respective iso120 and Q nomenclature and instead with a D, I or R amended, which will represent the dried, immersed and re-dried samples respectively. For example PP/EVA9/2.5/R is a sample of PP/EVA9/2.5/iso120 that has been immersed and subsequently re-dried. At the time of this investigation, all of the samples from the PP/EVA9/X/iso120 system were analysed in order to be thorough. However, in light of these results and since the next experiments were conducted to check the phenomenon found was comparable to other material systems, investigations into the PE/EVA9/X/Q system were streamlined: only one organoclay loading was chosen to be compared to the unfilled polymer blend.

The samples for the water immersion investigations were PE/EVA9/X/Q were X = 0, 1 and 9 wt.% organoclay loadings. These filler loadings were chosen in light of the electrical conductivity results presented in Chapter 6.2.1: filler loadings were chosen based on their smallest and greatest effect on the conductivity compared to the unfilled polymer blend given that it was hypothesised that water would increase conductivity.

7.2 Results and Discussion of Xylene Immersion

7.2.1 Investigating Xylene Uptake and Removal

Figure 7.1 shows the variation in sample mass of the PP/EVA9/X/Y composites with immersion time in xylene, and reveals a number of features of the xylene absorption process. First, in equilibrium, the mass of all three samples can be seen to have increased by 5-7%. Second, the initial data points acquired after just 4 hours reveal a comparable mass increase to that seen after 7 days. As such, the key aspects of these data are that xylene absorption occurs rapidly and that the mass of the absorbed xylene is largely independent of the amount of organoclay present. While the former necessarily indicates that any associated measurement of sample mass will be subject to uncertainties derived from the process used to remove xylene from the sample surface prior to measurement of the sample mass, the TGA and mass change measurements (shown in Figure 7.2) are, nevertheless, still in broad quantitative agreement.

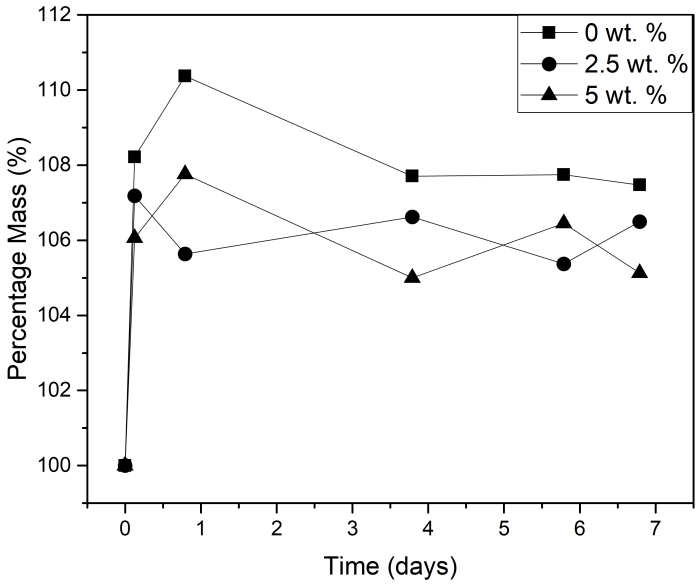

Figure 7.1: *Mass changes upon immersion of the PP/EVA9/X/Y composites in xylene. The error on each measurement is around 0.5% and the daily drift of the balance was taken into account.*

Figure 7.2 shows TGA data obtained from both dried and immersed samples from the PP-EVA-organoclay sample system. Consider first the results obtained from the dried samples. The absence of any detectable changes in mass at low temperatures indicates that negligible volatile species remained within the systems after drying. Further, the actual organoclay loading level present in each of the filled systems were 1.5 and 4.7 wt.% for the composition goals of 2.5 and 5 wt.% respectively. These calculated organ-

oclay loadings were unchanged by the xylene immersion. For simplicity, herein, the samples will still be referred to by their nominal target composition.

The inset in Figure 7.2 shows low temperature TGA data obtained from samples that had been immersed in xylene. Since the reported boiling temperature of the various isomers of xylene range from 138-144 °C, this feature, together with the absence of any comparable mass losses in the dried samples, strongly implies that this change in mass is related to desorption of xylene, which occurs progressively up to around 150 °C.

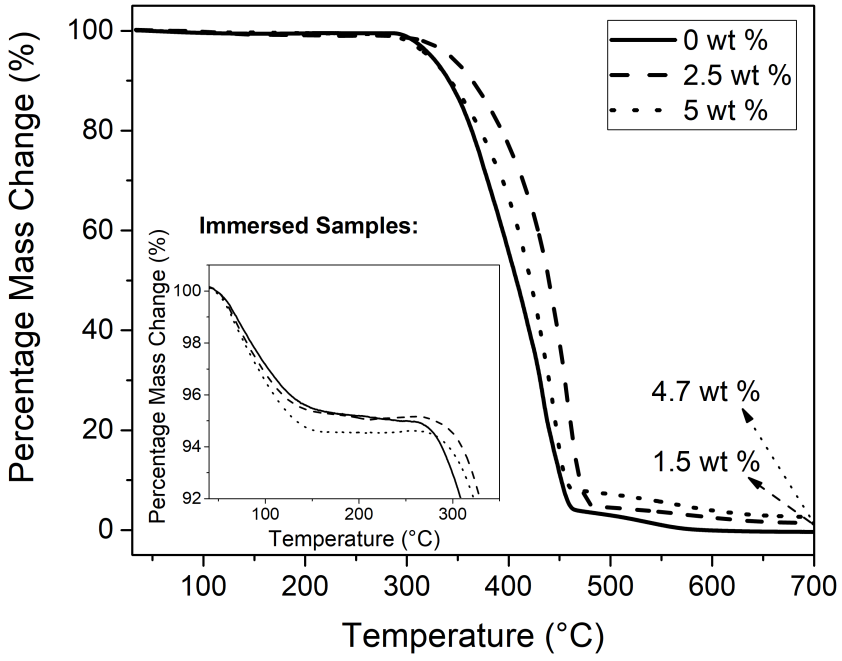

Figure 7.2: *Data from TGA conducted in air on PP/EVA9/X/D samples and the respective PP/EVA9/X/I samples (inset). The achieved organoclay loading has also been labelled.*

Figure 7.3 shows the mass change upon immersion and subsequent removal of the xylene under vacuum for the PP/EVA9/0/Y sample as a representative example. It can be seen that the xylene uptake occurs within a matter of hours (on the graph it appears on the 'Dried Samples' line due to the size of the scale on the x-axis). Drying took several days to remove the xylene returning the mass to the original amount - possibly due to the need to overcome the intermolecular forces formed between the xylene and the organoclay. The error on each measurement is around 0.5% and the daily drift of the balance was taken into account. Even so, the cause of the datum at 20 hours is unclear and is likely an erroneous result caused by vibrations from other equipment on the same desk reducing the accuracy of the balance.

Figure 7.4 shows the mass changes recorded following immersion and subsequent re-drying of the PE/EVA9/X/Y composites. Marked on the graph are the points at which

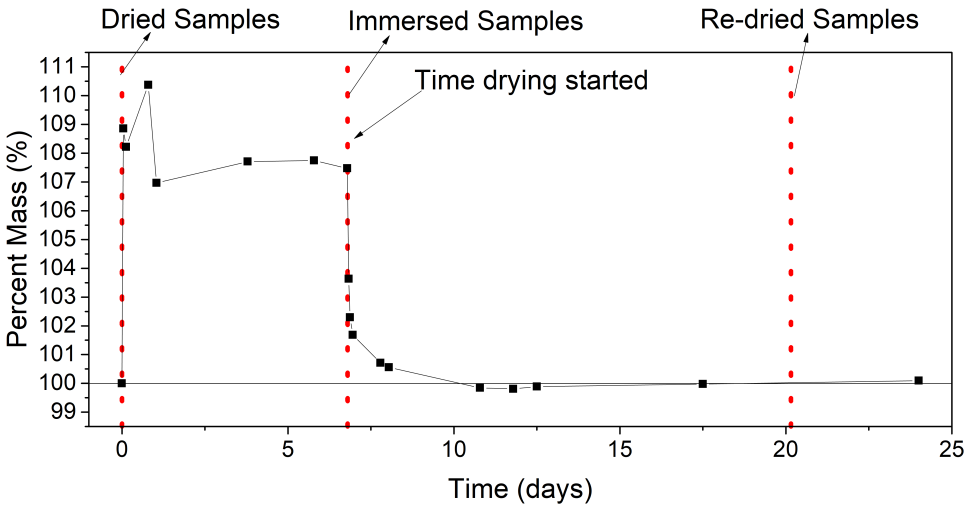

Figure 7.3: *Mass changes upon immersion and subsequent removal of xylene from PP/EVA9/0/Y. The error on each measurement is around 0.5% and the daily drift of the balance was taken into account.*

dielectric measurements were taken. From these data, it is evident that absorption occurs rapidly before plateauing at levels equating to around 10 wt.% of the initial sample mass in the case of PE/EVA9/0/I and PE/EVA9/5/I. However, the uncertainties in these values are such that these numerical differences are not statistically significant, indicating that the absorption of xylene is not significantly affected by the presence of the organoclay. This is presumably because xylene, being a good solvent for the dissolution of PE and EVA, is readily compatible with them.

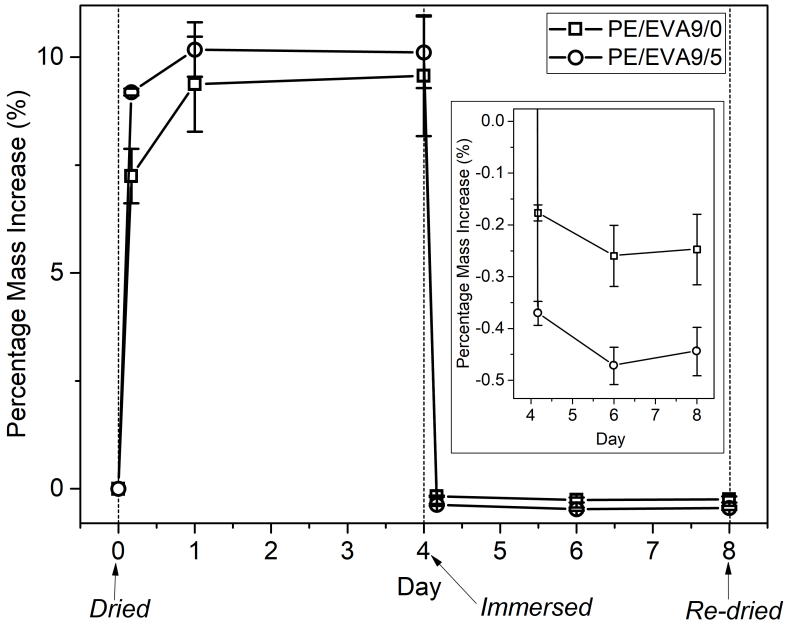

Figure 7.4: *Mass changes upon immersion and subsequent removal of xylene from the PE/EVA9/X/Y composites.*

Figure 7.5 shows ATR FT-IR data acquired from the PP/EVA9/X/Y samples of each material after one week of drying in a vacuum oven. In the materials containing organoclay there is an additional broad peak around 1075 cm^{-1}, corresponding to the Si-O bonding in the clay. ATR gives information on the sample surface, which is particularly of interest to check for possible degradation. It is notable that no absorption peaks can be seen in spectral regions that would correspond to degradation of the polymer during the extended drying procedure. This indicates that the drying procedure did not chemically alter the films.

Figure 7.6 shows transmission FT-IR data obtained from PP/EVA9/5 samples compared to xylene. The data show the presence of absorption peaks associated with xylene in the immersed sample, which are absent in the dried and re-dried samples. Since comparison of the FT-IR spectra obtained from these revealed no other differences, it can be concluded that the process of xylene immersion did not affect the system in any other way.

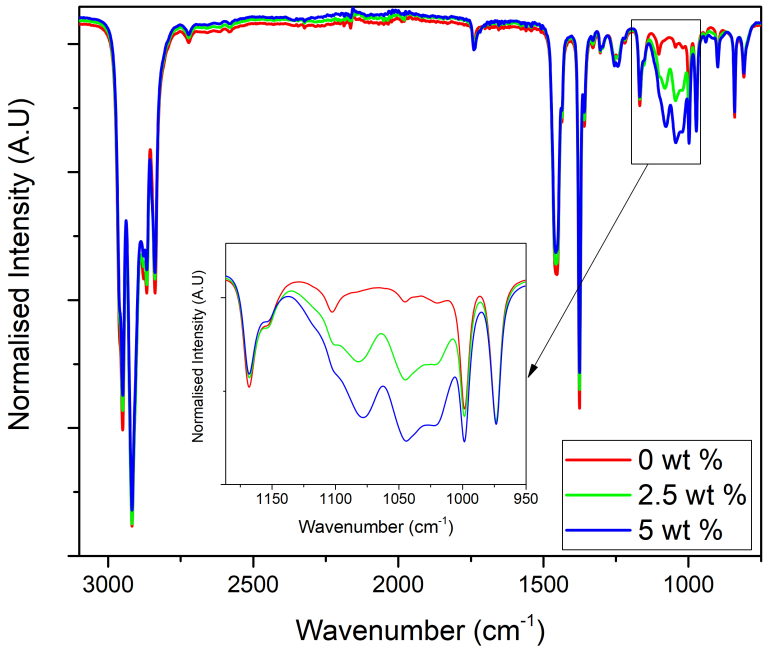

Figure 7.5: *ATR FT-IR data, normalised using Z-scores, of the PP/EVA9/X/D samples showing no evidence of polymer degradation (for example, oxidation) and the organoclay loading (highlighted by the inset).*

The FT-IR results for the PE/EVA9/0/Y and PE/EVA9/5/Y are shown in Figure 7.7(a) and 7.7(b) respectively. In both figures, the FT-IR spectrum of xylene is also included as a reference. From the traces labelled 1, xylene, it is evident that the FT-IR spectrum of this solvent contains a number of characteristic peaks within the spectral region shown, which fall within featureless regions of the spectrum of both PE/EVA9/0/D and PE/EVA9/5/D (traces labelled 2). Consequently, the presence of xylene in the PE/EVA9/0/I and PE/EVA9/5/I samples (traces labelled 3) is readily detected. In the case of PE/EVA9/0/R and PE/EVA9/5/R (traces labelled 4), weak absorption around 690 cm^{-1} and between 740 cm^{-1} and 820 cm^{-1} suggest that a small amount of xylene is retained, despite the samples being stored under dynamic vacuum (ca. 2 mbar) at 70 °C for 4 days and the mass change monitoring suggesting that the mass had stabilised. However, careful examination reveals shifts in these xylene-related peak maxima in the re-dried samples compared with both the xylene solvent itself and the immersed specimens. It is suggested that this effect is associated with local molecular interactions that influence the relevant vibrational modes; elsewhere, effects such as hydrogen bonding, variations in local disorder and vibronic coupling have been reported to shift and/or broaden FT-IR peaks in a manner akin to that seen here.[195,196]

The data reveal something different to the PP/EVA9/X/Y data shown in Figure 7.6. It is proposed that this is likely due to the different affinities of xylene with PE and PP in

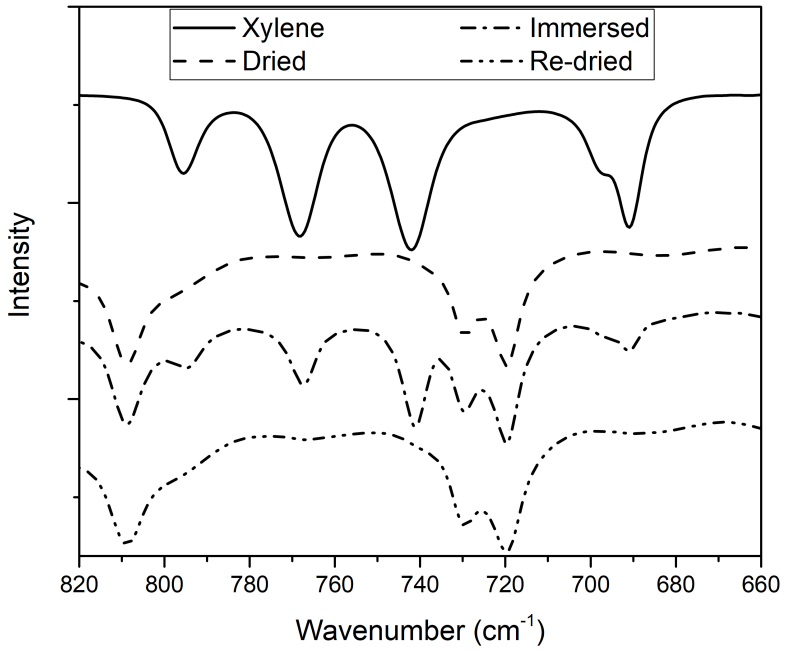

Figure 7.6: *Transmission mode FT-IR data, normalised using Z-scores and off-set for clarity, from the fingerprint region of PP/EVA9/5/Y samples containing 5 wt.% organoclay compared to xylene to identify the samples that contain xylene.*

the different composites.

Using XRD, the changes to the organoclay in the PE/EVA9/X/Y composites following xylene immersion and subsequent removal were investigated. The results are shown in Figure 4.6 and have been detailed, as part of the discussion on observing the organoclay in the composites, in Chapter 4.5. However the results pertinent to the xylene immersion experiments will be summarised here. The presence of xylene increased the interlayer distance of the organoclay, yet the removal of the xylene in the re-drying process resulted in a smaller interlayer distance than that of the dried sample. These results imply, respectively, that the xylene causes swelling of the polymer and organoclay, and that some material is physically removed in the re-drying process, causing a permanent physical change to the composites.

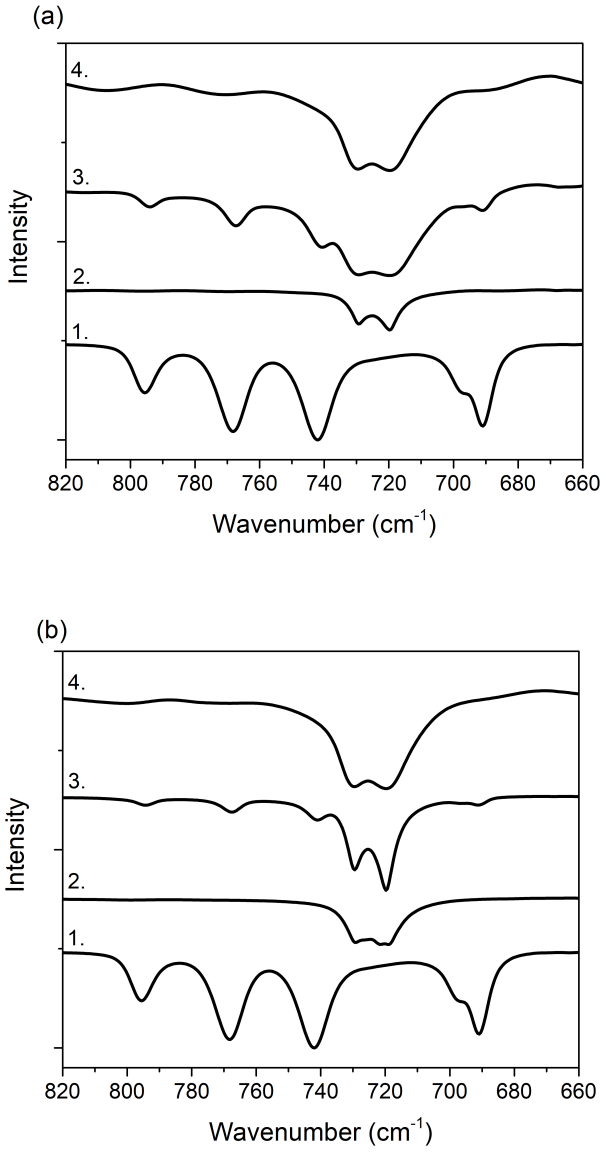

Figure 7.7: *FT-IR data, normalised using Z-scores and off-set for clarity, of dried, immersed and re-dried composites of (a) the PE/EVA9/0/Y and (b) the PE/EVA9/5/Y, compared to xylene.*

7.2.2 The Dielectric Response

7.2.2.1 Dielectric Spectroscopy

Dielectric spectroscopy data for both the PE/EVA9/X/Y and PP/EVA9/X/Y composites at each of the dried, immersed and re-dried conditionings are shown, respectively, in Figures 7.8 and 7.9 are discussed below.

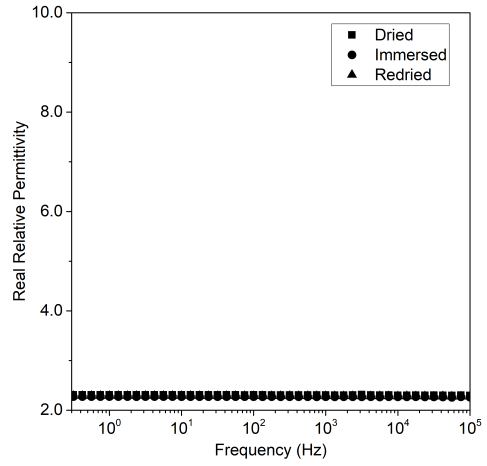

(a) Real relative permittivity of PE/EVA9/0/Y

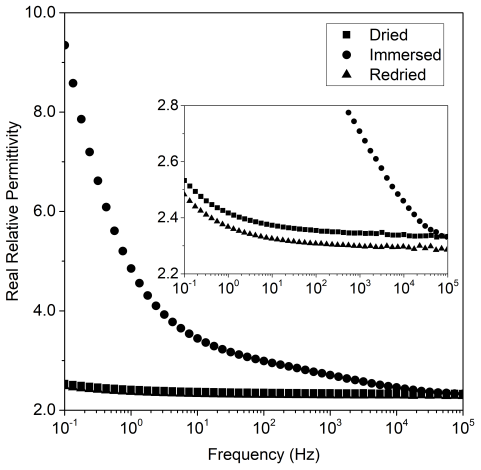

(b) Real relative permittivity of PE/EVA9/5/Y

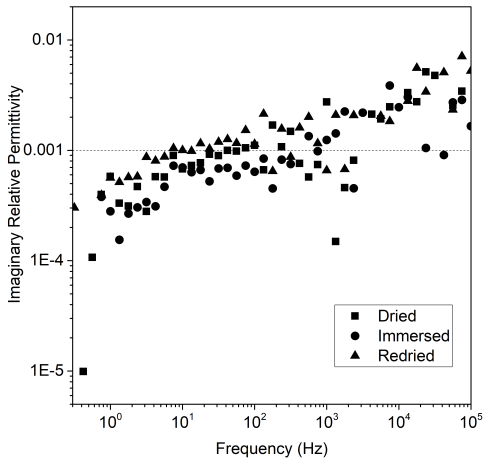

(c) Imaginary relative permittivity of PE/EVA9/0/Y

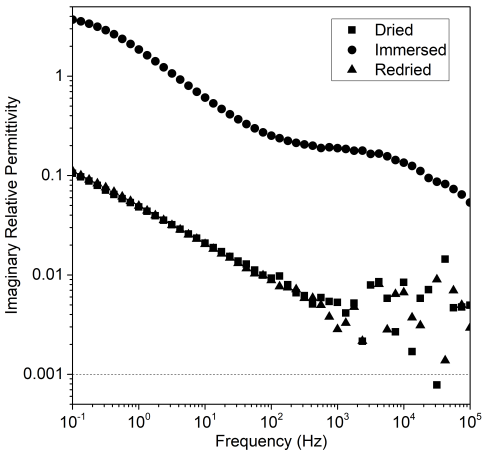

(d) Imaginary relative permittivity of PE/EVA9/5/Y

Figure 7.8: *Dielectric spectroscopy data of the PE/EVA9/X/Y composites at the various stages of the xylene immersion tests. The horizontal dashed line indicates the equipment limit.*

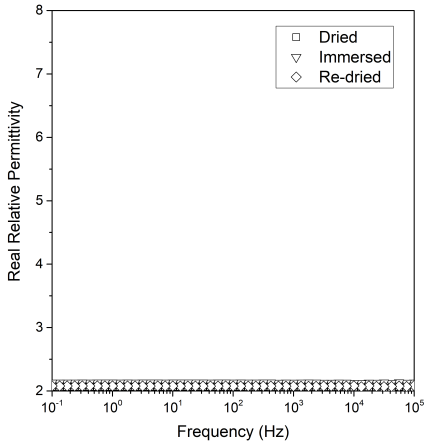

(a) Real relative permittivity of PP/EVA9/0/Y

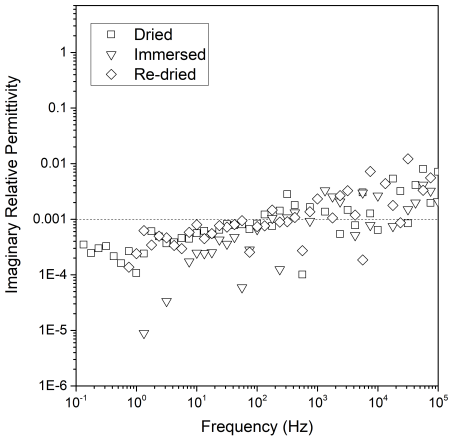

(b) Imaginary relative permittivity of PP/EVA9/0/Y

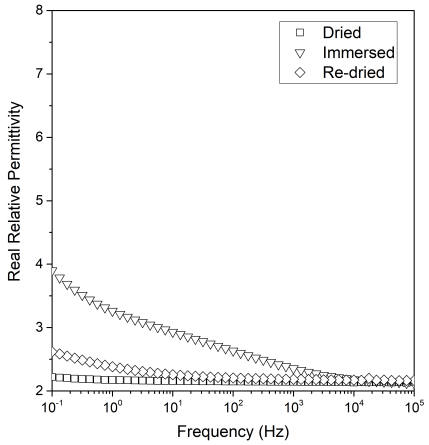

(c) Real relative permittivity of PP/EVA9/2.5/Y

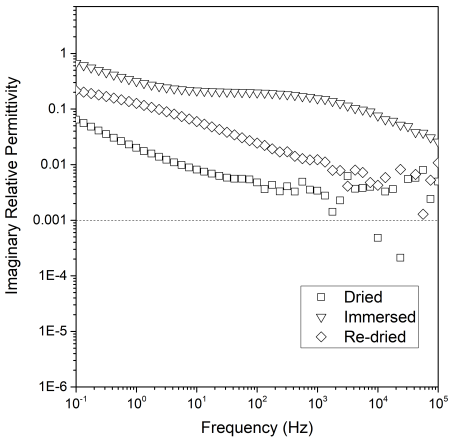

(d) Imaginary relative permittivity of PP/EVA9/2.5/Y

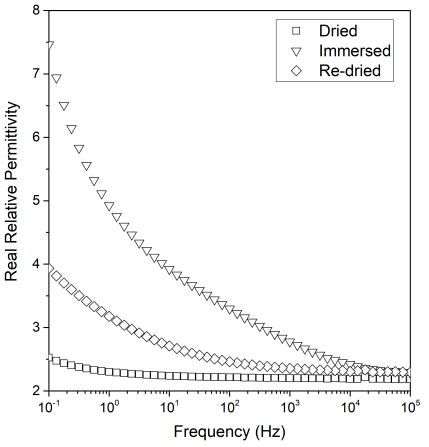

(e) Real relative permittivity of PP/EVA9/5/Y

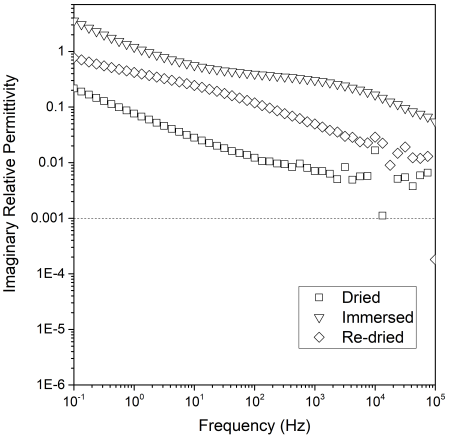

(f) Imaginary relative permittivity of PP/EVA9/5/Y

Figure 7.9: *Dielectric spectroscopy data of the PP/EVA9/X/Y composites at the various stages of the xylene immersion tests. The horizontal dashed line indicates the equipment limit.*

For polymer blends, it is possible to estimate the anticipated value of the real part of the relative permittivity, ϵ', using any one of a number of effective medium mixing theories.[134] Using the Lichtenecker logarithmic mixing rule,[135] results in a value of 2.4, based upon values of 2.3 for iPP[136] and 2.7 for EVA containing 9 % of VA, approximating the latter to be the same as EVA containing 12 % VA.[179] Evidently, the precise permittivity values shown in Figure 7.9(a) fall somewhat below this value, which is a consequence of uncertainties/variations in the sample thickness and the impact this has on deriving an effective permittivity value from the measured capacitance.

Nevertheless, the key feature of these data and the complementary imaginary permittivity data shown in 7.9(b) is that neither parameter is affected by absorption of xylene. The xylene used contains a mixture of the xylene isomers, but, for a representative example, para-xylene has a real relative permittivity value of 2.26 at 1 kHz[197] and, therefore, the inclusion of a small quantity of this solvent would not be expected to dramatically affect ϵ'. Some dielectric relaxation studies of systems containing chemically similar solvents to xylene have been undertaken: in the case of solutions of polystyrene in toluene, a weak β relaxation around 150 Hz is reported and attributed to rotation of toluene molecules.[198] As such, the absence of any detectable relaxations in the systems containing absorbed xylene is unsurprising.

Real and imaginary dielectric spectroscopy data for the PE/EVA9/X/Y composites are shown in Figure 7.8. The real relative permittivity, ϵ', of PE is 2.3 at 1 kHz,[136] which is approximately the ϵ' value obtained for PE/EVA9/X/Y and obtained by Zazoum *et al.*[139] for an 80:20 LDPE:HDPE blend (the same ratio used herein albeit the polymers were from different suppliers). Their data show a straight horizontal line, with ϵ' around 2.3, across the same frequencies measured herein. This means the results presented herein being around ϵ' = 2.25 for the PE/EVA9/0/D sample is unsurprising given PE is the largest constituent of the composite.

Figures 7.9(c), 7.9(d), 7.9(e), 7.9(f), 7.8(b) and 7.8(d) show dielectric data obtained from the systems containing the organoclay from both types of composites. First, consider the data obtained prior to exposure to the xylene, from which it is evident that the addition of the organoclay has little effect on the measured absolute value of ϵ', with high frequency values falling in the range 2.0 to 2.2 for the PP/EVA9/X/Y composites and 2.25 for the PE/EVA9/X/Y composites. At low frequencies, a small increase in ϵ' is evident for both the PP and PE-based samples containing organoclay.

In dielectric data, charge transport processes manifest themselves in a dependence of the form:

$$\epsilon'' \propto \omega^{-1}$$

where ω is the frequency of the field.[187,173] In a nanocomposite composed of polylactide and an MMT-based organoclay, Pluta *et al.*[187] reported the exponent in the above

equation was between -1 and 0. This, was attributed to a combination of charge transport, electrode polarisation and interfacial polarisation processes. Elsewhere, Fabiani *et al.*,[178] described the dielectric behaviour of EVA containing an organically-modified fluorohectorite clay and reported a loss peak at around 10 to 20 Hz, which they attributed to dielectric processes at polymer-filler interfaces. As such, it is proposed that, the variations of ϵ'' that are evident in Figures 7.9(d), 7.9(f), and 7.8(d) result from a combination of dipolar and charge transport processes.

The effect of organoclays on the dielectric response of a wide range of different polymer systems has been reported in the literature. Izci *et al.*[199] report that, at 10^{-2} Hz, the permittivity of their polypropylene-based nanocomposite increases with organoclay loading a peak that had already been shifted to higher frequency due to the polymer-clay interface. Elsewhere, Zazoum *et al.*[139] report similar findings on a PE-based nanocomposite. In both cases, without the organoclay, the base polymer showed no dielectric relaxations. These findings align with those reported herein.

When both xylene and the organoclay are present, dramatic changes in the dielectric response of the system are evident for both the PP/EVA9/X/Y and PE/EVA9/X/Y composites. Specifically, a pronounced increase in ϵ' is evident with decreasing frequency which, from the imaginary data, appears to be associated with two processes, a distinct dielectric loss process around 10 to 10^3 Hz, plus a low frequency dispersion which may either be related to Maxwell-Wagner polarization or to increasing DC conduction.

For both the PE and PP-based composites investigated, when comparing the unfilled, dried systems and the unfilled immersed systems with the filled counterparts, the results clearly demonstrate that the dielectric response of the filled composites immersed in xylene is not due to the presence of any single component (namely xylene or organoclay) acting in isolation. Therefore it is suggested that the dielectric effects shown above occur as a result of organoclay-xylene interactions. That is, the presence of the xylene effectively solvates dipolar species in the clay so facilitating a molecular response to the applied field and, thereby, leading to the increased losses that are observed. In general, organoclays contain amphiphilic molecules that are introduced within the galleries, both to increase compatibility with the host matrix and to increase the interlayer spacing and, thereby, ease exfoliation.[48,200] In such systems, the VA from the copolymer EVA interacts with the silicate clay layers, while the non-polar chains on the organoclay promote compatibility with non-polar matrix polymers. As such, it is suggested that a potential molecular explanation for increased losses seen when both the xylene and organoclay are present relate to solvation of the compatibiliser by the absorbed xylene, together with swelling of the galleries, as seen in the XRD results in Figure 4.6.

The consequence of both the solvation and swelling is enhanced mobility of compati-

biliser ions within the interlayer clay galleries, which facilitates coupling to the applied electric field more strongly than for samples containing organoclay but no xylene. Furthermore, given the observed reduction in organoclay periodicity shown by XRD data in Figure 4.6 for PE/EVA9/5/R compared with PE/EVA9/5/D, it is feasible that during the immersion step extraction of some compatibiliser molecules may occur, which may then result in increased ionic conduction. However, while this may contribute to the observed losses, the frequency dependence of ϵ'' at low frequencies clearly indicates that this is not the dominant factor. As such, it is suggested that a major contributory factor in the strongly increased losses seen when both the organoclay and xylene are present is solvent/compatibiliser interactions serving to facilitate coupling of the latter with the applied field. Indeed, the nature and dispersion of the compatibiliser has been shown to produce different permittivity traces, highlighting its role in interfacial polarisation in dielectric spectroscopy.[178,185]

It is proposed that the variations in the real permittivity of the unfilled samples are an artefact of the chosen sample handling methodology and not of any tangibile change in the permittivity following xylene immersion. As discussed in connection with the mass changes observed in Figures 7.1 and 7.4, absorption and desorption of xylene occurs relatively rapidly in these systems; consequently, by ensuring that no xylene remained on the sample surface prior to making measurements, varying degrees of desorption occurred during the 30 minutes drying time over which the sample was exposed to the uncontrolled ambient laboratory environment.

Comparison of the dielectric data obtained from PP/EVA9/X/D and PP/EVA9/X/R indicates the presence of the increased low frequency losses implying that some xylene, nevertheless, remained entrained within the latter systems. In contrast to this, comparison of the dielectric behaviour of PE/EVA9/5/D and PE/EVA9/5/R reveals no such difference, which indicates that any differences in the samples, caused by immersion in xylene, is negligible from a dielectric perspective for the frequency range observed.

Sample	α (kV/mm)	Change in α from dried sample	β	Thickness (mm)
PP/EVA9/0/D	144 ± 8	–	6.9	0.11 ± 0.002
PP/EVA9/0/I	140 ± 6	-3%	9.3	0.12 ± 0.007
PP/EVA9/0/R	136 ± 6	-6%	8.6	0.08 ± 0.003
PP/EVA9/2.5/D	176 ± 4	–	16.6	0.10 ± 0.008
PP/EVA9/2.5/I	144 ± 4	-18%	22.5	0.08 ± 0.003
PP/EVA9/2.5/R	171 ± 6	-3%	14.7	0.07 ± 0.002
PP/EVA9/5/D	160 ± 6	–	10.5	0.09 ± 0.004
PP/EVA9/5/I	133 ± 4	-17%	13.9	0.09 ± 0.005
PP/EVA9/5/R	153 ± 6	-4%	11.9	0.09 ± 0.004

Table 7.1: *Weibull data from the AC dielectric breakdown data studying the effect of the xylene on the PP/EVA9/X/Y composites*

7.2.2.2 Dielectric Breakdown

Since it would appear that there are xylene-mediated dielectric effects, it is appropriate to consider how the relaxation processes evident in Figures 7.9 and 7.8 influence breakdown strength of materials.

AC dielectric breakdown test data for the PP/EVA9/X/Y samples fitted well to the two parameter Weibull distribution with 90 % confidence limits. Figure 7.10 contains representative AC breakdown data obtained from dried, immersed and re-dried samples containing 2.5 wt.%, presented in the form of Weibull plots. Parameters derived from such an analysis for all systems are presented in Table 7.1; the quoted uncertainties in the Weibull scale parameter, correspond to 90 % confidence intervals.

The immersion of the PP/EVA9/X/Y samples in xylene resulted in an overall percentage mass increase of around 7 % regardless of the organoclay presence (shown in Figure 7.1). However, there was no significant difference in the AC breakdown strength between the samples immersed in xylene regardless of the presence of organoclay. This means that the presence of xylene effectively extinguishes the effect of organoclay on the AC breakdown strength, which was shown previously to increase with organoclay loading in dry samples (see Figure 6.11).

In the case of the PP/EVA9/0/Y samples, where the variation in breakdown strength seen is comparable to the uncertainties in these measurements, indicate that, in isolation, the presence of the xylene in the sample without organoclay does not significantly affect the breakdown strength. However, in the systems containing the organoclay, the presence of the xylene, which in the unfilled system is benign, leads to a significant reduction in breakdown strength. This indicates that interactions between the xylene and the organoclay serve to promote a mechanism that causes breakdown to occur at a

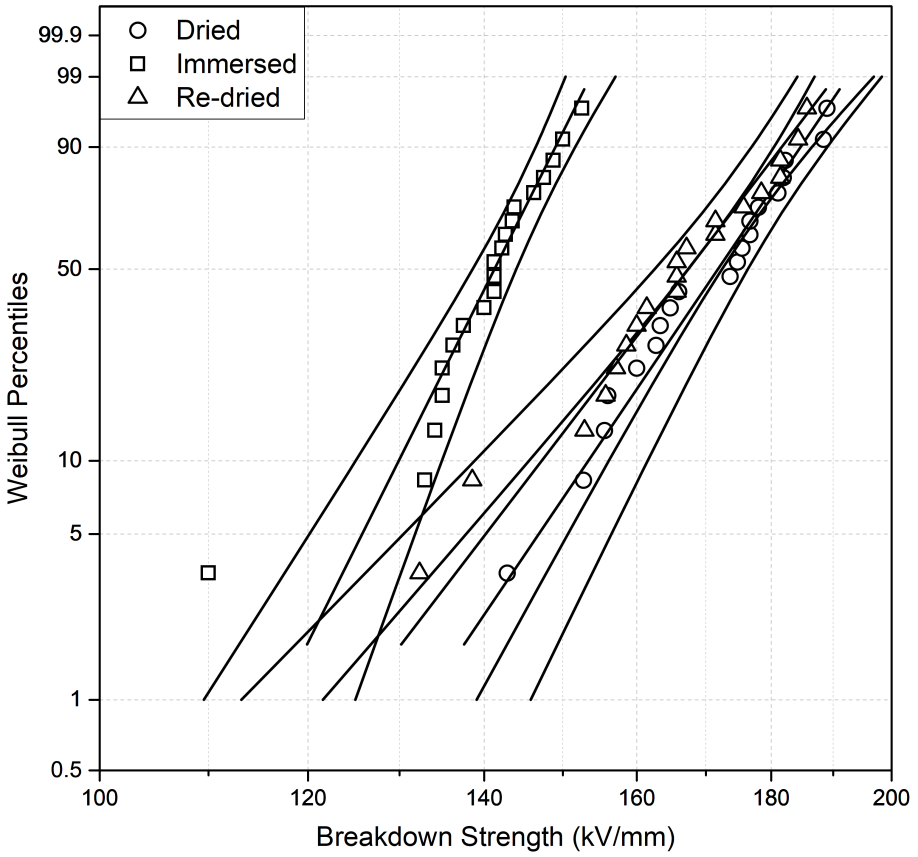

Figure 7.10: *AC dielectric breakdown strength data for the dried, immersed and re-dried samples of PP/EVA9/2.5/Y*

reduced electric field. This finding corroborates with work elsewhere that studied the effects of the breakdown strength on samples synthesised in humid conditions. The tests look at the affinity of water to their hydroxyl-covered nanoparticles but it is believed a similar mechanism is occurring in the work herein with the xylene-organoclay affinities.[36]

This phenomenon is similar to work described elsewhere, which reported on the effects of absorbed water on breakdown strength.[99] In the case of water, it is possible to propose a number of mechanisms by which its presence could adversely affect breakdown strength, involving dipolar and/or ionic processes. Here, the critical role played by the non-polar xylene combined with the mediating effect of this species in increasing dielectric losses at 50 Hz (the frequency of the dielectric breakdown testing), suggests that the dipole processes are most pertinent. In all cases, the re-dried samples exhibited a breakdown strength that was somewhat lower than their respective, dried samples which is again consistent with the marginally increased dielectric losses seen in the

Sample	α (kV/mm)	Change in α from dried sample	β	Thickness (mm)
PE/EVA9/0/D	463 ± 22	–	8.9	0.09 ± 0.004
PE/EVA9/0/I	360 ± 33	-22%	4.7	0.10 ± 0.005
PE/EVA9/0/R	427 ± 28	-8%	6.7	0.09 ± 0.003
PE/EVA9/5/D	399 ± 13	–	12.6	0.10 ± 0.004
PE/EVA9/5/I	313 ± 19	-22%	7.1	0.10 ± 0.005
PE/EVA9/5/R	367 ± 8	-8%	20.5	0.09 ± 0.004

Table 7.2: *Weibull data from the DC dielectric breakdown data studying the effect of the xylene on the PE/EVA9/X/Y composites*

re-dried samples in Figure 7.9.

To explore further the origins of the marginally reduced breakdown strength and increased dielectric losses seen in the re-dried materials for the PP/EVA9/X/Y system, these were subject to further analysis. Measurements of the change in sample mass during drying following immersion in xylene showed that, after one week, the mass had returned to the original level, which indicates that the mass of any retained xylene is less than the associated experimental uncertainties. FT-IR analysis of the re-dried sample also revealed no evidence for retained xylene. In concert, these observations lead to another possibility, namely that the electrical effects seen are not associated with retained xylene but are, rather, caused by the xylene immersion process inducing some irreversible change in the system. In the view of the proposal that absorption of xylene can solvate components within the systems, a possible implication of this is that extraction of such species occurs during immersion in xylene. To explore this possibility, after removal of the above specimens, the xylene was examined by FT-IR. In addition, pristine organoclay was also soaked in xylene before FT-IR analysis specifically to consider the possibility of compatibiliser extraction. None of these experiments provided evidence of any additions to the xylene solution.

By way of contrast and to help formulate a broader understanding of the effects of xylene immersion, DC dielectric breakdown tests were performed on the PE/EVA9/X/Y composites and the results are shown in Table 7.2.

Comparison of the behaviour of the PE/EVA9/0/Y sample set with equivalent data obtained from PE/EVA9/5/Y reveals that, irrespective of pre-conditioning regime, the inclusion of 5 wt.% of the organoclay consistently results in a reduction in the Weibull scale parameter by around 60 kV/mm. From the dielectric data presented above, it is evident that the inclusion of the organoclay increases the low frequency losses, which can be partially ascribed to enhanced charge transport. As such, it is suggested that the observed $\approx$ 60 kV/mm reduction in DC breakdown results directly from increased DC conduction in the presence of the organoclay. Comparable relationships between DC

conductivity and DC breakdown strength have been reported elsewhere.[201]

Comparison of the DC breakdown strength of PE/EVA9/0/D and PE/EVA9/0/R or PE/EVA9/5/D and PE/EVA9/5/R demonstrates that subjecting these systems to xylene absorption and subsequent desorption has a statistically insignificant effect on the derived Weibull scale parameter. This implies that any structural or compositional changes are electrically insignificant as far as breakdown processes are concerned, alike the permittivity findings presented in Chapter 7.2.2.1.

However, in both PE/EVA9/X/I systems, the presence of xylene results in a reduction in breakdown strength of around 30 %, which exceeds the uncertainties in these data. In the case of PE/EVA9/5/I, this may be related to xylene facilitating enhanced charge transport, with a negative correlation between DC conductivity and DC breakdown strength being widely reported on for systems similar to that studied herein, and beyond thermoplastics and organoclays.[178,201,36] That is, in this system, increased ionic conduction occurs as a consequence of solvated ions liberated from the organoclay; this is consistent with both the XRD and mass change data presented in Figures 4.6 and 7.4 respectively. However, this fails to explain the comparable reduction in DC breakdown strength exhibited by PE/EVA9/0/I. As such, while the possible influence of labile solvated compatibiliser molecules is not discounted, in the case of PE/EVA9/5/I, it is suggested that xylene, like some technologically important organic moieties, also appears to have a direct influence on charge transport processes. Indeed, similar results have been seen in the adverse electrical consequences of acetophenone, cumyl alcohol and α-methyl styrene in cross-linked PE.[202,203,204]

7.3 Effect of Water Immersion on the Composites: a counterpart to the Xylene Immersion Work

Environmental exposure of materials to water is inevitable, however absorption of this polar species can present a serious conditioning problem by altering the material properties. As a counterpoint to the xylene-immersion tests presented previously, water immersion tests will be examined so as to understand the effects of a polar solvent, which, in turn, will highlight the mechanism of the solvents influencing the dielectric properties.

The percentage mass change following water immersion was the same across all the samples: around 0.06 % increase and was stable after 1 day. Elsewhere for PE containing 5 or 10 wt.% silicon oxide or silicon nitride, the percentage change following water immersion was an order of magnitude higher at 0.6 % and stabilisation took around 4 days.[205] This suggests that organoclay is less susceptible to water uptake than silicon oxide and silicon nitride as the only other difference was the presence of EVA, which is

more hydrophilic than PE.

Figure 7.11 shows normalised transmission FT-IR data of the dry and immersed samples. These data show no significant difference between the dry and wet (immersed) samples apart for the larger peaks at around 3400 and 3600 cm^{-1} in PE/EVA9/9/Q. A change in peak size suggests that more of the corresponding bond type is present (in this case hydrogen bonding of O-H).[136] The increase in peak size in PE/EVA9/9/Q is due to the presence of water increasing the amount of hydrogen bonding occurring between the O-H groups in the water and the O-H groups in the organoclay clay. This peak is larger in PE/EVA9/9/Q than PE/EVA9/1/Q, despite the mass change measurements suggesting that an equivalent amount of water was present, because the former has a higher concentration of organoclay and hence more species to form hydrogen bonding with the water.

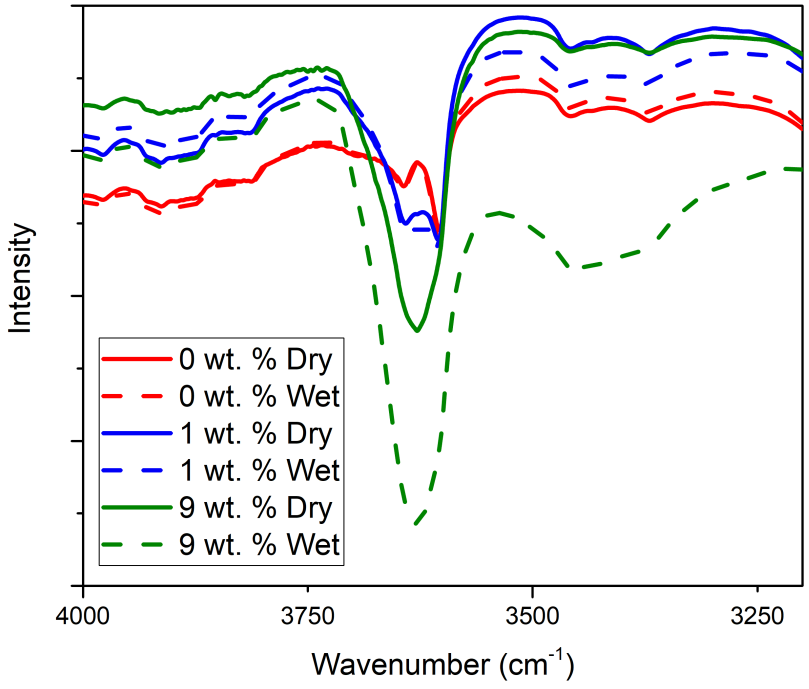

Figure 7.11: *Normalised FT-IR data in the region for observing the presence of water for the PE/EVA9/X/Q composites immersed in water (wet) compared to respective dry samples.*

Many researchers have considered the effect of water absorption on the dielectric response of nanocomposites, since the consequences of exposure to atmospheric water is an important practical consideration.[194,206,207,208,209] For example, Zhang *et al.*[207] exposed a range of nanocomposites containing nanoalumina to ambient conditions and found that in both the epoxy and PE-based systems, a water-related relaxation process resulted at the polymer-filler interface. Most notably, in the absence of nanoalumina, the relaxation of water was significantly slower in the epoxy matrix and not observed

in the PE-matrix, this difference was ascribed to there being an insignificant amount of water in the PE due to its non-polar nature.

Elsewhere, Lau *et al.*[194] considered the effect of water uptake in a morphologically-designed PE blend containing nanosilicas with different surface chemistries. They revealed, that the water uptake: (a) increased permittivity values; and (b) resulted in the development of dielectric loss processes that increased in strength and frequency. These effects were ascribed to accumulation of water molecules at nanoparticle/matrix interfaces, whereupon the variations seen are a consequence of changes in the aggregation state of the interfacial water and the different interactions that result. That is, initially, water molecules are tightly bound to the polar nanoparticle surface through hydrogen bonding while, as the water content increases, the influence of direct interfacial interactions decreases as more loosely-bound water structures form. These are, consequently, characterised by the associated peaks being displaced to higher frequencies. In the work of Lau *et al.*[194] the absorbed species directly interact with the applied electric field and, due to local environmental effects, the reduction in the frequency response from around 18 GHz[210,211] that characterises free water, to values in the Hz to kHz range.

DC conductivity measurements, shown in Table B.1 revealed no significant change following water immersion regardless of organoclay loading. On the other hand, the dielectric spectroscopy results revealed changes as shown in Figure 7.12. The phenomena observed for the PE/EVA9/0/Q and PE/EVA9/1/Q are unchanged by the water immersion and are equivalent to the results seen for the dry, PP-EVA-organoclay system presented in Figure 6.16. However, an observable change caused by the water can be seen for the PE/EVA9/9/Q sample in Figures 7.12(e) and 7.12(f). Between the measurements on Day 1 and Day 4 of water immersion, the loss peak was shifted to the higher frequencies. Similarly to Praeger *et al.*[182] studying PS-nanosilica systems, it is suggested that this can be attributed to the additional moisture increasing the relaxation rate, meaning that the dipoles can follow the alternating field until higher frequencies. Furthermore, the nature of the change in Figures 7.12(e) and 7.12(f) parallels the change caused by xylene immersion discussed previously: namely the solvent facilitates the organoclay coupling to the field. In the case of xylene immersion, it was observed that as the organoclay loading was increased, the loss peak also increased since there were more dipoles coupling to the alternating field. Similarly, for the water immersion tests, it can be seen that the 1 wt.% loading is too low for a detectable response and requires more organoclay for a response to be seen. This is in line with simulation findings by Hosier *et al.*[205] who modelled the formation of a percolating network (which would contribute to the conductive losses) created with the nanofiller and water shells across a PE matrix.

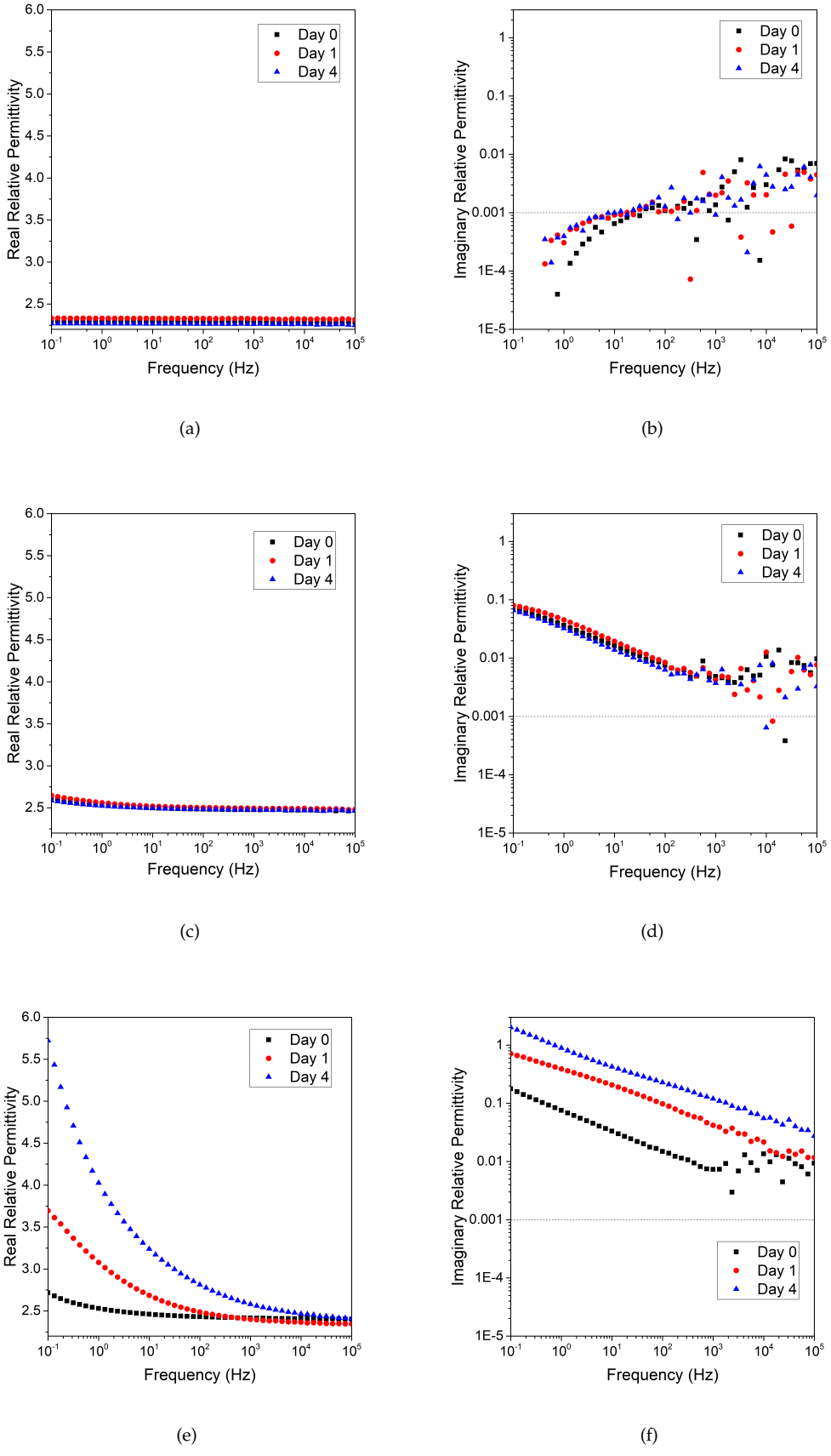

Figure 7.12: *Real relative permittivity results from water immersion tests of (a) PE/EVA9/0/Q, (c) PE/EVA9/1/Q and (d) PE/EVA9/9/Q with respective imaginary relative permittivity results in (b), (d) and (f). The horizontal dashed line indicates the equipment limit.*

7.4 Conclusion

The influence of xylene - a labile, nonpolar molecule - on dielectric response and breakdown behaviour has been examined in a polymer blend system containing an organoclay. In the absence of xylene, addition of the organoclay has little effect on the dielectric response of the system and, at low loading levels, appears to enhance the breakdown strength of the matrix. Equally, in the absence of the organoclay, the presence of xylene has an insignificant effect on both dielectric response and breakdown strength. However, when both the organoclay and the xylene are present together, strong synergistic effects are seen. Specifically, dielectric losses are markedly increased and, in parallel, AC breakdown strength is reduced. It is proposed that these effects are associated with solvation of amphiphilic species that are added to the virgin clay in order to render it more compatible with the host polymer, thereby easing dispersion during processing.

Water immersion tests were performed to investigate the effect that a polar solvent has on the composites compared to the non-polar xylene. The results revealed that the organoclay is much less prone to absorbing water than xylene however, when the organoclay loading was high enough the dielectric response caused by the two solvents was equivalent.

Furthermore, although dielectrics 'wet' with solvent are unlikely to find an application in industry, this work goes some way to recognising and understanding the signs of incomplete drying from solution blending or environmental exposure. This work provides data to aid discernment on the dryness of the samples and if the results seen are a result of the material or possibly the result of a solvent residue. In addition, while the results presented are practically, deleterious, this does not eliminate the possibility of other labile species acting in some advantageous way, by which macroscopic electrical properties are enhanced.

Chapter 8

Conclusions

The purpose of this work was to investigate and understand the link between the morphology and the electrical properties to allow one to develop materials to meet certain specifications more quickly and easily. Each of the five results chapter in this thesis have presented results from a single or group of analytical techniques and have discussed each of the sample systems, concurrently, throughout. However, although each chapter individually has drawn conclusions, here, overarching conclusions shall be made in order to appropriately address the thesis aim.

The results from investigating the PE-EVA-organoclay composites are catalogued in Chapters 3.3, 3.6, 4.2, 4.4, 5.3, 6.2.1, 6.3.2 and 6.4. At the relative compositions studied, even though PE-EVA and EVA-organoclay blends are possible, PE and organoclay are incompatible without the presence of EVA. On the other hand, for the PP-EVA-organoclay composites, PP and EVA are incompatible without organoclay. Making compatible systems is significant as it allows material systems to be homogeneous and therefore reliable and reproducible - making real-world application feasible. This work has investigated the properties of these material systems and their tolerances to different organoclay loadings and thermal treatments. Whilst doing this, links were established between the morphological and electrical properties to streamline future material development. The dispersion of the organoclay was found to be dependent on the ratio of organoclay to compatibiliser (EVA). The presence of organoclay initially increased the AC dielectric breakdown strength and the DC conductivity but these effects peaked at 5 wt.%. These electrical properties had decreased at the highest filler loadings, due to filler agglomerations, yet the results were still greater than in the corresponding unfilled samples. Another interesting finding was the decrease in percent crystallinity and organoclay crystallite size with organoclay loading - caused by the organoclay dispersion and nucleating effects which, in turn, influenced the electrical properties. This novel work was published into the literature (see Chapter 1.6.1 for details).

The results from investigating the PP-EVA-organoclay composites were catalogued in Chapters 3.4, 3.7, 4.2, 4.6, 5.4, 6.2.2, 6.3.3, 6.4. Despite being used primarily to compatibilise the polymer matrix, the organoclay significantly alters the electrical properties of the sample. The increasing organoclay content increases the DC conductivity and the AC dielectric breakdown strength, when compared to unfilled samples with the same thermal history, by the addition of charge carriers and pathways created at the interfaces. Additionally, thermal treatments of the materials, and the resulting crystallite size and phase separation, can be used to explain the electrical properties. The thermal treatments found that the quenched samples had the highest AC dielectric breakdown strength and highest DC conductivity. This can be attributed to either the crystallite size (determined through XRD) or the morphology with the interface and phase separation (observed under SEM). This gave an insight to the tolerances of the compatibiliser. The fact that the PE-based system is compatibilised by EVA while the PP-based system is compatibilised by the organoclay, initially, seems to be a discrepancy between what could otherwise be considered as similar material systems. Chemically, only a single methyl group on each monomer unit separates PP from PE. However, it is suggested that the addition of this methyl group alters the orientation of the polymer chain such that the ethylene monomers in the EVA copolymer cannot access or interact as effectively with PP than with the PE chain. The organoclay acts as a compatibiliser to the PP-EVA-based system via inhibiting chain movement in the melt phase. It is possible that a similar mechanism occurs in the PE-based system but the amount of chain movement will be significantly less than in the PP-EVA-based system since it is not as thermodynamically unfavourable for PE to co-exist with EVA. This novel work was published into the literature (see Chapter 1.6.1 for details).

The results from investigating the PP-PS-organoclay composites were catalogued in Chapters 3.5, 3.8, 4.2, 4.7, 5.5, 6.2.3, 6.3.4, 6.4. A key finding from the investigations into the PP-PS-organoclay composites is the differences observed between the PP7/PS3/X/Y and PP9/PS1/X/Y samples, i.e., the influence of the ratio of PP to PS. Similarly to the PP-EVA-organoclay system discussed previously, the organoclay compatibilised this polymer blend. It was found that the dielectric properties of the samples were dominated by the organoclay and not the morphological effects (created by the thermal treatment) in all cases apart for the 0.5 wt.% loading. Above this loading, the samples were considered percolating. Of all the materials studied, the PP-PS blend showed the lowest DC conductivity, yet the addition of organoclay resulted in changes to the dielectric properties in a similar way to the other material systems.

The effect of both polar and non-polar small solvent molecules on the PE-EVA-organoclay and PP-EVA-organoclay blends was investigated via immersing the samples in xylene and water. This work was undertaken to understand the potential effects that sample manufacture has on the samples and the results are reported in Chapter 7. The findings showed that, though neither the organoclay or xylene in the blends alone could cause

a dielectric response, synergistically they could. The findings revealed that when both xylene and organoclay were present, the dielectric response depended on the amount of xylene and the amount of organoclay present. This was attributed to the xylene solvating the amphiphilic nature of the clay and allowing the latter to respond to the applied field. In parallel to this, due to their ability to absorb energy from the field, the immersed samples containing organoclay performed significantly worse than their corresponding dry samples in AC dielectric breakdown tests. This novel work was published into the literature (see Chapter 1.6.1 for details). The water immersion test results revealed that the organoclay is much less prone to absorbing water than xylene however, when the organoclay loading was high enough the dielectric response caused by the two solvents was equivalent.

The thermal properties of all the material systems investigated herein were described in Chapter 3. The thermal degradation point was increased for all the samples containing organoclay compared to their respective base polymer matrix. However, according to a widely accepted test, only the PE-based system had created a nanocomposite. This does not detract from the composite properties displayed by the PP-EVA-organoclay or PP-PS-organoclay systems whose dependence on thermal treatment nevertheless makes the electrical properties of the material interesting. Across the materials studied, a variety of thermal treatments from the melt phase were employed. These included varying both the time the material spent in the melt phase and the speed at which it crystallised. In doing so, the effectiveness of the compatibiliser and the influence of organoclay vs. the influence of the morphology could be assessed. To name a few:

- for the PE-EVA-organoclay composites, the samples containing 1 and 5 wt.% loadings of organoclay had a relatively high conductivity following the SC or ISO thermal treatment due to self-assembly of the clay allowed by the time in the melt phase (far longer than the Q samples) creating a current pathway.
- the organoclay prevented phase separation in the PP-EVA-organoclay composites at 5 wt.% loading regardless of thermal treatment, however the 2.5 wt.% loading prevented phase separation in two out of the three thermal treatments.
- the conductivity and breakdown strength of the PP-PS-organoclay samples were influenced only at the lowest organoclay loading investigated (0.5 wt.%).

8.1 Conclusions on the Compatibility of the PE-EVA-Organoclay Composites

It has been seen that with a sufficient ratio between EVA and organoclay (found in the composites containing 1-5 wt.% organoclay), the former can successfully be employed

as a compatibiliser between PE and the organoclay to achieve a good dispersion of the organoclay. This was observed in the SEM micrographs and inferred through the XRD results, DC conductivity and TGA results in Chapters 5.3, 4.4, 6.2.1 and 3.3.1 respectively.

The XRD results (Figure 4.5) showed that the increase in XRD d_{001} spacing, a result of the degree of polymer intercalation, is dependent on the effective ratio of organoclay to compatibiliser. Specifically, as the ratio of organoclay to compatibiliser decreases the extent of polymer intercalation is decreased.

From the conductivity measurements (Figure 6.2) , it was found that the sample conductivity was dependent on the thermal treatment only at the low organoclay loading levels, giving an insight into the compatibility limit of the composites. For these samples, below the percolation loading level, the longer in the melt phase allowed for the arrangement of the organoclay tactoids to play a key role in increasing the conductivity. At the higher loadings, the organoclay was sufficiently concentrated that the relative arrangement achieved by the thermal treatments did not influence the conductivity.

Unlike in the other material systems, as mentioned previously, the TGA results (Figure 3.1) revealed that organoclay dispersion was sufficient to form a barrier effect and mean that samples analysed in air or nitrogen environments are equivalent. However, the TGA results also showed that at 13 wt.% loading the composite properties were different: the organoclay dispersion was insufficient to form a barrier as for the other composites with lower organoclay loadings. While it is generally accepted that in nanocomposite systems, optimised properties require good dispersion of the organoclay, the work presented here, it is suggested, indicates that where dielectric and electrical properties are concerned, improved dispersion is not the panacea it may be elsewhere. Rather, the mechanisms that determine bulk properties can be influenced by local physical and chemical factors and, indeed, organoclay loading.

From all of this it is clear that the influence of the presence of the organoclay manifests different properties depending on the dispersion, which, in turn, is dictated by the ratio between the organoclay and the EVA. Therefore it can be said that though the sample compositions studied herein were all compatible, the extent of compatibility varied.

8.2 Conclusions on the Compatibility of the PP-EVA-Organoclay and PP-PS-Organoclay Composites

Despite the TGA results for the PP-EVA-organoclay and PP-PS-organoclay composites (Figures 3.5 and 3.6 respectively) suggesting that a nanocomposite was not formed at the relative compositions studied, the XRD results (Figures 4.8 and 4.11 respectively)

showed polymer chain intercalation expanding the interlayer distances providing evidence that the polymer and organoclay were compatible. Furthermore, and perhaps the clearest evidence of compatibilsation of the composite by organoclay can be seen in the SEM micrographs in Chapters 5.4 and 5.5.

For the PP-PS-organoclay samples, TGA results in Chapter 3.5 suggested that dispersion was not sufficient to form a nanocomposite at the compositions studied. Furthermore the XRD results showed polymer chain intercalation had not changed the basal spacing implying that intercalation had not occurred. Though not as clear as for the PP-EVA-organoclay composites, SEM micrographs showed the organoclay acting as a compatibilising agent for the polymer blend.

The results from the PP-EVA-organoclay and PP-PS-organoclay composites show that, at the relative compositions studied, the organoclay can compatibilise these otherwise immiscible polymer blends. This profoundly changes the scope of the composite in electrical applications both through minimising phase separation and through the influence that the presence of the nanofiller has on the dielectric polymer blend.

The results for the PP-EVA-organoclay composites showing organoclay to be the compatibilising agent is particularly notable as the chemically similar PE-EVA-organoclay composites showed evidence that EVA was the compatibilising agent. The key difference between these two composites is the addition of a methyl group to the side of the ethylene monomers. This profoundly changes the shape of the polymer chains and therefore their ability to crystallise alongside each other due to changes in the dynamics of the intermolecular forces.

8.3 A summary of the general principles discovered that allow predictability in material development

One of the aims of this thesis was to investigate the interdependence of the material properties and in doing so, draw some conclusions about general principles that can inform material development decisions in the future. These findings can be summarised as:

- The dielectric properties are only influenced by thermal treatments when the filler loading is below the percolation threshold.
- Thermal treatments change the sample morphology significantly unless the blend is compatibilised sufficiently.
- Varying the thermal treatment causes a significant difference to the dielectric properties of unfilled polymer but has little impact on the dielectric properties of organoclay-filled polymers.

- Ensuring that the sample is solvent free is paramount as the effects of solvent in composites is significant, especially for the permittivity of organoclay-filled samples.
- When choosing two polymers to blend together, both the chemical shape and polarity are important considerations to ensure compatibility.

Chapter 9

Future Work

Just as this thesis has, in many ways, built upon the 2009 PhD thesis of Gabriele Gherbaz,[38] this thesis leaves many possible avenues for further study. I hope that my thesis can be considered part of a bigger project towards understanding and developing nanodielectrics and serve as a stepping stone for another PhD candidate in the future.

The work presented in this thesis demonstrates:

- the need to compatibilise polymer composites and the influence such endeavours can have on the material and
- the effect of small solvent molecules on the dielectric properties of the composites and therefore the need to ensure adequate preparation methods.

As shown in Chapter 5, imaging the composites to develop an understanding of the morphology of the composites is essential to the process of working towards a compatibilised system. Further work could be conducted in the area of imaging to better understand the morphology of the PP-PS blend and, in particular, the behaviour of PS. Furthermore TEM could be used to assess the dispersion of the organoclay as has been done elsewhere.[212,120,35]

One way to build upon Chapter 6 would be to investigate the permittivity of the composites over a variety of temperatures and a much lower frequency range. This would be useful particularly since these materials could find applications in capacitors, which themselves could be operational at temperatures other than the standard laboratory temperature, such as in computers and aircraft. Indeed, it was suggested that certain security-based applications may even desire a material that has a very different dielectric response above a certain temperature.

Furthermore, the space charge effect of these composites should be investigated as this is an especially important dielectric property if these composites were to be used in high voltage DC cables.

More generally, repeating some of this work with a synthetic clay (unlike the natural clay used herein) could be useful in understanding the effects of the inevitable impurities that the natural clay brings with it. Furthermore, using a different tacticity of PP (for example syndiotactic and atactic), and observing any changes to the compatibility between PP and EVA could be useful in probing exactly what causes the very different behaviour of PP and EVA compared to PE and EVA.

To build upon the solvent-immersion work presented in Chapter 7, it is suggested that one could repeat these investigations with other 'common-place' solvents or liquids. These could be chosen based on their use in composite preparation or perhaps likely exposure in a material application such as mineral and silicone oils, and cross-linking agents that could leach into the composites from neighbouring XLPE.[213]

In addition, the general principles drawn out in Chapter 8.3 should be tested to see how well they apply to other polymers and nanofillers. Perhaps a sensible starting point would be to replace EVA in the composites studied herein with copolymer ethylene-propylene rubber. This will change the polarity of the polymer making it less likely to be compatible with the organoclay but simultaneously more compatible with PP when considering the shape of the monomers.

Another area for future work is to investigate how the properties discovered herein using small-scale laboratory techniques change when considering manufacturing processes, for example in the production of capacitors or cables.

Appendix A

Appendix: Introducing the Characterisation Methods

Appendix A outlines and explains the investigative techniques employed to test the electrical, morphological and thermal properties properties of dielectric materials and the phenomena on which these measurements rely. The equipment and methods are discussed in Chapter 2.

A.1 Introducing Dielectric Spectroscopy: The Frequency-Dependent Dielectric Response

Polymers are often used as a dielectric because they have a low dielectric loss over a wide frequency range including at high frequencies (GHz). However other factors must be taken into account when selecting a dielectric for a capacitor including the size restrictions, costs, maximum working voltage and the frequency of the application.

The frequency response of the dielectric is measured by applying an AC voltage and recording the magnitude and phase angle of the current relative to the applied the voltage. From this, the capacitance and impedance are deduced - to determine the real and imaginary pars of the permittivity respectively.

Permittivity is a complex number comprising of real and imaginary parts as explained below and shown in Equations A.1 and A.2 (the negative sign a convention in Physics).

$$\epsilon_r(\omega) = \epsilon'_r(\omega) - j\epsilon''_r(\omega) \tag{A.1}$$

Which, for the purposes of this thesis, will be shortened to:

$$\epsilon = \epsilon' - j\epsilon'' \tag{A.2}$$

The real relative permittivity, also know as dielectric constant, $\epsilon_{\,r}(\omega)$, gives the charge storage ability of the material at a given frequency. The real relative permittivity of a sample is a dimensionless value given by the ratio of the absolute permittivity ($\epsilon(\omega)$) of the sample compared to the permittivity of a vacuum (ϵ_o), shown in Equation A.3.

$$\epsilon_r(\omega) = \epsilon(\omega)/\epsilon_o \tag{A.3}$$

The real relative permittivity at room temperature and an applied field of 1 kHz is 2.6 for PS and 2.3 for both PE and PP, while for water is 78.[136]

Impedance gives the imaginary part of the permittivity and is defined as the opposition of the material to the field. It is comprised of the combination of a real part (the resistance) and an imarginary part (the reactance). The reactance arises from either the capacitive or inductive properties of a material. Capacitance occurs when the current is ahead (or 'leads') the voltage change, as is the case for dielectric materials.

A.1.1 Plotting and Interpreting the Results

The real permittivity is directly related to electrical susceptibility, which means that the real relative permittivity depends on the polarisability of the material in an electric field. Dielectric spectroscopy tells one about the polarisability of a species (for example the dipoles) within a material as a function of field frequency. This can be described on the molecular scale by considering the dipoles that respond to the applied external field and the time it takes the dipoles to return to being randomly orientated - called relaxation.

During a dielectric relaxation, the energy stored by the field is transferred to heat via random molecular collisions. At low frequency fields, the phase difference between the field-induced dipole moment, p, and the electric field, E, is zero which means that the rate of relaxation is much faster than the rate of change of the field so the polarisation follows the field. However, when at high enough frequencies, the relaxation time is longer than the frequency of the field so p can no longer follow E. When the period of frequency of the field and the polarisation are the same, energy from the field is being converted into heat at the most efficient rate, this is called the resonant frequency.

Different species have a natural resonant frequency related to their physical nature and local environment. At the high frequencies (around 10^{15}) only the electronic polarisation of atomic orbitals can respond to the alternating field, whilst at lower frequencies (around 10^6), orientational polarisation of the dipole moments occurs.[214] For the polar

bonds in the organoclay, the response is dependent on the interaction between the polar groups on the organoclay and the polymer matrix. When there is solvent present decreasing the viscosity of the local environment to the organoclay, the polar parts of the organoclay can respond to the applied field. In this way, dielectric spectroscopy can give an understanding of the structural interactions and the surroundings of the components in the composite.

For the reasons described, when a dipole aligns to the applied external field, the real permittivity increases. This means that, at and around the resonant frequency, on the graph of real relative permittivity against frequency, the increased dielectric constant over a frequency range results in a permittivity peak. Such peaks are often referred to as loss peaks since they represent the material dissipating energy from the applied external field.

An alternative way to scrutinise the dielectric spectroscopy results involves plotting an Argand diagram in the form of the imaginary permittivity on the y-axis and the real permittivity on the x-axis. This has become known as a Cole-Cole plot, named after the authors of the seminal paper published in 1941.[188]

A.1.2 Predicting the Real Permittivity

It is possible to estimate the value of $\epsilon_{r}(\omega)$, using any one of a number of effective medium mixing theories including the equations: Lichtenecker, Maxwell-Garnett and Landau-Lifshitz.[134,80] The Lichtenecker equation was used herein due to its relative ease and simplicity of the calculations (since this was only meant to be a tool to obtain a prediction to check that the experimental results were reasonable), and has been used several times in work similar to that presented herein.[80,135]

The Lichtenecker equation (shown in Equation 2.9) presents an effective and commonly used function for a two-phase composite. However, the limitations of this equation include that it assumes a specific micro-geometry whereby the two phases are perfectly inter-dispersed and exist in spheres. This, together with the limitations of the available data tables, likely accounts for the consistently higher predicted values than the measured values of $\epsilon_{r}(\omega)$.[215]

A.2 Introducing the Dielectric Breakdown Strength

The maximum voltage withstood by a material, divided by its thickness, gives the dielectric breakdown strength of the material with the prefix AC or DC depending on the field conditions. Polymers are used in capacitors to increase the capacitance between the electrodes compared to air, which fails as an insulator at lower fields than a polymer

dielectric. Since breakdown results in destruction of the insulating material and current to flow between the electrodes, and the material is no longer suitable as an insulator, breakdown strength is a key parameter for the electrical engineer.

There are several possible mechanisms by which a breakdown can occur although determining which predominates is complicated. Furthermore, other factors such as temperature, humidity, sample thickness, sample ageing (if the field is applied for more than around 5 minutes before breakdown occurs), frequency of the applied field and the nature of the electrodes can all play a part in the breakdown. A brief description of possible breakdown mechanisms is given below.[214,216,129]

Electromechanical breakdown occurs due to the compressional force experienced by the dielectric due to the attraction of the two metal electrodes. The decrease in the thickness of the sample effectively increases the electric field it experiences, which leads to more thermal heating that eventually lead to deformation and material breakdown. This can be exacerbated by pre-existing cracks or weak points in the dielectric.

For an intrinsic breakdown to occur the applied field must accelerate a free electron (an electron in the conduction band), which then collides with and ionises an atom. This liberated electron can be promoted into the conduction band from the valence band if the collision transferred sufficient energy and can go onto ionise other atoms along with the original electron. This produces an avalanche effect with the promotion of further electrons causing a rapid increase in current leading to a breakdown by vapourising the material and creating a hole across the dielectric - sometimes visible with the naked eye.[216]

Internal discharges occur when the material contains pockets of gas (micro-voids), which breakdown before the material itself. This is called a partial discharge since the material does not fully breakdown. However, this can lead to a breakdown in several ways: by ionising an inner surface of the sample or by the local heating of the discharge melting or chemically altering the dielectric. Both of which effectively erode the material meaning breakdown occurs at a lower field than without a prior partial discharge occurring.

Thermal breakdown occurs when the dielectric losses are high since the sample heats up from the power dissipated from the electric field. When the heating rate exceeds the rate heat can be conducted away, the sample temperature increases meaning more electrons have the thermal energy to be promoted from the valence band to the conduction band. This means that the sample becomes more conducting and this current (possibly combined with some accelerated electrons via the intrinsic breakdown mechanism) leads to a breakdown. Due to the temperature dependence of this mechanism, the breakdown strength is lower at higher experimental temperatures.

Over time, insulation ageing makes breakdown more likely at lower fields. Oxida-

tion, ionisation, temperature cycling, water-initiated electrical treeing and mechanical stresses can cause the material to breakdown in addition to partial discharge of voids becoming more likely with time. Many of these processes may not happen during the breakdown tests but rather during the lifetime of the insulator in the application.

An external breakdown occurs when the surface of the insulator becomes conducting and offers a flash-over pathway, which, although the insulator is not permanently damaged, the insulator has failed. During the lifetime of an insulator, contaminants such as oil, water, or general dirt accumulate on the surface. External breakdown is another example of a breakdown mechanism that is unlikely to occur during the laboratory tests and instead during the insulator lifetime - unless the oil in which the tests are conducted has been contaminated.

Any, or a combination, of these mechanisms are possible with the samples considered in this study (although the occurrence of internal discharges were minimised since care was taken during sample pressing and selection to remove trapped bubbles and ageing effects should be minimised by having a sufficiently high ramp rate). This gives the breakdown a statistical nature, which is analysed using the Weibull Distribution, as detailed in Chapter 2.4.1.

A.3 Introducing Conductivity

Polymer dielectrics are regarded as insulators however, DC conductivity measurements are necessary to establish the current of the dielectric. A review paper published by Chiu *et al.*[217] gives an overview of the mechanisms of conduction in dielectric films. Broadly, there are two categories of conduction mechanisms: those that are electrode-limited and those that are bulk-limited. Since the former only applies to very thin films and so does not apply to the films tested in this thesis, only the bulk-limited mechanisms will be outlined here. Parameters effecting the conduction mechanism include, but are not limited to, the trap energy level, the trap density, carrier mobility and the density of states in the conduction band. Further, the conduction mechanisms can be influenced by the electric field, the nature of the species of the dielectric, the thickness of the dielectric, the temperature, and the electrodes employed.

A standard way to visualise the conductivity of a material is by representing the valence electronic orbitals containing the electrons available for promotion with a conduction band existing at a higher energy. When in these bands, the electrons are considered to be in energy wells called traps. At absolute zero, there is no thermionic promotion of the electrons from the valence into the conduction band but as the temperature rises, more electrons have the energy to be promoted from the valence band into the conduction band. This leaves an electron in the conduction band able to carry a current and a hole in the valence band also available for charge movement. For insulators, there

is an energy gap between the valence and conduction bands, this means that electrons are less likely to exist in the conduction band for insulators compared to metals where no such energy gap occurs. Any impurities in the polymer may produce a band at an energy level between the conduction and valence bands and facilitate a conduction mechanism by effectively decreasing the potential energy barrier between the valence and conduction bands.

The Poole-Frenkel effect describes how the potential energy required to promote electrons from the valence to the conduction band is effectively lowered when a field is applied due to the electrons being 'pulled' by the field. This makes it more likely to have electrons in the conduction band and therefore leads to a higher current and conductivity. This effect is more notable at higher electric fields and temperatures due to electrons being more likely to have the energy required to overcome the potential barrier.

Hopping conduction involves the tunnelling of the electrons between trap sites meaning that it does not have to possess the energy to overcome the barrier. Along with the hopping distance and the electron concentration, this mechanism depends on the frequency of thermal vibration of the electrons in the traps. Higher temperatures facilitate this mechanism. This mechanism of conduction dominates at low fields since at higher fields, the potential barrier is lowered and electrons move by the Poole-Frenkel effect rather than tunnelling.

Ohmic conduction may only be observed if there are no other conduction mechanisms occurring, such as at low applied fields. The conduction is a result of the movement of the electrons in the conduction band and the holes in the valence band. The resistance to this conduction is independent of frequency.

Where the Poole-Frenkel effect and ohmic conduction mechanisms occur at high and low fields respectively, the space-charge-limited conduction occurs at moderate fields. In an insulator, there is usually a limited number of electrons that can be promoted into the conduction band, limiting conduction. However, when there is an ohmic contact between the insulator and the electrode, electrons are injected. These are mostly trapped near the electrodes but some can be thermally promoted into the conduction band allowing the flow of charge carriers. When the density of charges injected exceeds the density of electrons promoted thermally in ohmic conduction, the mechanism is said to be space-charge-limited.

Ions can be present in dielectric films as a result of impurities or defects. An applied field can cause the movement of these ions between defect sites by providing them with enough energy to overcome the potential energy barrier. This form of conduction is termed ionic conduction.

Grain-boundary-limited conduction occurs in polycrystalline dielectric materials where

the grain boundary and the grain of the crystals have different conductivities. The potential energy barrier depends on the relative dielectric constant inversely, meaning that the occurrence of this phenomena is largely dependent on the nature of the material and not mainly the temperature and electric field as has been the case for some of the other mechanisms.

Upadhyay *et al.*[2] report on the different conduction mechanisms in the different regions of PE. The conduction in the crystalline regions is dominated by phonon scattering making the conduction independent of temperature, while conduction in the amorphous regions is dominated by impurities scattering the charge carriers since conduction occurs via charge hopping and interfacial regions. Upadhyay *et al.*[2] conclude that the interfacial regions has a dominating effect, therefore the amount and size of these crystalline and amorphous regions, in giving rise to the interfacial regions, governs the conductivity of the material.

A.4 The Interplay between the Dielectric Properties

When the conductivity of a sample increases, the DC dielectric breakdown strength of the sample decreases, a well-accepted and reported phenomenon.[50,129,99,178] Herein, an increase in DC conductivity was seen upon the addition of organoclay and xylene to the composites. These additions increase the conductivity by creating an energy band between the conduction and the valence bands meaning that less energy is required for the electrons to reach the conduction band. This lower energy barrier will mean that more electrons will have sufficient energy be able to exist in the conduction band and so the conductivity of the material is higher than without the dopants. Therefore at lower fields than in their un-doped counterparts, the ever-growing cascade of electron-electron promotions into the conduction band occur leading to material breakdown.

A.5 Introducing Thermal Gravimetric Analysis

TGA enables the study of the thermal decomposition of a material by measuring the mass loss as the sample is heated. This allows the identification of the thermal limits of the sample and the organoclay loading. The former is achieved via studying the temperature at which thermal degradation begins, while the latter, by comparing the mass remaining at the end of the experiment to the mass remaining when pure organoclay was tested. The diffusion-control, decomposition kinetics and the effects of char formation can also be investigated using TGA.[72]

A published criterion of the sample pyrolysis in air and nitrogen appearing the same if the sample had sufficient organoclay dispersion to form a nanocomposite can be ex-

plained by considering the barrier effect.[85,124] Normally, one would expect pyrolysis in an atmosphere containing oxygen to occur at a lower temperature than pyrolysis in nitrogen. However, the clay retards oxygen diffusion reaching the polymer so the pyrolysis takes place as if in the absence of oxygen (as it would in the nitrogen atmosphere). This means that, if the clay is sufficiently dispersed to form a barrier across the whole sample, the samples tested in air and nitrogen will appear equivalent.

Furthermore, char formation from the organoclay blocks oxygen diffusion and the escape of the degraded gaseous products so the degradation temperature of a sample containing organoclay would be higher than the equivalent sample without organoclay.

A.6 Introducing Differential Scanning Calorimetry

DSC measures the heat flow to a sample being heated at a set rate compared to an empty sample container. Since melt and glass transitions will change the amount of heat flow required to keep the sample heating at a set rate, when the transitions occur, the deviation causes peaks to appear in the spectrum. The peak position gives the temperature and the peak area gives the enthalpy of the transition. The same can be applied on an experiment performed by cooling the sample from the melt phase to obtain the crystallisation temperature and enthalpy.

The percent crystallinity of the sample can be obtained using the area of the peaks and an equation described in Chapter 2.3.1.

DSC can be used to determine the optimum conditions for cooling and crystallising the samples from the melt phase by holding the sample at a chosen temperature and measuring the time it takes to crystallise. A temperature should be chosen whereby the sample crystallises slowly enough that the crystal structure of the composite can be investigated but not so slowly that the crystallisation takes more than around an hour. This is in order to be time-conscientious and to be sure that crystallisation occurs at the desired temperature and not crystallising only when the sample is removed from the heat.

In published DSC work on a nanocomposite of PE with an organoclay from a master batch, Vaughan *et al.*[57] found that when well-dispersed the organoclay promotes nucleation but inhibits the formation of the crystalline structures, and the authors linked this to AC dielectric breakdown results. Elsewhere, for a PS-organoclay nanocomposite, it was found that the glass transition temperature was increased by the presence of organoclay compared to that of pure PS, a phenomenon ascribed to the PS polymer chains being confined between or adjacent to the clay layers.[67]

A.7 Introducing X-ray Diffraction

The crystallite nature of a sample can be investigated using X-ray diffraction, including the determination of the crystal structure and lattice spacing. This is achieved by radiating X-rays at a sample over a range of incidence angles and measuring the X-rays that get reflected back. These X-rays form peaks in a graph of intensity against angle.

Since the exfoliation of the organoclay occurs due to the polymer matrix moving between the organoclay layers, the greater the exfoliation means larger d-spacing (distance between the clay layers), which can be observed in a diffraction pattern. Published XRD analysis has shown that the interlayer distance of the organoclay can be increased by the intercalation of PE[31] and EVA[15] and the interlayer distance of the organoclay is increased more when EVA is also present in the matrix compared to a solely PP matrix.[22,15] The peaks can also give evidence as to whether there has been degradation of the organic part of the organoclay (for example during the sample processing) by there being a decrease in interlayer distance. Furthermore, a broadening of the organoclay peak is indicative of partial exfoliation due to the lower crystallinity that the polymer intercalation causes through random orientations.[149,49,55,39]

The average crystallite size gives an indication about the phase boundaries present in a sample. Since phase boundaries present charge trapping sites, this information can be used to understand the electrical properties of the sample such as conductivity.[154] This information about the morphology of the sample and can be determined by applying the Scherrer equation to the diffraction data since the full-width at half-maximum of the diffraction peaks can be related to the crystallite size. The use of this equation has been described in Chapter 2.3.2. Errors in the results from the Scherrer equation primarily arise due to peak broadening effects caused by factors other than the crystal, these include crystal dislocations, micro-stresses, grain boundaries and crystal imperfections due to contaminants.[128]

A.8 Introducing Fourir-Transform Infrared Spectroscopy

This technique indicates the types of bonds present by exposing the sample to infrared radiation and observing which wavelengths of the light have been absorbed. Each type of bond has a characteristic absorption wavelength - these are listed widely available data tables. FT-IR is performed in transmission mode or ATR mode depending on the application. When the inside of the material needed assessing the transmission mode was used but for considering only the surface, ATR was used. Assessing the types of bonds present can be used to check for species such as solvent and organoclay as well as assessing possible oxidation changes caused by the drying or thermal conditioning processes.

FT-IR is frequently used in literature in studies detailing the preparation and characterisation of nanocomposites. The use of FT-IR in identifying the presence of the Si-O moieties after the addition of the organoclay to the polymer matrix, and oxide groups due to degradation of the matrix from thermal treatments have both been widely reported.[34,48,209,218]

A.8.1 Normalising the Data

The Z-score (also known as the Standard Normal Variate Correction) is a value assigned to each data point in a data set that quantifies how far from the mean data point that specific point is, in terms of the number of standard deviations. This normalisation method involves adjusting the data so that it has an average of zero and a standard deviation of one.

The Z-score of each data point can be calculated using Equation A.4, where z represents the Z-score, x represents the data point that needs to be normalised to a data set, $\bar{x}$ is the mean of the data set and σ is the standard deviation of the data set.

$$z = x - \bar{x}/\sigma \tag{A.4}$$

This method means that it is not necessary for there to be a peak common to all the data sets to which the data can otherwise be normalised, hence this method is powerful for interpreting FT-IR data.

A.9 Introducing Scanning Electron Microscopy

SEM uses electrons to image the surface of a sample to a nanometre scale. Electrons have a shorter wavelength than light, enabling SEM to have a better resolution than an optical microscope. SEM was used in this study as the resolution was required to view the lamellae and organoclay, which are both in the order of nanometres. For this, the electrons are generated by a filament (made of tungsten, lanthanum hexaboride or similar) and get directed towards the sample by lenses creating a spot of around a nanometre. The beam is passed through deflector plates which allow the beam to be manipulated into a scanning raster pattern. The interaction of the electrons with the surface of the material produces X-rays and secondary and backscattered electrons that are detected and interpreted into a grey-scale image of the sample. The grey-scale image gives an idea of the depth of field and the identity of the material at one position compared to another. This can give information about the sample morphology.

The nature of the morphology influences the electrical properties of the material as published in two papers by the same research group.[10,219] In the first, they found that breakdown behaviour of an HDPE:LDPE blend varied with morphology but not with blend composition.[10] Further, they reported that the morphology depends on the crystallisation method and is largely insensitive to changes in the molecular composition. Whilst in another paper, they found that all the quenched samples showed a fine lamellar texture regardless of composition.[219] Work in this thesis will be viewed in light of this published work and seek to link the morphology with the results from the electrical tests.

Appendix B

Appendix: Supplementary Material

Appendix B includes data that is relevant but otherwise would impede the flow of the discussion in this thesis.

Sample	Conductivity of dry sample (S/cm)	Conductivity of sample immersed for 1 day (S/cm)	Conductivity of sample immersed for 4 days (S/cm)
PE/EVA9/0/Q	9.56E-17 $\pm$ 5.72E-17	8.01E-18	7.33E-17
PE/EVA9/1/Q	2.37E-16 $\pm$ 1.42E-16	5.2E-16	3.60E-16
PE/EVA9/9/Q	1.27E-12 $\pm$ 7.91E-13	3.34E-12	1.67E-12

Table B.1: *DC conductivity data for the PE/EVA9/X/Q water immersion tests.*

Bibliography

[1] J. I. Wang and I. R. Harrison. *Method of Experimental Physics: Polymers*, volume 16 B. Academic Press, Pennsylvania (1980). ISBN 0124759572.

[2] A. K. Upadhyay and C. C. Reddy. *On the mechanism of charge transport in low density polyethylene*. Journal of Applied Physics, **122, 6** (2017). doi:10.1063/1.4997941.

[3] R. B. Seymour and T. Cheng. *Introduction to History of Polyolefins*, pages 1–7. Springer Netherlands, Dordrecht (1986). ISBN 978-94-009-5472-4. doi:10.1007/978-94-009-5472-4_1.

[4] J. P. Jones, J. P. Llewellyn, and T. J. Lewis. *The contribution of field-induced morphological change to the electrical aging and breakdown of polyethylene*. IEEE Transactions on Dielectrics and Electrical Insulation, **12, 5**:951–966 (2005). doi:10.1109/TDEI.2005.1522189.

[5] M. Faker, M. K. Razavi Aghjeh, M. Ghaffari, and S. A. Seyyedi. *Rheology, morphology and mechanical properties of polyethylene/ethylene vinyl acetate copolymer (PE/EVA) blends*. European Polymer Journal, **44, 6**:1834–1842 (2008). doi:10.1016/j.eurpolymj.2008.04.002.

[6] T. G. Gopakumar, J. A. Lee, M. Kontopoulou, and J. S. Parent. *Influence of clay exfoliation on the physical properties of montmorillonite/polyethylene composites*. Polymer, **43, 20**:5483–5491 (2002). doi:10.1016/S0032-3861(02)00403-2.

[7] M. Tanniru, Q. Yuan, and R. D. K. Misra. *On significant retention of impact strength in clay-reinforced high-density polyethylene (HDPE) nanocomposites*. Polymer, **47, 6**:2133–2146 (2006). doi:10.1016/j.polymer.2006.01.063.

[8] O. Y. Alothman. *Processing and characterization of high density polyethylene/ethylene vinyl acetate blends with different VA contents*. Advances in Materials Science and Engineering, **10, 1** (2012). doi:10.1155/2012/635693.

[9] R. J. Young and P. A. Lovell. *Introduction to Polymers*. CRC Press, Boca Raton, FL, third edition. ISBN 13:978-1-4398-9415-6.

[10] I. L. Hosier, A. S. Vaughan, and S. G. Swingler. *On the effects of morphology and molecular composition on the electrical strength of polyethylene blends*. Journal of

Polymer Science Part B: Polymer Physics, **38, 17**:2309–2322 (2000). doi:10.1002/1099-0488(20000901)38:173.3.CO;2-Z.

[11] R. Crétois, L. Delbreilh, E. Dargent, N. Follain, L. Lebrun, and J. M. Saiter. *Dielectric relaxations in polyhydroxyalkanoates/organoclay nanocomposites*. European Polymer Journal, **49, 11**:3434–3444 (2013). doi:10.1016/j.eurpolymj.2013.07.009.

[12] M. Modesti, A. Lorenzetti, D. Bon, and S. Besco. *Effect of processing conditions on morphology and mechanical properties of compatibilized polypropylene nanocomposites*. Polymer, **46, 23**:10237–10245 (2005). doi:10.1016/j.polymer.2005.08.035.

[13] *Market Study: Polypropylene*. Ceresana Market Research, Germany, fourth edition (2017).

[14] J. Karger-Kocsis, editor. *Polypropylene Structure, blends and composites*. Springer Science+Business Media, Dordrecht, 1 edition (1995). doi:10.1007/978-94-011-0523-1.

[15] C. G. Martins, N. M. Larocca, D. R. Paul, and L. A. Pessan. *Nanocomposites formed from polypropylene/EVA blends*. Polymer, **50, 7**:1743–1754 (2009). doi:10.1016/j.polymer.2009.01.059.

[16] H. A. Khonakdar, S. H. Jafari, A. Haghighi-Asl, U. Wagenknecht, L. Haussler, and U. Reuter. *Thermal and Mechanical Properties of Uncrosslinked and Chemically Crosslinked Polyethylene/Ethylene Vinyl Acetate Copolymer Blends*. Journal of Applied Polymer Science, **103**:3261–3270 (2007). doi:10.1002/app.25268.

[17] DuPont. *United States Patent 2703794* (1955).

[18] M. Brogly, M. Nardin, and J. Schultz. *Effect of vinylacetate content on crystallinity and second-order transitions in ethylene-vinylacetate copolymers*. Journal of Applied Polymer Science, **64**:1903–1912 (1997). doi:10.1002/(SICI)1097-4628(19970606)64:10⟨1903::AID-APP4⟩3.0.CO;2-M.

[19] G. Wypych. *Handbook of Polymers*. ChemTec Publishing, 5 edition (2012). ISBN 978-1-895198-47-8. doi:10.1016/b978-1-895198-47-8.50162-4.

[20] A. M. Henderson. *Ethylene-Vinyl Acetate (EVA) Copolymers: A General Review*. IEEE Electrical Insulation Magazine, **9, 1**:30–38 (1993). doi:10.1109/57.249923.

[21] A. Maciel, A. Del-Real, M. V. Garcia-Garduiio, E. Oliva, . Manero, and V. M. Castaiiob. *Morphology and Elastic Properties of PP/EVA Polymer Blends*. Polymer International, **41, 3**:227–236 (1996). doi:10.1002/(SICI)1097-0126(199611)41:3⟨227::AID-PI584⟩3.0.CO;2-C.

[22] V. Goodarzi, S. H. Jafari, H. A. Khonakdar, S. A. Monemian, and M. Mortazavi. *An assessment of the role of morphology in thermal/thermo-oxidative degradation mechanism of PP/EVA/clay nanocomposites*. Polymer Degradation and Stability, **95, 5**:859–869 (2010). doi:10.1016/j.polymdegradstab.2010.01.009.

[23] V. Goodarzi, S. H. Jafari, H. A. Khonakdar, and J. Seyfi. *Morphology, rheology and dynamic mechanical properties of PP/EVA/clay nanocomposites*. Journal of Polymer Research, **18, 6**:1829–1839 (2011). doi:10.1007/s10965-011-9590-x.

[24] M. Shafiee, S. A. Ahmad Ramazani, and M. Danaei. *Investigation of the gas barrier properties of PP/clay nanocomposite films with EVA as a compatibiliser prepared by the melt intercalation method*. Polymer - Plastics Technology and Engineering, **49, 10**:991–995 (2010). doi:10.1080/03602559.2010.482075.

[25] I. L. Hosier, A. S. Vaughan, and W. Tseng. *Effect of polyethylene on morphology and dielectric breakdown in EVA blends*. 2007 International Conference on Solid Dielectrics, ICSD, pages 184–187 (2007). doi:10.1109/ICSD.2007.4290783.

[26] Y. Wang, Q. Zhang, and Q. Fu. *Compatibilization of immiscible poly (propylene)/polystyrene blends using clay*. Macromolecular Rapid Communications, **24, 3**:231–235 (2003). doi:10.1002/marc.200390026.

[27] W. Cheewawuttipong, D. Fuoka, S. Tanoue, H. Uematsu, and Y. Iemoto. *Thermal and mechanical properties of polypropylene/boron nitride composites*. Energy Procedia, **34**:808–817 (2013). doi:10.1016/j.egypro.2013.06.817.

[28] M. Bahmanyar, S. Sedaghat, A. Ramazani S.A., and H. Baniasadi. *Preparation of Ethylene Vinyl Acetate Copolymer/Graphene Oxide Nanocomposite Films via Solution Casting Method and Determination of the Mechanical Properties*. Polymer-Plastics Technology and Engineering, **54, 2**:218–222 (2015). doi:10.1080/03602559.2014.958772.

[29] C. Zhao, H. Qin, F. Gong, M. Feng, S. Zhang, and M. Yang. *Mechanical, thermal and flammability properties of polyethylene/clay nanocomposites*. Polymer Degradation and Stability, **87, 1**:183–189 (2005). doi:10.1016/j.polymdegradstab.2004.08.005.

[30] A. Panwar, V. Choudhary, and D. K. Sharma. *Review: A review: polystyrene/clay nanocomposites*. Journal of Reinforced Plastics and Composites, **30, 5**:446–459 (2011). doi:10.1177/0731684411399132.

[31] E. M. Araújo, R. Barbosa, C. R. S. Morais, L. E. B. Soledade, A. G. Souza, and M. Q. Vieira. *Effects of organoclays on the thermal processing of PE/clay nanocomposites*. Journal of Thermal Analysis and Calorimetry, **90**:841–848 (2007). doi:10.1007/s10973-006-7504-7.

[32] R. Guégan. *Organoclay applications and limits in the environment*. Comptes Rendus Chimie, **22, 2-3**:132–141 (2019). doi:10.1016/j.crci.2018.09.004.

[33] S. M. Ali Dadfar, I. Alemzadeh, S. M. Reza Dadfar, and M. Vosoughi. *Studies on the oxygen barrier and mechanical properties of low density polyethylene/organoclay nanocomposite films in the presence of ethylene vinyl acetate copolymer as a new type of compatibilizer*. Materials and Design, **32, 4**:1806–1813 (2011). doi:10.1016/j.matdes.2010.12.028.

[34] M. Zanetti, P. Bracco, and L. Costa. *Thermal degradation behaviour of PE/clay nanocomposites*. Polymer Degradation and Stability, **85, 1**:657–665 (2004). doi:10.1016/j.polymdegradstab.2004.03.005.

[35] J. J. Decker, K. P. Meyers, D. R. Paul, D. A. Schiraldi, A. Hiltner, and S. Nazarenko. *Polyethylene-based nanocomposites containing organoclay: A new approach to enhance gas barrier via multilayer coextrusion and interdiffusion*. Polymer, **61**:42–54 (2015). doi:10.1016/j.polymer.2015.01.061.

[36] N. Jaeverberg, B. Venkatesulu, H. Edin, and H. Hillborg. *Prebreakdown current and DC breakdown strength of alumina-filled poly(ethylene-co-butyl acrylate) nanocomposites: Part II - Prebreakdown currents*. IEEE Transactions on Dielectrics and Electrical Insulation, **21, 5**:2135–2145 (2014). doi:10.1109/TDEI.2014.003857.

[37] L. Hui, J. K. Nelson, and L. S. Schadler. *The influence of moisture on the electrical performance of XLPE/silica nanocomposites*. Proceedings of the 2010 IEEE International Conference on Solid Dielectrics, ICSD 2010, pages 10–13 (2010). doi:10.1109/ICSD.2010.5568040.

[38] G. Gherbaz. *Nanostructured Polymers : Morphology and Properties*. Ph.D. thesis, University of Southampton (2009).

[39] Y. Zhong and D. De Kee. *Morphology and properties of layered silicate-polyethylene nanocomposite blown films*. Polymer Engineering and Science, **45, 4**:469–477 (2005). doi:10.1002/pen.20306.

[40] A. Leszczyńska, J. Njuguna, K. Pielichowski, and J. R. Banerjee. *Polymer/montmorillonite nanocomposites with improved thermal properties. Part I. Factors influencing thermal stability and mechanisms of thermal stability improvement*. Thermochimica Acta, **453, 2**:75–96 (2007). doi:10.1016/j.tca.2006.11.002.

[41] S. Kumar, J. P. Jog, and U. Natarajan. *Preparation and Characterization of Poly(methyl methacrylate) Clay Nanocomposites via Melt Intercalation: The Effect of Organoclay on the Structure and Thermal Properties*. Journal of Applied Polymer Science, **89**:1186–1194 (2003). doi:https://doi.org/10.1002/app.12050.

[42] P. Meneghetti and S. Qutubuddin. *Synthesis, thermal properties and applications of polymer-clay nanocomposites*. Thermochimica Acta, **442**:74–77 (2006). doi:10.1016/j.tca.2006.01.017.

[43] X. Fu and S. Qutubuddin. *Polymerclay nanocomposites: exfoliation of organophilic montmorillonite nanolayers in polystyrene*. Polymer, **42, 2**:807–813 (2001). doi:10.1016/S0032-3861(00)00385-2.

[44] Rajkiran R. Tiwari and U. Natarajan. *Influence of Organic Modification on Mechanical Properties of Melt Processed Intercalated Poly(methyl methacrylate) Organoclay Nanocomposites*. J Appl Polym Sci, **105**:2433–2443 (2007). doi:10.1002/app.

[45] B. Bate and S. Burns. *Complex dielectric permittivity of organically modified bentonite suspensions (0.21.3 GHz)*. Canadian Geotechnical Journal, **51, 7**:782–794 (2014). doi: 10.1139/cgj-2013-0286.

[46] H. L. Tyan, C. M. Leu, and K. H. Wei. *Effect of reactivity of organics-modified montmorillonite on the thermal and mechanical properties of montmorillonite/polyimide nanocomposites*. Chemistry of Materials, **13, 1**:222–226 (2001). doi:10.1021/cm000560x.

[47] M. L. López-Quintanilla, S. Sánchez-Valdés, L. F. Ramos De Valle, and F. J. Medellín-Rodríguez. *Effect of some compatibilizing agents on clay dispersion of polypropylene-clay nanocomposites*. Journal of Applied Polymer Science, **100, 6**:4748–4756 (2006). doi: 10.1002/app.23262.

[48] Y. Prachum, R. H. A. Strauss, and S. Kiatkamjornwong. *The Physical and Mechanical Properties of Beta-Nucleated Polypropylene/Montmorillonite Nanocomposites*. Journal of Applied Polymer Science, **122**:1066–1076 (2011). doi:10.1002/app.34209.

[49] S. Filippi, C. Marazzato, P. Magagnini, A. Famulari, P. Arosio, and S. V. Meille. *Structure and morphology of HDPE-g-MA/organoclay nanocomposites: Effects of the preparation procedures*. European Polymer Journal, **44, 4**:987–1002 (2008). doi:10.1016/j.eurpolymj.2008.01.011.

[50] G. C. Montanari, D. Fabiani, F. Palmieri, D. Kaempfer, R. Thomann, and R. Mülhaupt. *Modification of electrical properties and performance of EVA and PP insulation through nanostructure by organophilic silicates*. IEEE Transactions on Dielectrics and Electrical Insulation, **11, 5**:754–762 (2004). doi:10.1109/TDEI.2004.1349780.

[51] M. Bhattacharya. *Polymer nanocomposites-A comparison between carbon nanotubes, graphene, and clay as nanofillers*. Materials, **9, 4**:1–35 (2016). doi:10.3390/ma9040262.

[52] P. G. S. Campos, M. C. A. Fantini, and D. F. S. Petri. *Grafting of tetrahydrophthalic and maleic anhydride onto polyolefins in solution*. Journal of the Brazilian Chemical Society, **15, 4**:532–540 (2004). doi:10.1590/S0103-50532004000400015.

[53] M. Zanetti and L. Costa. *Preparation and combustion behaviour of polymer/layered silicate nanocomposites based upon PE and EVA*. Polymer, **45, 13**:4367–4373 (2004). doi:10.1016/j.polymer.2004.04.043.

[54] I. L. Hosier, A. S. Vaughan, and S. G. Swingler. *An investigation of the potential of ethylene vinyl acetate/polyethylene blends for use in recyclable high voltage cable insulation systems*. Journal of Materials Science, **45, 10**:2747–2759 (2010). doi: 10.1007/s10853-010-4262-5.

[55] J. Mahmoudi, M. Eesaee, and M. Vakilian. *Electrical and Mechanical Characterization of High-density Polyethylene/Ethylene Vinyl Acetate/Organoclay Nanocomposite*. IEEE Transactions on Dielectrics and Electrical Insulation, **20, 5**:1772–1779 (2013). doi: 10.1109/TDEI.2013.6633708.

[56] Q. Zhang, H. Yang, and Q. Fu. *Kinetics-controlled compatibilization of immiscible polypropylene/ polystyrene blends using nano-SiO2 particles*. Polymer, **45, 6**:1913–1922 (2004). doi:10.1016/j.polymer.2004.01.037.

[57] A. S. Vaughan, S. G. Swingler, and Y. Zhang. *Polyethylene Nanodielectrics: The Influence of Nanoclays on Structure Formation and Dielectric Breakdown*. In *IEEE Trans.*, volume 126, pages 1057–1063. Japan (2005). doi:10.1541/ieejfms.126.1057.

[58] W. L. Elban, J. A. Howarter, M. C. Richardson, P. E. Stutzman, A. M. Forster, A. J. Nolte, and G. A. Holmes. *Influence of solvent washing on interlayer structure of alkylammonium montmorillonites*. Applied Clay Science, **61**:29–36 (2012). doi:10.1016/j.clay.2012.03.001.

[59] S. Sinha Ray and M. Okamoto. *Polymer/layered silicate nanocomposites: A review from preparation to processing*. Progress in Polymer Science (Oxford), **28, 11**:1539–1641 (2003). doi:10.1016/j.progpolymsci.2003.08.002.

[60] R. Salehiyan, H. Y. Song, M. Kim, W. J. Choi, and K. Hyun. *Morphological Evaluation of PP/PS Blends Filled with Different Types of Clays by Nonlinear Rheological Analysis*. Macromolecules, **49, 8**:3148–3160 (2016). doi:10.1021/acs.macromol.6b00268.

[61] S. Sinha Ray, S. Pouliot, M. Bousmina, and L. A. Utracki. *Role of organically modified layered silicate as an active interfacial modifier in immiscible polystyrene/polypropylene blends*. Polymer, **45, 25**:8403–8413 (2004). doi:10.1016/j.polymer.2004.10.009.

[62] R. Ayoob, F. Alhabill, T. Andritsch, and A. Vaughan. *Enhanced dielectric properties of polyethylene/hexagonal boron nitride nanocomposites*. Journal of Materials Science, **53, 5**:3427–3442 (2018). doi:10.1007/s10853-017-1786-y.

[63] G. Rivers, A. Rogalsky, P. Lee-Sullivan, and B. Zhao. *Thermal analysis of epoxy-based nanocomposites: Have solvent effects been overlooked?* Journal of Thermal Analysis and Calorimetry, **119, 2**:797–805 (2015). doi:10.1007/s10973-013-3613-2.

[64] O. M. Istrate, M. A. Gunning, C. L. Higginbotham, and B. Chen. *Structure-property relationships of polymer blend/clay nanocomposites: Compatibilized and noncompatibilized polystyrene/propylene/clay*. Journal of Polymer Science, Part B: Polymer Physics, **50, 6**:431–441 (2012). doi:10.1002/polb.23018.

[65] S. Chuayjuljit and C. Worawas. *Nanocomposites of EVA/polystyrene nanoparticles/-montmorillonite*. Journal of Composite Materials, **45, 6**:631–638 (2011). doi:10.1177/0021998310376116.

[66] A. B. Morgan and J. D. Harris. *Exfoliated polystyrene-clay nanocomposites synthesized by solvent blending with sonication*. Polymer, **45, 26**:8695–8703 (2004). doi:10.1016/j.polymer.2004.10.067.

[67] S. V. Krishna and G. Pugazhenthi. *Properties and Thermal Degradation Kinetics of Polystyrene/Organoclay Nanocomposites Synthesized by Solvent Blending Method: Effect of Processing Conditions and Organoclay Loading*. Journal of Applied Polymer Science, **120**:1322 (2011). doi:10.1002/app.

[68] D. J. Carastan and N. R. Demarquette. *Microstructure of nanocomposites of styrenic polymers*. Macromolecular Symposia, **233**:152–160 (2006). doi:10.1002/masy.200690012.

[69] S. Tantipattarakul, A. S. Vaughan, and T. Andritsch. *On the influence of morphology and chemical defects on charge transport dynamics in polyethylene: thermal ageing and concentration gradient*. Journal of Physics D: Applied Physics, **52, 39**:395302 (2019). doi:10.1088/1361-6463/ab2f38.

[70] P. Jacoby. *Beta nucleating masterbatch offers enhanced properties in polypropylene products*. Plastics, Additives and Compounding, **9, 3**:32–35 (2007). doi:10.1016/S1464-391X(07)70068-5.

[71] P. Mancinelli, T. Heid, D. Fabiani, A. Saccani, M. Toselli, and M. Fréchette. *Thermal in Situ Reduction of Graphene Oxide in Epoxy-based Nanodielectrics : Influence on Dielectric Properties*. 2013 Annual Report Conference on Electrical Insulation and Dielectric Phenomena Thermal, pages 768–771 (2013).

[72] A. Mikitaev, M. Ligidov, and G. Zaikov. *Polymers, Polymer Blends, Polymer Composites and Filled Polymers*. Nova Science Publishers, New York (2006). ISBN 9781608762385.

[73] I. Plea, P. V. Noingher, S. Schlögl, C. Sumereder, and M. Muhr. *Properties of polymer composites used in high-voltage applications*. Polymers, **8, 5** (2016). doi:10.3390/polym8050173.

[74] P. Kodgire, R. Kalgaonkar, S. Hambir, N. Bulakh, and J. P. Jog. *PP/clay nanocomposites: Effect of clay treatment on morphology and dynamic mechanical properties*. Journal of Applied Polymer Science, **81, 7**:1786–1792 (2001). doi:10.1002/app.1611.

[75] M. Eesaee, E. David, N. R. Demarquette, and D. Fabiani. *Electrical Breakdown Properties of Clay-Based LDPE Blends and Nanocomposites*. Journal of Nanomaterials, **2018** (2018). doi:10.1155/2018/7921725.

[76] K. S. Shah, R. C. Jain, V. Shrinet, A. K. Singh, and D. P. Bharambe. *High density polyethylene (HDPE) clay nanocomposite for dielectric applications*. IEEE Transactions on Dielectrics and Electrical Insulation, **16, 3**:853–861 (2009). doi:10.1109/TDEI.2009.5128526.

[77] M. Frounchi, S. Dadbin, Z. Salehpour, and M. Noferesti. *Gas barrier properties of PP/EPDM blend nanocomposites*. Journal of Membrane Science, **282, 1-2**:142–148 (2006). doi:10.1016/j.memsci.2006.05.016.

[78] C. D. Green, A. S. Vaughan, G. R. Mitchell, and T. Liu. *Structure Property Relationships in Polyethylene/Montmorillonite Nanodielectrics*. IEEE Transactions on Dielectrics and Electrical Insulation, **15, 1**:134–143 (2008). doi:10.1109/T-DEI.2008.4446744.

[79] M. Roy, J. K. Nelson, R. K. Maccrone, L. S. Schadler, C. W. Reed, and R. Keefe. *Polymer nanocomposite dielectrics-the role of the interface*. Dielectrics and Electrical Insulation, IEEE Transactions, **12, 4**:629–643 (2005). doi:10.1109/tdei.2005.1511089.

[80] M. Roy, J. K. Nelson, R. K. MacCrone, and L. S. Schadler. *Candidate mechanisms controlling the electrical characteristics of silica/XLPE nanodielectrics*. Journal of Materials Science, **42, 11**:3789–3799 (2007). doi:10.1007/s10853-006-0413-0.

[81] M. M. Shahin, R. H. Olley, and M. J. Blissett. *Refinement of Etching Techniques to Reveal Lamellar Profiles in Polyethylene Banded Spherulites*. Journal of Polymer Science Part B: Polymer Physics, **37**:2279–2286 (1999). doi:10.1002/(SICI)1099-0488(19990815)37:16⟨2279::AID-POLB30⟩3.0.CO;2-L.

[82] R. H. Olley and D. C. Bassett. *An improved permanganic etchant for polyolefines*. Polymer, **23, 12**:1707–1710 (1982). doi:10.1016/0032-3861(82)90110-0.

[83] M. Karlsson, X. Xu, K. Gaska, H. H. S. M. Gubanski, and U. W. Gedde. *DC Conductivity M eas urements of LDPE : Influence of Specimen Preparation Method and Polymer M orphology*. In *25th Nordic Insulation Symposium on Materials, Components and Diagnostics, NORD-IS 17* (2017).

[84] I. L. Hosier, A. S. Vaughan, and S. G. Swingler. *An investigation of the potential of polypropylene and its blends for use in recyclable high voltage cable insulation systems*. Journal of Materials Science, **46, 11**:4058–4070 (2011). doi:10.1007/s10853-011-5335-9.

[85] M. C. Costache, D. D. Jiang, and C. A. Wilkie. *Thermal degradation of ethylene-vinyl acetate coplymer nanocomposites*. Polymer, **46, 18**:6947–6958 (2005). doi:10.1016/j.polymer.2005.05.084.

[86] K. Y. Lau, A. S. Vaughan, G. Chen, I. L. Hosier, and A. F. Holt. *Absorption current behaviour of polyethylene/silica nanocomposites*. In *Journal of Physics: Conference Series*, volume 472, page 012003 (2013). ISBN doi:10.1088/1742-6596/472/1/012003. ISSN 1742-6588. doi:10.1088/1742-6596/472/1/012003.

[87] T. Tanaka. *Dielectric nanocomposites with insulating properties*. IEEE Transactions on Dielectrics and Electrical Insulation, **12, 5**:914–928 (2005). doi:10.1109/TDEI.2005.1522186.

[88] S. Kolesov. *The Influence of Morphology on the Electric Strength of Polymer Insulation*. IEEE Transactions on Electrical Insulation, **15, 5**:382–388 (1980). doi:10.1109/TEI.1980.298330.

[89] H. J. Maria, N. Lyczko, A. Nzihou, C. Mathew, S. C. George, K. Joseph, and S. Thomas. *Transport of organic solvents through natural rubber/nitrile rubber/organically modified montmorillonite nanocomposites*. Journal of Materials Science, **48, 15**:5373–5386 (2013). doi:10.1007/s10853-013-7332-7.

[90] G. Mazzanti and M. Marzinotto. *Extruded cables for high-voltage direct current transmission*. Institute of Electrical and Electronics Engineers, Hoboken, New Jersey (2013). ISBN 9781118096666.

[91] I. L. Hosier, M. Praeger, A. S. Vaughan, and S. G. Swingler. *The effects of hydration on the DC breakdown strength of polyethylene composites employing oxide and nitride fillers*. IEEE Transactions on Dielectrics and Electrical Insulation, **24, 5**:3073–3082 (2017). doi:10.1109/TDEI.2017.006579.

[92] K. Y. Lau, A. S. Vaughan, G. Chen, and I. L. Hosier. *Polyethylene nanodielectrics: The effect of nanosilica and its surface treatment on electrical breakdown strength*. In *Annual Report - Conference on Electrical Insulation and Dielectric Phenomena, CEIDP*, pages 21–24 (2012). ISBN 978-1-4673-1252-3. ISSN 00849162. doi:10.1109/CEIDP.2012.6378712.

[93] S. S. Brandstetter, L. F. Drummy, J. C. Horwath, D. L. Schweickart, and R. A. Vaia. *Breakdown voltage of thermoplastics with clay nanometer-sized fillers*. In *Proceedings of the 2008 IEEE International Power Modulators and High Voltage Conference, PMHVC*, pages 287–290 (2008). ISBN 9781424415359. ISSN 1930-885X. doi:10.1109/IPMC.2008.4743638.

[94] K. Lau, A. Vaughan, G. Chen, I. Hosier, A. Holt, and K. Ching. *On the space charge and DC breakdown behavior of polyethylene/silica nanocomposites*. IEEE Transactions on Dielectrics and Electrical Insulation, **21, 1**:340–351 (2014). doi:10.1109/TDEI.2014.6740758.

[95] A. T. Hoang, L. Pallon, D. Liu, Y. V. Serdyuk, S. M. Gubanski, and U. W. Gedde. *Charge transport in LDPE nanocomposites part I - experimental approach*. Polymers, **8, 3**:1–19 (2016). doi:10.3390/polym8030087.

[96] A. S. Vaughan, C. D. Green, Y. Zhang, and G. Chen. *Nanocomposites for high voltage applications: Effect of sample preparation on AC breakdown statistics*. In *Annual Report - Conference on Electrical Insulation and Dielectric Phenomena, CEIDP*, pages 732–735 (2005). ISBN 0780392574. ISSN 00849162. doi:10.1109/CEIDP.2005.1560787.

[97] F. Guastavino, L. Della Giovanna, E. Torello, M. Hoyos, and P. Tiemblo Magro. *Electrical Treeing in LDPE-EVA Blend Based Nanocomposites*. 2014 IEEE Conference on Electrical Insulation and Dielectric Phenomena (CEIDP), pages 780–783 (2014). doi:10.1109/CEIDP.2014.6995879.

[98] A. S. Vaughan, G. Gherbaz, S. G. Swingler, and N. Abd Rashid. *Polar / non-polar Polymer Blends : On structural evolution and the electrical properties of blends of polyethylene*

and ethylene - vinyl acetate. Annual Report Conference on Electrical Insulation and Dielectric Phenomena, CEIDP, pages 272–275 (2006).

[99] I. Hosier, M. Praeger, A. Holt, A. Vaughan, and S. Swingler. *On the Effect of Functionaliser Chain Length and Water Content in Polyethylene/Silica Nanocomposites: Part I Dielectric Properties and Breakdown Strength*. IEEE Transactions on Dielectrics and Electrical Insulation, **24, 3**:1698–1707 (2017). doi:10.1109/TDEI.2017.005788.

[100] A. Oya and Y. Kurokawa. *Factors controlling mechanical properties of clay mineral / polypropylene nanocomposites*. Journal of Materials Science, **35**:1045 – 1050 (2000). doi:10.1023/A:1004773222849.

[101] Y. Dong and D. Bhattacharyya. *Investigation on the competing effects of clay dispersion and matrix plasticisation for polypropylene/clay nanocomposites. Part II: Crystalline structure and thermo-mechanical behaviour*. Journal of Materials Science, **47, 9**:4127–4137 (2012). doi:10.1007/s10853-012-6267-8.

[102] R. Nowacki, B. Monasse, E. Piorkowska, A. Galeski, and J. M. Haudin. *Spherulite nucleation in isotactic polypropylene based nanocomposites with montmorillonite under shear*. Polymer, **45, 14**:4877–4892 (2004). doi:10.1016/j.polymer.2004.04.058.

[103] D. Li, J. Zhang, W. Xu, and Y. Fu. *Effect of SiO2/EVA on the Mechanical Properties, Permeability, and Residual Solvent of Polypropylene Packaging Films*. Polymer Composites, **37**:101–107 (2016). doi:DOI10.1002/pc.23159.

[104] C. Zilg, D. Kaempfer, R. Thomann, R. Muelhaupt, and G. C. Montanari. *Electrical Properties of Polymer Nanocomposites based upon Organophilic Layered Silicates*. Electrical Insulation and Dielectric Phenomena, 2003. Annual Report. Conference on, pages 546–550 (2003). doi:10.1109/ceidp.2003.1254913.

[105] J. Ma, Z. Qi, and Y. Hu. *Synthesis and characterization of polypropylene/clay nanocomposites*. Journal of Applied Polymer Science, **82, 14**:3611–3617 (2001). doi:10.1002/app.2223.

[106] A. Taguet, P. Cassagnau, and J. M. Lopez-Cuesta. *Structuration, selective dispersion and compatibilizing effect of (nano)fillers in polymer blends*. Progress in Polymer Science, **39, 8**:1526–1563 (2014). doi:10.1016/j.progpolymsci.2014.04.002.

[107] A. Bulinski, S. S. Bamji, M. Abou-Dakka, and Y. Chen. *Dielectric properties of polypropylene loaded with synthetic organoclay*. In *Electrical Insulation and Dielectric Phenomena, 2009. CEIDP '09. IEEE Conference on*, pages 666–671. IEEE (2009). ISBN 9781424445592. ISSN 00849162. doi:10.1109/CEIDP.2009.5377780.

[108] B. Hoffmann, C. Dietrich, R. Thomann, C. Friedrich, and R. Mulhaupt. *Morphology and rheology of polystyrene nanocomposites based upon organoclay*. Macromolecular Rapid Communications, **21, 1**:57–61 (2000). doi:10.1002/(SICI)1521-3927(20000101)21:1⟨57::AID-MARC57⟩3.0.CO;2-E.

[109] C. Il Park, W. Choi, M. Kim, and O. Ok Park. *Thermal and Mechanical Properties of Syndiotactic Polystyrene / Organoclay Nanocomposites with Different*. Journal of Polymer Science Part B Polymer Physics, **42**:1685–1693 (2003). doi:10.1002/polb.20040.

[110] S. Sinha Ray, M. Bousmina, and A. Maazouz. *Morphology and Properties of Organoclay Modified Polycarbonate/Poly(methyl methacrylate) Blend*. Polymer Engineering and Science, Special Issue: Polymeric Nanocomposites, **46, 8**:1121–1129 (2006). doi:10.1002/pen.20598.

[111] C. Bendjaouahdou and S. Bensaad. *The effects of organoclay on the morphology and balance properties of an immiscible polypropylene/natural rubber blend*. Energy Procedia, **36**:574–590 (2013). doi:10.1016/j.egypro.2013.07.066.

[112] H. Angus and A. Greenberg. *Melt blending of polypropylene-blend- polyamide 6-blend-organoclay systems*. Polymer International, **56**:50–56 (2007). doi:10.1002/pi.2109.

[113] P. H. P. Macaúbas and N. R. Demarquette. *Morphologies and interfacial tensions of immiscible polypropylene/polystyrene blends modified with triblock copolymers*. Polymer, **42, 6**:2543–2554 (2001). doi:10.1016/S0032-3861(00)00655-8.

[114] B. G. Soares, R. V. Barbosa, and J. C. Covas. *Polystyrene/EVA melt blends compatibilized with EVA-graft-polystyrene*. Journal of Applied Polymer Science, **65, 11**:2141–2149 (1997). doi:10.1002/(SICI)1097-4628(19970912)65:11⟨2141::AID-APP10⟩3.0.CO;2-6.

[115] C.-L. Zhang, L.-F. Feng, X.-P. Gu, S. Hoppe, and G.-H. Hu. *Blend composition dependence of the compatibilizing efficiency of graft copolymers for immiscible polymer blends*. Polymer Engineering and Science, **50, 11**:2243–2251 (2010). doi:10.1002/pen.21715.

[116] T. Wu, D. Yuan, F. Qiu, R. yuan Chen, G. zhen Zhang, and J. ping Qu. *Polypropylene/polystyrene/clay blends prepared by an innovative eccentric rotor extruder based on continuous elongational flow: Analysis of morphology, rheology property, and crystallization behavior*. Polymer Testing, **63**:73–83 (2017). doi:10.1016/j.polymertesting.2017.07.012.

[117] R. R. Tiwari and D. R. Paul. *Effect of organoclay on the morphology, phase stability and mechanical properties of polypropylene/polystyrene blends*. Polymer, **52, 4**:1141–1154 (2011). doi:10.1016/j.polymer.2011.01.019.

[118] R. Salehiyan, W. J. Choi, J. H. Lee, and K. Hyun. *Effects of mixing protocol and mixing time on viscoelasticity of compatibilized PP/PS blends*. Korea Australia Rheology Journal, **26, 3**:311–318 (2014). doi:10.1007/s13367-014-0035-z.

[119] F. Abbasi, A. Tavakoli, and M. K. Razavi Aghjeh. *Rheology, morphology, and mechanical properties of reactive compatibilized polypropylene/polystyrene blends via FriedelCrafts alkylation reaction in the presence of clay*. Journal of Vinyl and Additive Technology, **24, 1**:18–26 (2018). doi:10.1002/vnl.21522.

[120] S. Cho, J. S. Hong, S. J. Lee, K. H. Ahn, J. A. Covas, and J. M. Maia. *Morphology and rheology of polypropylene/polystyrene/clay nanocomposites in batch and continuous melt mixing processes*. Macromolecular Materials and Engineering, **296**:341–348 (2011). doi:10.1002/mame.201000194.

[121] E. Helal, L. G. Amurin, D. J. Carastan, R. R. de Sousa, E. David, M. Frechette, and N. R. Demarquette. *Tuning the Mechanical and Dielectric Properties of Clay-containing Thermoplastic Elastomer Nanocomposites*. Polymer Engineering and Science, **58**:E174–E181 (2018). doi:doi.org/10.1002/pen.24844.

[122] Y. Q. Rao and J. M. Pochan. *Mechanics of polymer-clay nanocomposites*. Macromolecules, **40, 2**:290–296 (2007). doi:10.1021/ma061445w.

[123] I. L. Hosier, A. S. Vaughan, and S. G. Swingler. *Structure property relationships in polyethylene blends: the effect of morphology on electrical breakdown strength*. Journal of Materials Science, **2**:4523–4531 (1997). doi:10.1023/A:1018617200285.

[124] M. Zanetti, G. Camino, R. Thomann, and R. Mülhaupt. *Synthesis and thermal behaviour of layered silicate-EVA nanocomposites*. Polymer, **42, 10**:4501–4507 (2001). doi:10.1016/S0032-3861(00)00775-8.

[125] E. Gmelin and S. Sarge. *Calibration of differential scanning calorimeters*. Pure and Applied Chemistry, **67, 11**:1789–1800 (1995). doi:10.1351/pac199567111789.

[126] W. Sichina. *DSC as problem solving tool: measurement of percent crystallinity of thermoplastics*. Perkin Elmer Instruments, and PETech (2000).

[127] J. H. Chen, F. C. Tsai, Y. H. Nien, and P. H. Yeh. *Isothermal crystallization of isotactic polypropylene blended with low molecular weight atactic polypropylene. Part I. Thermal properties and morphology development*. Polymer, **46, 15**:5680–5688 (2005). doi:10.1016/j.polymer.2005.03.107.

[128] A. K. Singh. *Advanced X-ray Techniques in Research And Industries*. Ios Pr Inc (2005). ISBN 1586035371.

[129] L. Dissado and J. Fothergill. *Electrical Degradation and Breakdown in Polymers*. The Institution of Engineering and Technology, London, UK, 1 edition (1992). ISBN 978-0-86341-196-0. doi:10.1049/ir:19920168.

[130] E. David, M. Fréchette, B. Zazoum, C. Daran-Daneau, A. D. Ngô, and H. Couderc. *Dielectric properties of PE/clay nanocomposites*. Journal of Nanomaterials, **2013** (2013). doi:10.1155/2013/703940.

[131] G. C. Stone and R. G. V. Heeswijk. *Paramater estimation for the Weibull distribution*. IEEE Transactions on Electrical Insulation, **EI-12, 4**:253–261 (1977). doi:10.1109/TEI.1977.297976.

[132] J. C. Fothergill. *Estimating the cumulative probability of failure data points to be plotted on Weibull and other probability paper*. IEEE Transactions on Electrical Insulation, **25, 3**:489–492 (1990). doi:10.1109/14.55721.

[133] B. Zazoum, E. David, and A. D. Ngô. *Structural and dielectric studies of LLDPE/O-MMT nanocomposites*. Transactions on Electrical and Electronic Materials, **15, 5**:235–240 (2014). doi:10.4313/TEEM.2014.15.5.235.

[134] P. Mallet, C. A. Guérin, and A. Sentenac. *Maxwell-Garnett mixing rule in the presence of multiple scattering: Derivation and accuracy*. Physical Review B - Condensed Matter and Materials Physics, **72, 1**:1–9 (2005). doi:10.1103/PhysRevB.72.014205.

[135] G. Peng, C.-C. Wu, C.-C. Diao, and C.-F. Yang. *Investigation of the composites of epoxy and micro-scale BaTi4O9 ceramic powder as the substrate of microwave communication circuit*. Microsystem Technologies, **24**:343–349 (2018). doi:10.1007/s00542-017-3367-z.

[136] D. R. Lide. *"Dielectric Constant of Selected Polymers", in CRC Handbook of Chemistry and Physics*. CRC Press, Boca Raton, FL (2005).

[137] D. Andjelkovic and N. Rajakovic. *Influence of accelerated aging on mechanical and structural properties of cross-linked polyethylene (XLPE) insulation*. Electrical Engineering, **83**:83–87 (2001). doi:10.1007/s002020000054.

[138] A. Arora, V. Choudhary, and D. K. Sharma. *Effect of clay content and clay/surfactant on the mechanical, thermal and barrier properties of polystyrene/organoclay nanocomposites*. Journal of Polymer Research, **18, 4**:843–857 (2011). doi:10.1007/s10965-010-9481-6.

[139] B. Zazoum, E. David, and A. D. Ngô. *LDPE / HDPE / Clay Nanocomposites : Effects of Compatibilizer on the Structure and Dielectric Response*. Journal of Nanotechnology (2013). doi:10.1155/2013/138457.

[140] P. Supaphol and J. E. Spruiell. *Thermal properties and isothermal crystallization of syndiotactic polypropylenes: Differential scanning calorimetry and overall crystallization kinetics*. Journal of Applied Polymer Science, **75**:44–59 (2000). doi:10.1002/(SICI)1097-4628(20000103)75:1⟨44::AID-APP6⟩3.0.CO;2-1.

[141] K. Y. Lau, M. A. M. Piah, and K. Y. Ching. *Correlating the breakdown strength with electric field analysis for polyethylene / silica nanocomposites*. Journal of Electrostatics, **86**:1–11 (2017). doi:10.1016/j.elstat.2016.12.021.

[142] K. Nakamura, S. Shimizu, S. Umemoto, A. Thierry, B. Lotz, and N. Okui. *Temperature Dependence of Crystal Growth Rate for α and β Forms of Isotactic Polypropylene*. Polymer Journal, **40, 9**:915–922 (2008). doi:10.1295/polymj.PJ2007231.

[143] R. A. C. Amoresi, A. A. Felix, E. R. Botero, N. L. C. Domingues, E. A. Falcão, M. A. Zaghete, and A. W. Rinaldi. *Crystallinity, morphology and high dielectric permittivity*

of NiO nanosheets filling Poly(vinylidene fluoride). Ceramics International, **41**:14733–14739 (2015). doi:10.1016/j.ceramint.2015.07.199.

[144] L. A. Al Juhaiman, D. A. Al-Enezi, and W. K. Mekhamer. *Preparation and characterization of polystyrene/organoclay nanocomposites from raw clay*. Digest Journal of Nanomaterials and Biostructures, **11, 1**:105–114 (2016).

[145] B. D. Cullity. *Elements Of X Ray Diffraction*. Addison-Wesley Publishing Company Inc., Reading, Massachusetts, 1st edition (1956).

[146] T. Lan, P. D. Kaviratna, and T. J. Pinnavaia. *Mechanism of clay tactoid exfoliation in epoxy-clay nanocomposites*. Chemistry of Materials, **7, 11**:2144–2150 (1995). doi:10.1021/cm00059a023.

[147] J. S. Borah, N. Karak, and T. K. Chaki. *Effect of organoclay platelets on morphology and properties of LLDPE/EMA blends*. Materials Science and Engineering A, **528, 6**:2820–2830 (2011). doi:10.1016/j.msea.2010.12.067.

[148] H. D. Lu, Y. Hu, Q. H. Kong, Y. B. Cai, Z. Chen, and W. C. Fan. *Influence of gamma irradiation on high density polyethylene/ethylene-vinyl acetate/clay nanocomposites*. Polymers for Advanced Technologies, **15, 10**:601–605 (2004). doi:10.1002/pat.518.

[149] A. Behradfar, A. Shojaei, and N. Sheikh. *Rheological and mechanical characteristics of low density polyethylene/ethylene-vinyl acetate/organoclay nanocomposites*. Polymer Engineering and Science, **50, 7**:1315–1325 (2010). doi:10.1002/pen.21660.

[150] G. Liang, J. Xu, S. Bao, and W. Xu. *Polyethylene / Maleic Anhydride Grafted Polyethylene / Organic-Montmorillonite Nanocomposites. I. Preparation, Microstructure, and Mechanical Properties*. Journal of Applied Polymer Science, **91**:3974–3980 (2004). doi:10.1002/app.13612.

[151] S. K. Srivastava, M. Pramanik, and H. Acharya. *Ethylene/vinyl acetate copolymer/clay nanocomposites*. Journal of Polymer Science, Part B: Polymer Physics, **44, 3**:471–480 (2006). doi:10.1002/polb.20702.

[152] D. L. Ho, R. M. Briber, and C. J. Glinka. *Characterization of organically modified clays using scattering and microscopy techniques*. Chemistry of Materials, **13, 5**:1923–1931 (2001). doi:10.1021/cm0008617.

[153] M. Okamoto, S. Morita, Y. H. Kim, T. Kotaka, and H. Tateyama. *Synthesis and structure of smectic clay/poly(methyl methacrylate) and clay/polystyrene nanocomposites via in situ intercalative polymerization*. Polymer, **41, 10**:3887–3890 (2000). doi:10.1016/S0032-3861(99)00655-2.

[154] K. Kalaitzidou, H. Fukushima, P. Askeland, and L. T. Drzal. *The nucleating effect of exfoliated graphite nanoplatelets and their influence on the crystal structure and electrical*

conductivity of polypropylene nanocomposites. Journal of Materials Science, **43, 8**:2895–2907 (2008). doi:10.1007/s10853-007-1876-3.

[155] A. J. Lovinger, J. O. Chua, and C. C. Gryte. *Studies on the α and β forms of isotactic polypropylene by crystallization in a temperature gradient*. Journal of Polymer Science: Polymer Physics Edition, **15**:641–656 (1977). doi:10.1002/pol.1977.180150405.

[156] B. H. Yuan, C. L. Bao, L. Song, N. N. Hong, K. M. Liew, and Y. Hu. *Preparation of functionalized graphene oxide/polypropylene nanocomposite with significantly improved thermal stability and studies on the crystallization behavior and mechanical properties*. Chemical Engineering Journal, **237**:411–420 (2014). doi:DOI10.1016/j.cej.2013.10.030.

[157] T. H. Kim, L. W. Jang, D. C. Lee, H. J. Choi, and M. S. Jhon. *Synthesis and Rheology of Intercalated Polystyrene / Na + -Montmorillonite Nanocomposites*. Macromolecular Rapid Communications, **23**:191–195 (2002). doi:10.1002/1521-3927(20020201)23:3⟨191::AID-MARC191⟩3.0.CO;2-H.

[158] X. Dai, Z. Zhang, C. Wang, Q. Ding, J. Jiang, and K. Mai. *A novel montmorillonite with β-nucleating surface for enhancing β-crystallization of isotactic polypropylene*. Composites Part A: Applied Science and Manufacturing, **49**:1–8 (2013). doi:10.1016/j.compositesa.2013.01.016.

[159] Y. Chen, H. Yang, S. Yang, P. Ren, Q. Zhang, and Z. Li. *Polypropylene films with high barrier performance via crystal morphology manipulation*. Journal of Materials Science, **52, 9**:5449–5461 (2017). doi:10.1007/s10853-017-0789-z.

[160] F. Medellín-Rodríguez, J. Mata-Padilla, B. Hsiao, M. Waldo-Mendoza, E. Ramírez-Vargas, and S. Sánchez-Valdes. *The Effect of Nanoclays on the Nucleation, Crystallization, and Melting Mechanisms of Isotactic Polypropylene*. Polymer Engineering and Science, **47, 11**:1889–1897 (2007). doi:DOI10.1002/pen.20902.

[161] A. F. Osman, T. F. M. Fitri, M. Rakibuddin, F. Hashim, S. A. T. Tuan Johari, R. Ananthakrishnan, and R. Ramli. *Pre-dispersed organo-montmorillonite (organo-MMT) nanofiller: Morphology, cytocompatibility and impact on flexibility, toughness and biostability of biomedical ethyl vinyl acetate (EVA) copolymer*. Materials Science and Engineering C, **74**:194–206 (2017). doi:10.1016/j.msec.2016.11.137.

[162] P. Meenakshi, S. E. Noorjahan, R. Rajini, U. Venkateswarlu, C. Rose, and T. P. Sastry. *Mechanical and microstructure studies on the modification of CA film by blending with PS*. Bulletin of Materials Science, **25, 1**:25–29 (2002). doi:10.1007/BF02704590.

[163] A. S. Al-Hobaib, M. S. Alsuhybani, K. M. AL-Sheetan, and M. R. Shaik. *Reverse osmosis membranes prepared by interfacial polymerization in n-heptane containing different co-solvents*. Desalination and Water Treatment, **57, 36**:16733–16744 (2015). doi:10.1080/19443994.2015.1083888.

[164] C. D. Green, A. S. Vaughan, G. Stevens, S. J. Sutton, T. Geussens, and M. Fairhurst. *Recyclable power cable comprising a blend of slow-crystallized polyethylenes*. IEEE Transactions on Dielectrics and Electrical Insulation, **20, 1**:1–9 (2013). doi:10.1109/TDEI.2013.6451335.

[165] V. Goodarzi, S. Hassan Jafari, H. Ali Khonakdar, B. Ghalei, and M. Mortazavi. *Assessment of role of morphology in gas permselectivity of membranes based on polypropylene/ethylene vinyl acetate/clay nanocomposite*. Journal of Membrane Science, **445**:76–87 (2013). doi:10.1016/j.memsci.2013.04.073.

[166] R. Succi, T. Han, and A. Cavallini. *An Investigation on the Dielectric Properties of Thermally-Aged Kapton and its Capability to Withstand Partial Discharges*. In *2019 IEEE Conference on Electrical Insulation and Dielectric Phenomena*, pages 426–429. IEEE, Richland, Washington, USA (2019).

[167] F. Ehtaiatkar, M. J. Folkes, and S. C. Steadman. *In situ production of polyethylene fibres from polymer blends*. Journal of Materials Science, **24, 8**:2808–2814 (1989). doi:10.1007/BF02385630.

[168] Y. Mecheri, L. Boukezzi, A. Boubakeur, and M. Lallouani. *Dielectric and mechanical behavior of cross-linked polyethylene under thermal aging*. In *2000 Annual Report Conference on Electrical Insulation and Dielectric Phenomena (Cat. No.00CH37132)*, volume 2, pages 560–563 (2000). ISBN 0-7803-6413-9. ISSN 00849162. doi:10.1109/CEIDP.2000.884022.

[169] G. Montanari, F. Palmieri, L. Testa, A. Motori, A. Saccani, and F. Patuelli. *Polarization processes of nanocomposite silicate-EVA and PP materials*. In *IEEJ Transactions on Fundamentals and Materials*, volume 126, pages 1090–1096 (2006). ISSN 03854205 13475533. doi:10.1541/ieejfms.126.1090.

[170] S. Stankovich, D. A. Dikin, R. D. Piner, K. A. Kohlhaas, A. Kleinhammes, Y. Jia, Y. Wu, S. B. T. Nguyen, and R. S. Ruoff. *Synthesis of graphene-based nanosheets via chemical reduction of exfoliated graphite oxide*. Carbon, **45, 7**:1558–1565 (2007). doi:10.1016/j.carbon.2007.02.034.

[171] W. Zhou, S. Qi, Q. An, H. Zhao, and N. Liu. *Thermal conductivity of boron nitride reinforced polyethylene composites*. Materials Research Bulletin, **42, 10**:1863–1873 (2007). doi:10.1016/j.materresbull.2006.11.047.

[172] M. Abou-Dakka. *Evolution of Space Charges and Conductivity with DC Aging of Polyethylene-Synthetic and Natural Clay Composites*. Journal of Nanomaterials, pages 1–8 (2012). doi:10.1155/2012/463748.

[173] Y. Li, X. Huang, Z. Hu, P. Jiang, S. Li, and T. Tanaka. *Large dielectric constant and high thermal conductivity in poly(vinylidene fluoride)/barium titanate/silicon carbide three-phase nanocomposites*. ACS Applied Materials and Interfaces, **3, 11**:4396–4403 (2011). doi:10.1021/am2010459.

[174] P. Maiti, P. H. Nam, M. Okamoto, N. Hasegawa, and A. Usuki. *Influence of crystallization on intercalation, morphology, and mechanical properties of polypropylene/clay nanocomposites*. Macromolecules, **35, 6**:2042–2049 (2002). doi:10.1021/ma010852z.

[175] V. Tomer, G. Polizos, C. A. Randall, and E. Manias. *Polyethylene nanocomposite dielectrics: Implications of nanofiller orientation on high field properties and energy storage*. Journal of Applied Physics, **109, 7** (2011). doi:10.1063/1.3569696.

[176] E. David and M. Fréchette. *Polymer nanocomposites-major conclusions and achievements reached so far*. IEEE Electrical Insulation Magazine, **29, 6**:29–36 (2013). doi:10.1109/MEI.2013.6648751.

[177] R. C. Smith, C. Liang, M. Landry, J. K. Nelson, and L. S. Schadler. *The mechanisms leading to the useful electrical properties of polymer nanodielectrics*. IEEE Transactions on Dielectrics and Electrical Insulation, **15, 1**:187–196 (2008). doi:10.1109/T-DEI.2008.4446750.

[178] D. Fabiani, G. Montanari, and L. Testa. *Effect of aspect ratio and water contamination on the electric properties of nanostructured insulating materials*. IEEE Transactions on Dielectrics and Electrical Insulation, **17, 1**:221–230 (2010). doi:10.1109/TDEI.2010.5412021.

[179] AZoM. *AZo Materials* (2001).

[180] S. Z. A. Dabbak, H. A. Illias, B. C. Ang, N. A. A. Latiff, and M. Z. H. Makmud. *Electrical properties of polyethylene/polypropylene compounds for high-voltage insulation*. Energies, **11, 6** (2018). doi:10.3390/en11061448.

[181] Ü. Alkan, Y. Karabul, A. E. Bulgurcuolu, M. Klllç, Z. G. Özdemir, and O. Içelli. *Polypropylene/basalt thick film composites: Structural, mechanical and dielectric properties*. E-Polymers, **17, 5**:417–425 (2017). doi:10.1515/epoly-2017-0035.

[182] M. Praeger, A. S. Vaughan, and S. G. Swingler. *A dielectric spectroscopy study of the polystyrene/nanosilica model system*. Proceedings of IEEE International Conference on Solid Dielectrics, ICSD, pages 859–862 (2013). doi:10.1109/ICSD.2013.6619765.

[183] R. Mujal-Rosas, J. Orrit-Prat, X. Ramis-Juan, M. Marin-Genesca, and A. Rahhali. *Study on dielectric, thermal, and mechanical properties of the ethylene vinyl acetate reinforced with ground tire rubber*. Journal of Reinforced Plastics and Composites, **30, 7**:581–592 (2011). doi:10.1177/0731684411399135.

[184] R. J. Sengwa and S. Choudhary. *Dielectric relaxations and structures of nanoclay in solution cast poly(Ethylene Oxide)-montmorillonite clay nanocomposites*. Journal of Macromolecular Science, Part B: Physics, **50**:1313–1324 (2011). doi:10.1080/00222348.2010.507451.

[185] Y. Wang and W. C. Chen. *Dielectric probing of relaxation behaviors in PMMA/organoclay nanocomposites: Effect of organic modification*. Composite Interfaces, **17, 9**:803–829 (2010). doi:10.1163/092764410X539217.

[186] T. C. M. Chung. *Functionalization of Polypropylene with High Dielectric Properties: Applications in Electric Energy Storage*. Green and Sustainable Chemistry, **02, 02**:29–37 (2012). doi:10.4236/gsc.2012.22006.

[187] M. Pluta, J. K. Jeszka, and G. Boiteux. *Polylactide/montmorillonite nanocomposites: Structure, dielectric, viscoelastic and thermal properties*. European Polymer Journal, **43, 7**:2819–2835 (2007). doi:10.1016/j.eurpolymj.2007.04.009.

[188] K. S. Cole and R. H. Cole. *Dispersion and Absorption in Dielectrics I. AC characteristics*. J. Chem. Phys., **9, 1913**:341–351 (1941). doi:10.1063/1.1750906.

[189] H. J. Choi, C. H. Hong, and M. S. Jhon. *Cole-Cole Analysis on Dielectric Spectra of Electrorheological Suspensions*. International Journal of Modern Physics B, **21, 28**:4974–4980 (2007). doi:10.1142/S0217979207045918.

[190] A. L. Sharma and A. K. Thakur. *Relaxation behavior in clay-reinforced polymer nanocomposites*. Ionics, **21, 6**:1561–1575 (2015). doi:10.1007/s11581-014-1336-4.

[191] K. C. Kao. *Dielectric Phenomena in Solids* (2004). ISBN 0123965616.

[192] V. Raja, A. K. Sharma, and V. V. Rao. *Impedance spectroscopic and dielectric analysis of PMMA-CO-P4VPNO polymer films*. Materials Letters, **58, 26**:3242–3247 (2004). doi:10.1016/j.matlet.2004.05.061.

[193] R. Ayoob, T. Andritsch, and A. S. Vaughan. *Water absorption behaviour in polyethylene boron nitride nanocomposites*. Proceedings of the 2016 IEEE International Conference on Dielectrics, ICD 2016, **2**:784–787 (2016). doi:10.1109/ICD.2016.7547733.

[194] K. Y. Lau, A. S. Vaughan, G. Chen, I. L. Hosier, and a. F. Holt. *On the dielectric response of silica-based polyethylene nanocomposites*. Journal of Physics D: Applied Physics, **46, 9** (2013). doi:10.1088/0022-3727/46/9/095303.

[195] G. Tourillon and F. Garnier. *Effect of dopant on the physicochemical and electrical properties of organic conducting polymers*. Journal of Physical Chemistry, **87, 13**:2289–2292 (1983). doi:10.1021/j100236a010.

[196] S. Glenis, M. Benz, E. LeGoff, M. G. Kanatzidis, J. L. Schindler, and C. R. Kannewurf. *Polyfuran: A New Synthetic Approach and Electronic Properties*. Journal of the American Chemical Society, **115, 26**:12519–12525 (1993). doi:10.1021/ja00079a035.

[197] P. Perez, T. E. Block, and C. M. Knobler. *Refractive Index and Dielectric Constant of Mixtures of Carbon Tetrachloride with Benzene, p-Xylene, and Mesitylene*. Journal of Chemical and Engineering Data, **16, 3**:333–335 (1971). doi:10.1021/je60050a035.

[198] N. Taniguchi, O. Urakawa, and K. Adachi. *Calorimetric study of dynamical heterogeneity in toluene solutions of polystyrene*. Macromolecules, **37, 20**:7832–7838 (2004). doi:10.1021/ma048788j.

[199] E. Izci and N. Bowler. *Dielectric Properties of Isotactic Polypropylene and Montmorillonite Nanocomposites*. In *Procedings of the 2010 IEEE International Conference on Solid Dielectrics (ICSD 2010)*, pages 1–4. IEEE, Potsdam, Germany (2010). ISBN 978-1-4244-7945-0. doi:10.1109/ICSD.2010.5568047.

[200] A. Vatansever, T. Inan, H. Dogan, and A. Sirkecioglu. *Effect of organic modifier type of montmorillonite on the poly (butyl acrylate-co-methyl methacrylate)/montmorillonite nanocomposite*. Polymer Bulletin, **73, 4**:909–925 (2016). doi:10.1007/s00289-015-1526-x.

[201] F. N. Alhabill, R. Ayoob, T. Andritsch, and A. S. Vaughan. *Effect of resin/hardener stoichiometry on electrical behavior of epoxy networks*. IEEE Transactions on Dielectrics and Electrical Insulation, **24, 6**:3739–3749 (2017). doi:10.1109/TDEI.2017.006828.

[202] J. C. Fothergill, G. C. Montanari, G. C. Stevens, C. Laurent, G. Teyssedre, L. A. Dissado, U. H. Nilsson, and G. Platbrood. *Electrical, microstructural, physical and chemical characterization of HV XLPE cable peelings for an electrical aging diagnostic data base*. IEEE Transactions on Dielectrics and Electrical Insulation, **10, 3**:514–527 (2003). doi:10.1109/TDEI.2003.1207480.

[203] N. Hirai, R. Minami, K. Shibata, Y. Ohki, M. Okashita, and T. Maeno. *Effect of Byproducts of Dicumyl Peroxide- on Space Charge Formation in Low-density Polyethylene*. In *IEEE conference CEIDP 2001*, pages 478–483. IEEE, Kitchener, Ontario, Canada (2001). doi:10.1109/CEIDP.2001.963585.

[204] T. Takeda, N. Hozumi, H. Suzuki, and T. Okamoto. *Factors of hetero space charge generation in XLPE under dc electric field of 20 kV/mm*. Electrical Engineering in Japan (English translation of Denki Gakkai Ronbunshi), **129, 2**:13–21 (1999). doi:10.1002/(SICI)1520-6416(19991115)129:2⟨13::AID-EEJ2⟩3.0.CO;2-V.

[205] I. L. Hosier, M. Praeger, A. S. Vaughan, and S. G. Swingler. *The Effects ofWater on the Dielectric Properties of Silicon-Based Nanocomposites*. IEEE Transactions on Nanotechnology, **16, 2**:169–179 (2017). doi:10.1109/TNANO.2017.2703982.

[206] R. Ayoob, F. Alhabill, T. Andritsch, and A. Vaughan. *The effect of water absorption on the dielectric properties of polyethylene hexagonal boron nitride nanocomposites*. J. Phys. D: Appl. Phys., **51, 6** (2018). doi:10.1088/1361-6463/aaa306.

[207] C. Zhang and G. C. Stevens. *The dielectric response of polar and non-polar nanodielectrics*. IEEE Transactions on Dielectrics and Electrical Insulation, **15, 2**:606–617 (2008). doi:10.1109/TDEI.2008.4483483.

[208] E. David, C. Daran-Daneau, M. F. Frechette, B. Zazoum, A. D. Ngô, and S. Savoie. *Dielectric response of LLDPE/Clay nanocomposite melt compounded from a masterbatch*. In *Conference Record of IEEE International Symposium on Electrical Insulation*, pages 641–645 (2012). ISBN 9781467304887. ISSN 01642006. doi:10.1109/ELINSL.2012.6251550.

[209] K. Faghihi, M. Taher, and M. Hajibeygi. *Preparation and characterization of new polyamide/montmorillonite nanocomposites containing azo moiety in the main chain*. Arabian Journal of Chemistry, **9**:S1496–S1502 (2016). doi:10.1016/j.arabjc.2012.03.010.

[210] S. Mashimo, S. Kuwabara, S. Yagihara, and K. Higasi. *Dielectric relaxation time and structure of bound water in biological materials*. Journal of Physical Chemistry, **91, 25**:6337–6338 (1987). doi:10.1021/j100309a005.

[211] K. J. Tielrooij, D. Paparo, L. Piatkowski, H. J. Bakker, and M. Bonn. *Dielectric relaxation dynamics of water in model membranes probed by terahertz spectroscopy*. Biophysical Journal, **97, 9**:2484–2492 (2009). doi:10.1016/j.bpj.2009.08.024.

[212] Y. Kurokawa, H. Yasuda, C. Corporation, M. Kashiwagi, and A. Oyo. *Structure and properties of a montmorillonite a polypropylene nanocomposite*. Journal of Materials Science Letters, **6**:1670–1672 (1997).

[213] N. Hussin. *The Effects of Crosslinking Byproducts on the Electrical Properties of Low Density Polyethylene*. Ph.D. thesis (2011). doi:10.1016/j.jsv.2010.04.020.

[214] S. O. Kasap. *Dielectric Materials and Insulation*. In *Principles of Electrical Engineering Materials and Devices*, chapter 7, pages 512–565. Tom Casson, Saskatchewan, Canada (1997). ISBN 0-256-16173-9.

[215] A. V. Goncharenko, V. Z. Lozovski, and E. F. Venger. *Lichtenecker's equation: applicability and limitations*. Optics Communications, **174, 1-4**:19–32 (2000). doi:10.1016/S0030-4018(99)00695-1.

[216] H. M. Rosenberg. *The Solid State*. Clarendon Press, Oxford, second edition (1978).

[217] F. C. Chiu. *A review on conduction mechanisms in dielectric films*. Advances in Materials Science and Engineering, **2014** (2014). doi:10.1155/2014/578168.

[218] P. Chammingkwan, K. Matsushita, T. Taniike, and M. Terano. *Enhancement in mechanical and electrical properties of polypropylene using graphene oxide grafted with end-functionalized polypropylene*. Materials, **9, 4** (2016). doi:10.3390/ma9040240.

[219] I. L. Hosier, A. S. Vaughan, and S. G. Swingler. *The effects of measuring technique and sample preparation on the breakdown strength of polyethlyene*. IEEE Transactions on Dielectrics and Electrical Insulation, **9, 3**:353–361 (2002). doi:10.1109/TDEI.2002.1007697.